FANTASTIC VESICLES & HOW TO FIND THEM

Direct Detection of Single Extracellular Vesicles in Complex, Clinically Relevant Biofluids

WOUTER WILLEM WOUD

Fantastic Vesicles and How to Find Them

Direct Detection of Single Extracellular Vesicles in Complex, Clinically Relevant Biofluids

Wouter Willem Woud

The research described in this thesis was performed at the Erasmus MC Transplant Institute, Department of Internal Medicine, University Medical Center, Rotterdam, The Netherlands.

Cover design:	BernArt Visuals
Lay-out:	Publiss | www.publiss.nl
Print:	Ridderprint | www.ridderprint.nl
Copyright:	Wouter W. Woud, 2023

Printing of this thesis was financially supported by the Nederlandse Transplantatie Vereniging (NTV), Erasmus Universiteit Rotterdam, Cytek Biosciences, and Cees Woud Natuursteen.

Fantastic Vesicles and How to Find Them

Direct detection of single extracellular vesicles
in complex, clinically relevant biofluids

Fantastische vesikels en hoe ze te vinden

Directe detectie van individuele extracellulaire vesikels in
complexe, klinisch relevante biovloeistoffen

Thesis
To obtain the degree of Doctor from the
Erasmus University Rotterdam,
by command of the
Rector Magnificus

Prof. dr. A. L. Bredenoord

and in accordance with the decision of the Doctorate Board.
The public defence shall be held on

Wednesday 28 June 2023 at 10:30 hrs

by

Wouter Willem Woud

born in Zaanstad, The Netherlands

Erasmus University Rotterdam

Doctoral Committee

Promotor:	Prof. dr. C. C. Baan
Other members:	Prof. dr. E. J. Hoorn Prof. dr. R. J. Porte Dr. E. N. M. Nolte-'t Hoen
Co-promotors:	Dr. M. J. Hoogduijn Dr. ir. K. Boer

TABLE OF CONTENTS


REJECTED
REJECTED
REJECTED

FANTASTIC VESICLES AND HOW TO FIND THEM

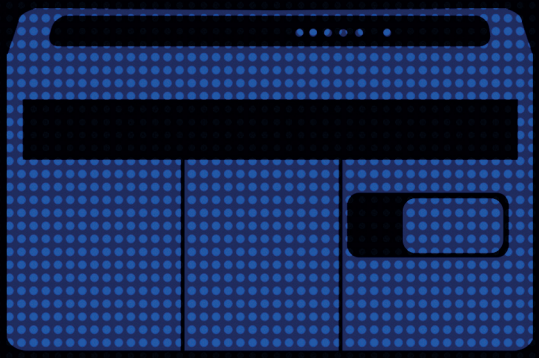

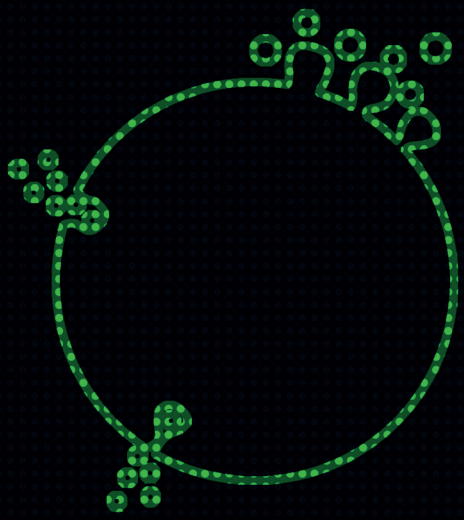

01

GENERAL INTRODUCTION AND OBJECTIVES

The wide wealthy world of communication

The living world is a collection of ecosystems in which the interactions between individual components determine the emergent properties of complex biological systems [1]. Such interactions are mainly driven through communication between or within species and organisms, which are subject to changing environmental conditions. As such, the state of a system is reflected by its occupying species, which may be studied to infer environmental changes. To illustrate: bees are considered an indicator species meaning that their vibrancy on earth reflects environmental conditions and aids in gauging the health of ecosystems. Simply put, reduced numbers of bees in a given hive indicate a decline in environmental conditions.

Similar to studying bees to infer environmental status, studying biomolecules released by cells – as means of intercellular communication – allows researchers to infer cellular status, and, by extension, the status of cellular systems as a whole. This is of paramount importance in the context of health and disease. Broadly speaking, cellular communication is performed through either direct contact with neighboring cells or the excretion of biomolecules into the extracellular space. A relatively recently discovered and exciting modality of such an excreted means of communication, and the subject of this thesis, are extracellular vesicles (EVs).

A brief history of EV-erything

EVs were first described in a series of manuscripts which identified potential structures that would *retrospectively* be described as EVs [2]. In 1946, Chargaff and West reported the discovery of a 'particulate fraction' which sedimented from human plasma at 31,000 g (but remained at solution at 5,000 g). At the time, these particles were suggested to be a form of cellular waste [3]. In 1967, Peter Wolf described a *"material in minute form, sedimentable by high-speed centrifugation and originating from platelets, but distinguishable from intact platelets"* – which we now know as the EV fraction. Wolf provided electron microscopy images of these particles, which he described as 'platelet dust' [4]. A few years later (1971), Neville Crawford published further images of these particles – which were now being described as 'microparticles' – and showed that these particles contained lipids and carried cargo such as the cellular energy source adenosine triphosphate (ATP) [5], thus suggesting that these particles were more than cellular debris or waste particles. These pioneering experiments were the first to describe the presence and structure of such cell-free components and hinted at their potential biological importance.

Since then, EVs have been identified as a heterogeneous group of lipid bilayered membrane structures (30-8000 nm in diameter [6]), and are classified into three major subtypes based on their mode of biogenesis (Figure 1). In addition to their mode of release, EV size is often used for characterization: exosomes are regarded as the smallest type of EVs (30 – 100 nm in diameter), microvesicles range from 100 to 1000 nm in diameter, and apoptotic bodies may reach sizes up to several micrometers [7]. However, there is some controversy on nomenclature and sizes as different types of EVs overlap in their size distribution [8, 9]. Therefore, the term 'Extracellular Vesicle', as used in this thesis, is used as a generic term for all secreted vesicles.

EVs carry proteins on their surface and a variety of macromolecules as cargo (e.g., lipids, proteins, enzymes, nucleic acids, protein-coding mRNAs and regulatory microRNAs [10, 11]), which are thought to reflect the status of their cell of origin. Upon contact with or internalization by recipient cells, EVs have the ability to transfer information from one cell to another, thus modulating recipient cell behavior [12]. Therefore, EVs have been recognized as mediators of intercellular communication during both normal physiological as well as in pathological processes [10, 13]. As EVs are excreted by virtually all cell types in the human body, they can be found in all body fluids, such as the blood [6], saliva [14] and urine [15, 16].

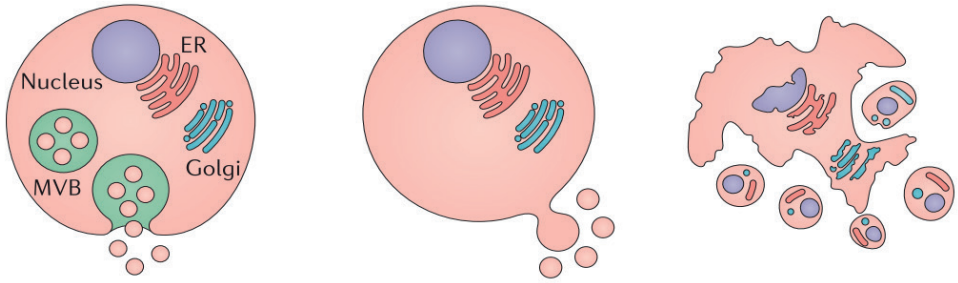

Figure 1 - Exosomes, Microvesicles, and Apoptotic bodies.
Exosomes (left) are released into the extracellular domain through fusion of multivesicular bodies (MVB) with the cell membrane. Microvesicles (middle) are formed through outward budding of the cell membrane, and apoptotic bodies (right) are fragments of cells which have undergone apoptosis. Adapted from Karpmann, et al. [17].

The relative stability of EVs (their cargo is protected from fragmentation and degradation by the lipid bilayer [18]), and their ubiquitous presence in (relatively) easily obtainable bodily fluids have sparked the interest in EVs as potential biomarkers for disease diagnosis and prognosis [19]. As EVs exist at numbers exceeding 1000 particles for each cell of origin, their analysis offers quantitative advantages over less abundant entities such as circulating tumor cells [20], donor-derived cell-free DNA [21], or antibodies against cytoplasmic proteins [22].

EVs as potential biomarkers in kidney transplantation

Kidney transplantation is the preferred treatment for patients suffering from irreversible, end-stage renal disease - providing increased patient survival over dialysis [23]. However, the shortage of available donor kidneys (grafts), the increasing number of patients on the waiting list, and the general aging of the population has led to an increased use of expanded-criteria donor (ECD) grafts as well as grafts procured from donation after circulatory death (DCD) [24] – both of which are associated with poorer transplant outcomes when compared to organs from standard criteria donors [25, 26]. An essential problem with the usage of these kidneys is the lack of quality measures needed to guide the clinician in deciding whether to accept or decline the organ. In the past decade, hypothermic machine perfusion (HMP) has gained interest as a promising preservation technique for deceased donor organs [27], showing improved clinical outcomes after kidney transplantation compared with static cold storage [28]. The most recent development in organ preservation is normothermic machine perfusion (NMP). In contrast to HMP, NMP aims to restore cellular metabolism and function to the organ, which is achieved through circulation of a warm, oxygenated red blood cell based solution through the organ prior to transplantation [29, 30]. Because metabolism is activated, NMP offers the possibility to assess graft status prior to transplantation through monitoring of the perfusion dynamics and analysis of biomarkers (such as EVs) in the perfusion fluids [25, 29, 31, 32].

After transplantation - despite potent immunosuppressive therapy - acute rejection of the graft occurs in as much as 21% of transplantations during the first 6 months after transplantation [21]. Though the function of kidney allografts are routinely monitored through serum creatinine and urea, and urinary protein concentrations, these markers are relatively insensitive for allograft rejection as a rise in their concentrations does not specifically indicate immunologic rejection

[33]. Consequently, an elevation of these markers is often followed by a kidney transplant biopsy, which, despite being the gold standard to diagnose rejection, is an invasive procedure with a risk of complications including bleeding and infection [34]. Combined, these issues reveal the critical need for more accurate, early and minimally invasive biomarker platforms to diagnose kidney allograft rejection.

The potential of EVs as biomarker for the detection of allograft rejection has been described – in animal models – by a few groups [35-40]. These studies have shown that donor-derived EVs are released into the circulation post transplantation, and provide indications that concentrations of donor-derived EVs diminish during rejection well before alterations in classical biomarkers or histologic manifistation of injury can be observed. These findings suggest that detection and monitoring of donor-derived circulating EVs may herald rejection in a more time-sensitive manner compared to classical markers.

Challenging to measure

Despite the interest in and clinical relevance of EVs as biomarker, EV analysis is hampered by a variety of factors. First of all, their physical characteristics, such as their small size, low epitope copy number [41], the variety of protein markers depending on the cell source, the confinement of some markers to the luminal side of the EV, and the low abundance of pathological EVs [11, 42] all contribute to the complexity of EV analysis. Additionally, no unique antigens representative for specific EV classes and subpopulations have been reported to date. Instead, tetraspanins (CD9/CD63/CD81) are recognized as common EV antigens. These proteins are enriched on EVs and are involved in EV biogenesis, cargo selection, and cell targeting [43, 44].

Second, the identification of EVs in blood plasma is further hindered by the molecular complexity of plasma, which contains multiple elements (e.g. protein aggregates, cell debris and the far more abundant lipoproteins) that interfere with EV analysis [11, 45]. Lipoproteins are submicron structures of lipids and apolipoproteins that are excreted into the circulation by the liver and intestines. They are classified into several subgroups, and their biophysical properties in terms of size and density largely overlap with those of EVs. However, a distinguishing feature is the presence of an aqueous core in EVs, whereas the core of lipoproteins is comprised of lipids [11].

Third, apart from their biological diversity and their large overlap in biophysical properties with other entities, a lack of robust EV detection methods and ambiguities in how data should be interpreted for EV analysis makes interpretation between studies challenging [46, 47]. Currently, the gold standard approach for EV analysis is based on the isolation or concentration of EVs. Ultracentrifugation, density-gradient, and size exclusion chromatography are the most widely used EV isolation techniques [48], despite yielding low-purity EV samples due to the co-isolation of non-desired molecules such as lipoproteins [11, 45].

Additionally, a variety of analytical platforms are available. Nanoparticle tracking analysis (NTA) allows the determination of the size distribution and a rough indication of the concentration of individual nanoparticles in suspension[49], but provides limited phenotyping capabilities. In turn, transmission electron microscopy (TEM) is able to image particles <1 nm, but is time consuming and not suitable for looking at shifts in EV populations. Other methods, such as ELISA and Western blot analysis, offer bulk phenotyping abilities but lack quantification [9, 15, 50, 51]. Thus, a tool for the accurate determination of the concentration and phenotyping of single EVs in complex samples such as plasma represents an unmet need.

The holy grail: direct detection of single EVs in complex samples

The only technique that has the potential to detect, size, and phenotype thousands to millions of EVs per minute is flow cytometry (FC) [52]. However, most clinical flow cytometers, and their corresponding assays, are designed for cell measurements and are not readily adapted to measure EVs; as the majority of EVs are <300 nm in diameter, conventional FCs struggle to discriminate these particles from background signals [11, 53, 54]. Another problem with flow cytometry is that the generated signals are expressed in arbitrary units, which hinders comparison of results between different instruments [47]. To address these issues, more sensitive instruments are introduced into the field, and guidelines regarding methods and data reporting are being developed for both flow cytometry (Minimum Information about a Flow Cytometry experiment, MIFlowCyt) and EV research [47].

In summary, the ideal EV analysis platform would be able to 1) detect and discriminate single EVs <300 nm in diameter above background signals of the instrument, 2) determine the size, concentration and phenotype of single EVs, 3)

operate at a relatively high-throughput rate of thousands to millions of EVs per minute, 4) be used without the need for prior EV isolation (thus omitting sample selection biases whilst simultaneously reducing sample handling time), and 5) discriminate the identified EVs from other contaminating components in the bio-fluid of interest.

Objectives of this thesis

Sensitive and standardized methods for single EV analysis are needed if EVs are to be translated into clinical practice. In recent years, imaging flow cytometry (IFCM) has emerged as a technique that enables the discrimination and analysis of single EVs with increased sensitivity compared to conventional FC. The ability of IFCM to detect submicron particles has been demonstrated using fluorescent polystyrene beads [55-58] or the use of cell supernatant-derived EVs [50]. At the moment of writing, several studies have reported the detection of EVs - obtained after performing isolation procedures - from plasma using IFCM [55, 56, 58, 59]. However, the used isolation procedures may have changed some EV properties: ultrafiltration might disintegrate larger EVs (thus generating smaller particles which, in turn, skew EV quantification upward) [60] whereas ultracentrifugation might cause aggregation and encapsulation of EVs (skewing EV quantification downward) [61]. Thus, it is unlikely that these results represent all EVs in plasma [62].

The main objective of this thesis is to explore whether IFCM is a suitable platform for the direct detection of single EVs in molecular complex samples such as plasma *without* the need to perform EV isolation techniques. This thesis is composed of two parts:

- Part I presents the development of a standardized IFCM-based methodology which allows for the direct detection, characterization and quantification of single EVs in molecular complex samples such as perfusate, plasma or urine.
- Part II aims to validate the standardized methodology to detect EV subsets in the context of kidney transplantation.

In **chapter 2,** we aim to validate the proof-of-concept that kidneys release nanoparticles (such as protein aggregates and EVs) *ex-vivo*. In this chapter, we examine the release of nanoparticles into the perfusion fluid by expanded-criteria donor (ECD) kidneys during normothermic machine perfusion (NMP). To this end,

perfusate samples taken before, during, and after the NMP procedure are analyzed with nanoparticle tracking analysis (NTA) to quantitate and determine the size distribution of nanoparticles released during NMP.

Though NTA currently is a gold-standard technique for EV-quantitation and size analysis, it is unsuitable for complex samples such as plasma or urine (due to its limited phenotyping capabilities). In **chapter 3**, we aim to provide a standardized (size- and fluorescence calibrated) IFCM-based methodology which is able to discriminate, phenotype, and determine the concentration of individual human plasma-derived EVs ≤400 nm in diameter – *without* prior isolation of EVs. This methodology aims to discriminate EVs from contaminating agents such as lipoproteins and protein aggregates in molecular complex samples such as plasma, and forms the backbone of this thesis. In **chapter 4**, we present an adaptation of this methodology aiming to detect single EVs in urine – another complex bio fluid with its own set of challenges in the context of EV detection.

In **chapter 5**, we characterize the nanoparticles released by ECD kidneys during NMP, and confirm that these are representative of EVs. Following the identification of EVs in the perfusion fluids, we aim to identify distinct EV subsets and examine whether these are potentially correlated with donor and NMP viability characteristics. As a first step towards clinical applicability, we next set out to determine whether the developed methodology is able to detect and follow-up single, (donor) tissue-derived EVs in plasma samples of kidney transplant recipients (**chapter 6**).

Chapter 7 provides a summary of the results described in this thesis. **Chapter 8** discusses these results and provides a perspective on future implications of our findings.

REFERENCES

1. Friedman J, Gore J. Ecological systems biology: The dynamics of interacting populations. Current Opinion in Systems Biology. 2017;1:114-21.
2. Couch Y, Buzas EI, Di Vizio D, Gho YS, Harrison P, Hill AF, et al. A brief history of nearly EV-erything - The rise and rise of extracellular vesicles. J Extracell Vesicles. 2021;10(14):e12144.
3. Chargaff EW, R. The biological significance of the thromboplastic protein of blood. Journal of Biological Chemistry. 1946;166(1):189-97.
4. Wolf P. The Nature and Significance of Platelet Products in Human Plasma. Brit J Haemat. 1967;13(3):269-88.
5. Crawford N. The Presence of Contractile Proteins in Platelet Microparticles Isolated from Human. Brit J Haemat. 1971;21(53):53-69.
6. Arraud N, Linares R, Tan S, Gounou C, Pasquet JM, Mornet S, et al. Extracellular vesicles from blood plasma: determination of their morphology, size, phenotype and concentration. J Thromb Haemost. 2014;12(5):614-27.
7. Gyorgy B, Szabo TG, Pasztoi M, Pal Z, Misjak P, Aradi B, et al. Membrane vesicles, current state-of-the-art: emerging role of extracellular vesicles. Cell Mol Life Sci. 2011;68(16):2667-88.
8. Gould SJ, Raposo G. As we wait: coping with an imperfect nomenclature for extracellular vesicles. J Extracell Vesicles. 2013;2.
9. Witwer KW, Buzas EI, Bemis LT, Bora A, Lasser C, Lotvall J, et al. Standardization of sample collection, isolation and analysis methods in extracellular vesicle research. J Extracell Vesicles. 2013;2.
10. Pitt JM, Kroemer G, Zitvogel L. Extracellular vesicles: masters of intercellular communication and potential clinical interventions. J Clin Invest. 2016;126(4):1139-43.
11. Simonsen JB. What Are We Looking At? Extracellular Vesicles, Lipoproteins, or Both? Circ Res. 2017;121(8):920-2.
12. Kalra H, Drummen GP, Mathivanan S. Focus on Extracellular Vesicles: Introducing the Next Small Big Thing. Int J Mol Sci. 2016;17(2):170.
13. Abels ER, Breakefield XO. Introduction to Extracellular Vesicles: Biogenesis, RNA Cargo Selection, Content, Release, and Uptake. Cell Mol Neurobiol. 2016;36(3):301-12.
14. Han Y, Jia L, Zheng Y, Li W. Salivary Exosomes: Emerging Roles in Systemic Disease. Int J Biol Sci. 2018;14(6):633-43.
15. Salih M, Zietse R, Hoorn EJ. Urinary extracellular vesicles and the kidney: biomarkers and beyond. Am J Physiol Renal Physiol. 2014;306(11):F1251-9.
16. Wang S, Kojima K, Mobley JA, West AB. Proteomic analysis of urinary extracellular vesicles reveal biomarkers for neurologic disease. EBioMedicine. 2019;45:351-61.
17. Karpman D, Stahl AL, Arvidsson I. Extracellular vesicles in renal disease. Nat Rev Nephrol. 2017;13(9):545-62.
18. Minciacchi VR, Zijlstra A, Rubin MA, Di Vizio D. Extracellular vesicles for liquid biopsy in prostate cancer: where are we and where are we headed? Prostate Cancer Prostatic Dis. 2017;20(3):251-8.
19. Roy S, Hochberg FH, Jones PS. Extracellular vesicles: the growth as diagnostics and therapeutics; a survey. J Extracell Vesicles. 2018;7(1):1438720.

20. Krebs MG, Hou JM, Ward TH, Blackhall FH, Dive C. Circulating tumour cells: their utility in cancer management and predicting outcomes. Ther Adv Med Oncol. 2010;2(6):351-65.
21. Verhoeven J, Boer K, Peeters AMA, Clahsen-van Groningen MC, Roodnat JI, van de Wetering J, et al. A Novel High-Throughput Droplet Digital PCR-Based Indel Quantification Method for the Detection of Circulating Donor-derived Cell-free DNA After Kidney Transplantation. Transplantation. 2022.
22. Kierny MR, Cunningham TD, Kay BK. Detection of biomarkers using recombinant antibodies coupled to nanostructured platforms. Nano Rev. 2012;3.
23. Harhay MN, Rao MK, Woodside KJ, Johansen KL, Lentine KL, Tullius SG, et al. An overview of frailty in kidney transplantation: measurement, management and future considerations. Nephrol Dial Transplant. 2020;35(7):1099-112.
24. Summers DM, Watson CJ, Pettigrew GJ, Johnson RJ, Collett D, Neuberger JM, et al. Kidney donation after circulatory death (DCD): state of the art. Kidney Int. 2015;88(2):241-9.
25. Brat A, Pol RA, Leuvenink HG. Novel preservation methods to increase the quality of older kidneys. Curr Opin Organ Transplant. 2015;20(4):438-43.
26. Callaghan CJ, Harper SJ, Saeb-Parsy K, Hudson A, Gibbs P, Watson CJ, et al. The discard of deceased donor kidneys in the UK. Clin Transplant. 2014;28(3):345-53.
27. Rijkse E, de Jonge J, Kimenai HJAN, Hoogduijn MJ, de Bruin RWF, van den Hoogen MWF, et al. Safety and feasibility of 2 h of normothermic machine perfusion of donor kidneys in the Eurotransplant Senior Program. BJS Open. 2021;5(1).
28. Moers C, Smits JM, Maathuis MH, Treckmann J, van Gelder F, Napieralski BP, et al. Machine perfusion or cold storage in deceased-donor kidney transplantation. N Engl J Med. 2009;360(1):7-19.
29. Hosgood SA, Saeb-Parsy K, Wilson C, Callaghan C, Collett D, Nicholson ML. Protocol of a randomised controlled, open-label trial of ex vivo normothermic perfusion versus static cold storage in donation after circulatory death renal transplantation. BMJ Open. 2017;7(1):e012237.
30. Vallant N, Wolfhagen N, Sandhu B, Hamaoui K, Cook T, Pusey C, et al. A Comparison of Pulsatile Hypothermic and Normothermic Ex Vivo Machine Perfusion in a Porcine Kidney Model. Transplantation. 2021;105(8):1760-70.
31. Moers C, Varnav OC, van Heurn E, Jochmans I, Kirste GR, Rahmel A, et al. The value of machine perfusion perfusate biomarkers for predicting kidney transplant outcome. Transplantation. 2010;90(9):966-73.
32. Xu J, Buchwald JE, Martins PN. Review of Current Machine Perfusion Therapeutics for Organ Preservation. Transplantation. 2020;104(9):1792-803.
33. Josephson MA. Monitoring and managing graft health in the kidney transplant recipient. Clin J Am Soc Nephrol. 2011;6(7):1774-80.
34. Morgan TA, Chandran S, Burger IM, Zhang CA, Goldstein RB. Complications of Ultrasound-Guided Renal Transplant Biopsies. Am J Transplant. 2016;16(4):1298-305.
35. Campana S, De Pasquale C, Carrega P, Ferlazzo G, Bonaccorsi I. Cross-dressing: an alternative mechanism for antigen presentation. Immunol Lett. 2015;168(2):349-54.
36. Golebiewska JE, Wardowska A, Pietrowska M, Wojakowska A, Debska-Slizien A. Small Extracellular Vesicles in Transplant Rejection. Cells. 2021;10(11).

37. Gunasekaran M, Xu Z, Nayak DK, Sharma M, Hachem R, Walia R, et al. Donor-Derived Exosomes With Lung Self-Antigens in Human Lung Allograft Rejection. Am J Transplant. 2017;17(2):474-84.

38. Kennel PJ, Saha A, Maldonado DA, Givens R, Brunjes DL, Castillero E, et al. Serum exosomal protein profiling for the non-invasive detection of cardiac allograft rejection. J Heart Lung Transplant. 2018;37(3):409-17.

39. Tower CM, Reyes M, Nelson K, Leca N, Kieran N, Muczynski K, et al. Plasma C4d+ Endothelial Microvesicles Increase in Acute Antibody-Mediated Rejection. Transplantation. 2017;101(9):2235-43.

40. Zhang H, Huang E, Kahwaji J, Nast CC, Li P, Mirocha J, et al. Plasma Exosomes From HLA-Sensitized Kidney Transplant Recipients Contain mRNA Transcripts Which Predict Development of Antibody-Mediated Rejection. Transplantation. 2017;101(10):2419-28.

41. Welsh JA, van der Pol E, Bettin BA, Carter DRF, Hendrix A, Lenassi M, et al. Towards defining reference materials for measuring extracellular vesicle refractive index, epitope abundance, size and concentration. J Extracell Vesicles. 2020;9(1):1816641.

42. Blijdorp CJ, Tutakhel OAZ, Hartjes TA, van den Bosch TPP, van Heugten MH, Rigalli JP, et al. Comparing Approaches to Normalize, Quantify, and Characterize Urinary Extracellular Vesicles. J Am Soc Nephrol. 2021.

43. Jankovicova J, Secova P, Michalkova K, Antalikova J. Tetraspanins, More than Markers of Extracellular Vesicles in Reproduction. Int J Mol Sci. 2020;21(20).

44. Raposo G, Stoorvogel W. Extracellular vesicles: exosomes, microvesicles, and friends. J Cell Biol. 2013;200(4):373-83.

45. Karimi N, Cvjetkovic A, Jang SC, Crescitelli R, Hosseinpour Feizi MA, Nieuwland R, et al. Detailed analysis of the plasma extracellular vesicle proteome after separation from lipoproteins. Cell Mol Life Sci. 2018;75(15):2873-86.

46. Konoshenko MY, Lekchnov EA, Vlassov AV, Laktionov PP. Isolation of Extracellular Vesicles: General Methodologies and Latest Trends. Biomed Res Int. 2018;2018:8545347.

47. Welsh JA, Van Der Pol E, Arkesteijn GJA, Bremer M, Brisson A, Coumans F, et al. MIFlowCyt-EV: a framework for standardized reporting of extracellular vesicle flow cytometry experiments. J Extracell Vesicles. 2020;9(1):1713526.

48. Gardiner C, Vizio DD, Sahoo S, Théry C, Witwer KW, Wauben M, et al. Techniques used for the isolation and characterization of extracellular vesicles: results of a worldwide survey. Journal of Extracellular Vesicles. 2016;5:10.3402/jev.v5.32945.

49. van der Pol E, Coumans FA, Grootemaat AE, Gardiner C, Sargent IL, Harrison P, et al. Particle size distribution of exosomes and microvesicles determined by transmission electron microscopy, flow cytometry, nanoparticle tracking analysis, and resistive pulse sensing. J Thromb Haemost. 2014;12(7):1182-92.

50. Gorgens A, Bremer M, Ferrer-Tur R, Murke F, Tertel T, Horn PA, et al. Optimisation of imaging flow cytometry for the analysis of single extracellular vesicles by using fluorescence-tagged vesicles as biological reference material. J Extracell Vesicles. 2019;8(1):1587567.

51. Lener T, Gimona M, Aigner L, Borger V, Buzas E, Camussi G, et al. Applying extracellular vesicles based therapeutics in clinical trials - an ISEV position paper. J Extracell Vesicles. 2015;4:30087.

52. Kuiper M, van de Nes A, Nieuwland R, Varga Z, van der Pol E. Reliable measurements of extracellular vesicles by clinical flow cytometry. Am J Reprod Immunol. 2021;85(2):e13350.
53. Larson MC, Luthi MR, Hogg N, Hillery CA. Calcium-phosphate microprecipitates mimic microparticles when examined with flow cytometry. Cytometry A. 2013;83(2):242-50.
54. Gyorgy B, Modos K, Pallinger E, Paloczi K, Pasztoi M, Misjak P, et al. Detection and isolation of cell-derived microparticles are compromised by protein complexes resulting from shared biophysical parameters. Blood. 2011;117(4):e39-48.
55. Erdbrugger U, Rudy CK, Etter ME, Dryden KA, Yeager M, Klibanov AL, et al. Imaging flow cytometry elucidates limitations of microparticle analysis by conventional flow cytometry. Cytometry A. 2014;85(9):756-70.
56. Headland SE, Jones HR, D'Sa AS, Perretti M, Norling LV. Cutting-edge analysis of extracellular microparticles using ImageStream(X) imaging flow cytometry. Sci Rep. 2014;4:5237.
57. Lannigan J, Erdbruegger U. Imaging flow cytometry for the characterization of extracellular vesicles. Methods. 2017;112:55-67.
58. Mastoridis S, Bertolino GM, Whitehouse G, Dazzi F, Sanchez-Fueyo A, Martinez-Llordella M. Multiparametric Analysis of Circulating Exosomes and Other Small Extracellular Vesicles by Advanced Imaging Flow Cytometry. Front Immunol. 2018;9:1583.
59. Ricklefs FL, Maire CL, Reimer R, Duhrsen L, Kolbe K, Holz M, et al. Imaging flow cytometry facilitates multiparametric characterization of extracellular vesicles in malignant brain tumours. J Extracell Vesicles. 2019;8(1):1588555.
60. Jang SC, Kim OY, Yoon CM, Choi DS, Roh TY, Park J, et al. Bioinspired exosome-mimetic nanovesicles for targeted delivery of chemotherapeutics to malignant tumors. ACS Nano. 2013;7(9):7698-710.
61. Linares R, Tan S, Gounou C, Arraud N, Brisson AR. High-speed centrifugation induces aggregation of extracellular vesicles. J Extracell Vesicles. 2015;4:29509.
62. Shao H, Im H, Castro CM, Breakefield X, Weissleder R, Lee H. New Technologies for Analysis of Extracellular Vesicles. Chem Rev. 2018;118(4):1917-50.

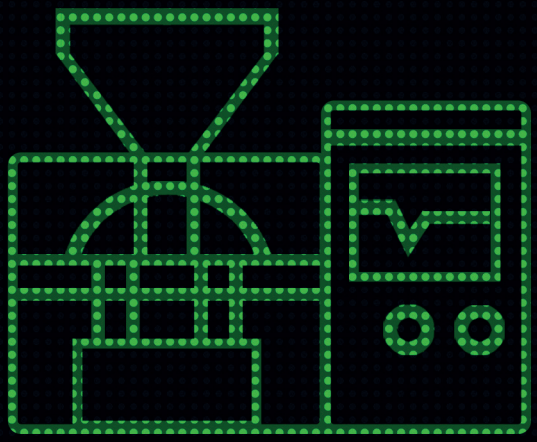

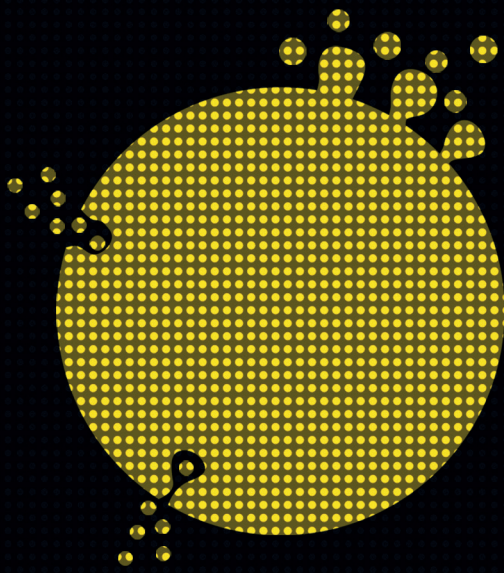

02

NANOPARTICLE RELEASE BY EXTENDED CRITERIA DONOR KIDNEYS DURING NORMOTHERMIC MACHINE PERFUSION

Wouter W. Woud[1], Ana Merino[1], Martin J. Hoogduijn[1], Karin Boer[1], Martijn W.F. van den Hoogen[1], Carla C. Baan[1], Robert C. Minnee[2]

[1] Department of Internal Medicine, section Nephrology and Transplantation,
[2] Department of Surgery, Division of Hepato-Pancreato-Biliary and Transplant Surgery, Erasmus MC, University Medical Centre Rotterdam, The Netherlands

Transplantation 103(5):p e110-e111, May 2019.

The poor outcomes of transplantations with kidneys from extended criteria donors (ECD) requires new methods of organ preservation and assessment given the more severe ischemia/reperfusion injuries (IRI) compared to standard criteria donors[1]. Machine perfusion (MP), aimed at reducing IRI and increasing graft function, is extensively being researched and allows for the examination of the isolated kidneys *ex vivo* through analysis of perfusion fluids[1,2]. Donor-derived Extracellular Vesicles (EVs), which may reflect the conditional state of their tissue of origin, are known to be excreted *in vivo* in blood/urine and as such have been used to asses organ function post transplantation[3]. We postulate that analysis of nanoparticles, including EVs, in perfusion fluid during normothermic MP may allow for the assessment of kidney quality prior to transplantation.

In this pilot trial, three ECD kidneys, (2 donors after cardiac death (DCD), 1 donor after brain death (DBD), comparable warm ischemia times of 15 minutes followed by 12 hours of cold ischemia, age 66/73/65, all male) were perfused at 37 °C for 2 hours during which perfusate samples were taken at 30 minutes intervals. Samples were centrifuged at 16.000x *g* for 10 minutes to discard platelets and supernatant was diluted 10x in 0.22 µm filtered PBS prior to analysis by Nanoparticle Tracking Analysis (NTA) (Figure 1A) to determine nanoparticle size and concentration (Figure 1B). Samples were measured by the Malvern Panalytical NanoSight NS300 and analyzed with NTA software version 3.2.16. In brief, NTA tracks the Brownian motion of individual nanoparticles in suspension on a frame-by-frame basis and correlates this movement with particle size through the Stokes-Einstein equation. Per sample, 10 videos of 15 seconds with 20-60 particles in the field of focus were recorded with camera level 11 and analyzed with detection threshold 5. This threshold was found to eliminate most of the protein background in our analysis and allowed us to focus on more complex particles such as EVs.

In the perfusate samples the average particle size remained unchanged (~155 ± 7.6 nm, data not shown), while an ~7.75-fold increase in cumulative nanoparticle concentration was observed over time: $9.03E^{9}$ particles/mL after 120 minutes compared to $1.17E^{9}$ particles/mL after 0 minutes of perfusion (Figure 1C). Particle excretion was observed to be highest from the DBD kidney during the entire normothermic MP procedure. Whether this increased nanoparticle release reflects better kidney function requires further research; the released nanoparticles contain kidney-derived EVs which may be indicative for renal quality. These preliminary results indicate that analysis of perfusion fluid may be utilized to assess renal quality prior to transplantation.

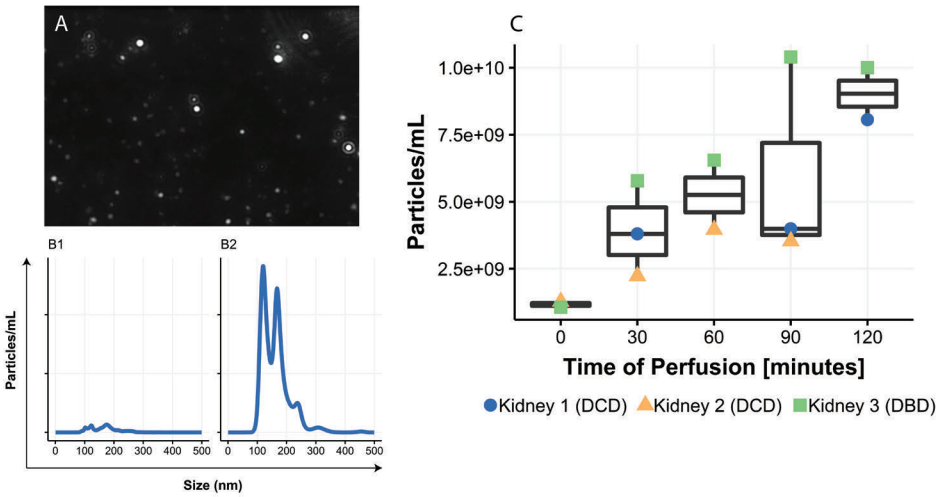

Figure 1 - Renal nanoparticle release measured by NTA.
A. Image of kidney derived nanoparticles during Nanoparticle Tracking Analysis (NTA) measurements.
B. Size distribution vs. particle concentration of **1.** perfusate after 0 minutes of perfusion and **2.** perfusate after 120 minutes of perfusion.
C. *Ex vivo* nanoparticle release by extended criteria donors (ECD) kidneys during Normothermic Machine Perfusion. Perfusate was obtained at 30 minutes intervals and measured with NTA. Accumulation of nanoparticles within the cumulative perfusion fluid was observed over time for all kidneys perfused, with highest excretion rate observed in the DBD kidney.

REFERENCES

1. Brat A, Pol RA, Leuvenink HG. Novel preservation methods to increase the quality of older kidneys. *Curr Opin Organ Transplant*. 2015;20(4):438-443.
2. Hosgood SA, Saeb-Parsy K, Wilson C, Callaghan C, Collett D, Nicholson ML. Protocol of a randomised controlled, open-label trial of ex vivo normothermic perfusion versus static cold storage in donation after circulatory death renal transplantation. *BMJ Open*. 2017;7(1):e012237.
3. Morelli AE. Exosomes: From Cell Debris to Potential Biomarkers in Transplantation. *Transplantation*. 2017;101(10):2275-2276.


REJECTED
REJECTED
REJECTED

PART I

Development:
The Needle in the Haystack

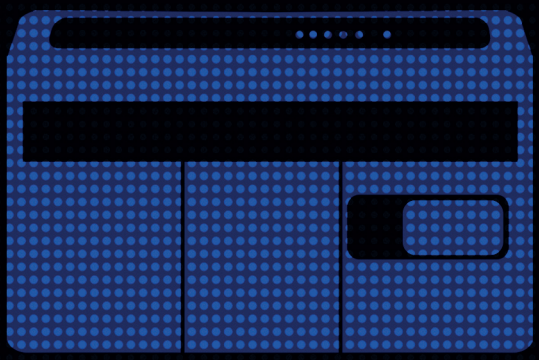

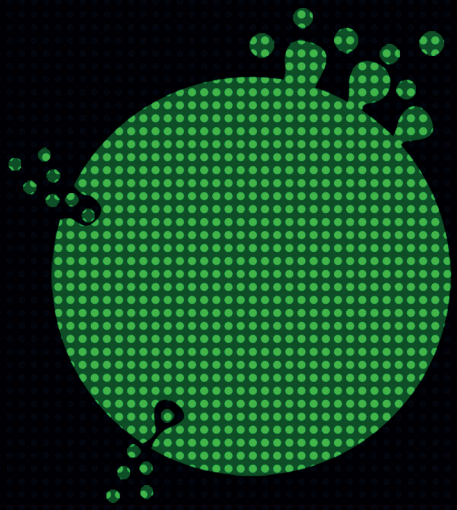

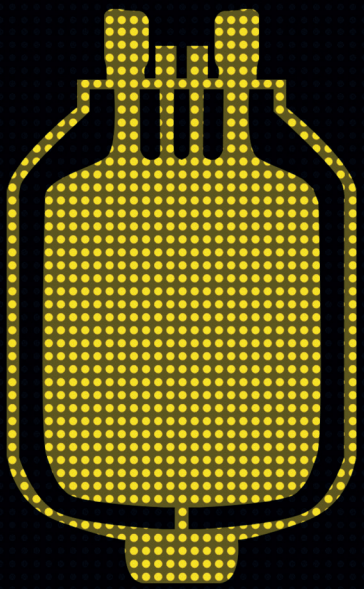

03

AN IMAGING FLOW CYTOMETRY-BASED METHODOLOGY FOR THE ANALYSIS OF SINGLE EXTRACELLULAR VESICLES IN UNPROCESSED HUMAN PLASMA

Wouter W. Woud[1], Edwin van der Pol[2,3], Erik Mul[4], Martin J. Hoogduijn[1], Carla C. Baan[1], Karin Boer[1], Ana Merino[1]

[1] Erasmus MC Transplant Institute, Department of Internal Medicine, University Medical Center Rotterdam, Rotterdam, The Netherlands.
[2] Biomedical Engineering & Physics, Laboratory Experimental Clinical Chemistry, Vesicle Observation Center, Amsterdam UMC, University of Amsterdam, Amsterdam, The Netherlands.
[3] Cancer Center Amsterdam, Imaging and Biomarkers, Amsterdam, The Netherlands.
[4] Department Central Cell Analysis Facility, Sanquin Research and Landsteiner Laboratory, Academic Medical Center, University of Amsterdam, Amsterdam, The Netherlands

Commun Biol ***5****, 633 (2022)*

ABSTRACT

Extracellular vesicles (EVs) are tissue-specific particles released by cells containing valuable diagnostic information in the form of various biomolecules. To rule out selection bias or introduction of artefacts caused by EV isolation techniques, we present a clinically feasible, imaging flow cytometry (IFCM)–based methodology to phenotype and determine the concentration of EVs with a diameter ≤400 nm in human platelet-poor plasma (PPP) *without* prior isolation of EVs.

Instrument calibration (both size and fluorescence) were performed with commercial polystyrene beads. Detergent treatment of EVs was performed to discriminate true vesicular events from artefacts. Using a combination of markers (CFSE & Tetraspanins, or CD9 & CD31) we found that >90% of double-positive fluorescent events represented single EVs.

Through this work, we provide a framework that will allow the application of IFCM for EV analysis in peripheral blood plasma in a plethora of experimental and potentially diagnostic settings. Additionally, this direct approach for EV analysis will enable researchers to explore corners of EV as cellular messengers in healthy and pathological conditions.

KEYWORDS

Unprocessed Human Plasma; Extracellular Vesicles; Imaging Flow Cytometry; Quantify; Phenotype; Diagnostic Platform

INTRODUCTION

Extracellular vesicles (EVs) are lipid bilayer membrane structures (30-8000 nm in diameter [1]) released by cells. They are involved in cellular communication through transfer of surface receptors and/or a variety of macromolecules carried as cargo (e.g., lipids, proteins, nucleic acids, protein-coding mRNAs and regulatory microRNAs) [2,3]. As EVs are excreted by virtually all cell types in the human body, they can be found in most body fluids, such as the blood [1], saliva [4] and urine [5,6]. Often regarded as a "snapshot" of the status of the cell of origin, EVs are examined for their biochemical signatures to assess the presence of various diseases, e.g., cancer or viral infections [7,8], and are considered excellent minimally invasive biomarkers in so-called liquid biopsies [9-11]. While no unique antigens representative for specific EV classes and subpopulations have been reported to date, tetraspanins (CD9/CD63/CD81) are recognized as common antigens. These proteins are enriched on EVs and are involved in EV biogenesis, cargo selection, and cell targeting [12,13].

Despite the increased interest in EVs as biomarker, their quantification and characterization is hampered by physical characteristics such as their small size and low epitope copy number [14], the variety of their protein markers depending on the cell source, and the confinement of some markers to the luminal side of the EVs [3,15]. The identification of EVs in blood plasma is further hindered by the molecular complexity of the plasma, which contains multiple elements (e.g., lipoproteins, cell debris and soluble proteins), that interfere with EV analysis [3,16]. Moreover, a lack of robust methods and ambiguities in how data should be interpreted for EV analysis makes data interpretation between studies challenging [17,18].

Currently, the gold standard approach for EV analysis is based on the isolation or concentration of EVs. Ultracentrifugation, density-gradient, and size exclusion chromatography are the most widely used EV isolation techniques [19], despite yielding low-purity EV samples due to the co-isolation of non-desired molecules such as lipoproteins [3,16]. Additionally, a variety of analytical platforms are available. Nanoparticle tracking analysis (NTA) allows the determination of the size distribution and a rough indication of the concentration [20] of individual nanoparticles in suspension, but provides limited phenotyping capabilities. In turn, transmission electron microscopy (TEM) is able to image particles <1 nm, but is time consuming. Other methods, such as ELISA and Western blot analysis, offer bulk phenotyping abilities but lack quantification [5,21-23]. Thus, a tool for the accurate determination of the concentration and phenotyping of single EV in complex samples such as plasma represents an unmet need.

Flow Cytometry (FC) is a tool to quantify and phenotype particles in suspension. However, while EVs can reach sizes up to ~8000 nm in diameter, the majority of EV are <300 nm and are therefore difficult to discriminate from background noise by conventional FC [3,24,25].

In recent years, imaging flow cytometry (IFCM) has emerged as a technique that enables the discrimination and analysis of single EV. The ability of IFCM to detect submicron particles has been demonstrated by several research groups using fluorescent polystyrene beads [26-29] or the use of cell supernatant-derived EV [21]. To date, several studies have reported the detection of EVs - obtained after performing isolation procedures - from plasma using IFCM [26,27,29,30]. However, due to the used isolation procedures, it is difficult to evaluate whether these results represent all EVs in plasma, or if some subpopulations are missed [31].

To rule out selection bias or introduction of artefacts caused by EV isolation techniques, we here demonstrate an IFCM-based methodology to phenotype and determine the concentration of human plasma-derived EVs with a diameter ≤400 nm - *without* prior isolation of EVs. By omitting the need for sample isolation, this method is able to directly show the status of an individual, which will be greatly beneficial in the monitoring of EVs in health and disease, and will enable researchers to explore new corners of EV biology.

RESULTS

Outline of the article

The objective of this article is to provide an assay that will allow researchers to study single EVs directly in diluted, labeled human plasma using IFCM. The following procedures were conducted to validate our assay: size calibration of the IFCM based on scatter intensities, background analysis of the IFCM, detergent treatment of EVs, dilution experiments, and fluorescence calibration. In addition, two labeling strategies based on CFSE+Tetraspanin+ and CD9+CD31+ were evaluated by mixing human plasma with mouse plasma at different ratios.

Detection of sub-micron fluorescent polystyrene beads

EV analysis at the single EV level requires an instrument that is able to detect a heterogeneous sub-micron sized population. To this end, we tested the ability of

IFCM to discriminate single-size populations of fluorescent sub-micron beads by measuring two commercially available mixtures of FITC-fluorescent polystyrene (PS) beads of known sizes (Megamix-Plus FSC – 900, 500, 300 and 100 nm, and Megamix-Plus SSC – 500, 240, 200, 160 nm). Within the Megamix-Plus FSC mix, we acquired a 300/500 nm bead ratio of 2.2, which is within the manufacturers internal reference qualification range (1.7 – 2.7 ratio). Next, we mixed both bead sets in a 1:1 ratio ('Gigamix') and performed acquisition. Figure 1a shows that IFCM is able to discern all seven fluorescent bead populations, as well as the 1 µm-sized Speed Beads (SB), via the FITC (Ch02) and side scatter (SSC - Ch06) intensities.

Calibration of scatter intensities through Mie theory

The output of IFCM signal intensities are presented in arbitrary units (a.u.), which hinders data comparability (and reproducibility) with different flow cytometers. Since light scattering of spherical objects is dependent on particle size and refractive index, Mie theory can be used to relate the scatter intensity of events to their size given their refractive index [32]. Generally, Mie theory is applied to calibrate the scatter channels of a FC (forward- and/or sideward-scattered light - FSC or SSC, respectively); however, IFCM utilizes a brightfield detection channel (BF, Ch04) as opposed to FSC.

Mie theory was applied on both scatter detection channels (BF and SSC). As a first step, we extracted the BF and SSC median scatter intensities of each identified size population of PS beads (Figure 1b). Coefficient of variation (CV) analysis for each single PS bead population showed scores ≥8% for the BF detector irrespective of bead size, whereas CV scores for the SSC detection channel were observed to increase with decreasing bead sizes – indicating that the detection of smaller particles is close to the detection limit of the SSC detector in our setup.

Next, BF and SSC data of the PS beads were scaled onto Mie theory, resulting in a scaling factor (F) of 1.3518 and a coefficient of determination (R^2) of 0.00 for the BF detector and a scaling factor of 8.405 and an R^2 of 0.91 for the SSC detector (Figure 1c). Thus, signals from sub-micron PS beads measured with the BF detector do not provide quantitative information. The SSC detector, on the other hand, can be readily calibrated. For the SSC detector, the theoretical model indicates a plateau for EVs with a diameter between ~400 to ~800 nm, which translates into a low resolution when determining EV sizes based on SSC intensities within this region. To ensure inclusion of sub-micron EVs, a gate was set at SSC below the scattering intensity corresponding to the plateau, namely 400 nm EVs, corresponding to a value of 900 a.u. SSC intensity.

These data show that 1) IFCM is able to readily discern sub-micron sized EVs based on their emitted fluorescence and SSC intensities, and 2) SSC – but not BF – light scattering intensities can be used to approximate particle sizes (following Mie calculations). The standardization of SSC signal intensities followed by the setting of a sub-micron gate provides a tool to selectively analyze all fluorescent EVs in complex samples such as plasma, as long as these particles emit detectable fluorescent intensities.

a

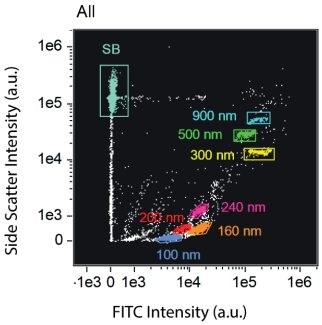

b

PS Bead Size	Counts	Percentage of Total	Median BF (a.u.)	CV	Median SSC (a.u.)	CV
900 nm	483	2.18	22076.44	8.59	50893.45	7.43
500 nm	2100	9.48	12705.39	12.96	29127.35	6.09
300 nm	1871	8.44	40905.82	8.3	13783.06	4.75
240 nm	2009	9.06	1700.82	13.02	1282.13	8.93
200 nm	3403	15.36	805.34	16.66	537.22	11.05
160 nm	7806	35.23	2622.92	14.43	526.39	15.49
100 nm	4485	20.24	774.26	22.12	119.98	37.67

c

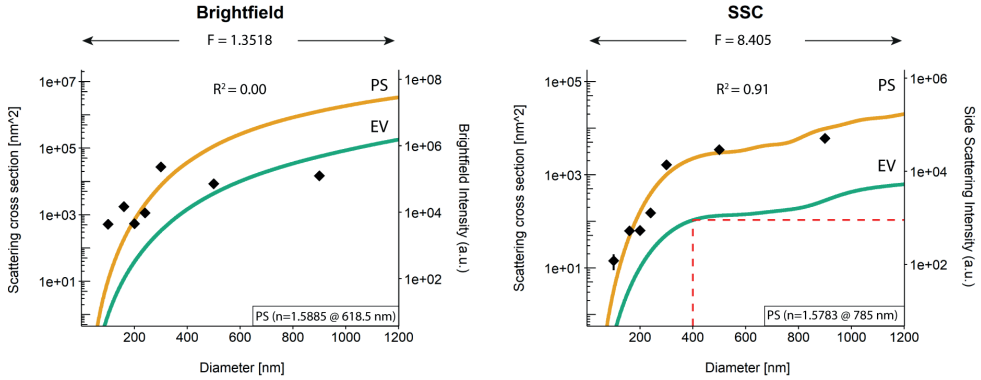

Figure 1 – Calibration of scatter intensities through Mie theory.
a) Gigamix polystyrene (PS) bead populations with sizes from 900 nm down to 100 nm were identified on the basis of SSC and FITC fluorescent intensities.
b) Counts and median scatter intensities of each PS bead population as detected by the brightfield (BF) and side scatter (SSC) detectors (Ch04 and Ch06, respectively).
c) Diameter vs Scattering cross section graphs. PS beads (green lines) were modelled as solid spheres with a refractive index of 1.5885 for a wavelength of 618.5 nm (brightfield) and 1.5783 for a wavelength of 785.0 nm (SSC). EVs (orange lines) were modelled as core-shell particles, with a core refractive index of 1.38 and a shell refractive index of 1.48 and a shell thickness of 6 nm for both wavelengths. The obtained scatter intensities of the PS beads as described in **b** were overlayed and a least-square-fit was performed to correlate theory and practice. Based on these correlations, SSC signal intensities were found to be indicative of particle size and a SSC cut-off of 900 a.u – corresponding to particles of 400 nm – was used in the rest in this work. F: scaling factor between scattering intensity and scattering cross section; n: refractive index.

IFCM gating strategy for the detection of single particles ≤400 nm in plasma

EVs represent a heterogeneous group with different cellular origin. The analysis of single EVs, as well as the different subsets, will provide a better understanding of the pathophysiological state of the individual. Therefore, we designed a gating strategy to analyze individual sub-micron sized particles based on 1) the analysis of events within a pre-defined sub-micron size range, and 2) exclusion of multi-spot fluorescent events from our analysis.

Based on the previous results, we selected all events with SSC intensities ≤ 900 a.u. - corresponding with particles of 400 nm and below. (Figure 2a – I). Next, we checked for multiplet detection within each separate fluorescent detection channel based on the number of fluorescent spots within the pixel grid for each acquired event: these spots were quantified by combining the "Spot Count" feature with the intensity masks for each of the channels used per experiment. Although the camera can spatially resolve signals originating from multiple simultaneously imaged EVs, the software anticipates that the signals are originating from multiple locations within 1 cell. By selecting all events that showed 0 or 1 spot, representing either negative or single-positive events for a fluorescent marker, we were able to exclude multiplet events from our analysis (Figure 2a – II, III). As a last step, we calculated the distance between individual fluorescent spots detected in different fluorescent channels to exclude any false double-positive events (defined as 2 different single-positive particles within the same event). To this end, we created a new mask by combining the intensity masks of the channels in use per experiment using Boolean logic (e.g., MC_Ch02 OR MC_Ch05), and combined this new mask with the "Min Spot Distance" feature to calculate the distance between the fluorescent spots across the detection channels used. We then excluded all fluorescent events that did not occupy the same location on the pixel grid (Figure 2a – IV). Ultimately, this gating strategy allows for the identification and subsequent analysis of single fluorescent sub-micron sized particles ≤400 nm in PPP and is applied throughout the rest of this work.

Establishment of IFCM background fluorescence

Given their physical characteristics, EVs yield faint fluorescent signals – compared too cells – when measured with IFCM. Therefore, we assessed the fluorescent background levels induced by our staining protocol. As no washing steps are performed, the discrimination of EVs from fluorescent background signals is

required to exclude false-positive particles from analysis. 0.20 µm filtered PBS (fPBS - Buffer Control) and platelet-poor plasma (PPP) samples from 5 healthy individuals was stained with CFDA-SE (carboxyfluorescein diacetate succiminidyl ester) or a mixture of tetraspanin-specific antibodies (anti-CD9/anti-CD63/anti-CD81) labeled with APC. CFDA-SE is a non-fluorescent molecule converted to fluorescent CFSE (carboxyfluorescein succiminidyl ester) by intravesicular esterases. This helps to discriminate EV from lipoproteins, as the latter do not contain esterase activity.

PPP samples left unstained or singly stained with CFSE (Ch02) or the tetraspanin-specific antibody mixture (Ch05) were used to set the gating areas (Figure 2b) and compensation matrix. Following our gating strategy, analysis of unstained fPBS or unstained PPP or fPBS + CFSE resulted in ~E^5 single-positive objects/mL within the CFSE gating area. In contrast, PPP samples single stained with CFSE showed an average of $4.23E^7 \pm 7.28E^6$ objects/mL (mean ± standard deviation), representing a 100-fold higher CFSE single-positive particle concentration compared to the unstained samples and fPBS (Figure 2c, left panel).

Similarly, analysis of positive fluorescent events upon staining with the tetraspanin-specific antibody mixture showed that fPBS + anti-tetraspanin antibodies (fPBS Mix) yielded $5.98E^6$ objects/mL – a 3.6-fold increase over the concentrations of fPBS Unstained ($1.65E^6$ objects/mL). Additionally, an isotype control was added to analyze the specificity of the antibodies in the tetraspanin mixture. Positive particle concentrations were obtained for both fPBS and PPP Isotypes, ($6.16E^5$ and $1.97E^5 \pm 1.07E^5$ objects/mL, respectively). Analysis of PPP + anti-tetraspanin antibodies (PPP Mix) revealed an average of $1.69E^8 \pm 1.44E^8$ objects/mL – a 28-fold higher particle concentration than fPBS + anti-tetraspanin antibodies, a 350-fold higher particle concentration than PPP Unstained ($4.86E^5 \pm 2.6E^5$ objects/mL), and an approximate 860-fold higher particle concentration than PPP Isotypes (Figure 2c, right panel). An approximate 4-fold higher concentration of fluorescent particles was observed in the PPP Mix vs CFSE after subtraction of background concentrations before comparison.

Together, these findings show that positive fluorescently stained events can be successfully discriminated from background signals and that the anti-tetraspanin antibody binding in our protocol is specific. Moreover, as unstained samples and isotype controls yielded ~E^5 (for CFSE) and fPBS with anti-tetraspanin antibodies yielded ~ E^6 objects/mL in their respective fluorescent channels, we established the level of the background concentrations in our setup for single positive fluorescent events at E^5 and E^6 objects/mL, for CFSE ant anti-tetraspanin antibodies respectively.

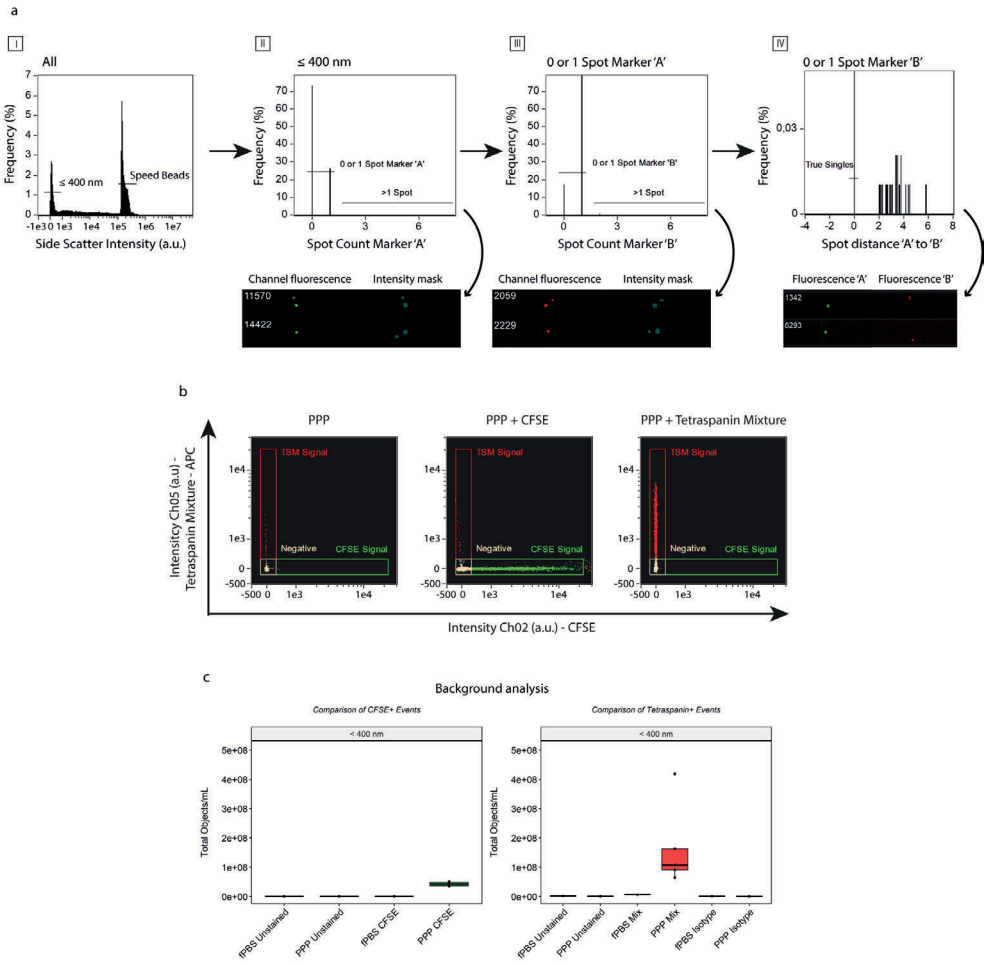

Figure 2 – Gating strategy for the detection of single EV through exclusion of coincident events and fluorescent background analysis.
a) Generalized concept. First, particles with SSC intensities ≤ 900 a.u. are selected, effectively selecting all (fluorescent) particles ≤ 400 nm (I). Subsequently, coincidence detection is carried out based on the number of fluorescent spots within the pixel grid determined with the standard intensity mask. Events showing 0 or 1 spot within each channel are selected and used in the subsequent analysis (II & III); events showing more than 1 spot are excluded from analysis. Lastly, the distance between the individual fluorescent spots on the different detection channels is calculated and events not overlapping on the pixel grid are excluded (IV). Visual examples of excluded events are shown below each graph.
b) Representative example of unstained and single-stained PPP samples (stained with CFDA-SE or the anti-tetraspanin mixture -composed of anti-CD9/anti-CD63/anti-CD81-APC) used in the setting of the gating areas and identification of fluorescent events. X-axis: fluorescence intensity of CFSE, detected in channel 2 (Ch02). Y-axis: fluorescent intensity of the anti-tetraspanin mixture detected in channel 5 (Ch05).
c) Background analysis of fluorescent events (left: CFSE, right: anti-tetraspanin mixture) for unstained fPBS (Buffer Control), 5 unstained PPP, 1 single-stained fPBS and 5 single-stained PPP. Black dots: individual PPP samples.

Human plasma single EV can be discriminated from artifact signals through detergent treatment

After optimizing the protocol to identify single fluorescent sub-micron sized particles above background in PPP of healthy individuals, we tested the protocols' ability to discriminate legitimate EV signals from artefact signals. We hypothesized that single EV could be identified as double-positive events after staining with both CFDA-SE and the anti-tetraspanin mixture, as these events would represent structurally intact, esterase containing sub-micron sized particles bearing common EV antigens. To test this hypothesis, we examined the fluorescent populations of particles ≤400 nm in diameter in 1 fPBS and the same 5 PPP samples by combining both fluorescent stains. Following our gating strategy, gating areas were re-established on the basis of unstained and single-stained fPBS and PPP samples, as well as isotype controls. Gating cut-offs were determined to encompass all obtained fluorescent events for all PPP samples. Visual interrogation of the events in the identified fluorescent gates confirmed that the events analyzed met the criteria imposed by the gating strategy: (co-localized) single-spot fluorescence (Figure 3a).

After acquisition of double-stained PPP (Figure 3b - I), we used detergent treatment (30 minutes incubation with 20 µL 10% (v/v) TritonX-100) to disrupt the lipid bilayer of EV and thereby remove EV signals from the measurement (Figure 3b – II). Fluorescent particles such as free antibodies or disrupted membrane fragments bearing antigens-antibodies remaining after detergent treatment were measured to allow the identification of artifact events, and the number of fluorescent events still present after detergent treatment were compared with the number of total fluorescent events before detergent treatment on a gate-by-gate basis to identify false positive signals (Figure 3c-e).

Analysis of CFSE single-positive events before detergent treatment showed a total of $3.25E^{7} \pm 1.16E^{6}$ objects/mL acquired for PPP samples, and a 31% reduction was observed after detergent treatment resulting in $2.25E^{7} \pm 1.03E^{6}$ objects/mL (~69% of total CFSE-single positive fluorescent events) (Figure 3c).

Analysis of antibody mixture single-positive events showed a total of $1.47E^{8} \pm 9.35E^{7}$ objects/mL events acquired for PPP samples, and $5.31E^{7} \pm 6.88E^{7}$ objects/mL after detergent treatment (~36% of total events (Figure 3d).

Analysis of double-positive events revealed $5.96E^7 \pm 3.69E^7$ objects/mL total double-positive particles across the 5 PPP samples measured, with a very limited number of artifact particles present after detergent treatment: $3.47E^6 \pm 4.48E^6$ objects/mL (~6% of total acquired events). This revealed that almost all double-positive particles measured ($5.61E^7 \pm 3.36E^7$ objects/mL, ~94% of the total concentration before detergent treatment), were structurally intact, esterase-containing EV displaying common EV protein signatures in the form of tetraspanin markers (Figure 3e).

By treating our samples with detergent we were able to identify to what extend our protocol discriminates legit EV signals from artefact signals. We observed that double-positive events were largely comprised of true EVs whereas the single-positive populations showed a high degree of fluorescent particles still present after detergent treatment. Therefore, we concluded that the colocalization of two fluorophores (found as double-positive events before detergent treatment) represent CFSE+/Tetraspanin+ EV.

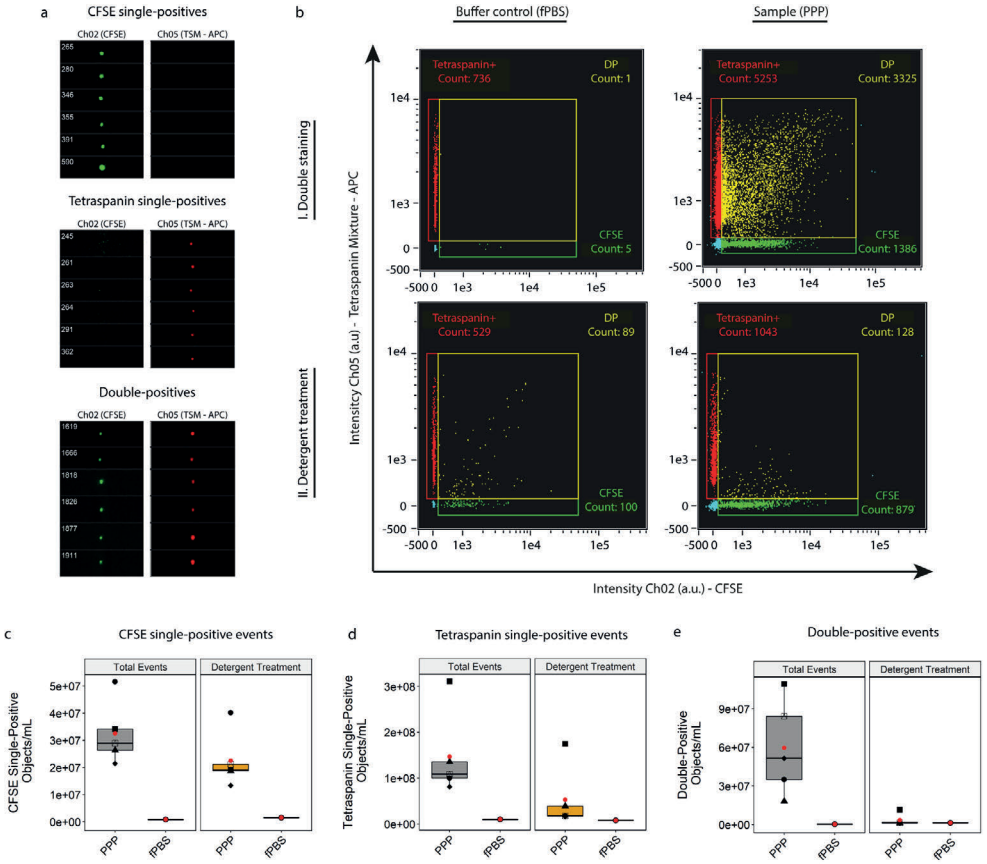

Figure 3 – Identification of true EV from PPP.
a) Images of representative CFSE single-positive, tetraspanin single-positive and double-positive particles obtained from a double-stained PPP sample before detergent treatment.
b) Double-stained (CFDA-SE & anti-tetraspanin mixture) fPBS or PPP without (I) and with (II) detergent treatment to determine potential artifact signals. Detergent treatment was performed by incubating the samples for 30 minutes with 20 µL 10% (v/v) TritonX-100 stock solution.
c) Analysis of CFSE single-positive,
d) Tetraspanin single-positive, and
e) double-positive fluorescent events in 5 PPP samples and fPBS before and after detergent treatment (gray and orange boxes, respectively) to discriminate true EV from artifact signals on a gate-by-gate basis. Double-positive events were found to represent mostly true EV signals (~94% of total acquired double-positive events). Red dots: means of sample spread. Symbols: individual PPP samples.

Fluorescent calibration for standardized reporting

As mentioned before, flow cytometers differ in their fluorescent sensitivity and dynamic range, and therefore data comparison between different instruments is hindered. In order to improve data comparison fluorescent calibration must be performed to convert arbitrary units (a.u.) into standardized units. To this end, we used commercially available Rainbow Calibration Particles (RCP) with known reference values in terms of the Equivalent number of Reference Fluorophores (ERF).

Using the same settings as applied for EV measurements, we measured the Mean Fluorescent Intensity (MFI) of each of the four RCP bead populations (1 blanc – 3 fluorescent) generated for each channel used in our setup (Figure 4a). Using the blank bead populations, we established the lower detection thresholds for fluorescent detection channels Ch02 (CFSE) and Ch05 (APC). We then calculated the respective logarithmic values of each peak (Figure 4b), and performed a linear regression analysis of the ERF values against the MFI for peaks 2 to 4, omitting the blanc beads as these represent PS beads without fluorophores (Figure 4c). In the example of the double-stained PPP sample presented in Figure 3b without fluorescent calibration, we next converted the measured fluorescent intensities for CFSE and APC of each event into their respective ERF values (Figure 4d). Lower fluorescent thresholds were converted accordingly and resulted in 35.40 and 6.40 ERF for CFSE and APC, respectively. Upper fluorescent thresholds were calculated at 3776 and 123 ERF for CFSE and APC, respectively. For the double-positive fluorescent population, this conversion resulted in median values of 138.09 ERF CFSE and 27.88 ERF APC.

These data show that the fluorescent intensities generated by imaging flow cytometry can be readily converted into standardized units, which, in turn, enhances the comparability of the generated data with other instruments using the same filter sets.

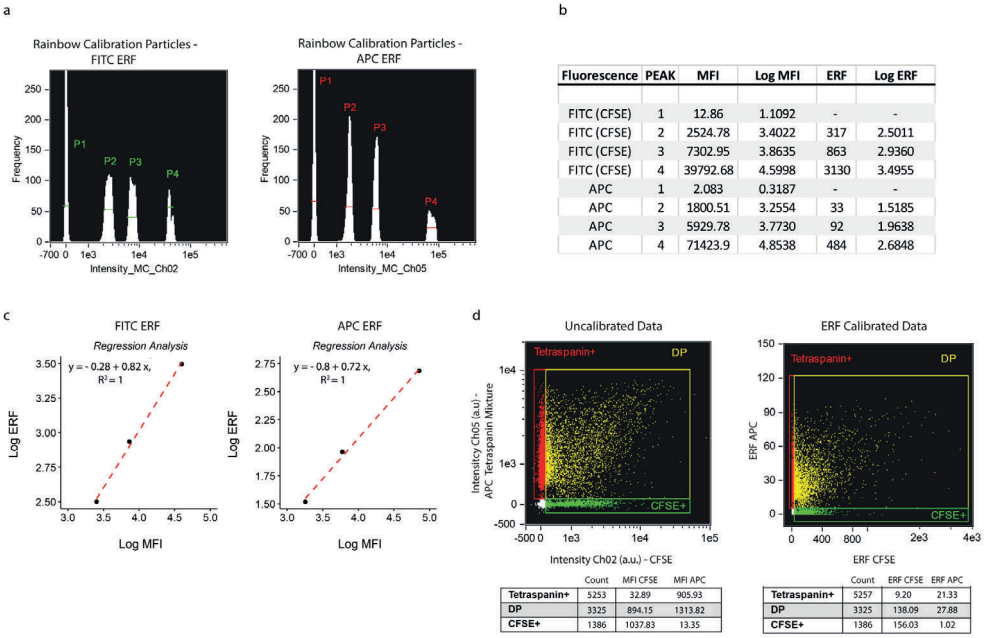

Fluorescence	PEAK	MFI	Log MFI	ERF	Log ERF
FITC (CFSE)	1	12.86	1.1092	-	-
FITC (CFSE)	2	2524.78	3.4022	317	2.5011
FITC (CFSE)	3	7302.95	3.8635	863	2.9360
FITC (CFSE)	4	39792.68	4.5998	3130	3.4955
APC	1	2.083	0.3187	-	-
APC	2	1800.51	3.2554	33	1.5185
APC	3	5929.78	3.7730	92	1.9638
APC	4	71423.9	4.8538	484	2.6848

	Count	MFI CFSE	MFI APC
Tetraspanin+	5253	32.89	905.93
DP	3325	894.15	1313.82
CFSE+	1386	1037.83	13.35

	Count	ERF CFSE	ERF APC
Tetraspanin+	5257	9.20	21.33
DP	3325	138.09	27.88
CFSE+	1386	156.03	1.02

Figure 4 – Fluorescent calibration allows reporting of fluorescent intensities in standardized units.
a) The median fluorescent intensities (MFI) of each peak of FITC and APC ERF (Equivalent number of Reference Fluorophores) calibration beads was measured with the same instrument/acquisition settings applied as used for EV acquisition.
b) Calculation of the log of the MFI and ERF values (provided by the bead manufacturer).
c) For each of the used detection channels, the log of the MFI corresponding to the fluorescent peaks (P2-P4) was plotted on the x-axis, and the log of the ERF values on the y-axis; linear regression analysis was performed.
d) Representative example of uncalibrated data (left) and corresponding ERF calibrated data (right).

Testing EV coincidence occurrence through serial dilution

The detection of multiple EV as a single event can lead to false interpretation of the data (e.g. underestimation of the concentration of particles of interest). To examine the accuracy of quantification of EV from PPP by our IFCM protocol, we double stained the 5 PPP samples with CFDA-SE and the anti-tetraspanin antibody mixture and performed a serial dilution experiment. The concentrations and ERF of double-positive particles in each PPP sample obtained after four 4-fold dilution steps were analyzed using a linear regression model, with the results shown in Figure 5. All data shown were used in the analysis and R^2 calculation.

We observed that the concentrations of double-positive events were linearly proportional to the dilution factor (Figure 5a) while the ERF of both fluorescent signals remained stable: mean 113.47 (range 55.07-157.55) for CFSE and mean 31.83 (range 28.2-36.8) for APC (Figure 5b), showing that the IFCM platform is capable of accurately quantifying individual EV. Serial dilution resulted into a larger spread of CFSE ERF values at lower dilutions (64x and 256x) only, which was interpreted to be a consequence of the lower number of particles analyzed. Additionally, double-positive EV concentrations at the aforementioned dilutions came close to the previously established background of our assay (~E^5 objects/mL).

The observed linear reduction in concentration of double-positive events according to the dilution factor, and the stable ERF signals for both fluorescent markers, confirm that the IFCM platform is able to quantify true single EV. Additionally, we were able to verify that our gating strategy correctly identifies and selects single EV (by excluding multiplet events).

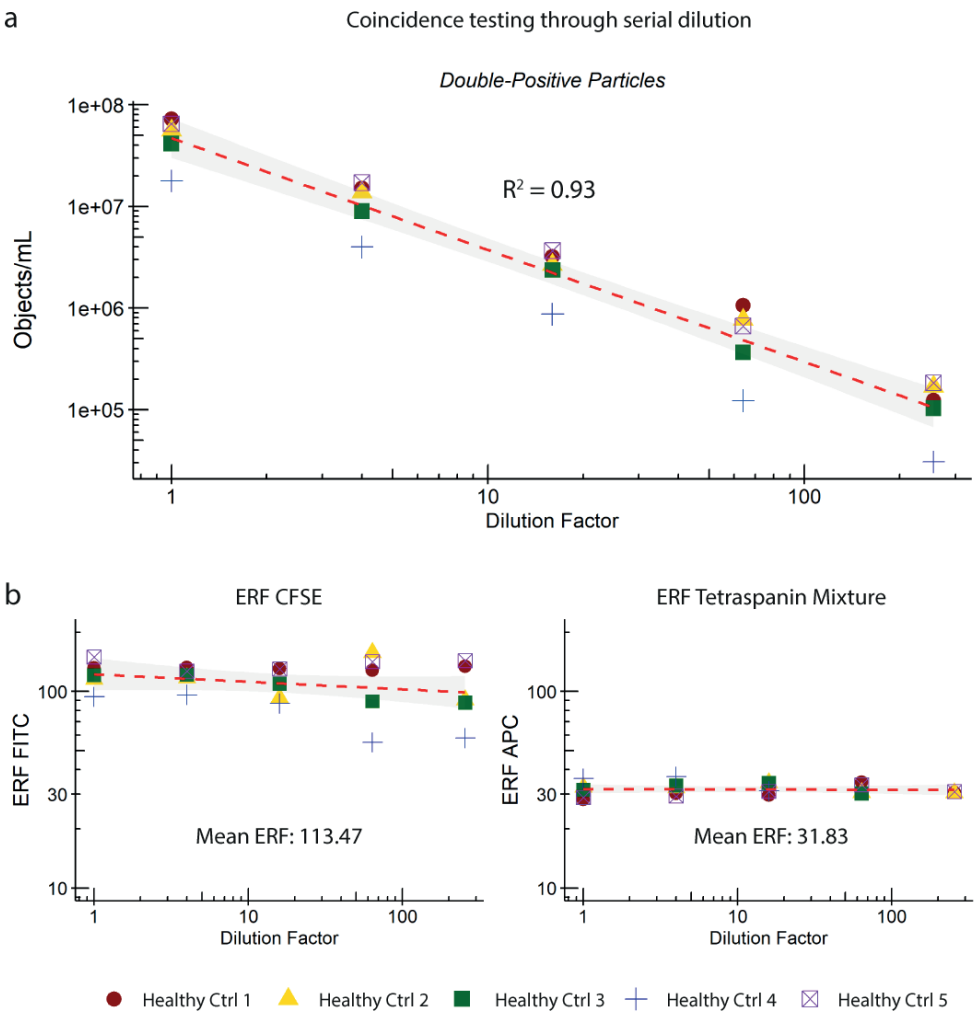

Figure 5 – Examination of the accurate quantification of single EV detection by IFCM. Analysis of serial dilutions of 5 double-stained (CFDA-SE & anti-tetraspanin mixture) PPP samples showed a linear correlation between **a**) the obtained concentration and **b**) Equivalent number of Reference Fluorophores (ERF) of fluorescent detection channels Ch02 (CFSE) and Ch05 (APC) with dilution factor (4-fold).

Tetraspanin distribution on human plasma-derived single EV

After having established that our IFCM methodology identifies and quantifies single EV through staining with CFDA-SE and the anti-tetraspanin antibody mixture, we aimed to analyze whether we could detect different subsets of EV. Therefore, we assessed the contributions of the individual tetraspanins to the double-positive events pool. The 5 PPP samples were stained with CFDA-SE and either the anti-tetraspanin antibody mixture or one of its individual components (anti-CD9 [clone HI9a], anti-CD63 [clone H5C5] or anti-CD81 [clone 5A6]) at a concentration equal to that used within the mixture. The concentrations of double-positive events upon staining with each stain were compared (Figure 6a) and normalized with respect to the concentration of double-positive events (in objects/mL) obtained with the anti-tetraspanin antibody mixture (Figure 6b).

The tetraspanin marker CD9 was found to be the main contributor to the fluorescent signal and thus responsible for most of the double-positive EV identified in PPP when stained with the anti-tetraspanin antibody mixture: ~88 ± 11% of the double-positive events were still present when staining with only CD9 versus ~13 ± 3% for CD63 and ~9 ± 5% for CD81. In short, we show that our methodology is able to identify subsets of EV, and that tetraspanin marker CD9 – and not CD63 or CD81 - represent the bulk of CFSE+ single EV in PPP of healthy individuals.

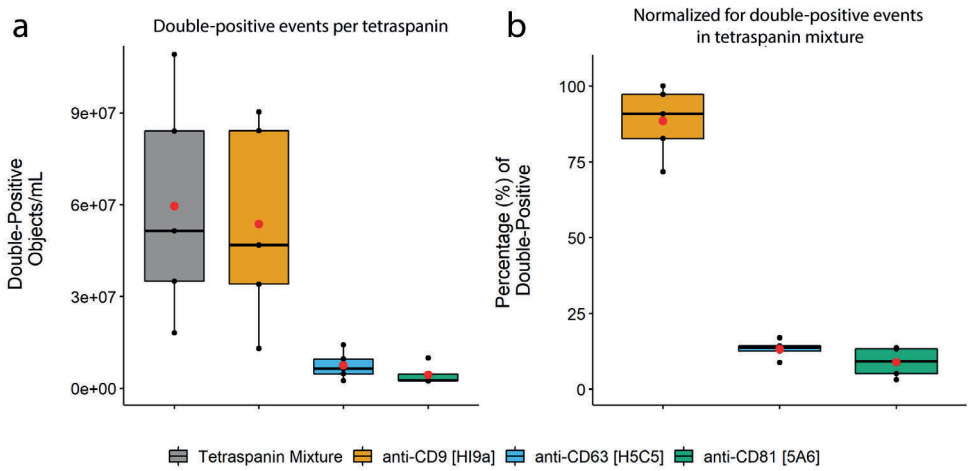

Figure 6 – Tetraspanin distribution within 5 PPP samples. All samples were stained with CFDA-SE and an anti-tetraspanin mixture or one of the anti-tetraspanin antibodies at a concentration equal to that used in the mixture.
a) Tetraspanin distribution determined using anti-CD9 [HI9a], anti-CD63 [H5C5] and anti-CD81 [5A6], and **b**) their relative frequencies of double-positive events compared to that obtained with the anti-tetraspanin mixture. Results shown represent events (double-positive objects/mL) obtained with each of these staining combinations and are colored as follows: gray boxes – anti-tetraspanin mixture, orange boxes – anti-CD9, blue boxes – anti-CD63, green boxes – anti-CD81. Red dots: means of sample spread. Black dots, individual PPP samples.

Colocalization of fluorophores indicates true EVs

So far, the identification and discrimination of single EV from contaminating agents such as lipoproteins in PPP samples has been based on the notion that lipoproteins do not contain esterases, and hence cannot become fluorescently labelled by CFSE. However, as not all EV may contain esterases the quantification of double-positive events (CFSE+/Tetraspanin+) likely represents an underrepresentation when it comes to total EV. An alternative approach to the identification of single EV in PPP samples on the basis of intravesicular esterases would be the staining of samples with monoclonal antibodies (mAbs) targeting EV surface proteins. Based on the results presented in Figure 6b, we used anti-CD9 [clone HI9a] as this antibody was shown to recapitulate the majority of the tetraspanin signal. Anti-CD31 [clone WM-59] was chosen as a secondary marker since CD31 is ubiquitously expressed within the vasculature and on diverse immune cell types, and therefore likely to be highly prevalent on EV in PPP.

Figure 7a shows the ERF calibrated (APC calibration performed as described in Figure 4, for BV421 calibration see Supplementary Figure 1) IFCM results after double staining of both fPBS and a representative PPP sample with anti-CD9-APC and anti-CD31-BV421 and subsequent detergent treatment. The lower fluorescent threshold for Ch01 (BV421) was established at 677.71 ERF; upper fluorescent threshold was established at 112,201 ERF. A visual representation of the events before detergent treatment within each gate is shown in Figure 7b. As stated before, only single spot fluorescent events (with colocalized fluorescent spots for double-positive events) were analyzed.

Focusing on double-positive particles, we acquired a total of $5.12E^7 \pm 1.02E^7$ objects/mL before detergent treatment and $3.61E^6 \pm 5.46E^6$ objects/mL (~7% of total events) after detergent treatment, thus showing that ~93% of the double-positive events detected in the PPP sample could be classified as true single EVs with this strategy. Mean ERF values of the double-positive events in all 5 PPP samples (before detergent treatment) were calculated at ~7,620 (range 3,640 – 9,240) and 20.4 (range 15 – 27.9) for BV421 and APC, respectively. Additionally, analysis of fPBS + mAbs (both anti-CD9 and anti-CD31 antibodies), PPP + isotype controls and fPBS + isotope controls yielded particle concentrations within the previously established fluorescent background range (~E^5 objects/mL), both before and after detergent treatment - indicating that the double-positive single EV detected in the PPP + mAb samples were detected well above the level of the background concentrations (Figure 7c).

Thus, the staining of PPP samples with anti-CD9 and anti-CD31 showed that double-positive events (before detergent treatment) can be successfully identified as true single EV. Although this staining approach (the combination of two surface markers expressed on EV) differs from the previously used staining approach (the combination of CFDA-SE and the anti-tetraspanin antibody mixture), both strategies resulted in the identification of true EV on the basis of the colocalization of two fluorophores within the same event – indicating that this colocalization is membrane facilitated and therefore can be used as a criteria to identify EV in unprocessed PPP.

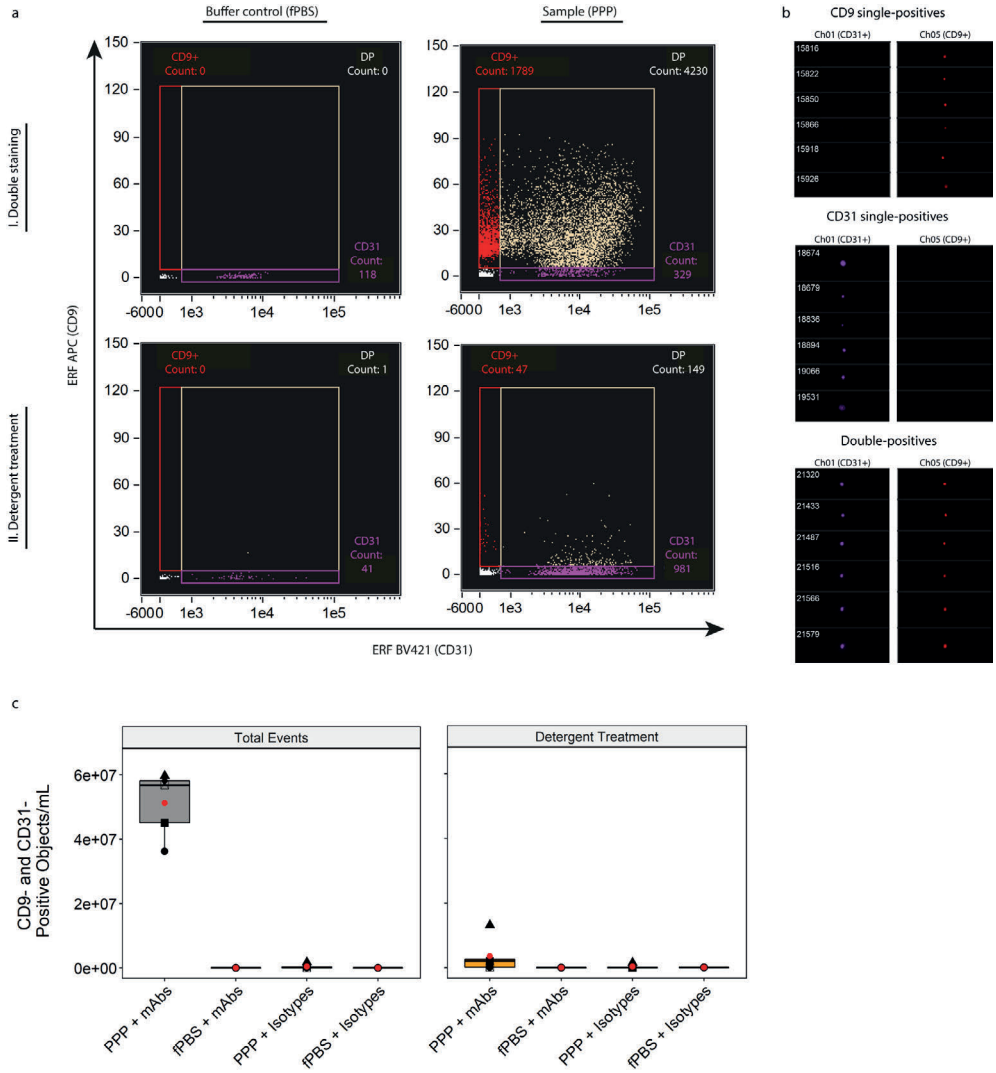

Figure 7 - Identification of single EVs on the basis of vesicular surface markers.
a) Representative, fluorescence calibrated data obtained for buffer control (fPBS, left column) and PPP (right column) samples stained with anti-CD31-BV421 and anti-CD9-APC mAbs. Detergent treatment was performed by incubating the samples for 30 minutes with 20 µL 10% (v/v) TritonX-100 stock solution. Red gate: Single-positive CD9 events, purple gate: single-positive CD31 events, tan gate: double-positive events. I, double staining and II, double staining after detergent treatment.
b) Visual interrogation of the gated populations in the representative PPP sample.
c) Quantification of double-positive fluorescent events in 5 PPP samples and fPBS, stained with mAbs or isotypes, before and after detergent treatment. Approximately 93% of double-positive events in PPP stained with mAbs represent PPP-derived single EV that were detected well above the fluorescent background. Red dots: means of sample spread. Symbols: individual PPP samples.

IFCM facilitates specific EV subset analysis in contaminated/diluted PPP samples

To demonstrate the discriminative capabilities of our methodology, and to show that our staining procedure is specific, we mixed human and mouse PPP at various ratios (10% increments) and stained these samples with CFDA-SE and both anti-human CD31-BV421 and anti-mouse CD31-APC mAbs. For the analysis, all CFSE-positive events <400 nm were selected, and human and mouse single EVs were identified based on the species-specific antibody, thus ensuring the analysis of double-positive events.

Quantification of total human and mouse single EV in 100% human or mouse PPP revealed a ~13-fold higher concentration in human: $2.29E^7 \pm 6.25E^6$ (CFSE+ anti-human CD31+, Figure 8a) vs $1.8E^6 \pm 3.46E^5$ (CFSE+ anti-mouse CD31+, Figure 8b) objects/mL, respectively. As expected, human EV concentrations showed a linear increase as the fraction of human PPP increased ($R^2 = 0.95$), while mouse EV showed the opposite trend (linear decreased as the fraction of human PPP increased – R^2 0.81). Anti-human and anti-mouse concentrations obtained after staining the 100% human and mouse samples with their corresponding isotype controls were used to establish the background concentrations of our protocol (as indicated by the dashed red lines in Figures 8a, b), and showed that the detection of anti-human/mouse EV is specific and above background. Additionally, no mAb cross-reactivity between species was observed.

Together, these data show that our method enables the discrimination and accurate quantification of distinct single EV populations in unprocessed, mixed PPP samples.

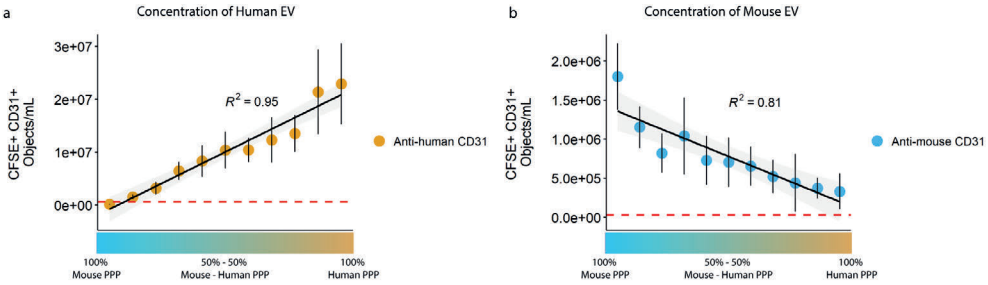

Figure 8 – Quantification of single EVs in mixed human and mouse PPP samples. Samples were stained with CFDA-SE and anti-human and anti-mouse CD31 (conjugated to BV421 and APC, respectively). Quantification of **a**) CFSE+ anti-human CD31+ single EV ≤400 nm showed a linear increase corresponding to the increase in human PPP abundance (R^2 = 0.95), while **b**) CFSE+ anti-mouse CD31+ single EV ≤400 nm showed a linear decrease corresponding to the decrease in mouse PPP abundance (R^2 = 0.81). Data were obtained through three independent experiments using the same human and mouse PPP samples. X-axis: v/v ratio of mouse – human PPP. Data shown represent the mean ± standard error. Red dashed lines: background concentrations of our protocol as indicated by the measurement of isotype controls.

DISCUSSION

We developed an IFCM-based methodology to identify, phenotype and determine the concentration of single EVs from molecular complex blood plasma without prior isolation, providing an advantage over currently available analytical techniques, which *do* require EV isolation. We present an easy-to-use sample processing and staining protocol (Figure 9), and provide a gating strategy for the identification of single EVs. Following this gating strategy, EV subpopulations in PPP could be readily discerned based on the colocalization of two fluorescent markers bound to EV membranes. Additionally, platform standardization through both size and fluorescence calibration allows reproducibility and comparison of acquired data, showing the potential of our method for translation into clinical application.

Given that neither the isolation of EVs from PPP nor sample washing after staining with fluorescently labelled mAbs was performed, it was imperative to assess the fluorescent background levels induced by our sample handling protocol. Using control samples, we showed minimal background fluorescence and clear discrimination of specific fluorescent events above background. Approaches taken by other groups analyzing EV in PPP using IFCM involve sample isolation [30] and/or washing steps to remove unbound mAbs [26,30]; here we show that such sample isolation and/or washing steps can be omitted by detecting and eliminating the

background produced by samples. We established the background level of the IFCM with respect to sub-micron particle quantification at ~E^5 objects/mL (after sample dilution correction). Previously published work by Görgens et al. showed that IFCM is able to accurately quantify single EV (cell culture-derived) up to concentrations of ~E^8 objects/mL [21]. Together, these data suggest that single EV quantification with IFCM is optimal for samples between E^5 – E^8 objects/mL (as demonstrated in this work).

To identify single EVs present in the PPP samples, we designed a gating strategy based on the imaging capabilities of IFCM. Several key features or advantages that contribute to IFCM being a more powerful platform for EV analysis compared to conventional FC include the slower flow rate, CCD-camera based detection (enabling higher quantum efficiency compared to conventional photon multiplier tubes), and integration of detected signals over time using TDI [21]. Additionally, IFCM allows automatic triggering on all channels during acquisition, and thus EVs devoid of SSC signals may still be detected based on their fluorescent probes. Conversion of scatter intensities from arbitrary units into standardized units (using light scatter theory and Mie calculations [32]) enhances reproducibility across different FC platforms. By performing these calculations for the BF and SSC detector channels, we demonstrated that measured PS bead signal intensities in the BF channel did not correlate with the theorized model. Thus, although the BF channel has its merits for cell-based research, it should not be used for EV-based research. The high degree of correlation between predicted and measured scatter intensities (R^2 = 0.91) for the SSC detection channel underlines the utility of the SSC channel to relate scatter signals to standard units.

Both size and fluorescence calibrations are key in the validation of sub-micron sized particle detection and reproducibility of the generated data, respectively [18]. In line with previously published literature, we have shown that IFCM is able to discriminate PS particles down to 100 nm on the basis of their emitted fluorescent intensities [21]. Regarding fluorescent calibration, we standardized the generated fluorescent intensities into ERF values using Rainbow Calibration Particles (RCP). It should be noted that ERF assignments to RCP are derived from a reference instrument, and comparisons across instruments are expected to vary with filter and laser configuration, variations that can be measured and accounted for by cross-calibration against MESF or antibody capture beads [33].

A common artefact encountered when measuring sub-micron particles with conventional FC is swarm detection, which is defined as a special case of coincidence detection where instead of two or a few particles, multiple (tenths to hundreds) of particles at or below the detection limit are simultaneously and continuously present in the laser beam of the flow cytometer and measured as single counts. This may occur during detection of EV in highly concentrated samples, and can lead to erroneous data interpretation [34]. While swarm detection can be prevented by dilution of highly concentrated samples, coincidence detection may still occur (albeit at lower frequencies). To identify coincidence detection, and exclude potential multiplets from our analysis, we designed a gating strategy that selects all events displaying 0 or 1 fluorescent spot on acquired images, thus ascertaining the analysis of events representative for single (and not multiple) particles. The identification of multiple, spatially separated fluorescent particles within acquired images provides insight into the degree of coincidence detection in a given sample - which is not possible with conventional FC. To demonstrate that our methodology correctly identifies and quantifies single EV, we performed coincidence testing through serial dilution [35]. Analysis of the concentration of CFSE+/Tetraspanin+ EV upon serial dilution yielded a linear correlation with the dilution factor while ERF remained stable.

In this work we examined two fluorescent labeling strategies to identify and discriminate EV: 1) application of CFDA-SE staining in conjunction with an anti-tetraspanin antibody mixture, and 2) staining with two mAbs targeting two different EV surface proteins. With both approaches, single EV were identified through the colocalization of two fluorescent markers, thus excluding the possibility of soluble protein detection. The combination of isotype and detergent treatment controls demonstrated the specificity of the mAbs for EV labelling (and not lipoproteins), and the dissociation of lipid structures, respectively. Therefore, both of these controls are highly recommended, if not mandatory, for the correct interpretation of acquired results. Single EV concentrations as reported in this work are in line with concentrations reported by other groups obtained after the purification/isolation of PPP samples [29,36]. This shows the advantage of our methodology over existing analytical techniques as no isolation, and therefore less manipulation, of EV are performed in our approach.

Another FC-based method to directly measure EV in plasma, performed on a Beckman Coulter CytoFlex and using a strategy that encompasses the labelling of EV with a fluorescent lipid probe (vFRed) in combination with CFDA-SE or an anti-

tetraspanin mixture similar to ours, has recently been published [33]. In this study, membrane fluorescence was calibrated in terms of vesicle size (surface area) by using a synthetic vesicle size standard, as provided in the vFC EV Analysis kit from Cellarcus Biosciences. However, the staining with a lipid membrane dye should be consistent for applicability. Thus, either the amount of dye needs to be approximately matched to the number of EV, or an excess of dye should be used so that the membrane becomes saturated with dye [32]. Additionally, the staining of lipoproteins is unavoidable when performing lipid staining strategies on PPP samples.

It must be noted that the identification and quantification of single EV through the IFCM method presented here is also subject to limitations. First, a minimum of 3 pixels is required before an event is recorded by IFCM as an object; fluorescent events not passing this threshold may consequently be missed. Second, our gating strategy excludes multiplets from analysis, and only single-spot fluorescent events are quantified. This may yield underestimations of EV concentration in very concentrated samples (as the frequency of multiplets may be higher than that of singlets during the acquisition of such samples) [21]. In such cases, serial dilution experiments may prove valuable to reduce multiplet detection and obtain a high frequency of single events. Alternatively, our gating strategy could be expended upon: rather than excluding events representing multiplets, the individual particles might be quantified and – following multiplication of the obtained concentrations with a factor representing their identified multiplet value – added to the total obtained concentrations of singlets.

Combined, we propose five criteria for the successful analysis of single EVs in PPP through IFCM: 1) standardization of SSC signal intensities to allow estimation of particle sizes; 2) single-spot fluorescence to ensure single-particle analysis and no coincident events; 3) colocalization of a minimum of two fluorophores to assess the presence of two markers in the same particle or event; 4) disappearance after detergent treatment to confirm that the detected events represent structures composed of lipid membranes and hence are of biological origin; and 5) a linear correlation between concentration and dilution factor to further imply that single EVs are analyzed. These criteria are summarized in Table 1 for quick reference.

In conclusion, we present an IFCM-based methodology and provide a framework that will allow researchers to directly study plasma-derived EVs, expanding on the usage of EV as non-invasive biomarkers in the clinic. We expect that this

methodology, after validation of markers of interest, will be useful for EV analysis in many different sample types and in a plethora of clinical settings.

#	Criteria	Reasoning
1	Standardization of SSC signals	Allows estimation of particle sizes
2	Single Spot Fluorescence	Single particle analysis / no coincidence events
3	Colocalization of fluorophores	Indicating the presence of markers in the same particle/event
4	Signal disappears after Detergent Lysis	Confirmation that detected events are of biological origin
5	Linear correlation with Dilution factor	Single particle analysis & confirmation that events are biological

Table 1 - Criteria for events to be classified as true single EV by IFCM.

MATERIALS & METHODS

Processing and storage of human blood plasma (Steps I – III)

The collection and processing of samples from 5 healthy human individuals (2 males, 3 females, average age: 43.4 years, age range: 31-56 years) was approved by the Medical Ethical Review Board (MERB number MEC-2018-1623) and conducted in accordance with the Declaration of Helsinki. All individuals provided written informed consent.

In brief, 12 mL of blood was collected (one drawing) from each individual into two BD Vacutainer® K3-EDTA-coated collection tubes (BD Biosciences, San Jose, USA) (Figure 9 – step I). Whole blood was centrifuged (Heraeus Multifuge 1S) at 1910 x *g* for 10 minutes at room temperature (Figure). The plasma layer was then collected - leaving ~1 mm of plasma above the buffy coat - and centrifuged (Heraeus Fresco) at 16,000 x *g* for 10 minutes at room temperature in 1mL aliquots using Safe-Lock Eppendorf tubes (Eppendorf AG, Hamburg, Germany). The resulting platelet-poor plasma (PPP) was first pooled before being divided into 700-µL aliquots in cryovials containing 28 µL of a 25x concentrated protease inhibitor cocktail solution (4% v/v) (cOmplete Protease inhibitor cocktail tablets, Roche, Mannheim, Germany) according to the manufacturers' instructions and stored at -80 °C (Figure 9 – step III).

Processing and storage of mouse blood plasma

All the procedures and animal housing conditions were carried out in strict accordance with current EU legislation on animal experimentation and were approved by the Institutional Committee for Animal Research (DEC protocol EMC No. AVD101002016635). Six weeks male C57BL/6J (JAX,GSP) mice (Jackson Labs, Bar Harbor, ME) were housed in Erasmus MC animal facility and housed in groups of 2-3/cage. They were maintained on a 12:12 h light-dark cycle and allowed ad libitum access to water and standard rodent food. The mice were anesthetized and blood (approximately 0.8 mL) was collected via the left ventricle using a 23-25 gauge needle. To ensure euthanasia of the animal post-procedure, mice were killed by cervical dislocation.

Antibody preparation (Step IV)

All monoclonal antibodies (mAbs) were centrifuged for 10 minutes at 16,000 x *g* to reduce the number of (potential) mAb clumps (Figure 9 – step IV). A volume of the top layer of each centrifuged mAb solution was carefully harvested (according to the dilutions needed, described below) and diluted in 0.22 µm-filtered PBS (fPBS) before being added to the samples (Figure 9 – step VI). The sample staining protocol is described under step VI.

The mAbs used to stain human PPP were anti-CD9–APC, clone HI9a (6 µg/mL, BioLegend, San Diego, USA); anti-CD63–APC, clone H5C6 (200 µg/mL, BioLegend); and anti-CD81–APC, clone 5A6 (200 µg/mL, BioLegend. Human and mouse PPP were both stained with anti-human CD31–BV421, clone WM-59 (50 µg/mL, BioLegend) and anti-mouse CD31-APC, clone 390 (200 µg/mL, BioLegend). Isotype controls used were IgG1,k-BV421, clone MOPC-21 (100 µg/mL, BioLegend); IgG1,k-APC, clone MOPC-21 (200 µg/mL, BioLegend); and IgG2a,k-APC, clone RTK2758 (200 µg/mL, BioLegend).

Optimal mAb concentrations were determined by performing separate titration experiments for each mAb on human PPP and fPBS samples in parallel. The optimal concentration of each mAb was defined as the concentration that yielded the best discrimination between sample (PPP) and background (fPBS). All tetraspanin mAbs were diluted 30-fold in fPBS before staining (Final concentrations: CD9: 200 ng/mL, CD63: 6.6 µg/mL, CD81: 6.6 µg/mL); CD31-BV421 (anti-human) and CD31-APC (anti-mouse) were diluted 1000-fold (Final concentration: 50 ng/mL) and 62.5-fold (Final

concentration: 3.2 µg/mL), respectively. The anti-tetraspanin antibody mixture was made by combining anti-CD9/anti-CD63/anti-CD81 in the same stock solution.

Preparation of a carboxyfluorescein diacetate succinimidyl ester stock solution (Step V)

A carboxyfluorescein diacetate succinimidyl ester (CFDA-SE) stock solution was made with the Vybrant™ CFDA-SE Cell Tracer Kit from Invitrogen immediately prior to use according to the manufacturer's instructions. In brief, CFDA-SE powder was spun down using a table-top centrifuge, and 18 µL of dimethylsulfoxide (DMSO) was added. The mixture was thoroughly resuspended and incubated at room temperature for 10 – 15 minutes in the dark. Then, the dissolved CFDA-SE was added to a total volume of 1.782 mL of fPBS to create a 50 µM CFDA-SE stock solution. Similar to the protocol used to prepare mAbs, this stock solution was centrifuged for 10 minutes at 16,000 x *g* to reduce potential CFDA-SE clumps (Figure 9 – step V); the top layer was carefully harvested – leaving ~100 µL of liquid in the tube – before being added to the samples.

Sample labeling (Step VI)

Staining was performed overnight at 4 °C in the dark in a total volume of 130 µL. This volume was build-up by 30 µL of sample, a volume of mAb stock solutions (described under step IV) as needed and brought to the total volume of 130 µL with fPBS; 12.5 uL of the stock solutions containing mAbs labelled with –APC and 5 µL of the stock solutions containing mAbs labeled with –BV421 were added, resulting in the following concentrations used per test: CD9 – 2.5 ng, CD63 – 83 ng, CD81 – 83 ng, CD31 (anti-human) – 1 ng, CD31 (anti-mouse) – 40 ng per test. Equivalent amounts of isotype control were used for each antibody.

For specificity and sensitivity analysis, human and mouse PPP were mixed at varying ratios with the total volume of PPP maintained at 30 µL. Samples were then incubated overnight at 4 °C to ensure optimal saturation of the available EV epitopes (Figure 9– step VI); this incubation time was determined empirically by adding the anti-tetraspanin antibody mix to fPBS and PPP samples and performing acquisition at set intervals (1/3/6 hours and O/N).

CFDA-SE labeling was performed on the day of data acquisition by adding 100 µL of the 50 µM CFDA-SE stock solution to the samples, followed by 30 minutes

of incubation at room temperature in the dark. Control samples not stained with CFDA-SE were incubated with 100 µL fPBS instead. All samples were brought to a total volume of 380 µL using fPBS before IFCM measurements.

Controls

Assay controls were used in all experiments, as recommended by the MIFlowCyt-EV framework [18] (Supplementary Table 1 and 2). These controls consisted of fPBS, fPBS with reagents, unstained samples, single-stained samples, isotype controls (matched with their corresponding fluorophore-conjugated mAbs at the same concentrations) and samples subjected to detergent treatment.

A 10% (v/v) Triton X-100 stock solution was made by dissolving 1 mL of TritonX-100 in 9 mL of fPBS. Detergent treatment was performed by the addition of 20 µL of the Triton X-100 stock solution (final concentration: 0.5% (v/v) per test), followed by 30 minutes of incubation at room temperature in the dark prior to acquisition. Note that samples were first acquired as described in the section "Data acquisition (Step VII)" before detergent treatment and corresponding re-acquisition was performed. Supplementary Table 3 gives an overview of these controls as well as the rationale behind their use. All controls contained 4% (v/v) 25x concentrated protease inhibitor cocktail solution (cOmplete Protease inhibitor cocktail tablets, Roche, Mannheim, Germany) in accordance with the PPP samples.

Usage of polystyrene beads for calibration purposes

A mix of commercial fluorescent polystyrene (PS) beads was used to calibrate fluorescence and light scattering signals. Megamix-Plus FSC (lot 203372) and Megamix-Plus SSC (lot 210812) beads (BioCytex) were mixed at a 1:1 ratio, resulting in a mix containing green fluorescent bead populations with sizes of 100, 300 and 900 nm from the Megamix-Plus FSC bead set, and 160, 200 and 240 nm from the Megamix-Plus SSC bead-set and 500 nm from both; this mix was termed Gigamix.

Rainbow Calibration Particles (RCP-05-5, lot AL01, Spherotech) with known Equivalent number of Reference Fluorophores (ERF) values for C30/FITC/APC (as determined on a Beckman Coulter CytoFLEX) were used in the standardization of the fluorescent detection channels Ch01,Ch02 & Ch05, respectively. For each detection channel, the MFI of each peak from the four bead populations (1 blanc – 3 fluorescent) were measured, and a linear regression analysis was performed of

the log of these values against the log of the known ERF values. The resulting linear function was used to relate the log of BV421/CFSE/APC fluorescent intensities to the log of ERF values.

Light scatter theory and Mie calculations for IFCM

Light scattering signals of bead populations from Gigamix were fitted with Mie theory using a previously described model [32]. The BF detector was modelled as a forward scattered light detector collecting light using a lens with a numerical aperture (NA) of 0.9, which corresponds to the NA of the 60x objective. The center wavelength of brightfield detection was 618.5 nm. The SSC detector was modelled as a detector that is placed perpendicular to the propagation direction of the laser beam. The NA of the collection lens was 0.9 and the wavelength was 785.0 nm. PS beads were modelled as solid spheres with a refractive index of 1.5885 for a wavelength of 618.5 nm (brightfield) and 1.5783 for a wavelength of 785.0 nm (SSC). EVs were modelled as core-shell particles with a core refractive index of 1.38, shell refractive index of 1.48 and a shell thickness of 6 nm for both wavelengths as the dispersion relation for the core and shell of EVs is unknown. Beads were measured in water, and EVs in PBS. Therefore, the refractive indices of PBS and water were assumed to be 1.3345 and 1.3325, respectively, at a wavelength of 618.5 nm (BF) and 1.3309 and 1.3289, respectively, at a wavelength of 785.0 nm (SSC).

Effective scattering cross sections of the calibration beads were calculated by integrating the amplitude scattering matrix elements over 576 collection angles [32]. Data and theory were log10-transformed to scale the data onto the theory using a least-square-fit.

Data acquisition (Step VII)

All samples were analyzed on an ImageStreamX MKII instrument (ISx; Luminex, Texas, USA) equipped with 4 lasers set to the following powers: 405 nm: 120 mW, 488 nm: 200 mW, 642 nm: 150 mW, and 775 nm (SSC): 1.25 mW. The instrument calibration tool ASSIST® was used upon each startup to optimize performance and consistency. The ISx was equipped with three objectives (20x/40x/60x) and 1 CCD camera. Settings previously established by Görgens et al. [21] were used in our experiments. All data were acquired using the 60x objective (numerical aperture of 0.9 – wherein 1 pixel images an area of 0.1 μm^2) with fluidics settings set to “low speed/high sensitivity” – resulting in a flow speed of 43.59 ± 0.07 mm/sec (mean ± standard deviation).

We adjusted the default sample core size of 7 µm to 6 µm using the "Defaults Override" option within INSPIRE software (version 200.1.681.0), as recommended by the manufacturer. Data were acquired over 180 seconds for standardization among samples with the autofocus setting activated and the "Remove Speedbead" option unchecked. These settings are shown in Supplementary Table 4 for quick reference.

BV421 fluorescence signals were collected in channel 1 (435–505-nm filter), CFSE signals in channel 2 (505–560-nm filter) and APC signals in channel 5 (642–745-nm filter). Channel 4 was used as the brightfield channel, and channel 6 (745–785-nm filter) was used for SSC detection. Particle enumeration was achieved through the advanced fluidic control of the ISx coupled with continuously running SBs (used by the IFCM to measure sample velocity for camera synchronization during acquisition, and enables particle enumeration during analysis), and application of the "objects/mL" feature within the ISx Data Exploration and Analysis Software (IDEAS®).

Data analysis

Data analysis was performed using Amnis IDEAS software (version 6.2). The image display mapping was linearly adjusted for all fluorescent events for each channel and then applied to all files from their respective experiments. The IDEAS software utilizes 'masks' – defined as the algorithm which selects pixels within an image based on their intensity and localization – to define the analysis area of each event within the pixel grid. The "masks combined" (MC) standard setting was used to quantify all fluorescence intensities in the channels used during acquisition corresponding to the fluorochromes used (Ch01, Ch02 & Ch05). Fluorescent events from singly stained PPP samples were used in the setting of compensation matrices (to compensate for spectral overlap between fluorochromes) such that straight fluorescent populations were obtained when depicted in scatterplots. Single-positive gating areas were established based on these single-positive fluorescent populations, and double-positive gates were set based on the boundaries of the single-positive gates. Unstained samples were used in the definition of the low-end of the various gates. Fluorescent thresholds were verified using cut-off values from the blanc fluorescent bead populations in the Rainbow Calibration Particles.

Statistics and Reproducibility

Statistical analysis was performed using R version 4.0.2 and RStudio (RStudio Team (2016). RStudio: Integrated Development for R. RStudio, Inc., Boston, MA; URL: http://www.rstudio.com/) version 1.1.463. All concentrations reported in this work were corrected for sample dilution (before acquisition – 380 µL total volume per test containing 30 µL sample = ~12.33-fold dilution factor) and are shown as the mean ± standard deviation unless specified otherwise. In all experiments conducted, PPP samples from the same 5 healthy individuals were used (n = 5 biologically independent samples). In the mouse vs human experiments, three independent experiments were conducted using the same mouse and human PPP samples (three replicates).

ACKNOWLEDGMENTS

The authors would like to thank Peter Rhein (Luminex) for his support and discussions throughout the project.

AUTHOR CONTRIBUTIONS

W.W.W. participated in the research design, execution of the research, data analysis, and article drafting and is the corresponding author. E.vd.P. participated in the calibration of scatter intensities through Mie theory. E.M. participated in data acquisition and provided IFCM expertise. M.J.H., C.C.B., and K.B. participated in the research design. A.M. participated in the research design, data acquisition and data analysis. All authors reviewed the manuscript and approved its final version.

COMPETING INTERESTS

The authors declare no competing interests.

DATA AVAILABILITY

All source data underlying the figures presented in this work are provided as 'Supplementary Data 1-8' (separate tabs for each figure). Any other relevant data are available from the corresponding author upon reasonable request.

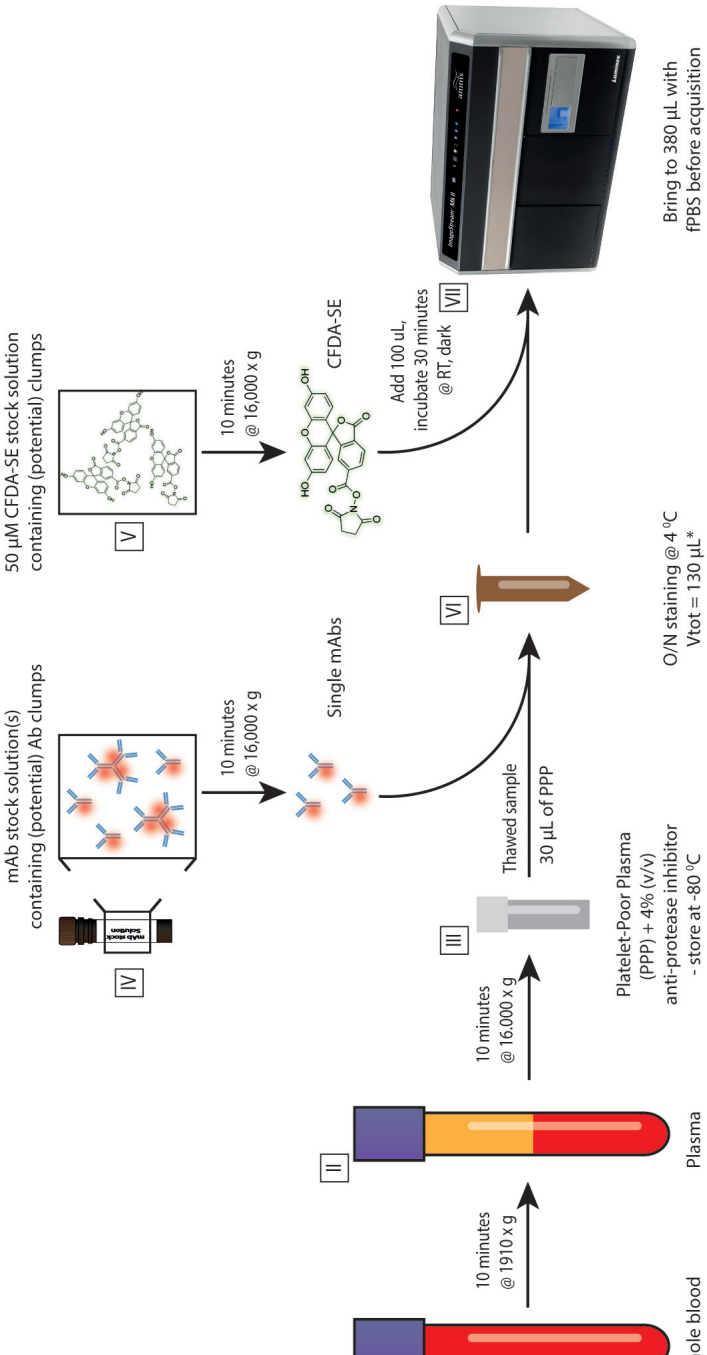

Figure 9 – Schematic overview of the sample processing and staining protocol. EDTA whole blood (I) is centrifuged for 10 minutes at 1910 x g, after which the plasma top layer (II) is harvested and subjected to centrifugation for 10 minutes at 16,000 x g. The resulting platelet-poor plasma (PPP) is collected and stored as aliquots in cryovials containing an anti-protease inhibitor stock solution (4% v/v) at -80 °C (III). Prior to use, monoclonal antibodies and CFDA-SE stock solutions are centrifuged for 10 minutes at 16,000 x g to reduce the number of potential clumps of fluorescent particles (IV & V). mAbs are added to 30 µL of PPP, and samples are brought to a total volume of 130 µL using filtered PBS (VI) and incubated overnight (O/N) at 4 °C in the dark. CFDA-SE is added on the day of acquisition and incubated for 30 minutes at room temperature in the dark. Samples are brought to a total volume of 380 µL using filtered PBS and are assessed using a Luminex ISx MKII imaging flow cytometer (VII). After initial acquisition, detergent treatment is performed for each sample by adding 20 µL 10% (v/v) TritonX-100 solution followed by 30 minutes incubation at room temperature. Permission to use the image of the Imagestream (ISx) Imaging Flow cytometer (VII) was granted by Luminex.

REFERENCES

1 Arraud, N. *et al.* Extracellular vesicles from blood plasma: determination of their morphology, size, phenotype and concentration. *J Thromb Haemost* **12**, 614-627, doi:10.1111/jth.12554 (2014).

2 Pitt, J. M., Kroemer, G. & Zitvogel, L. Extracellular vesicles: masters of intercellular communication and potential clinical interventions. *J Clin Invest* **126**, 1139-1143, doi:87316 10.1172/JCI87316 (2016).

3 Simonsen, J. B. What Are We Looking At? Extracellular Vesicles, Lipoproteins, or Both? *Circ Res* **121**, 920-922, doi:CIRCRESAHA.117.311767 (2017).

4 Han, Y., Jia, L., Zheng, Y. & Li, W. Salivary Exosomes: Emerging Roles in Systemic Disease. *Int J Biol Sci* **14**, 633-643, doi:10.7150/ijbs.25018 (2018).

5 Salih, M., Zietse, R. & Hoorn, E. J. Urinary extracellular vesicles and the kidney: biomarkers and beyond. *Am J Physiol Renal Physiol* **306**, F1251-1259, doi:ajprenal.00128.2014 (2014).

6 Wang, S., Kojima, K., Mobley, J. A. & West, A. B. Proteomic analysis of urinary extracellular vesicles reveal biomarkers for neurologic disease. *EBioMedicine* **45**, 351-361, doi:S2352-3964(19)30402-5 (2019).

7 Han, L., Lam, E. W. & Sun, Y. Extracellular vesicles in the tumor microenvironment: old stories, but new tales. *Mol Cancer* **18**, 59, doi:10.1186/s12943-019-0980-8 (2019).

8 Urbanelli, L. *et al.* The Role of Extracellular Vesicles in Viral Infection and Transmission. *Vaccines (Basel)* **7**, doi:vaccines7030102 (2019).

9 Vallabhajosyula, P. *et al.* Tissue-specific exosome biomarkers for noninvasively monitoring immunologic rejection of transplanted tissue. *J Clin Invest* **127**, 1375-1391, doi:87993 10.1172/JCI87993 (2017).

10 McBride, J. D., Rodriguez-Menocal, L. & Badiavas, E. V. Extracellular Vesicles as Biomarkers and Therapeutics in Dermatology: A Focus on Exosomes. *J Invest Dermatol* **137**, 1622-1629, doi: 10.1016/j.jid.2017.04.021 (2017).

11 Karpman, D., Stahl, A. L. & Arvidsson, I. Extracellular vesicles in renal disease. *Nat Rev Nephrol* **13**, 545-562, doi:nrneph.2017.98 (2017).

12 Jankovicova, J., Secova, P., Michalkova, K. & Antalikova, J. Tetraspanins, More than Markers of Extracellular Vesicles in Reproduction. *Int J Mol Sci* **21**, doi:ijms21207568 (2020).

13 Raposo, G. & Stoorvogel, W. Extracellular vesicles: exosomes, microvesicles, and friends. *J Cell Biol* **200**, 373-383, doi:jcb.201211138 (2013).

14 Welsh, J. A. *et al.* Towards defining reference materials for measuring extracellular vesicle refractive index, epitope abundance, size and concentration. *J Extracell Vesicles* **9**, 1816641, doi:10.1080/20013078.2020.1816641 (2020).

15 Blijdorp, C. J. *et al.* Comparing Approaches to Normalize, Quantify, and Characterize Urinary Extracellular Vesicles. *J Am Soc Nephrol*, doi:ASN.2020081142 (2021).

16 Karimi, N. *et al.* Detailed analysis of the plasma extracellular vesicle proteome after separation from lipoproteins. *Cell Mol Life Sci* **75**, 2873-2886, doi:10.1007/s00018-018-2773-4 (2018).

17 Konoshenko, M. Y., Lekchnov, E. A., Vlassov, A. V. & Laktionov, P. P. Isolation of Extracellular Vesicles: General Methodologies and Latest Trends. *Biomed Res Int* **2018**, 8545347, doi:10.1155/2018/8545347 (2018).

18 Welsh, J. A. *et al.* MIFlowCyt-EV: a framework for standardized reporting of extracellular vesicle flow cytometry experiments. *J Extracell Vesicles* **9**, 1713526, doi:10.1080/20013078.2020.1713526 (2020).

19 Gardiner, C. *et al.* Techniques used for the isolation and characterization of extracellular vesicles: results of a worldwide survey. *Journal of Extracellular Vesicles* **5**, 10.3402/jev.v3405.32945, doi:10.3402/jev.v5.32945 (2016).

20 van der Pol, E. *et al.* Particle size distribution of exosomes and microvesicles determined by transmission electron microscopy, flow cytometry, nanoparticle tracking analysis, and resistive pulse sensing. *J Thromb Haemost* **12**, 1182-1192, doi:10.1111/jth.12602 (2014).

21 Gorgens, A. *et al.* Optimisation of imaging flow cytometry for the analysis of single extracellular vesicles by using fluorescence-tagged vesicles as biological reference material. *J Extracell Vesicles* **8**, 1587567, doi:10.1080/20013078.2019.1587567 2019).

22 Lener, T. *et al.* Applying extracellular vesicles based therapeutics in clinical trials - an ISEV position paper. *J Extracell Vesicles* **4**, 30087, doi:30087 (2015).

23 Witwer, K. W. *et al.* Standardization of sample collection, isolation and analysis methods in extracellular vesicle research. *J Extracell Vesicles* **2**, doi:10.3402/jev.v2i0.20360 (2013).

24 Larson, M. C., Luthi, M. R., Hogg, N. & Hillery, C. A. Calcium-phosphate microprecipitates mimic microparticles when examined with flow cytometry. *Cytometry A* **83**, 242-250, doi:10.1002/cyto.a.22222 (2013).

25 Gyorgy, B. *et al.* Detection and isolation of cell-derived microparticles are compromised by protein complexes resulting from shared biophysical parameters. *Blood* **117**, e39-48, doi:blood-2010-09-307595 (2011).

26 Erdbrugger, U. *et al.* Imaging flow cytometry elucidates limitations of microparticle analysis by conventional flow cytometry. *Cytometry A* **85**, 756-770, doi:10.1002/cyto.a.22494 (2014).

27 Headland, S. E., Jones, H. R., D'Sa, A. S., Perretti, M. & Norling, L. V. Cutting-edge analysis of extracellular microparticles using ImageStream(X) imaging flow cytometry. *Sci Rep* **4**, 5237, doi:srep05237 (2014).

28 Lannigan, J. & Erdbruegger, U. Imaging flow cytometry for the characterization of extracellular vesicles. *Methods* **112**, 55-67, doi: 10.1016/j.ymeth.2016.09.018. (2017).

29 Mastoridis, S. *et al.* Multiparametric Analysis of Circulating Exosomes and Other Small Extracellular Vesicles by Advanced Imaging Flow Cytometry. *Front Immunol* **9**, 1583, doi:10.3389/fimmu.2018.01583 (2018).

30 Ricklefs, F. L. *et al.* Imaging flow cytometry facilitates multiparametric characterization of extracellular vesicles in malignant brain tumours. *J Extracell Vesicles* **8**, 1588555, doi:10.1080/20013078.2019.1588555 (2019).

31 Shao, H. *et al.* New Technologies for Analysis of Extracellular Vesicles. *Chem Rev* **118**, 1917-1950, doi:10.1021/acs.chemrev.7b00534 (2018).

32 de Rond, L., Coumans, F. A. W., Nieuwland, R., van Leeuwen, T. G. & van der Pol, E. Deriving Extracellular Vesicle Size From Scatter Intensities Measured by Flow Cytometry. *Curr Protoc Cytom* **86**, e43, doi:10.1002/cpcy.43 (2018).

33 Sandau, U. S. *et al.* Methamphetamine use alters human plasma extracellular vesicles and their microRNA cargo: An exploratory study. *J Extracell Vesicles* **10**, e12028, doi:10.1002/jev2.12028 (2020).

34 Libregts, S., Arkesteijn, G. J. A., Nemeth, A., Nolte-'t Hoen, E. N. M. & Wauben, M. H. M. Flow cytometric analysis of extracellular vesicle subsets in plasma: impact of swarm by particles of non-interest. *J Thromb Haemost* **16**, 1423-1436, doi:10.1111/jth.14154 (2018).

35 Nielsen, M. H., Beck-Nielsen, H., Andersen, M. N. & Handberg, A. A flow cytometric method for characterization of circulating cell-derived microparticles in plasma. *J Extracell Vesicles* **3**, doi:10.3402/jev.v3.20795 (2014).

36 Tian, Y. *et al.* Quality and efficiency assessment of six extracellular vesicle isolation methods by nano-flow cytometry. *J Extracell Vesicles* **9**, 1697028, doi:10.1080/20013078.2019.1697028 (2020).

SUPPLEMENTARY DATA

a

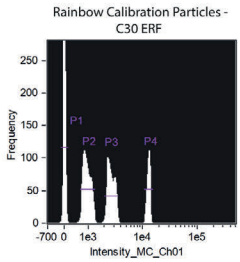

b

Fluorescence	PEAK	MFI	Log MFI	ERF	Log ERF
C30 (BV421)	1	13.7	1.1367	-	-
C30 (BV421)	2	972.55	2.9879	3550	3.5502
C30 (BV421)	3	2706	3.4323	9228	3.9651
C30 (BV421)	4	12921.39	4.1113	25364	4.4042

c

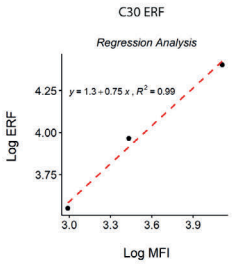

d

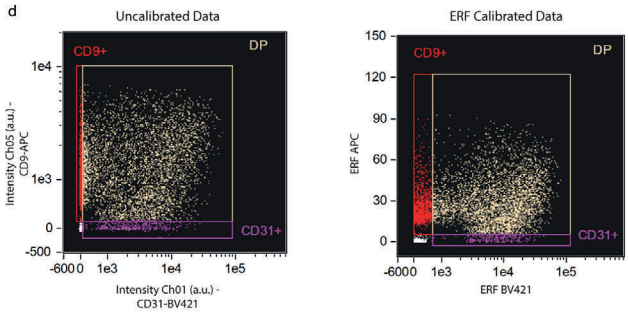

	Count	MFI Ch01	MFI Ch05
CD9+	1789	22.64	924.74
DP	4230	3254.04	1316.33
CD31+	467	2430.8	28.06

	Count	ERF Ch01	ERF Ch05
CD9+	1789	207.06	21.65
DP	4230	8596.4	27.92
CD31+	329	6907.35	3.42

Supplementary Figure 1 – Fluorescent calibration of BV421
a) The median fluorescent intensities (MFI) of each fluorescent peak of BV421 ERF calibration beads was measured with the same instrument/acquisition settings applied as used for EV acquisition.
b) Calculation of the log of the MFI and ERF values (provided by the bead manufacturer).
c) For both detection channels, the log of the MFI was plotted on the x-axis, and the log of the ERF values on the y-axis. A linear regression analysis was performed, respectively.
d) Representative example of uncalibrated data (left) and corresponding ERF calibrated data (right).

Framework Criteria	What to report	Please complete each criterion
1.1 Preanalytical variables conforming to MISEV guidelines.	Preanalytical variables relating to EV sample including source, collection, isolation, storage, and any others relevant and available in the performed study.	From each of the 5 (human) healthy individuals , 12 mL of blood was collected (one drawing) into two BD Vacutainer® K3-EDTA-coated collection tubes (BD Biosciences, San Jose, USA). Whole blood was centrifuged (Heraeus Multifuge 1S) at 1910 x g for 10 minutes at room temperature. The plasma layer was then collected - leaving ~1 mm of plasma above the buffy coat - and centrifuged (Heraeus Fresco) at 16,000 x g for 10 minutes at room temperature. The resulting platelet-poor plasma (PPP) was divided into 700-µL aliquots in cryovials containing 28 µL of a 25x concentrated protease inhibitor cocktail solution (4% v/v) (cOmplete Protease inhibitor cocktail tablets, Roche, Mannheim, Germany) according to the manufacturers' instructions and stored at -80 °C. All the procedures and animal housing conditions were carried out in strict accordance with current EU legislation on animal experimentation and were approved by the Institutional Committee for Animal Research (DEC protocol EMC No. AVD101002016635). Six weeks male C57BL/6J (JAX,GSP) mice (Jackson Labs, Bar Harbor, ME) were housed in Erasmus MC animal facility and housed in groups of 2-3/cage. They were maintained on a 12:12 h light-dark cycle and allowed ad libitum access to water and standard rodent food. The mice were anesthetized and blood (approximately 0.8 mL) was collected via the left ventricle using a 23-25 gauge needle. To ensure euthanasia of the animal post-procedure, mice were killed by cervical dislocation.
1.2 Experimental design according to MIFlowCyt guidelines.	EV-FC manuscripts should provide a brief description of the experimental aim, keywords, and variables for the performed FC experiment(s) using MIFlowCyt checklist criteria: 1.1, 1.2, and 1.3, respectively. Template found at www.evflowcytometry.org.	**1.1 Aim:** To develop an assay for the direct measurement of Extracellular Vesicles (EV) in unprocessed (human) plasma samples. **1.2 Keywords:** Unprocessed Human Plasma; Extracellular Vesicles; Imaging Flow Cytometry; Quantify; Phenotype; Diagnostic Platform. **1.3 Experiment variables:** Platelet-poor plasma (PPP) samples from 5 healthy individuals and/or six week old male C57BL/6J (JAX,GSP) mice (Jackson Labs, Bar Harbor, ME) were stained with CFDA-SE, anti-tetraspanin antibodies (CD9, CD63, CD81) and CD31, and measured with Imaging Flow Cytometry (IFCM).

Framework Criteria	What to report	Please complete each criterion
2.1 Sample staining details	State any steps relating to the staining of samples. Along with the method used for staining, provide relevant reagent descriptions as listed in MIFlowCyt guidelines (Section 2.4 Fluorescence Reagent(s) Descriptions).	**mAbs used:** The monoclonal antibodies (mAbs) used to stain human PPP were anti-CD9–APC, clone HI9a (6 µg/mL, BioLegend, San Diego, USA); anti-CD63–APC, clone H5C6 (200 µg/mL, BioLegend); and anti-CD81–APC, clone 5A6 (200 µg/mL, BioLegend. Human and mouse PPP were both stained with anti-human CD31–BV421, clone WM-59 (50 µg/mL, BioLegend) and anti-mouse CD31-APC, clone 390 (200 µg/mL, BioLegend). Isotype controls used were IgG1,k-BV421, clone MOPC-21 (100 µg/mL, BioLegend); IgG1,k-APC, clone MOPC-21 (200 µg/mL, BioLegend); and IgG2a,k-APC, clone RTK2758 (200 µg/mL, BioLegend). **mAb preperation:** All mAbs were centrifuged for 10 minutes at 16,000 x g to reduce the number of (potential) mAb clumps. A volume of the top layer of each centrifuged mAb solution was carefully harvested (according to the dilutions needed, described below) and diluted in 0.22 µm-filtered PBS (fPBS) before being added to the samples. **mAb pre-dilutions** All tetraspanin mAbs were diluted 30-fold in fPBS before staining (Final concentrations: CD9: 0.2 µg/mL, CD63: 6.6 µg/mL, CD81: 6.6 µg/mL); CD31-BV421 (anti-human) and CD31-APC (anti-mouse) were diluted 1000-fold (Final concentration: 50 ng/mL) and 62.5-fold (Final concentration: 3.2 µg/mL), respectively. The anti-tetraspanin antibody mixture was made by combining anti-CD9/anti-CD63/anti-CD81 in the same stock solution. **CFDA-SE Stock solution preperation:** A carboxyfluorescein diacetate succinimidyl ester (CFDA-SE) stock solution was made with the Vybrant™ CFDA-SE Cell Tracer Kit from Invitrogen immediately prior to use according to the manufacturer's instructions: CFDA-SE powder was spun down using a table-top centrifuge, and 18 µL of dimethylsulfoxide (DMSO) was added. The mixture was thoroughly resuspended and incubated at room temperature for 10 – 15 minutes in the dark. The dissolved CFDA-SE was added to a total volume of 1.782 mL of fPBS to create a 50 µM CFDA-SE stock solution. Similar to the protocol used to prepare mAbs, this stock solution was centrifuged for 10 minutes at 16,000 x g to reduce potential CFDA-SE clumps; the top layer was carefully harvested before being added to the samples.

Framework Criteria	What to report	Please complete each criterion
2.1 Sample staining details	State any steps relating to the staining of samples. Along with the method used for staining, provide relevant reagent descriptions as listed in MIFlowCyt guidelines (Section 2.4 Fluorescence Reagent(s) Descriptions).	**Sample staining:** 30 uL of sample was added to a pre-defined volume of fPBS (dependant on the volume of mAb staining - total volume after mAb addition was set at 130 µL): 12.5 uL of the stock solutions containing mAbs labelled with –APC and 5 µL of the stock solutions containing mAbs labeled with –BV421 were added, resulting in the following concentrations used per test: anti-CD9 – 2.5 ng, anti-CD63 – 83 ng, anti-CD81 – 83 ng, anti-CD31 (anti-human) – 1 ng, anti-CD31 (anti-mouse) – 40 ng per test. Equivalent amounts of isotype control was used for each antibody. Samples were then incubated overnight at 4 °C to ensure optimal saturation of the available EV epitopes; this incubation time was determined by adding the anti-tetraspanin antibody mix to fPBS and PPP samples and performing acquisition at set intervals (1/3/6 hours and O/N). CFDA-SE labeling was performed on the day of data acquisition by adding 100 µL of the 50 µM CFDA-SE stock solution to the samples, followed by 30 minutes of incubation at room temperature in the dark. Control samples not stained with CFDA-SE were incubated with 100 µL fPBS instead. All samples were brought to a total volume of 380 µL using fPBS before IFCM measurements.
2.2 Sample washing details	State any steps relating to the washing of samples.	No sample washing was performed; background fluorescence induced by our protocol is described in detail in this work.
2.3 Sample dilution details	All methods and steps relating to sample dilution.	For sample staining (descibed above), 30 uL of sample was incubated O/N in a total volume of 130 uL, resuling in 4.25-fold sample dilution. This volume was topped-up with 250 uL fPBS to a total volume of 380 uL, resulting in a total dilution of ~12.6-fold. For serial dilution experiments, samples were diluted four times (4-fold each step) by mixing 100 uL of sample with 300 uL of fPBS.

Framework Criteria	What to report	Please complete each criterion
3.1 Buffer alone controls.	State whether a buffer-only control was analyzed at the same settings and during the same experiment as the samples of interest. If utilized it is recommended that all samples be recorded for a consistent set period of time e.g. 5 minutes, rather than stopping analysis at a set recorded event count e.g. 100,000 events. This allows comparisons of total particle counts between controls and samples.	Buffer-only control of 0.22 µm-filtered PBS (fPBS) was recorded during the same experiment at the same imaging flow cytometer with acquisition settings similar to all other samples, including laser power and flow rate. All samples were recorded for 3 minutes to allow comparisons of total particle counts between controls and samples. In gerneral, <10 fluorescent events were acquired within this time period for each of the established gating regions.
3.2 Buffer with reagent controls.	State whether a buffer with reagent control was analyzed at the same settings, same concentrations, and during the same experiment as the samples of interest. If used state what the results were.	Buffer with reagent controls (single-stained with 12.5 µL anti-CD9 – 2.5 ng/test, 12.5 µL anti-CD63 – 83 ng/test, 12.5 µL anti-CD81 – 83 ng/test, 5 µL anti-CD31 (anti-human) – 1 ng/test, 5 µL anti-CD31 (anti-mouse) – 40 ng/ test, 100 µL of the 50 µM CFDA-SE stock solution) were recorded during the same experiment at the same imaging flow cytometer with acquisition settings similar to all other samples, including laser power and flow rate. All samples were recorded for 3 minutes to allow comparisons of total particle counts between controls and samples. In general, after 3 minutes, 600-700 fluorescent events (-APC) were recorded in buffer-control with anti-tetraspanin cocktail, <10 events in buffer-control with anti-CD9, ~100-200 events in buffer-control with anti-CD63, ~400-500 events in buffer-control with anti-CD81, ~<50 events in buffer-control with anti-mouse anti-CD31, ~200 events in buffer-control with anti-human anti-CD31 (-BV421), and <10 events in buffer-controls with CFDA-SE (CFSE)
3.3 Unstained controls.	State whether unstained control samples were analyzed at the same settings and during the same experiment as stained samples. If used, state what the results were, preferably in standard units.	Unstained control samples were measured at the same dilution as matched stained and isotype control samples, and were recorded during the same experiment at the same imaging flow cytometer with acquisition settings similar to all other samples, including laser power and flow rate. No substantial changes in fluorescence signal were observed between unstained and matched isotype controls.

Framework Criteria	What to report	Please complete each criterion
3.4 Isotype controls.	The use of isotype controls is applicable to immunofluorescence labelling only. State whether isotype controls were analyzed at the same settings and during the same experiment as stained samples. If utilized, state which antibody they are matched to, the concentration used, and what the results were (Section 4.2, 4.3, 4.4). Due to conjugation differences between manufacturers if should be stated if the isotype controls are from the same manufacturer as the matched antibodies.	Isotype controls samples were measured at the same dilution and at the same concentration as matched stained controls and were recorded during the same experiment at the same imaging flow cytometer with acquisition settings similar to all other samples, including laser power and flow rate. No substantial changes in fluorescence signal were observed between unstained and matched isotype controls. **Isotype - mAb matching:** IgG1,k-BV421, clone MOPC-21 (100 µg/mL, BioLegend) matched with anti-human CD31–BV421, clone WM-59 (50 µg/mL, BioLegend); IgG1,k-APC, clone MOPC-21 (200 µg/mL, BioLegend) matched with anti-CD9–APC, clone HI9a (6 µg/mL, BioLegend, San Diego, USA); anti-CD63–APC, clone H5C6 (200 µg/mL, BioLegend); and anti-CD81–APC, clone 5A6 (200 µg/mL, BioLegend), IgG2a,k-APC, clone RTK2758 (200 µg/mL, BioLegend) matched with anti-mouse CD31-APC, clone 390 (200 µg/mL, BioLegend). No isotype control for CFDA-SE was used. All isotype controls are from the same manufacturer as the matched antibodies.
3.5 Single-stained controls.	State whether single-stained controls were included. If used state whether the single-stained controls were recorded using the same settings, dilutions, and during the same experiment as stained samples and state what the results were, preferably in standard units (Section 4.2, 4.3, 4.4).	Single-stained control samples were included for every mAb used in this work, and were measured at the same dilution and at the same concentration as matched stained controls and were recorded during the same experiment at the same imaging flow cytometer with acquisition settings similar to all other samples, including laser power and flow rate. Single-stained controls aided in the establishment of the compensation matrix (to eliminate spectral overlap between detection channels). The following results were obtained for a representative single-stained PPP sample: **anti-CD9, anti-CD63, anti-CD81 (mix)** Counts: 7666, Median Fluorescent Intenstiy: 906, Equivalent number of Reference Fluorophores: 52 - **CFSE** Counts: 3234, Median Fluorescent Intenstiy: 816, Equivalent number of Reference Fluorophores: 134 - **anti-human anti-CD31** Counts: 3341 Median Fluorescent Intenstiy: 4101, Equivalent number of Reference Fluorophores: 12701.

Framework Criteria	What to report	Please complete each criterion
3.6 Procedural controls.	State whether procedural controls were included. If used, state the procedure and if the procedural controls were acquired at the same settings and during the same experiment as stained samples.	No procedural controls were used as no further sample processing was performed after labelling with reagents.
3.7 Serial dilutions.	State whether serial dilutions were performed on samples and note the dilution range and manner of testing. The fluorescence and/or scatter signal intensity would ideally be reported in standard units (see Section 4.3, 4.4) but arbitrary units can also be used. This data is best reported by plotting the recorded number events/ concentration over a set period of time at different sample dilution. The median fluorescence intensity at each of the dilutions should also ideally be plotted on the same or a separate plot.	Serial dilution samples were measured at the same (initial) dilution and at the same concentration as matched stained controls and were recorded during the same experiment at the same imaging flow cytometer with acquisition settings similar to all other samples, including laser power and flow rate. Four times 4-fold dilution was performed by mixing 100 uL of (stained) sample with 300 uL of fPBS. Correlation analysis showed a linear correlation between the concentration of double-positive fluorescent EV (CFSE+Tetraspanin+) and dilution rate (R^2=0,93). Fluorescent intensities remained stable: ~113 ERF CFSE and ~32 ERF APC.
3.8. Detergent treated EV-samples	State whether samples were detergent treated to assess lability. If utilized, state what detergent was used, the end concentration of the detergent, and what the results were of the lysis.	A 10% (v/v) Triton X-100 stock solution was made by dissolving 1 mL of TritonX-100 in 9 mL of fPBS. All samples (buffer alone, buffer plus reagents, unstained samples, single-stained samples, and double-stained samples) were treated with 20 µL of the Triton X-100 stock solution (final concentration: 0.5% (v/v) per test), followed by 30 minutes of incubation at room temperature in the dark prior to acquisition. Comparison of fluorescent concentrations in the PPP samples obtained before and after detergent lysis for CFSE+, Tetraspanin+, and CFSE+Tetraspanin+ regions showed ~31%, ~64% and ~94% reduction, respectively. For CD9+CD31+ EV, a ~93% reduction was observed after detergent lysis.

Framework Criteria	What to report	Please complete each criterion
4.1 Trigger Channel(s) and Threshold(s).	The trigger channel(s) and threshold(s) used for event detection. Preferably, the fluorescence calibration (Section 4.3) and/or scatter calibration (Section 4.4) should be used in order to report the trigger channel(s) and threshold(s) in standardized units.	Based on unstained, single-stained and isotype control samples, detection for CFSE fluorescence was triggered with 488nm laser at full power (200 mW), detected in channel 2 (480-560 filter) at a threshold of 170 arbitrary units, equivalent to ~36 FITC ERF, deterimined using Spherotec Rainbow Calibration beads and the manufacturers calibration values. Similarly, APC fluorescence was triggered with 642 nm laser at full power (150 mW), detected in channel 5 (642-745 filter), at a threshold of 170 a.u., equivalent to ~6 ERF APC. BV421 fluorescence was triggered with 405 nm laser at full pwer (120 mW), detected in channel 1 (435-505 nm filter), at a threshold of 110 a.u., equivalent to ~678 C30 ERF.
4.2 Flow Rate / Volumetric quantification.	State if the flow rate was quantified/validated and if so, report the result and how they were obtained.	Flow speed was monitored during acquisition and acquisition was started when flow speed was between 43.5 - 43.7 mm/sec. Typically, with the IFCM set at 'low speed, high sensitivity', ~0.8 uL of sample was measured in the time span of 180 seconds.
4.3 Fluorescence Calibration.	State whether fluorescence calibration was implemented, and if so, report the materials and methods used, catalogue numbers, lot numbers, and supplied reference units for the standards. Fluorescence parameters may be reported in standardized units of MESF, ERF, or ABC beads. The type of regression used, and the resulting scatter plot of arbitrary data vs standard data for the reference particles should be supplied.	Arbitrary BV421, CFSE and APC fluorescence intensities were converted to ERF units using 500 nm Rainbow Calibration Particles (RCP-05-5, lot AL01, Spherotech) with known Equivalent number of Reference Fluorophores (ERF) values for C30/FITC/APC. For each detection channel, the MFI of each fluorescent peak (blanc peaks were omitted from the regression analysis) from the four bead populations (1 blanc – 3 fluorescent) were measured, and a linear regression analysis was performed of the log(10) of these values against the log(10) of the known ERF values. The resulting equations were used to convert BV421/CFSE/APC fluorescent intensities into ERF units.

Framework Criteria	What to report	Please complete each criterion
4.4 Light Scatter Calibration.	State whether and how light scatter calibration was implemented. Light scatter parameters may be reported in standardized units of nm2, along with information required to reproduce the model.	Light scattering signals were fitted with Mie theory using a previously described model. The BF detector was modelled as a forward scattered light detector collecting light using a lens with a numerical aperture (NA) of 0.9, which corresponds to the NA of the 60x objective. The center wavelength of brightfield detection was 618.5 nm. The SSC detector was modelled as a detector that is placed perpendicular to the propagation direction of the laser beam. The NA of the collection lens was 0.9 and the wavelength was 785.0 nm. PS beads were modelled as solid spheres with a refractive index (n) of 1.5885 for a wavelength of 618.5 nm (brightfield) and 1.5783 for a wavelength of 785.0 nm (SSC). EVs were modelled as core-shell particles with a core refractive index of 1.38, shell refractive index of 1.48 and a shell thickness of 6 nm for both wavelengths as the dispersion relation for the core and shell of EVs is unknown. Beads were measured in water, and EVs in PBS. Therefore, the refractive indices of PBS and water were assumed to be 1.3345 and 1.3325, respectively, at a wavelength of 618.5 nm (BF) and 1.3309 and 1.3289, respectively, at a wavelength of 785.0 nm (SSC). Effective scattering cross sections of the calibration beads were calculated by integrating the amplitude scattering matrix elements over 576 collection angles. Data and theory were log10-transformed to scale the data onto the theory using a least-square-fit.
5.1 EV diameter/ surface area/ volume approximation.	State whether and how EV diameter, surface area, and/or volume has been calculated using FC measurements.	BF and SSC data of the PS beads were scaled onto Mie theory, resulting in a scaling factor (F) of 1.3518 and a coefficient of determination (R2) of 0.00 for the BF detector and a scaling factor of 8.405 and an R2 of 0.91 for the SSC detector. For the SSC detector, the theoretical model indicated a plateau between ~400 to ~800 nm, which translates into a low resolution when determining EV sizes based on SSC intensities within this region. The highest dynamic range was observed up to 400 nm - corresponding to a value of 900 a.u. SSC intensity.
5.2 EV refractive index approximation.	State whether the EV refractive index has been approximated and how this was done.	EV refractive index has not been approximated in this work - for Mie theory application, EVs were modelled as core-shell particles with a core refractive index of 1.38, shell refractive index of 1.48 and a shell thickness of 6 nm for both wavelengths as the dispersion relation for the core and shell of EVs is unknown.
5.3 EV epitope number approximation.	State whether EV epitope number has been approximated, and if so, how it was approximated.	Other than conversion of fluorescent intensities into standardized units (ERF), no EV epitope numbers have been approximated in this work.

Framework Criteria	What to report	Please complete each criterion
6.1 Completion of MIFlowCyt checklist.	Complete MIFlowCyt checklist criteria 1 to 4 using the MIFlowCyt guidelines. Template found at www.evflowcytometry.org.	The MIFlowCyt checklist v1.0.0 has been completed and attached in the Supplementary Information.
6.2 Calibrated channel detection range	If fluorescence or scatter calibration has been carried out, authors should state whether the upper and lower limits of a calibrated detection channel were calculated in standardized units. This can be done by converting the arbitrary unit scale to a calibrated scaled, as discussed in Section 4.3 and 4.4, and providing the highest unit on this scale and the lowest detectable unit above the unstained population. The lowest unit at which a population is deemed 'positive' can be determined a variety of ways, including reporting the 99th percentile measurement unit of the unstained population for fluorescence. The chosen method for determining at what unit an event was deemed positive should be clearly outlined.	The lower fluorescence threshold for Ch01 (BV421), Ch02 (CFSE), and Ch05 (APC) was set at 110, 170, and 170 a.u., respectively. These values were obtained by analysing blanc-fluorescent Rainbow Calibration Particles (RCP-05-5, lot AL01, Spherotech), unstained PPP samples, and isotype control PPP samples. When scaled to ERF units, these values translated to 677.71 / 35.40 / 6.40 ERF, respectively. Upper fluorescent limits (high-end gating cut-off) for Ch01 (BV421), Ch02 (CFSE), and Ch05 (APC) was set at 100.000, 50.553, and 10.302 a.u., respectively. These gating cut-offs were determined to encompass all obtained fluorescent events. When scaled to ERF units, these values translated to 112,201 / 3776 / 123 ERF, respectively.

Framework Criteria	What to report	Please complete each criterion
6.3 EV number/ concentration.	State whether EV number/ concentration has been reported. If calculated, it is preferable to report EV number/ concentration in a standardized manner, stating the number/ concentration between a set detection range.	Detected concentrations of fluorescent EV are described in detail in the manuscript. All concentrations reported were obtained between the calibrated detection ranges for each channel, as described above.
6.4 EV brightness.	When applicable, state the method by which the brightness of EVs is reported in standardized units of scatter and/or fluorescence.	EV brightness was calculated for all fluorescent populations analyzed and described in the work; MFI values were converted into standardized-ERF values. For CFSE+Tetraspanin+ EV measured in the PPP samples, we observed a mean EV brightness of 119.57 ERF (range 99.6-156) for CFSE and 65.33 ERF (range 61.3-69.8) for APC. For CD9+CD31+ EV measured in the PPP samples, we observed a mean EV brightness of ~7,620 (range 3,640 – 9,240) and 20.4 (range 15 – 27.9) for BV421 and APC, respectively.
7.1. Sharing of data to a public repository.	Provide a link to the experimental data in a public data repository.	IFCM files can be obtained by contacting the corresponding author.

Supplementary Table 1 – Framework representing the Minimal Information about a Flow Cytometry (FC) experiment to allow standardized EV-FC-specific reporting (MIFlowCyt-EV template), as recommended by the Minimum Information for Studies of EVs (MISEV).

Requirement	Please Include Requested Information
1.1. Purpose	To develop a protocol for the direct measurement of Extracellular Vesicles (EV) in unprocessed (human) plasma samples.
1.2. Keywords	Unprocessed Human Plasma; Extracellular Vesicles; Imaging Flow Cytometry; Quantify; Phenotype; Diagnostic Platform
1.3. Experiment variables	Platelet-poor plasma (PPP) samples from 5 healthy individuals and/or six week old male C57BL/6J (JAX,GSP) mice (Jackson Labs, Bar Harbor, ME) were stained with CFDA-SE, anti-tetraspanin antibodies (CD9, CD63, CD81) and CD31, and measured with Imaging Flow Cytometry (IFCM).
1.4. Organization name and address	Erasmus Medical Center, University Medical Center Rotterdam, The Netherlands. Wytemaweg 80, 3015 CN, Rotterdam
1.5. Primary contact name and email address	Wouter W. Woud, wouterwwoud@gmail.com
1.6. Date or time period of experiment	2020 - 2021
1.7. Conclusions	Imaging Flow Cytometry (IFCM) can be used to identify, quantify and phenotype fluorescently tagged EV ≤240 nm in **unprocessed** (human) plasma samples.
1.8. Quality control measures	The instrument calibration tool ASSIST® was used upon each startup to optimize performance and consistency between experiments. Additionally, commercially available mixtures of FITC-fluorescent polystyrene beads of known sizes (Megamix-Plus FSC – 900, 500, 300 and 100 nm, and Megamix-Plus SSC – 500, 240, 200, 160 nm), as well as Rainbow Calibration Particles (RCP-05-5, lot AL01, Spherotech), were used in calibrating and standardization of the IFCM platform.
2.1.1.1. (2.1.2.1., 2.1.3.1.) Sample description	Platelet-poor plasma (PPP) obtained from 5 healthy individuals was used in this study. From each of the 5 healthy individuals, 12 mL of blood was collected (one drawing) into two BD Vacutainer® K3-EDTA-coated collection tubes (BD Biosciences, San Jose, USA). Whole blood was centrifuged (Heraeus Multifuge 1S) at 1910 x g for 10 minutes at room temperature. The plasma layer was then collected - leaving ~1 mm of plasma above the buffy coat - and centrifuged (Heraeus Fresco) at 16,000 x g for 10 minutes at room temperature. The resulting PPP was divided into 700-µL aliquots in cryovials containing 28 µL of a 25x concentrated protease inhibitor cocktail solution (4% v/v) (cOmplete Protease inhibitor cocktail tablets, Roche, Mannheim, Germany) according to the manufacturers' instructions and stored at -80 °C. Additionally, PPP was generated from mice. All the procedures and animal housing conditions were carried out in strict accordance with current EU legislation on animal experimentation and were approved by the Institutional Committee for Animal Research (DEC protocol EMC No. AVD101002016635). Six weeks male C57BL/6J (JAX,GSP) mice (Jackson Labs, Bar Harbor, ME) were housed in Erasmus MC animal facility and housed in groups of 2-3/cage. They were maintained on a 12:12 h light-dark cycle and allowed ad libitum access to water and standard rodent food. The mice were anesthetized and blood (approximately 0.8 mL) was collected via the left ventricle using a 23-25 gauge needle. To ensure euthanasia of the animal post-procedure, mice were killed by cervical dislocation.

Requirement	Please Include Requested Information
2.1.1.2. Biological sample source description	See above
2.1.1.3. Biological sample source organism description	Healthy human individuals – 2 male, 3 female, age range 31 – 56 (mean 43,4). Mouse – see above.
2.1.2.2. Environmental sample location	NA
2.3. Sample treatment description	Bloods were drawn, processed and stored as described above. For staining, 30 uL of PPP was added to a pre-defined volume of fPBS (dependant on the volume of mAb staining - total volume after mAb addition was set at 130 µL): 12.5 uL of the stock solutions containing mAbs labelled with –APC and 5 µL of the stock solutions containing mAbs labeled with –BV421 were added, resulting in the following concentrations used per test: anti-CD9 – 2.5 ng, anti-CD63 – 83 ng, anti-CD81 – 83 ng, anti-CD31 (anti-human) – 1 ng, anti-CD31 (anti-mouse) – 40 ng per test. Equivalent amounts of isotype control was used for each antibody. Samples were then incubated overnight at 4 °C to ensure optimal saturation of the available EV epitopes; this incubation time was determined by adding the anti-tetraspanin antibody mix to fPBS and PPP samples and performing acquisition at set intervals (1/3/6 hours and O/N). CFDA-SE labeling was performed on the day of data acquisition by adding 100 µL of the 50 µM CFDA-SE stock solution to the samples, followed by 30 minutes of incubation at room temperature in the dark. Control samples not stained with CFDA-SE were incubated with 100 µL fPBS instead. All samples were brought to a total volume of 380 µL using fPBS before IFCM measurements.
2.4. Fluorescence reagent(s) description	The monoclonal antibodies (mAbs) used to stain human PPP were anti-CD9–APC, clone HI9a (6 µg/mL, BioLegend, San Diego, USA); anti-CD63–APC, clone H5C6 (200 µg/mL, BioLegend); and anti-CD81–APC, clone 5A6 (200 µg/mL, BioLegend. Human and mouse PPP were both stained with anti-human CD31–BV421, clone WM-59 (50 µg/mL, BioLegend) and anti-mouse CD31-APC, clone 390 (200 µg/mL, BioLegend). Isotype controls used were IgG1,k-BV421, clone MOPC-21 (100 µg/mL, BioLegend); IgG1,k-APC, clone MOPC-21 (200 µg/mL, BioLegend); and IgG2a,k-APC, clone RTK2758 (200 µg/mL, BioLegend).
3.1. Instrument manufacturer	LUMINEX
3.2. Instrument model	ImageStream^{X} MkII

Requirement	Please Include Requested Information
3.3. Instrument configuration and settings	The ISx was equipped with three objectives (20x/40x/60x) and 1 CCD camera. All data were acquired using the 60x objective (numerical aperture of 0.9 – pixel area of 0.1 μm^2) with fluidics settings set to "low speed/high sensitivity". We adjusted the default core size of 7 µm to 6 µm using the "Defaults Override" option within INSPIRE software (version 200.1.681.0), as recommended by the manufacturer. Data were acquired over three minutes for standardization among samples with the autofocus setting activated and the "Remove Speedbead" option unchecked. BV421 fluorescence signals were collected in channel 1 (435–505-nm filter), CFSE signals in channel 2 (480–560-nm filter) and APC signals in channel 5 (642–745-nm filter). Channel 4 was used as the brightfield channel, and channel 6 (745–780-nm filter) was used for SSC detection. Excitation lasers were set as follows: 405 nm: 120 mW, 488 nm: 200 mW, 642 nm: 150 mW, and 775 nm (SSC): 1.25 mW. Particle enumeration was achieved through the advanced fluidic control of the ISx coupled with continuously running SBs and application of the "objects/mL" feature within the ISx Data Exploration and Analysis Software (IDEAS®).
4.1. List-mode data files	IFCM files can be obtained by contacting the corresponding author.
4.2. Compensation description	Fluorescent events from singly stained PPP samples were used in the setting of compensation matrices (to compensate for spectral overlap between fluorochromes) such that straight fluorescent populations were obtained when depicted in scatterplots. The following compensation matrix was established for all fluorophores used in this manuscript:

	Ch01	Ch02	Ch03	Ch04	Ch05	Ch06
Ch01	1	0,07	0	0,022	0,025	0
Ch02	0,111	1	0	0,022	0,02	0
Ch03	0	0	1	0,026	0	0
Ch04	0	0	0	1	0	0
Ch05	0,002	0,02	0	0,028	1	0
Ch06	0,013	0,035	0	0,034	0	1

4.3. Data transformation details	Arbitrary BV421, CFSE and APC fluorescence intensities were converted to ERF units using 500 nm Rainbow Calibration Particles (RCP-05-5, lot AL01, Spherotech) with known Equivalent number of Reference Fluorophores (ERF) values for C30/FITC/APC. For each detection channel, the MFI of each peak from the four bead populations (1 blanc – 3 fluorescent) were measured, and a linear regression analysis was performed of the log(10) of these values against the log(10) of the known ERF values. The resulting equations were used to convert BV421/CFSE/APC fluorescent intensities into ERF units.

Requirement	Please Include Requested Information
4.4.1. Gate description	The lower fluorescence threshold for Ch01 (BV421), Ch02 (CFSE), and Ch05 (APC) was set at 110, 170, and 170 a.u., respectively. These values were obtained by analyzing blanc-fluorescent Rainbow Calibration Particles (RCP-05-5, lot AL01, Spherotech), unstained PPP samples, and isotype control PPP samples. When scaled to ERF units, these values translated to 1397.171 / 38.40 / 28.03 ERF, respectively. Upper fluorescent limits (high-end gating cut-off) for Ch01 (BV421), Ch02 (CFSE), and Ch05 (APC) was set at 100.000, 50.553, and 10.302 a.u., respectively. These gating cut-offs were determined to encompass all obtained fluorescent events. When scaled to ERF units, these values translated to 89125 / 3656 / 133 ERF, respectively.
4.4.2. Gate statistics	Median Fluorescent Intensity (MFI) – Count – Objects/mL
4.4.3. Gate boundaries	See above

Supplemental Table 2 – Checklist representing the Minimal Information about a Flow Cytometry (FC) experiment to allow standardized EV-FC-specific reporting (MIFlowCyt-EV checklist), as recommended by the Minimum Information for Studies of EVs (MISEV).

Control type	Rationale
PBS	Blanc - Background control
PBS + mAbs	mAb mediated background control
PBS + Isotypes	Isotype mediated background control
Unstained sample	Autofluorescence of unstained sample
Sample + Single stain	Fluorescence compensation purpose
Sample + Isotype	Unspecific binding of antibodies used
Sample + Double stain	***Multiparameteric detection of sample of interest***
Sample + Double stain + Detergent Treatment	Confirmation that detected events are of biological nature

Supplementary Table 3 - Control types and the rationale for their use. Each control listed above is essential for the multiparametric detection of human plasma-derived single EV.

Parameter	Settings
Magnification:	60x
Lasers:	405nm – 488nm – 642nm - SSC (785 nm)
Voltage:	120mW – 200mW – 150mW – 1.25mW
Fluidics:	Low Speed & High Sensitivity
Autofocus:	ON
Remove Speedbead:	Unchecked
Core Widt:	6 µm (Override)
Acquisition time:	180 seconds

Supplementary Table 4 - Acquisition parameter settings for the multiparametric detection of single EV in human plasma samples using the ISx MKII imaging flow cytometer. Lasers were turned on as applicable for each experiment. SSC: Side Scatter.

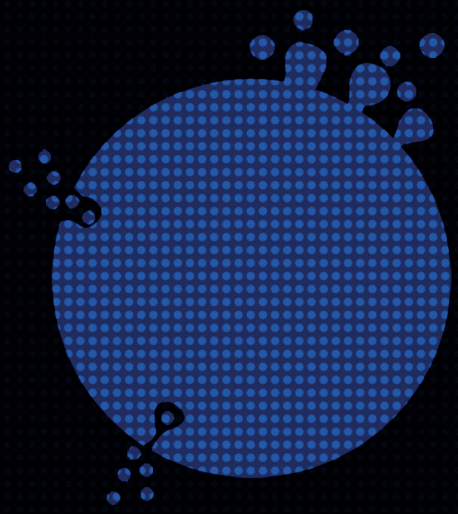

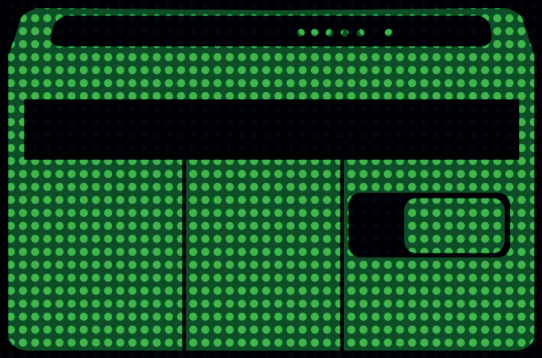

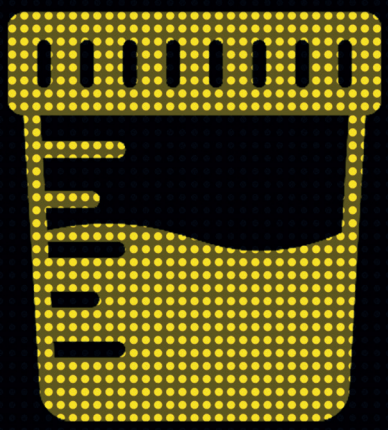

04

ISOLATION-FREE MEASUREMENT OF SINGLE URINARY EXTRACELLULAR VESICLES BY IMAGING FLOW CYTOMETRY

Liang Wu*[1,2], Wouter W. Woud*[1], Carla C. Baan[1], Dennis A. Hesselink[1], Edwin van der Pol[3,4,5], Guido Jenster[6], Karin Boer[1]

[1] Erasmus MC Transplant Institute, Department of Internal Medicine, University Medical Center Rotterdam, Rotterdam, The Netherlands.
[2]Department of Nephrology, The First Affiliated Hospital of Shaoyang University, 422000 Shaoyang, Hunan, China.
[3]Laboratory Experimental Clinical Chemistry, Amsterdam University Medical Centers, location AMC, Amsterdam, the Netherlands.
[4]Vesicle Observation Center, Amsterdam University Medical Centers, location AMC, Amsterdam, the Netherlands.
[5]Biomedical Engineering and Physics, Amsterdam University Medical Centers, location AMC, Amsterdam, the Netherlands.
[6]Department of Urology, Erasmus Medical Center, Rotterdam, The Netherlands.

Nanomedicine: Nanotechnology, Biology, and Medicine 48 (2023) 102638

* These authors contributed equally to this work

ABSTRACT

Urinary extracellular vesicles (uEVs) are promising biomarkers for various diseases. However, many tools measuring uEVs rely on time-consuming uEV isolation methods, which could induce sample bias. This study demonstrates the detection of single uEVs without isolation using imaging flow cytometry (IFCM). Unstained urine samples contained auto-fluorescent (A-F) particles when characterized with IFCM. Centrifugation successfully removed A-F particles from the unprocessed urine. Based on the disappearance of A-F particles, a gate was defined to distinguish uEVs from A-F particles. The final readouts of IFCM were verified as single EVs based on detergent treatment and serial dilutions. When developing this protocol to measure urine samples with abnormally high protein levels, 25 mg/mL dithiothreitol (DTT) showed improved uEV recovery over 200 mg/mL DTT. This study provides an isolation-free protocol using IFCM to quantify and phenotype single uEVs, eliminating the hindrance and influence of A-F particles, protein aggregates, and coincidence events.

KEYWORDS

Extracellular vesicles; Imaging flow cytometry; Isolation-free methodology; Human urine; Kidney transplantation.

INTRODUCTION

Extracellular vesicles (EVs) are phospholipid bilayers widely released by cells into body fluids, such as blood and urine. Their reported size ranges from 30 nm to 8000 nm, with most EVs <200 nm.[1–3] EVs reflect parental cell status via variations in EV concentration, composition, or cargo and are considered minimally invasive biomarkers.[1]

Urinary extracellular vesicles (uEVs) are ideal biomarkers as urine collection is non-invasive and easily repeated.[4] uEVs show meaningful values in diagnosing renal and urinary system diseases,[5–7] and illnesses of other systems, such as Parkinson's disease and liver cirrhosis.[8,9]

Despite the perspective as a clinical marker, uEV quantification and characterization are hampered because of their small size, urine contaminants, and lack of methods for accurate detection.[1,10] Nanoparticle tracking analysis (NTA), resistive pulse sensing (RPS), and flow cytometry (FCM) are the most commonly used single-EV-quantification techniques.[1] However, NTA and RPS are limited in phenotyping capabilities, struggling to distinguish uEVs from other particles, such as protein aggregates.[1,11] Although some modern flow cytometers can detect small EVs (< 100 nm) based on light scattering, most flow cytometers in clinical research labs have a size detection limit of >600 nm.[12] Moreover, some particles in urine emit autofluorescence, leading to false-positive signals in FCM, regardless of labeling.[13,14] The origin of these autofluorescent (A-F) particles is still unclear and how to distinguish them from uEVs needs more research. The direct measurement of uEV is also hampered by Tamm-Horsfall protein (THP), a highly abundant urinary protein, easily entrapping uEVs.[13–16]

Due to the limitations of traditional techniques and the complex composition of urine, uEV purification is commonly required before detection.[17] However, no (combination of) isolation methods, including ultracentrifugation, ultrafiltration, precipitation, or size exclusion chromatography, can reach 100 % uEV purity and yield due to significant loss of uEVs or co-isolation of other particles.[1,17] Some purification procedure likely alters uEV properties.[14,18–20] Ultrafiltration can disintegrate large EVs to generate smaller particles, misunderstood as natural EVs.[18] Ultracentrifugation might cause EV aggregation and encapsulation of multiple small uEV inside bigger uEV.[14,19,20]

Endowed with increased fluorescence detection sensitivity over conventional FCM,[21] and the capability of distinguishing particles based on high-resolution imaging,[22] imaging FCM (IFCM) allows quantification and characterization of uEVs to solve the mentioned difficulties and bypass EV isolation. IFCM has been demonstrated for single EV measurement in minimally processed plasma[23], cell supernatant,[22] and isolated uEVs,[24,25] but no methodology to detect uEVs from urine without relying on prior EV purification. The current study aims to provide a protocol to characterize uEVs by IFCM directly in stained urine by excluding A-F particles and diminishing the influence of THP.

RESULTS

Outline of the manuscript

The workflow of this study is schematically summarized in Figure 1. We aimed for standardized uEV-IFCM measurements independent of uEV purification for clinical usage. To this end, supporting techniques (TEM, NTA, TR-FIA) were used to indicate the size distribution, concentration, and uEV markers in unprocessed urine. The IFCM instrument was calibrated with standardized reference material for cross-platform comparisons and then used to quantify, phenotype and characterize uEVs in the minimally processed urine (unprocessed urine with labeling). Urine samples from healthy controls (HC) were initially used to establish the uEV-IFCM protocol, which was further developed using the urine of kidney transplant recipients (KTR).

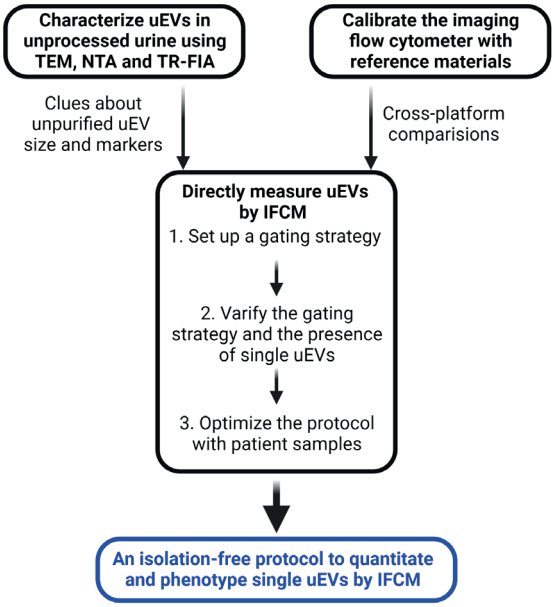

Figure 1 - Schematic workflow of this study.

Measuring uEVs by TEM, NTA, and TR-FIA

In HC urine samples imaged by TEM, uEV-like cup-shaped structures were observed with diameters between 50 and 100 nm (Figure 2A, large-area images in Supplementary Figure S2). With NTA, we summarized the single-particle-size reports from all HC urine samples. We found that 93-98 % of urine particles' diameter was <400 nm, but 2-7 % of all detected particles showed a size from 400 nm to 1200 nm (Figure 2B). The total concentration of particles measured by NTA was around 10^8/mL, which is an order of magnitude estimate of particles exceeding the lower limit of detection (LoD).[31] We estimate the LoD to be ~90 nm based on the distribution mode.

To select appropriate labeling for uEV detection by IFCM, we compared the relative expression levels of the tetraspanins CD9 and CD63 on uEVs using TR-FIA. In Figure 2C, CD63 was 6.7-fold higher than CD9 following the Europium intensity (p = 0.0302), corresponding with previous research.[32] Hence, CD63+ uEV was chosen as a targeted population to demonstrate the following isolation-free uEV-IFCM methodology.

Standardize the range of detected uEV size

After knowing the size range and marker of uEV in the unprocessed urine samples, a step-by-step gating strategy was developed to distinguish single CD63+ uEV particles from non-uEV components or coincidence events in IFCM.

As demonstrated with NTA (Figure 2B), we chose the detection range of <1200 nm to include virtually all uEVs. Based on the previously published calibration of our IFCM, an SSC cutoff value of 5279.179 arbitrary units, corresponding to 1200-nm (diameter) EVs, was obtained and used to include uEVs ≤ 1200 nm for all the following analyses.[23]

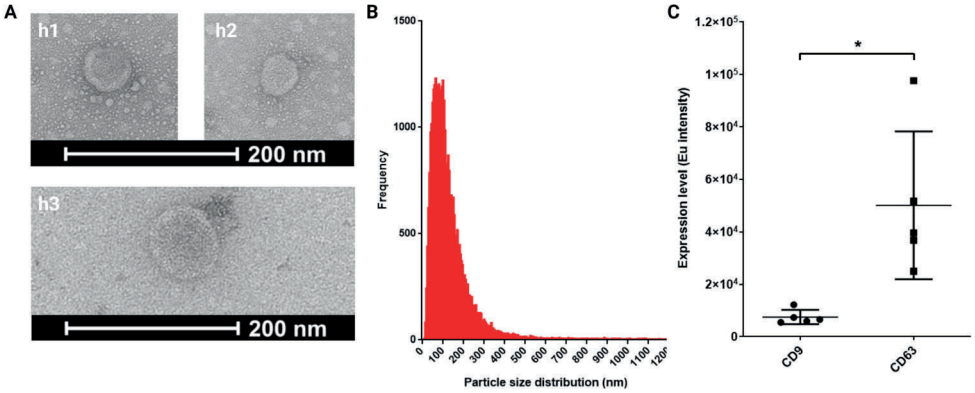

Figure 2 - uEV characteristics tested by TEM, NTA, and TR-FIA in the HC urine (n = 5).
A) uEV-like structures in TEM.
B) The size distribution of urinary particles in NTA.
C) uEV tetraspanin levels as reported by TR-FIA. *p < 0.05.

Exclude multiplets and false singlets

The fluorescence intensity of uEVs in multiplets cannot be individually characterized.[28] Following previous research, we also initially tried to utilize intensity masks to calculate the spot count feature.[22,23] However, the Intensity Mask mistook close doublets as singlets (Supplementary Figure S3A). Compared with Intensity masking, Peak Mask only selects pixels with peak intensity (Supplementary Figure S3B).[28] Therefore, spot numbers could be more precisely quantitated using the Peak Mask. The spot-to-background ratio of the Peak Mask should not be higher than the value of 1, lest the number of individual spots are underestimated. When the ratio was 3, this Peak mask ignored pixels with < 3-fold of the average intensity of the whole image, leading to missing dim spots (Supplementary Figure S3C). Notably,"<" of this ratio has no meaning because in the Peak mask

with the bright model, the intensity of included pixels must be higher than the background.[28] Therefore, the Peak Mask with a spot-to-cell background ratio of 1 was the most appropriate for identifying singlets and excluding events with >1 spot in fluorescence-detecting channels (Ch02 & Ch05). The next step, coincidence/false "singlets" (one green and one red object, but their positions did not overlap), were excluded based on the distance between Ch02 and Ch05 spots ≠ 0.

Distinguishing uEV-singlets from auto-fluorescent particles in labelled urine

In fDPBS, no positive particles (Figure 3A) were observed. Conversely, unprocessed urine (without staining) contained 1.6 ± 0.7 × 10^6 objects/mL positive particles (Figure 3B). These events are auto-fluorescent (A-F) particles and demonstrated positive fluorescent signals in fluorescence-detecting channels: Ch02, Ch03, and Ch05. Ch02 and Ch05 were used to detect Alexa488, and APC signals, respectively. No fluorescent reagent was used for Ch03, so it only presented the A-F signals. In the minimally processed urine (urine only with labeling), the distribution of A-F particles overlapped with positive uEVs (Figure 3C), necessitating the exclusion/removal of A-F particles. Lowering laser power or detergent treatment did not sufficiently remove A-F particles (Figure 3D). Hence, these A-F particles are not phospholipid bilayer structures, and their A-F signal is unrelated to the high laser power. A step of short-run centrifugation (10,000 g × 10 min) was found to remove 98.9 ± 0.3% of A-F particles (p = 0.0058; Figure 3D).

Though centrifugation effectively removed A-F particles, it could cause a loss of uEVs. We designed a gating strategy distinguishing non-A-F particles (uEVs) from A-F particles based on the absence of A-F particles in centrifuged urine and aimed to bypass centrifugation finally. First, urine was"cleane" using that centrifugation (Figure 3B to 3E). Next, centrifuged urine was stained with CD63-Alexa488 and CD63-APC to show positive uEVs (Figure 3F). The spillover from Ch02 to Ch03 was compensated (value: 0.19 in the compensation matrix), so uEVs were horizontally distributed in Figure 3G. Notably, applying this compensation to A-F particles in the unprocessed urine did not alter the A-F signal (Supplementary Figure S4). Based on the remaining events after this centrifugation, a gate,"Non-A-F Particle", was set in Ch03 with a cutoff value of 150 A-F intensity (arbitrary unit), which is equal to 5 MESF-PE (blue gate in Figure 3G). Then, the obtained compensation matrix and gate were applied to urine samples without centrifugation (blue gate in Figure 3H). By doing so, A-F particles were excluded from the following analysis without requiring centrifugation, and therefore, urine was kept minimally processed until uEV labeling, thus bypassing potential uEV loss. The"Non-A-F Particle" gate was

permanently applied to distinguish non-A-F particles from A-F particles in all the following uEV-IFCM analyses (Supplementary Figure S5). Typical images of distinguished positive uEVs and excluded A-F particles were presented in Figure 3I.

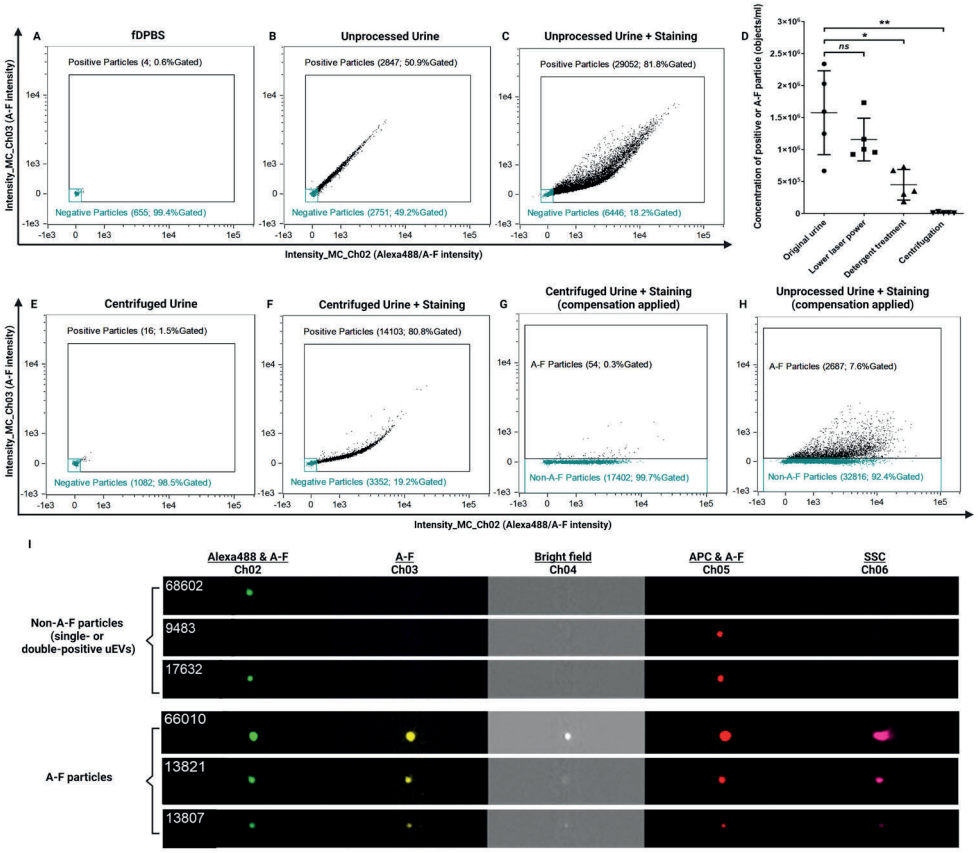

Figure 3 - Distinguish non-A-F particles/uEVs from A-F particles in the stained urine using IFCM. No compensation in **A**-**C**, **E, F**. Based on fDPBS (**A**), the gates"Negative Particle" and"Positive Particle" were established and applied to present A-F particles in the unprocessed urine (**B**). (**C**) A-F particles and positive uEVs could not be distinguished in urine with double-CD63 staining. (**D**) Methods for removing A-F particles in unprocessed urine (n = 5)."Original urine": unstained urine without any treatments. Compared to the control, the "Lower laser power" group used a quarter of the laser voltage of Ch02 and Ch05; "Detergent treatment" was incubated with 2.0% TritonX-100 at room temperature for 30 min; "Centrifugation" was centrifuged at 10.000 g for 10 min and removed the pellet. $^{**}p < 0.01$; $^{*}p < 0.05$; ns, no significance. (**E**) The absence of A-F particles in the urine supernatant after centrifugation (10.000 g 10 min). (**F**) Centrifuged urine was CD63-stained to present the distribution of non-A-F particles (uEVs). (**G**) A compensation matrix was applied in (**F**) to eliminate spillovers between Ch02 and Ch03, and the gate "Non-A-F Particles" was set up. (**H**) The compensation matrix and the gate "Non-A-F Particles" were applied to the CD63-stained urine (no centrifugation). (**I**) Typical images of positive uEVs and A-F particles in double-CD63-stained urine.

Detect fluorescently labelled uEV singlets

Next, we aimed to distinguish between single-positive and double-positive uEVs. The cutoff fluorescent intensity of APC -/+ was established by staining samples with CD63-Alexa488 and isotype (IgG1)-APC. Based on the APC threshold, we set up the green gate in Supplementary Figure S6B to include the Alexa488-single-positive uEVs. Likewise, the Alexa488 -/+ cutoff value was set by staining urine with IgG1-Alxea488 and CD63-APC and then obtaining the red gate in Supplementary Figure S6C for APC-single-positive uEVs. Doing so allowed us to establish a compensation matrix to minimize fluorescent spillover between Ch02 and Ch05. Fluorescent thresholds were set at 22 MESF-Alexa488, and 1463 MESF-APC. Using these fluorescent thresholds, we established a double-positive fluorescent region which allowed identification of double-positive uEVs (blue region in Supplementary Figure S6D) from single-positive uEVs. These thresholds were established based on multiple urine samples without gating differences observed, indicating that these gates can be repeatedly applied.

Here, we summarized the logic of the whole IFCM gating strategy (Figure 4). After excluding A-F particles, the analysis of double-CD63-stained HC urine samples demonstrated three uEV populations as the final readout: CD63-Alexa488 single-positive, CD63-APC single-positive, and double-positive uEV singlets.

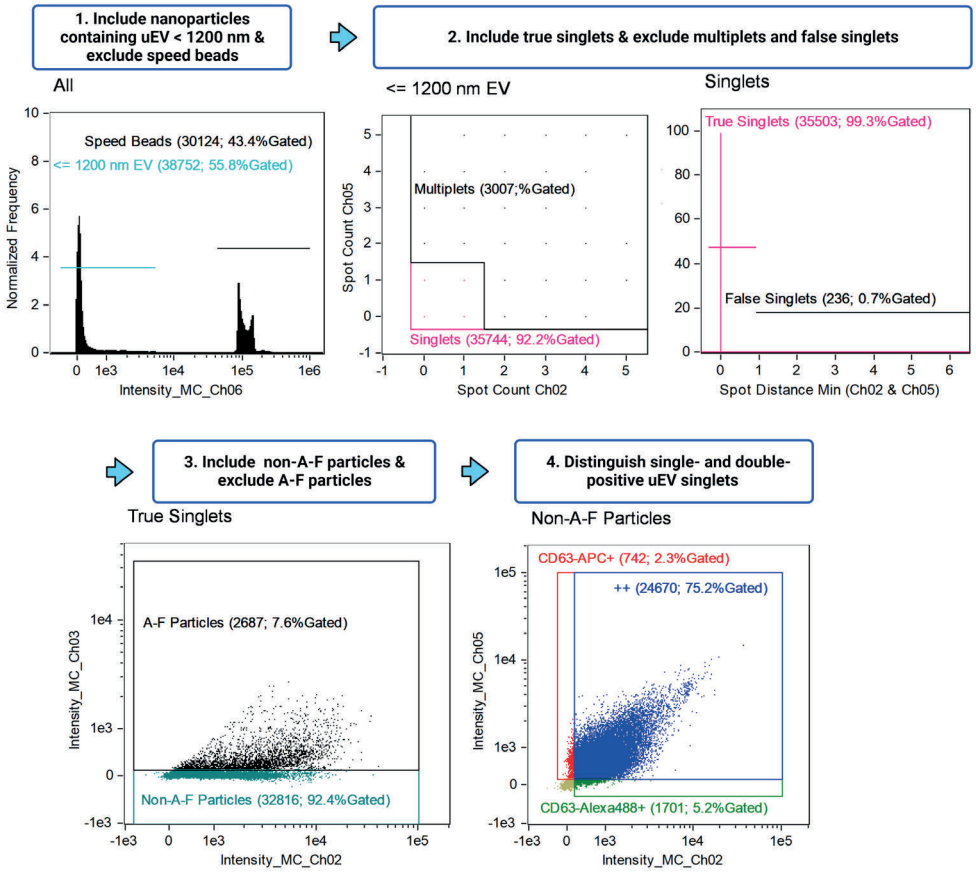

Figure 4 - The final IFCM gating strategy directly identifying CD63+ uEVs in the double-CD63-stained urine. Each gate's name displays the counts and percentage of gated events (Counts; %Gated).

Background analysis

Without performing any wash steps, it was essential to verify the presence of CD63+ uEVs. First, detergent treatment was used to check if the readouts of IFCM represent biological membrane structures. Before detergent treatment, for all HC urine samples (double-CD63-stained), we found that the majority of readouts were“+” particles, 3.8 ± 1.3 × 10^7 objects/mL (Figure 5A). After detergent treatment,“+” events decreased to 4.8 ± 2.7 × 10^5 objects/mL, representing a 98.5 ± 0.9% decrease compared to no detergent (p = 0.0034). As for the single-positive particles in the stained urine, 3.2 ± 2.5 × 10^6 objects/mL of events were“CD63-Alexa488” (Figure 5B), and 5.8 ± 0.6 × 10^5 objects/mL of events were“CD63-APC” (Figure 5C). After detergent treatment, the concentration of the single“CD63-Alexa488” events and the“CD63-APC” events was reduced by 91.3 ± 6.7% and 77.9 ± 30.1%, respectively (Figures 5B & 5C).

Next to detergent treatment, the double-positive concentrations in other controls were summarized in Figure 5A. Compared with unstained, isotype-stained, and double-stained plus detergent-treated urine, the average uEV-to-background concentration ratio for the double-positive region in double-stained urine is 3102.2-fold, indicating a convincing presence of CD63+ uEVs in the minimally processed urine. Compared to urine with other treatments, the average uEV-to-background ratios of Alexa488 single-positive and APC single-positive events in the double-stained urine were 10.9-fold and 26.6-fold, respectively (Figures 5B & 5C).

Double-positive particles are the majority of CD63+ uEVs and showed the highest uEV-to-background ratio, so they were selected to represent CD63+ uEVs in the subsequent analysis.

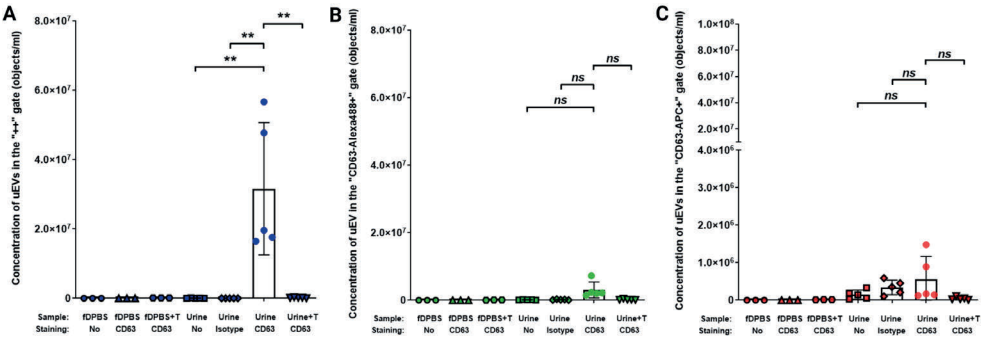

Figure 5 - Quantification of background signals and presence of CD63+ uEVs with IFCM. Concentrations of uEVs included in the double-positive gate (++; **A**), CD63-Alexa488 single-positive gate (**B**), and CD63-APC single-positive gate (**C**). Negative controls compared with the double-stained healthy urine samples (n = 5).“CD63”: staining samples with CD63-Alexa488 and CD63-APC;“Isotype” labeling urine with IgG1-Alexa488 and IgG1-APC;“+T”: urine incubated with 0.5% (v/v) TritonX-100 at room temperature for 30 min. “ns”: no significance; **$p < 0.01$.

Serial dilutions confirm the single-particle analysis

Serial dilutions were performed to verify the detection of single uEVs and the selection of singlets in the IFCM gating strategy.[33] We serially diluted HC urine samples 3- and 9-fold in fDPBS and observed a linear decrease in CD63+ uEV concentration (R^2 = 0.9992; Figure 6A). This decrease corresponded with the dilution factor, indicating the analysis of single that CD63+ uEVs.[33] Moreover, diluted samples maintained consistent MESF-Alexa488 and MESF-APC signals of the CD63+ uEVs (Figures 6B & 6C). These findings confirmed that our gating strategy correctly identifies and selects single uEVs.

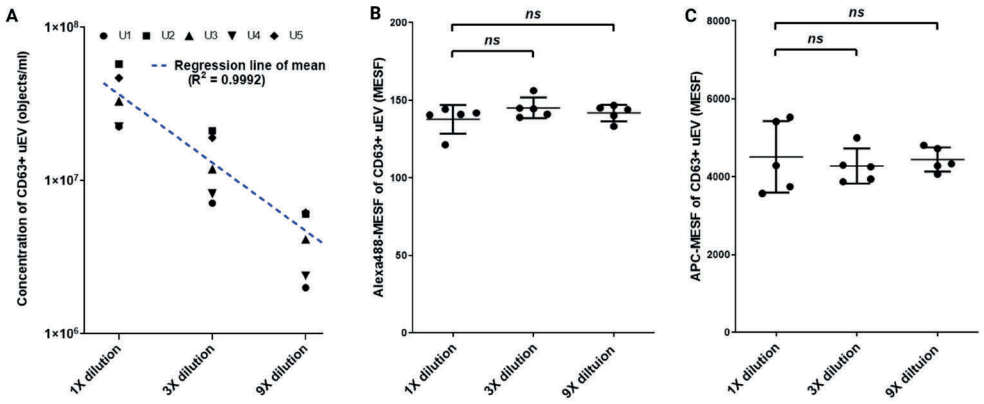

Figure 6 - Verification of uEV singlets in the serially diluted urine.
(**A**) Serial dilutions were performed on the double-stained healthy urine samples (n = 5), showing the linear regression on the mean values of CD63+ uEV concentration. R^2: coefficient of regression.
(**B**, **C**) Dilution effects on the MESF-Alexa488 and MESF-APC of CD63+ uEV. "ns": no significance.

4

Application and development of the isolation-free protocol for patient's uEV

Our protocol has been developed using HC urine samples and showed good inter- and intra-reproducibility in long-term and repeated measurements for clinical applications (CV < 6.1%; Supplementary Figure S7). However, patient's urine differs from healthy conditions, including higher pH and increased urinary protein levels (Supplementary Table S1). We found that normalizing urinary pH by the commonly used dilution with fDPBS did not alter the detection of uEV numbers (Supplementary Figure S8). Tamm-Horsfall protein (THP) is the most abundant urinary protein, likely polymerizing and entrapping uEVs, and THP level rises significantly during kidney dysfunctions.[15,16,34]

Using electron microscopy, most uEVs observed in healthy urine were identified as single/free structures (Supplementary Figure S2A & S2B). However, in KTR urine, many uEVs are enclosed in aggregate- or filament-like structures (Figure 7A, large-area pictures in Supplementary Figure S2C & S2D). These aggregates/filaments might be associated with higher urinary total protein in KTR urine compared with HC urine (p = 0.0050; Figure 7B). Using ELISA, KTR urine also showed significantly elevated urinary THP compared with HC urine (p = 0.0197; Figure 7C).

Dithiothreitol (DTT, 200 mg/mL) is a general reagent reducing THP polymerization,[16,35] though excess DTT also breaks the disulfide bond in other molecules, such as present on antibodies.[36] The final concentration of DTT should be carefully considered because there are no washing steps in our protocol. Due to the small sample volume (500 μL) used for each test, reducing the volume of DTT makes it hard to resuspend the urine pellet. Therefore, we opted to reduce the concentration of DTT: we used 25 mg/mL and 200 mg/mL DTT to examine the effect of DTT on uEV detection using IFCM.

Compared to the non-DTT group, 25 mg/mL of DTT did not affect CD63+ uEVs concentration in HC urine samples, whereas 200 mg/mL of DTT caused a 9.5 ± 5.2% decline of detected uEV amounts ($p = 0.0431$; Figure 7D). In KTR urine, 25 mg/mL DTT elevated 12.4 ± 10.4% in CD63+ uEV concentration compared to the non-DTT usage ($p = 0.0367$; Figure 7D). However, 200 mg/mL DTT showed a 13.83 ± 3.7% decrease in uEV numbers compared to the non-DTT group ($p = 0.0109$; Figure 7D) in KTR urine. Hence, 25 mg/mL of DTT was used in our developed protocol for applications in patient urine with high levels of THP.

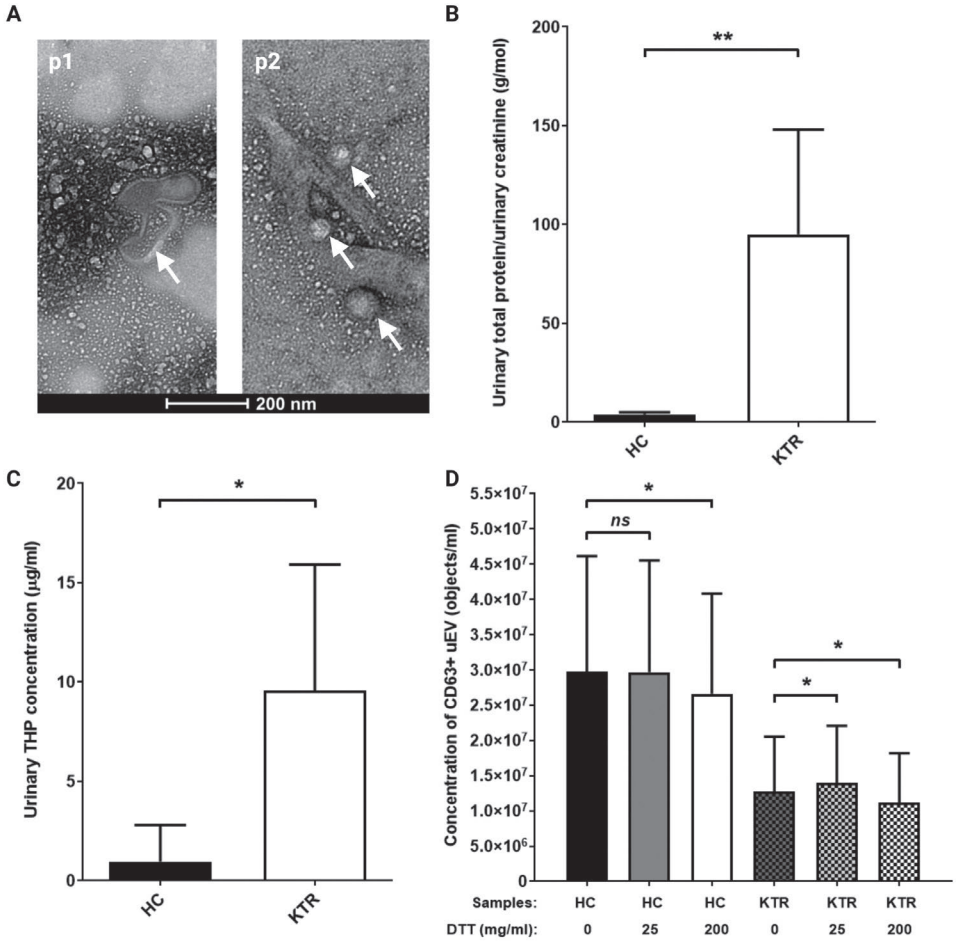

Figure 7 - DTT usage in the IFCM protocol.
A) uEVs in the KTR urine samples measured by TEM. White arrows indicate uEVs.
B, **C**) Total protein concentrations and THP of HC urine samples (n = 5) and KTR samples (n = 5). **$p < 0.01$; *$p < 0.05$.
D) DTT effects on CD63+ uEV numbers in the HC (n = 5) and KTR urine (n = 5).
"ns": no significance; "*" : $p < 0.05$.

DISCUSSION

We successfully characterized and phenotyped single uEVs in healthy and KTR urine without prior isolation using IFCM in this study. Our protocol is based on the absolute sizing of EVs with the Mie Theory to realize cross-platform reproducibility.[23,29,37] Conversion of SSC signals into particle size has been demonstrated for our instrument to selectively analyze plasma-derived EVs ≤400 nm.[23] Here, we expanded the analysis range to investigate uEVs ≤1200 nm because larger uEVs might also be meaningful as a biomarker. Podocytes can release uEVs (≥400 nm) containing abundant RNA and protein markers, serving as an indicator of kidney injury.[14,38] In addition to size, EV shape or membrane orientation might also be of interest, but EV signals with IFCM are indicated with only a few pixels. Therefore other uEV morphology information, such as shape, is challenging to be explored.

The most significant novelty and improvement is the exclusion of urinary A-F particles from uEVs in minimally processed urine. The presence of autofluorescence/A-F particles is a natural property of urine.[14,39] A-F particles presented similar fluorescent characteristics in all the urine samples (HC or KTR). Those particles can be substantially excluded from uEVs with the same gate and compensation matrix (Supplementary Figure S5), indicating possibly no necessity to adjust the gate or compensation matrix when measuring different urine samples. Following published FCM research,[13,14] we also found that A-F particles in all urine samples showed fluorescence with emission wavelengths 505-595 nm and 642-745 nm. The broad emission wavelength range indicates that A-F particles hinder specific fluorescent EV detection using many typical fluorophores, such as Alexa488, fluorescein isothiocyanate (FITC), PE, Alexa647, and APC. This problem might be avoided by using fluorophores with other emission wavelengths, such as near-infrared ones.[40]

Compared to uEVs, A-F particles might be larger/denser because A-F particles were removed by moderate-speed centrifugation while uEVs were maintained. Large uEVs are co-isolated with A-F particles in the low-centrifugation pellet.[14] Luca et al. tried a masking strategy to delimit A-F in particular channels but observed that 30-40 % of"positive uEV" remained after detergent lysis.[14] We found that detergent treatment could not entirely remove A-F particles (Figure 3B), suggesting a non-EV structure. We assume A-F particles likely remained in their readouts after their mask strategy. Droste et al. processed urine with a 200 nm filter and did not observe A-F particles using IFCM, but they detected about 10^4 objects/mL CD63+

uEVs.[24] In contrast, in our protocol without filtration, we found around 10^7 objects/mL of CD63+ uEVs. These findings suggest not using filtration or centrifugation when aiming to investigate the full (detectable) spectrum of uEVs.

We chose two CD63 antibodies to demonstrate our methodology. Researchers can easily replace the labeling for detecting other markers but should be cautious in the antibody selection. The single staining with CD63-Alexa488 detected around a 5-fold uEV concentration compared to CD63-APC (Compare Supplementary Figure S5B with S5C). This finding might be attributed to the fluorophore to protein (F/P) ratio of CD63-Alexa488 (5.20) being much higher than CD63-APC (1.22). A Higher F/P value means brighter fluorescence of each antibody-epitope complex and hence higher sensitivity in the EV detection by FCM.[41]

In this study, we developed our protocol for application in patient samples. During kidney injury, the kidney excretes more THP than in healthy conditions,[34] leading to more entrapment of uEVs.[15] In the patient samples, we found the recovery of uEVs using DTT (10%) is not as significant as previous reports (20%),[16,42] which might result from a lower concentration of DTT (25 mg/mL) we used than previous studies (200 mg/mL), because considering the detrimental effects of DTT on antibodies.[36,43]

The limitation of this study is the absence of other quantitative techniques available to compare our IFCM results. However, we do see a correlation between TR-FIA and IFCM (Supplementary Figure S9A). TR-FIA, independent of isolation, revealed that uEV concentration, not the epitope density on single uEVs, might determine the total uEV protein numbers. Our study met all the requirements of accurate IFCM measurement in the MISEV2018 guideline and MIFlowCyt-EV framework.[1,33] As a method paper, we demonstrate that IFCM is a feasible tool to quantitate and characterize uEVs without bias-concomitant isolation. With our protocol (Figure 8), uEV researchers can measure targeted subpopulations of uEVs from 500 µL of urine by simply changing the antibody to other markers. More patient urine samples should be enrolled to make the results more robust for clinical application.

Most EV studies relying on isolation used disunified isolation methods, which results in non-comparable data among them. Promoting standardized and isolation-free detection equals diminishing the research heterogeneity and integrating the data from single-center clinical studies. In conclusion, IFCM provides insight into the differences between single uEVs, A-F particles, and uEV multiplets, allowing for characterizing single uEVs without purification.

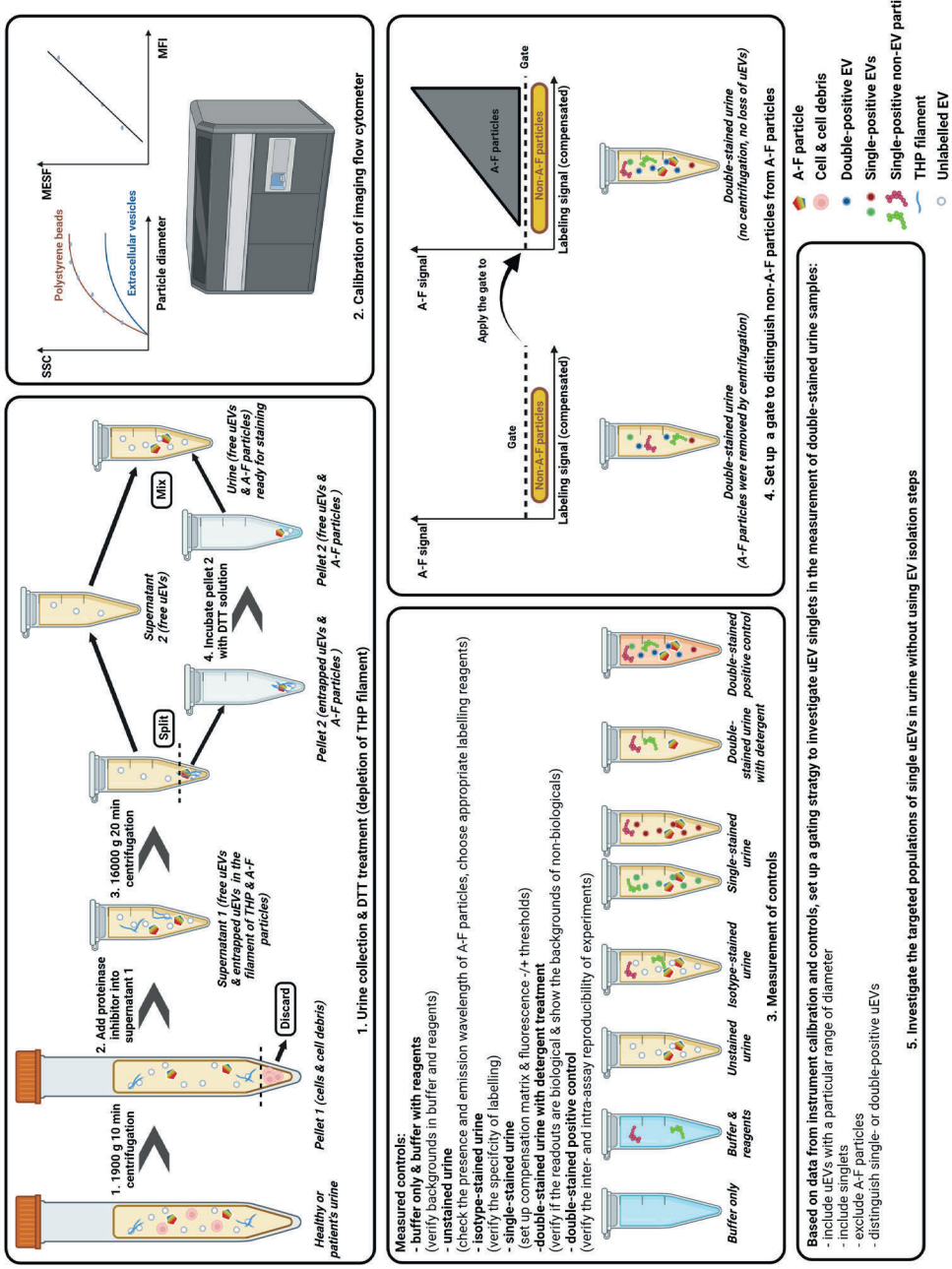

Figure 8 - Schematic summary of the isolation-free protocol measuring uEVs by IFCM.

MATERIALS & METHODS

Urine samples were measured by (1) transmission electron microscopy (TEM), (2) nanoparticle tracking analysis (NTA), (3) time-resolved fluorescence immunoassay (TR-FIA), and (4) IFCM without using any uEV isolation method. Supernatant harvested from COLO-205 cells was used as a positive control to investigate the inter- and intra-assay reproducibility during IFCM measurement. TEM, NTA, and TR-FIA protocols were introduced in supplementary materials, including the COLO-205 cell culturing, the measurement of urine protein, creatinine, pH, Tamm-Horsfall protein, and urine treatment with dithiothreitol (DTT).

Collection of urine samples

Urine was collected from 5 healthy controls (HC; Medical Ethical Review number 2018-1623) and 5 kidney transplant recipients (KTR) with acute kidney injury in the first 2 weeks post-transplantation (Medical Ethical Review number 2018-035), approved by the institutional review board of the Erasmus MC. Details regarding the collection of urine samples were demonstrated in the Supplementary material. The gender, age, pH, urinary total protein concentration, and urine creatinine concentration of included individuals are shown in Supplementary Table S1.

Labeling EVs from urine for IFCM

CD9 and CD63 are tetraspanins playing critical roles in EV generation and excretion.[26] Both are used as general uEV surface markers.[27] Urine and COLO-205 cell medium (positive control) were stained with antibodies (all from Biolegend, USA): CD63-Alexa488 (clone H5C6; fluorophore-to-protein ratio 5.20); CD63-APC (clone H5C6; fluorophore-to-protein ratio 1.22); IgG1-Alexa488 or IgG1-APC (both clone MOPC-21). Our study aims to investigate diverse uEV populations by combining markers conjugated with different fluorophores, so two CD63 antibodies were used to demonstrate the influence of fluorophore conjugation on the uEV-IFCM detection and compare the single- and double-positive backgrounds. Antibodies (100–200 μL) were centrifuged at 16,000 g at 4 °C for 10 min (FrescoTM 17 Microcentrifuge, Thermofisher Scientific), and only the supernatant was pipetted to avoid aggregates. Based on titration, the final concentration of all antibodies in the sample solution was 0.44 μg/mL. 112 μL of samples were incubated with 4 μL of 15-fold-diluted CD63-Alexa488 and 4 μL of 15-fold-diluted CD63-APC at 4 °C in the

dark overnight (dilution by 0.2-μm-pore-filtered Dulbecco's phosphate-buffered saline; fDPBS). IgG1-Alexa488 and IgG1-APC were used as isotypes. The stained sample was treated with 6 μL of 10% (v/v) Triton-X-100 at room temperature for 30 min to lyse biological structures, such as EVs.

Acquisition settings of ImageStreamx MkII

Multispectral IFCM was performed using Amins ImageStream MKII (ISx, Luminex, Seattle, WA, USA), with data acquisition by software INSPIRE® (version: 200.1.681, EMD Millipore). INSPIRE® runs a quality control procedure with built-in ASSIST® as the daily startup procedure. The settings of INSPIRE® in the acquisition: low-speed (velocity: 40 mm/s) & high sensitivity, 6 μm core diameter, 60X magnification, 488-nm laser power at channel 02 (Ch02) detecting Alexa488: 200 mW; 642-nm laser power at channel 05 (Ch05) detecting APC: 150 mW, 1.25 mW laser power at channel 06 (Ch06) detecting side scatter (SSC), and activated channel 04 (Ch04) for detection of bright field. To monitor sample flow and maintain the camera's focus in ISx, polystyrene speed beads (catalog no. 400041, Luminex) were loaded together with samples at 15%. Each acquisition lasted 180 s, the"Prim" function was clicked once for loading samples fast, and"Remove Speed Bead" was unchecked to maintain speed beads during acquisition.

IFCM analysis

Raw image files acquired from INSPIRE® were analyzed by ISx Data Exploration and Analysis Software (IDEAS® 6.2, EMD Millipore). "Mask" define a specific area within images to select and quantify pixels. Masks in Ch01 to Ch06 pictures were labeled from M01 to M06, and Mask Combined (MC) includes M01 to M06. Different functions can be applied to each Mask to adjust the position and region of selected pixels. Mask with the"Intensit" function contains pixels showing higher intensity than the backgrounds. The Mask with the"Pea" function (model: Bright) identifies the brightest pixels with the peak intensity in each event, designed for fluorescent spot recognition.[28] The intensity threshold of the Peak Mask is determined by its cell-to-background ratio. The name of M02 in Ch02, with Peak function, Bright model, and cell-to-background ratio 1, is simplified as Peak (M02, Ch02, Bright, 1). Masks, Peak (M02, Ch02, Bright, 1), and Peak (M05, Ch05, Bright, 1) were used to include the pixels of Alexa488+ and APC+ fluorescent spots. By using the Boolean logic function, Peak masks applied for Ch02 and Ch05 were combined as"Peak

(M02, Ch02, Bright, 1) OR Peak (M05, Ch05, Bright, 1".

"Feature" is further applied upon Mask to analyze quantitative and positional information of selected pixels. Mask selection significantly influences feature characteristics because Mask determines the region of analysis for any given Feature.[28] Hence, the combination of Feature and Mask is instrument/analysis-specific and independent of the sample. Intensity MC is designed to match Intensity Feature for quantifying fluorescence in Ch02, Ch03, Ch05, or SSC signals in Ch06. We chose Peak Masks (M02, Ch02, Bright, 1) and (M05, Ch05, Bright, 1) to be combined with "Spot Count Ch02" and "Spot Count Ch05" features, respectively, because Peak Mask can sensitively recognize fluorescent spot numbers in Ch02 and Ch05.[22,28] Distance between spots presented in a single event but different channels can be analyzed after combining Masks in those channels. The feature "Spot Distance Min" was applied on the composite mask "Peak (M02, Ch02, Bright, 1) OR Peak (M05, Ch05, Bright, 1)" to measure the minimal distance between Alexa488+ and APC+ spots within an image.[23] When this value of "Spot Distance (Ch02 & Ch05)" was 0, the positions of Alexa488+ and APC+ particles overlapped.[23]

An analysis template that summarizes all used features and accompanying masks can be found in Supplementary Table S2.

Calibration of the IFCM

Size-related calibration was performed by measuring SSC of beads of known diameter and refractive index (Gigamix, BioCytex, The Netherlands) followed by Mie theory using the scripts of Rosetta Calibration (v1.29, Exometry, The Netherlands).[29] EVs were modeled as core-shell particles with a core refractive index of 1.38, a shell refractive index of 1.48 and a shell thickness of 6 nm. The calibration based on SSC using Gigamix and Rosetta Calibration has previously been reported by our team using the same machine and acquisition settings.[23]

Calibration of the fluorescence intensity was based on three Quantum™ MESF (molecules of equivalent soluble fluorochrome) kits containing four populations of beads with varying amounts of Alexa488, APC, or PE (Bangs Laboratories, USA).[25] For each kit, the median fluorescence intensity (MFI) of beads was measured by IFCM and converted into MESF based on the instructions of the manufacturer (https://www.bangslabs.com/quickcal). Data was presented in Supplementary Table S3 & Figure S1. The regression coefficient values for each fluorochrome (R^2-

Alexa488: 0.9987; R^2-PE: 0.9948; R^2-APC: 0.9955) indicated that obtained MFI could be readily converted into MESF values.

EV-Track

Experimental details have been uploaded to the EV-TRACK (ID: EV220008), an open-access knowledgebase recommended by the International Society for Extracellular Vesicles to track worldwide EV research.[1,30]

Statistical Analysis

GraphPad Prism 8.0 (GraphPad Software, USA) was used to analyze and visualize the data. Data were presented as mean ± standard deviation. In the calibration of MESF in IFCM, the analysis templates calculated the correlation coefficient (R^2) values between MFI and MESF. The coefficient of variation (CV) reflected the reproducibility of IFCM. Paired t-tests were used to show the differences in uEVs numbers or urinary pH between urine samples with different treatments. Unpaired t-tests were utilized to show the differences in urinary protein levels between HCs and KTRs. Linear regression analysis demonstrated the association between IFCM and TR-FIA readouts. Statistical significance was defined by p-values < 0.05 (two-tailed).

ACKNOWLEDGMENTS

We thank the support from the China Scholarship Council (No. 202008430154) and Wenda Verschoor and Rens Kraaijeveld for helping solve the technical questions of IFCM and structure this paper. We acknowledge Natasja Dits at the Department of Urology (Erasmus Medical Center; EMC) for the TEM images and Manou van Alphen for the support of TR-FIA. All figures were created with BioRender.com.

DISCLOSURE

G. Jenster has a license agreement with Cell GS for the CD9 and CD63 TR-FIA (TRIFic). Other author reports no conflicts of interest in this work.

REFERENCES

1. Théry C, Witwer KW, Aikawa E, Alcaraz MJ, Anderson JD, Andriantsitohaina R, et al. Minimal information for studies of extracellular vesicles 2018 (MISEV2018): a position statement of the International Society for Extracellular Vesicles and update of the MISEV2014 guidelines. *J Extracell Vesicles*. 2018;7(1):2001-3078. doi:10.1080/20013078.2018.1535750
2. Liangsupree T, Multia E, Riekkola mL. Modern isolation and separation techniques for extracellular vesicles. *J Chromatogr A*. 2021;1636:461773. doi:10.1016/j.chroma.2020.461773
3. Arraud N, Linares R, Tan S, Gounou C, Pasquet JM, Mornet S, et al. Extracellular vesicles from blood plasma: Determination of their morphology, size, phenotype and concentration. *J Thromb Haemost*. 2014;12(5):614-627. doi:10.1111/JTH.12554
4. Wen J, Yang T, Mallouk N, Zhang Y, Li H, Lambert C, et al. Urinary Exosomal CA9 mRNA as a Novel Liquid Biopsy for Molecular Diagnosis of Bladder Cancer. *Int J Nanomedicine*. 2021;16:4805-4811. doi:10.2147/IJN.S312322
5. Wu L, Boer K, Woud WW, Udomkarnjananun S, Hesselink DA, Baan CC. Urinary extracellular vesicles are a novel tool to monitor allograft function in kidney transplantation: A systematic review. *Int J Mol Sci*. 2021;22(19):10499. doi:10.3390/ijms221910499
6. Liu YR, Ortiz-Bonilla CJ, Lee YF. Extracellular Vesicles in Bladder Cancer: Biomarkers and Beyond. *Int J Mol Sci*. 2018;19(9). doi:10.3390/IJMS19092822
7. Kamińska A, Roman M, Wróbel A, Gala-Błądzińska A, Małecki MT, Paluszkiewicz C, et al. Raman spectroscopy of urinary extracellular vesicles to stratify patients with chronic kidney disease in type 2 diabetes. *Nanomedicine Nanotechnology, Biol Med*. 2022;39:102468. doi:10.1016/J.NANO.2021.102468
8. Wang S, Kojima K, Mobley JA, West AB. Proteomic analysis of urinary extracellular vesicles reveal biomarkers for neurologic disease. *EBioMedicine*. 2019;45:351-361. doi:10.1016/j.ebiom.2019.06.021
9. Gonzalez E, Azkargorta M, Garcia-Vallicrosa C, Prieto-Elordui J, Elortza F, Blanco-Sampascual S, et al. Could protein content of Urinary Extracellular Vesicles be useful to detect Cirrhosis in Alcoholic Liver Disease? *Int J Biol Sci*. 2021;17(8):1864-1877. doi:10.7150/IJBS.59725
10. Erdbrügger U, Blijdorp CJ, Bijnsdorp I V., Borràs FE, Burger D, Bussolati B, et al. Urinary extracellular vesicles: A position paper by the Urine Task Force of the International Society for Extracellular Vesicles. *J Extracell Vesicles*. 2021;10(7):e12093. doi:10.1002/jev2.12093
11. Cimorelli M, Nieuwland R, Varga Z, van der Pol E. Standardized procedure to measure the size distribution of extracellular vesicles together with other particles in biofluids with microfluidic resistive pulse sensing. *PLoS One*. 2021;16(4). doi:10.1371/JOURNAL.PONE.0249603
12. van der Pol E, Sturk A, van Leeuwen T, Nieuwland R, Coumans F, Mobarrez F, et al. Standardization of extracellular vesicle measurements by flow cytometry through vesicle diameter approximation. *J Thromb Haemost*. 2018;16(6):1236-1245. doi:10.1111/jth.14009
13. Burger D, Thibodeau JF, Holterman CE, Burns KD, Touyz RM, Kennedy CRJ. Urinary podocyte microparticles identify prealbuminuric diabetic glomerular injury. *J Am Soc Nephrol*. 2014;25(7):1401-1407. doi:10.1681/ASN.2013070763
14. Musante L, Bontha SV, La Salvia S, Fernandez-Piñeros A, Lannigan J, Le TH, et al. Rigorous characterization of urinary extracellular vesicles (uEVs) in the low centrifugation pellet - a neglected source for uEVs. *Sci Rep*. 2020;10(1):1-14. doi:10.1038/s41598-020-60619-w

15. Xu X, Barreiro K, Musante L, Kretz O, Lin H, Zou H, et al. Management of Tamm–Horsfall Protein for Reliable Urinary Analytics. *Proteomics - Clin Appl*. 2019;13(6):1-10. doi:10.1002/prca.201900018
16. Fernández-Llama P, Khositseth S, Gonzales PA, Star RA, Pisitkun T, Knepper MA. Tamm-Horsfall protein and urinary exosome isolation. *Kidney Int*. 2010;77(8):736-742. doi:10.1038/ki.2009.550
17. Stam J, Bartel S, Bischoff R, Wolters JC. Isolation of extracellular vesicles with combined enrichment methods. *J Chromatogr B Anal Technol Biomed Life Sci*. 2021;1169. doi:10.1016/j.jchromb.2021.122604
18. Jang SC, Kim OY, Yoon CM, Choi DS, Roh TY, Park J, et al. Bioinspired exosome-mimetic nanovesicles for targeted delivery of chemotherapeutics to malignant tumors. *ACS Nano*. 2013;7(9):7698-7710. doi:10.1021/nn402232g
19. Pang B, Zhu Y, Ni J, Ruan J, Thompson J, Malouf D, et al. Quality assessment and comparison of plasma-derived extracellular vesicles separated by three commercial kits for prostate cancer diagnosis. *Int J Nanomedicine*. 2020;15:10241-10256. doi:10.2147/IJN.S283106
20. Linares R, Tan S, Gounou C, Arraud N, Brisson AR. High-speed centrifugation induces aggregation of extracellular vesicles. *J Extracell Vesicles*. 2015;4(1). doi:10.3402/jev.v4.29509
21. Botha J, Pugsley HR, Handberg A. Conventional, high-resolution and imaging flow cytometry: Benchmarking performance in characterisation of extracellular vesicles. *Biomedicines*. 2021;9(2):1-24. doi:10.3390/biomedicines9020124
22. Görgens A, Bremer M, Ferrer-Tur R, Murke F, Tertel T, Horn PA, et al. Optimisation of imaging flow cytometry for the analysis of single extracellular vesicles by using fluorescence-tagged vesicles as biological reference material. *J Extracell Vesicles*. 2019;8(1):1587567. doi:10.1080/20013078.2019.1587567
23. Woud WW, Pol E van der, Mul E, Hoogduijn MJ, Baan CC, Boer K, et al. An imaging flow cytometry-based methodology for the analysis of single extracellular vesicles in unprocessed human plasma. *Commun Biol*. 2022;40(1):633. doi:10.1101/2022.02.24.481807
24. Droste M, Tertel T, Jeruschke S, Dittrich R, Kontopoulou E, Walkenfort B, et al. Single Extracellular Vesicle Analysis Performed by Imaging Flow Cytometry and Nanoparticle Tracking Analysis Evaluate the Accuracy of Urinary Extracellular Vesicle Preparation Techniques Differently. *Int J Mol Sci Artic Int J Mol Sci*. 2021;22(22):12436. doi:10.3390/ijms222212436
25. Lannigan J, Erdbruegger U. Imaging flow cytometry for the characterization of extracellular vesicles. *Methods*. 2017;112:55-67. doi:10.1016/j.ymeth.2016.09.018
26. Mathieu M, Névo N, Jouve M, Valenzuela JI, Maurin M, Verweij FJ, et al. Specificities of exosome versus small ectosome secretion revealed by live intracellular tracking of CD63 and CD9. doi:10.1038/s41467-021-24384-2
27. Royo F, Zuñiga-Garcia P, Sanchez-Mosquera P, Egia A, Perez A, Loizaga A, et al. Different EV enrichment methods suitable for clinical settings yield different subpopulations of urinary extracellular vesicles from human samples. *J Extracell Vesicles*. 2016;5(1). doi:10.3402/jev.v5.29497
28. Amnis. IDEAS® Image Data Exploration and Analysis Software User's Manual. 2013;(July):231. https://www.luminexcorp.com/imagestreamx-mk-ii/?wpdmdl=41965
29. de Rond L, Coumans FAW, Nieuwland R, van Leeuwen TG, van der Pol E. Deriving Extracellular Vesicle Size From Scatter Intensities Measured by Flow Cytometry. *Curr Protoc Cytom*. 2018;86(1):e43. doi:10.1002/cpcy.43

30. Van Deun J, Mestdagh P, Agostinis P, Akay Ö, Anand S, Anckaert J, et al. EV-TRACK: transparent reporting and centralizing knowledge in extracellular vesicle research. *Nat Methods 2017 143*. 2017;14(3):228-232. doi:10.1038/nmeth.4185
31. van der Pol E, Coumans FAW, Grootemaat AE, Gardiner C, Sargent IL, Harrison P, et al. Particle size distribution of exosomes and microvesicles determined by transmission electron microscopy, flow cytometry, nanoparticle tracking analysis, and resistive pulse sensing. *J Thromb Haemost*. 2014;12(7):1182-1192. doi:10.1111/jth.12602
32. Duijvesz D, Versluis CYL, Van Der Fels CAM, Vredenbregt-Van Den Berg MS, Leivo J, Peltola MT, et al. Immuno-based detection of extracellular vesicles in urine as diagnostic marker for prostate cancer. *Int J Cancer*. 2015;137(12):2869-2878. doi:10.1002/ijc.29664
33. Welsh JA, Van Der Pol E, Arkesteijn GJA, Bremer M, Brisson A, Coumans F, et al. MIFlowCyt-EV: a framework for standardized reporting of extracellular vesicle flow cytometry experiments. *J Extracell Vesicles*. 2020;9(1). doi:10.1080/20013078.2020.1713526
34. Rampoldi L, Scolari F, Amoroso A, Ghiggeri G, Devuyst O. The rediscovery of uromodulin (Tamm-Horsfall protein): From tubulointerstitial nephropathy to chronic kidney disease. *Kidney Int*. 2011;80(4):338-347. doi:10.1038/ki.2011.134
35. Lozano-Ramos I, Bancu I, Oliveira-Tercero A, Armengol MP, Menezes-Neto A, Del Portillo HA, et al. Size-exclusion chromatography-based enrichment of extracellular vesicles from urine samples. *J Extracell Vesicles*. 2015;4(2015):1-11. doi:10.3402/jev.v4.27369
36. Crivianu-Gaita V, Romaschin A, Thompson M. High efficiency reduction capability for the formation of Fab' antibody fragments from F(ab)2 units. *Biochem Biophys Reports*. 2015;2:23-28. doi:10.1016/j.bbrep.2015.04.004
37. van der Pol E, de Rond L, Coumans FAW, Gool EL, Böing AN, Sturk A, et al. Absolute sizing and label-free identification of extracellular vesicles by flow cytometry. *Nanomedicine Nanotechnology, Biol Med*. 2018;14(3):801-810. doi:10.1016/j.nano.2017.12.012
38. Liu Y, Li S, Rong W, Zeng C, Zhu X, Chen Q, et al. Podocyte-Released Migrasomes in Urine Serve as an Indicator for Early Podocyte Injury. *Kidney Dis (Basel, Switzerland)*. 2020;6(6):422-433. doi:10.1159/000511504
39. Birková A, Oboril J, Kréta R, Čižmárová B, Hubková B, Šteffeková Z, et al. Human fluorescent profile of urine as a simple tool of mining in data from autofluorescence spectroscopy. *Biomed Signal Process Control*. 2020;56:101693. doi:10.1016/J.BSPC.2019.101693
40. Hong G, Antaris AL, Dai H. Near-infrared fluorophores for biomedical imaging. *Nat Biomed Eng*. 2017;1(1):1-22. doi:10.1038/s41551-016-0010
41. Gankema AAF, Li B, Nieuwland R, Pol E van der. Automated fluorescence gating and size determination reduce variation in measured concentration of extracellular vesicles by flow cytometry. *Cytom Part A*. Published online 2022. doi:10.1002/cyto.a.24665
42. Correll VL, Otto JJ, Risi CM, Main BP, Boutros PC, Kislinger T, et al. Optimization of small extracellular vesicle isolation from expressed prostatic secretions in urine for in-depth proteomic analysis. *J Extracell Vesicles*. 2022;11(2). doi:10.1002/jev2.12184
43. Li Y, Nese A, Lebedeva N V., Davis T, Matyjaszewski K, Sheiko SS. Molecular tensile machines: Intrinsic acceleration of disulfide reduction by dithiothreitol. *J Am Chem Soc*. 2011;133(43):17479-17484. doi:10.1021/ja207491r

SUPPLEMENTARY DATA

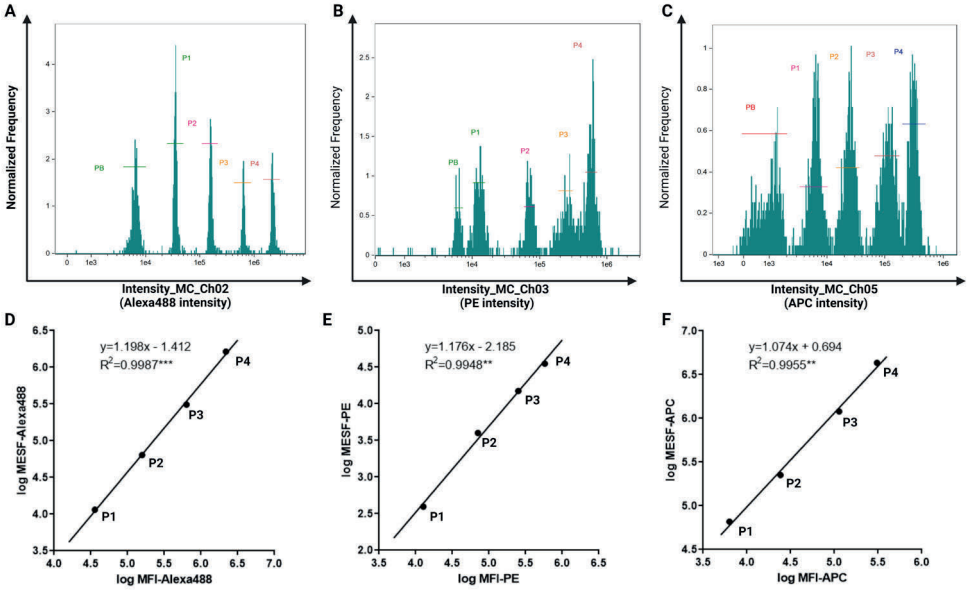

Supplementary Figure S1 - Calibration of MESF detection of IFCM based on standardized fluorescent beads. (**A** ~ **C**) IFCM measured 5 populations of beads per kit with standardized MESF-Alexa488 (**A**), MESF-PE (**B**), or MESF-APC (**C**). (**D** ~ **F**) The regression analysis between log MESF and log MFI for Alexa488 (**D**), PE (**E**), or APC (**F**). Regression formulas were calculated based on non-blank populations (P1-4), and the R^2 denoted the regression coefficient. Marks: ***$p < 0.001$; **$p < 0.01$. **Abbreviations:** MESF, molecules of equivalent soluble fluorochrome; MFI, median fluorescent intensity; IFCM, imaging flow cytometry; PB: blank population.

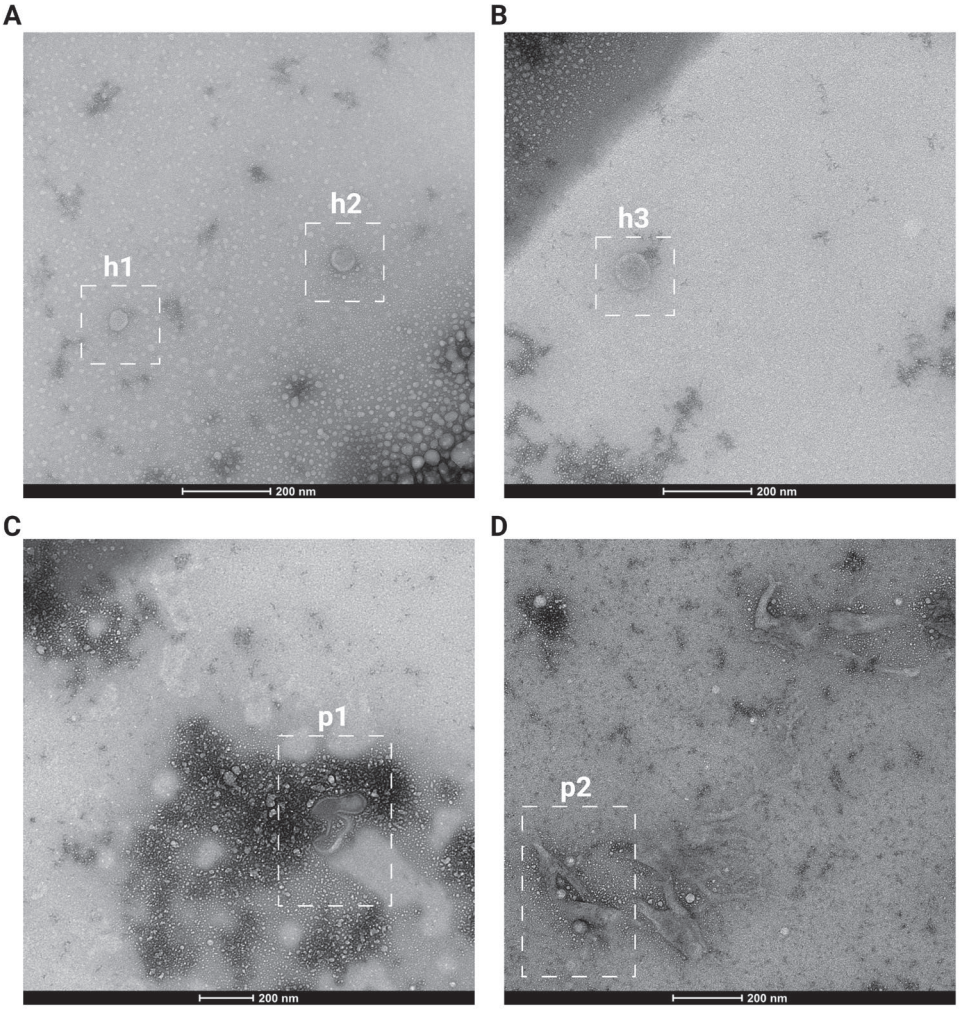

Supplementary Figure S2 - The large-area pictures obtained from transmission electron microscopy showing urinary extracellular vesicles from healthy individuals (**A** & **B**) and kidney transplant recipients (**C** & **D**).

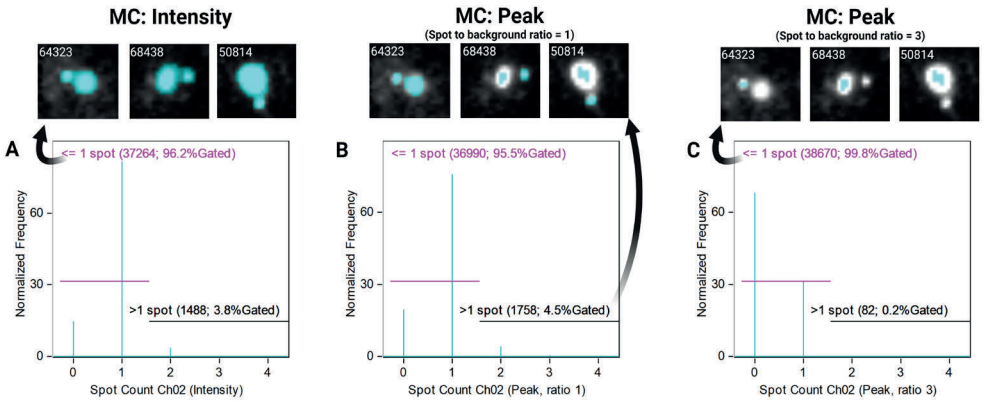

Supplementary Figure S3 - Distinguish singlets from multiplets by calculating spot count based on different MCs: Intensity MC (**A**) or Peak MC (**B** and **C**). (**C**) used a higher spot-to-background ratio than (**B**). At the top of (**A** ~ **C**), typical images of Ch02-positive doublets and corresponding MC (blue area) were shown. Object numbers were presented at the top left corner of each image. Black arrows denoted in which gate these events were included. Each gate's name gave the counts and percentage of gated events (Counts; %Gated). **Abbreviations:** MC, masks combined.

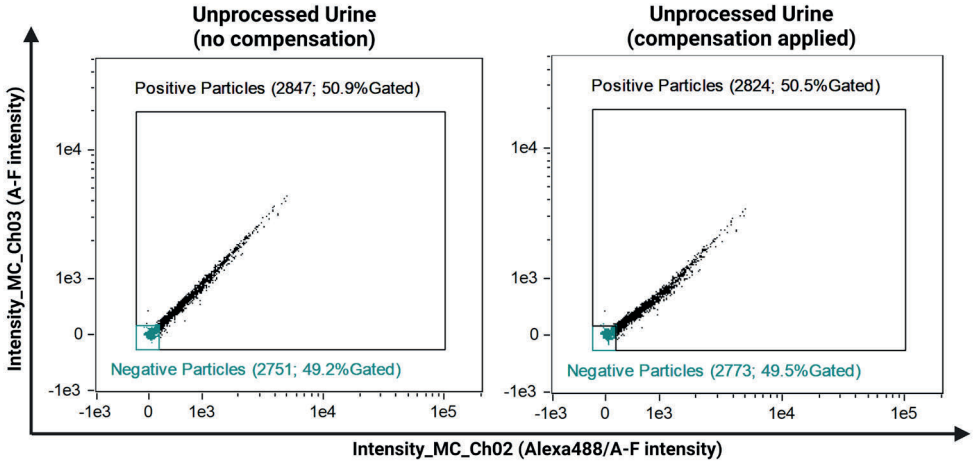

Supplementary Figure S4 - The fluorescent properties of autofluorescent particles in the unprocessed and unlabeled urine with or without compensation applied. The compensation matrix is the same as in Figures 3G & 3H in the results.

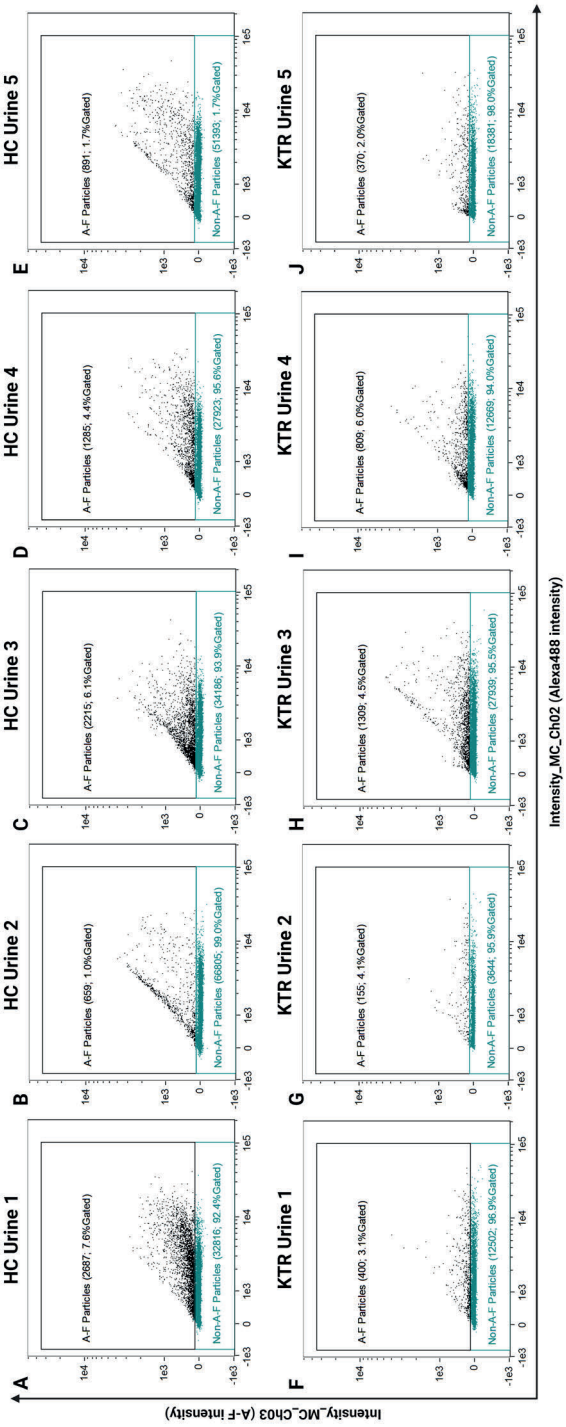

Supplementary Figure S5 - The "Non-A-F Particles" gate and compensation matrix obtained from Figure 3G can be applied to distinguish uEVs from A-F particles in other healthy control (HC) or kidney transplant recipient (KTR) urine samples. All urine samples were stained by CD63-Alexa488 and CD63-APC without any further treatments.

4

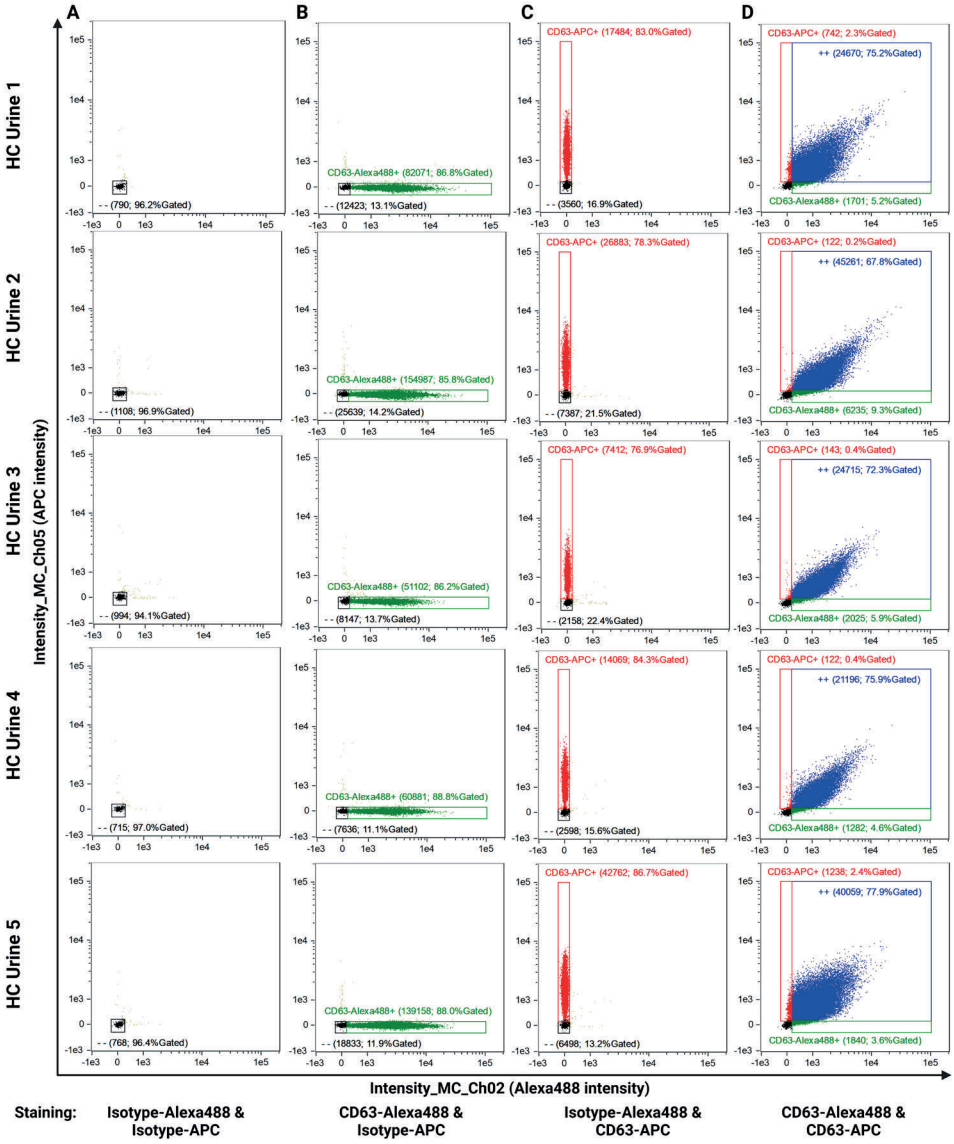

Supplementary Figure S6 - Isotype and single staining set up the fluorescence thresholds. Data from all healthy control (HC) urine samples were presented here. Each gate's name showed the counts and percentage of gated events (Counts; %Gated). **Abbreviations:** ++, double-positive.

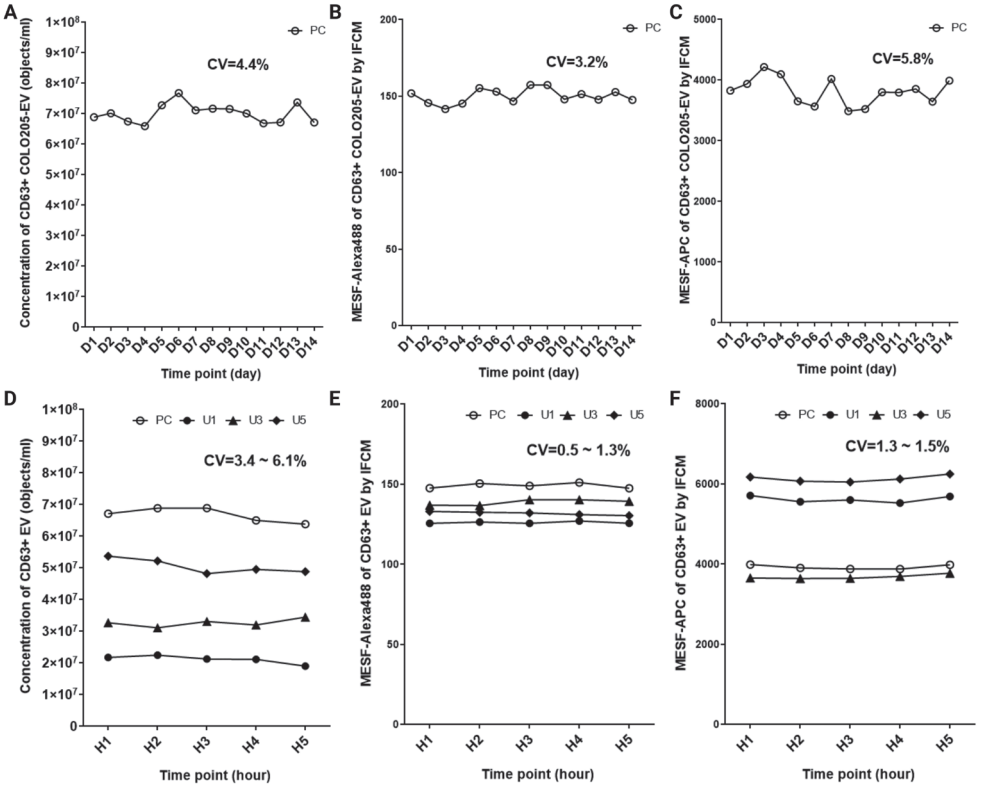

Supplementary Figure S7 - Inter- and intra-assay reproducibility to detect CD63+ uEV by IFCM. (**A - C**) Individually repeated IFCM experiments measured the concentration, MESF-Alexa488, and MESF-APC of CD63+ EV from the positive control (COLO205 cell line supernatant) on 14 separate days. The CV represented the reproducibility of IFCM. (**D - F**) One IFCM experiment repeatedly measured the concentration, MESF-Alexa488, and MESF-APC of CD63+ EV from the positive control (n=1) and healthy urine sample (n =3) at each hour. The range of CV was shown (n =4). **Abbreviations:** CV, coefficient of variation; MESF, molecular equivalent soluble fluorochrome; MFI, median fluorescence intensity; PC, positive control.

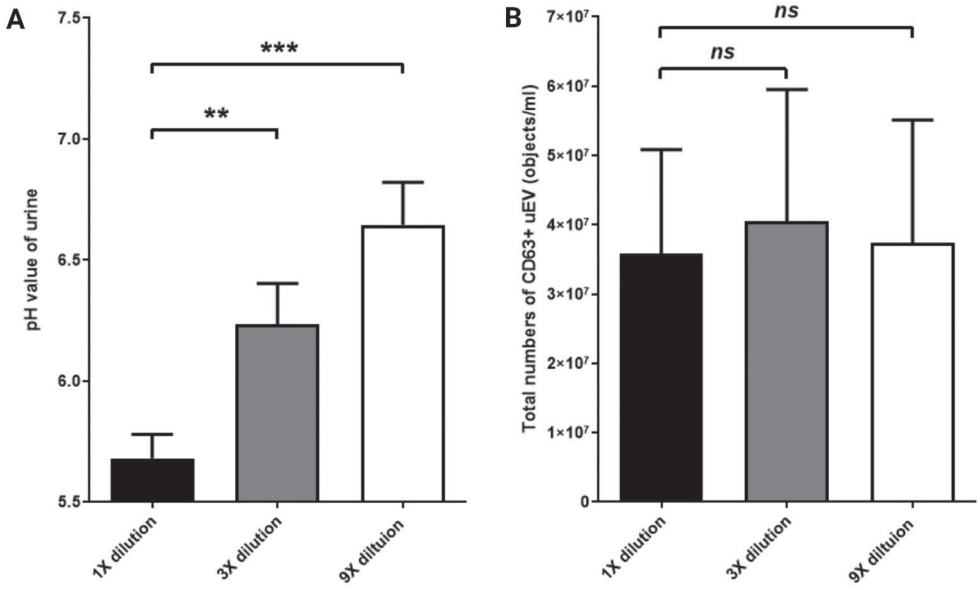

Supplementary Figure S8 - The influence of dilution on urinary pH and its effect on uEV detection by IFCM. (**A**) The effects of dilution on the total numbers of CD63+ uEV by IFCM. Marks: ***$p < 0.001$; **$p < 0.01$. (**B**) The total numbers of uEV were calculated by correcting the concentrations with dilution times. Marks: ns, no significance. **Abbreviations:** A-F, auto-fluorescence; IFCM, imaging flow cytometry.

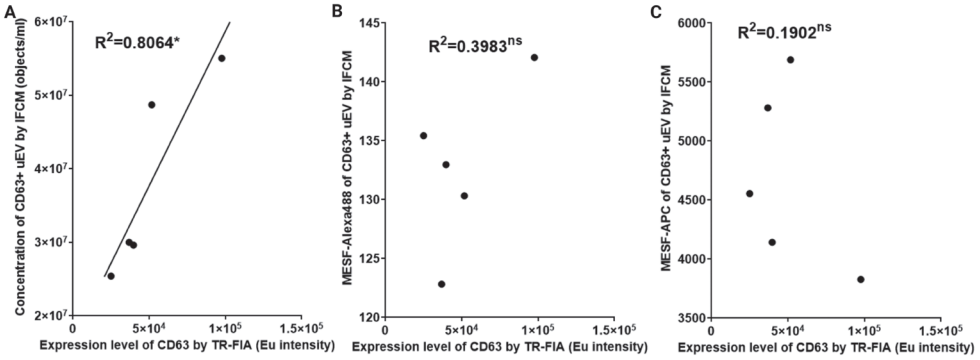

Supplementary Figure S9 - Comparison between IFCM and TR-FIA. (**A**) Correlation (linear regression) analysis between CD63+ uEV concentrations by IFCM and CD63 expression levels in healthy urine samples (n = 5). (**B** and **C**) Correlation (linear regression) analysis between the MESF of CD63+ uEV by IFCM and CD63 expression levels in healthy urine samples (n = 5). R^2 denoted the coefficient of regression. Marks: *$p < 0.05$; ns, no significance. **Abbreviations:** Eu, europium; IFCM, imaging flow cytometry; TR-FIA, time-resolved fluoroimmunoassay.

Clinical parameters	**Healthy controls (n = 5)**	**Kidney transplant recipient with acute kidney injury in 2 weeks post-transplantation (n = 5)**
Gender (male/female)	4/1	4/1
Pathology presented in biopsy	-	Rejection (n = 2); Acute tubular necrosis (n = 3)
Age (year)	27.80 ± 1.30	63.40 ± 7.73
Urine pH	5.68 ± 0.98	6.20 ± 0.45
Urinary total protein concentration (g/L)	0.07 ± 0.04	0.65 ± 0.30
Urinary creatinine concentration (mmol/L)	16.46 ± 7.76	8.80 ± 4.77

Supplementary Table S1 - Clinical parameters of enrolled subjects.

Built-in or self-made	**Feature**	**Mask**
Built-in	Intensity_MC_Ch02	MC
Built-in	Intensity_MC_Ch03	MC
Built-in	Intensity_MC_Ch05	MC
Built-in	Intensity_MC_Ch06	MC
Self-made	Spot Count Ch02	Peak (M02, Ch02, Bright, 1)
Self-made	Spot Count Ch05	Peak (M05, Ch05, Bright, 1)
Self-made	Spot Distance Min (Ch02 & Ch05)	Peak (M02, Ch02, Bright, 1) Or Peak (M05, Ch05, Bright, 1)

Supplementary Table S2 - All used features with MCs in the IFCM analysis.

Population	Beads-Alexa488				Beads-PE				Beads-APC			
	Median MESF	**Log MESF**	**Median MFI**	**Log MFI**	**Median MESF**	**Log MESF**	**Median MFI**	**Log MFI**	**Median MESF**	**Log MESF**	**Median MFI**	**Log MFI**
Blank population (PB)	NA	NA	6558.17	3.817	NA	NA	6227.22	3.794	NA	NA	1022.26	3.010
Population 1 (P1)	11489	4.060	35776.51	4.554	394	2.595	11489	4.10493	65829	4.818	11489	3.800
Population 2 (P2)	63949	4.806	157752.88	5.198	3997	3.602	63949	4.84879	224599	5.351	63949	4.385
Population 3 (P3)	311396	5.493	633621.63	5.802	14988	4.176	311396	5.400839	1200523	6.079	311396	5.055
Population 4 (P4)	1636893	6.214	2183260.06	6.339	35476	4.550	1636893	5.763067	4324094	6.636	1636893	5.488

Supplementary Table S3 - Characteristics of MESF-standardized beads.
Manufacturers provided the MESF values, and the MFI values were obtained in the detection by IFCM**.** The MFI values of non-blank populations (P1-4) were used to calculate the MESF. **Abbreviations:** MESF, molecules of equivalent soluble fluorochrome; MFI: median fluorescence intensity; NA: not available.


REJECTED
REJECTED
REJECTED

PART II

Validation: Detection of EVs in Kidney Transplantation

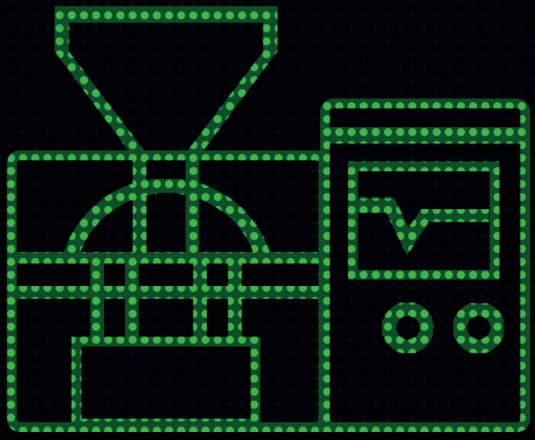

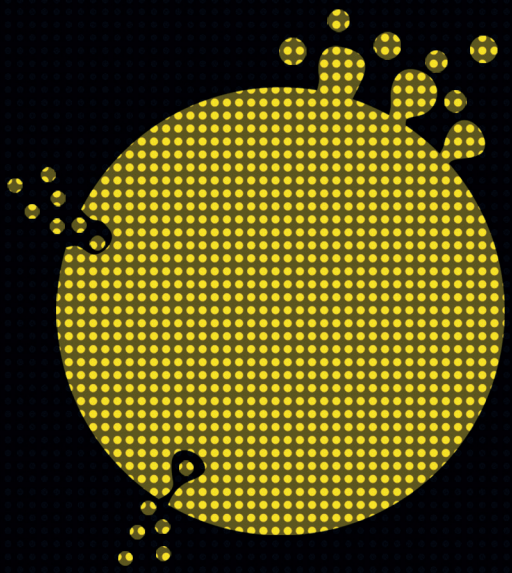

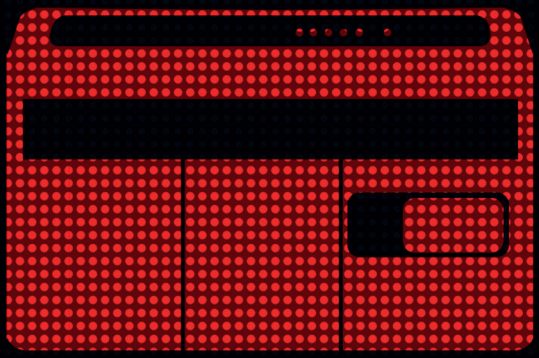

05

EXTRACELLULAR VESICLES RELEASED DURING NORMOTHERMIC MACHINE PERFUSION ARE ASSOCIATED WITH HUMAN DONOR KIDNEY CHARACTERISTICS

Wouter W. Woud[1], Asel S. Arykbaeva[2,3], Ian P.J. Alwayn[2,3], Carla C. Baan[1], Robert C. Minnee[4], Martin J. Hoogduijn[1] , Karin Boer[1]

[1]Erasmus MC Transplant Institute, Department of Internal Medicine, University Medical Center Rotterdam, Rotterdam,
[2]Department of Surgery, Leiden University Medical Center, Leiden,
[3]LUMC Transplant Center, Leiden University Medical Center, Leiden
[4]Erasmus MC Transplant Institute, Department of Surgery, Division of Hepato-Pancreato-Biliary and Transplant Surgery, Erasmus MC, University Medical Center Rotterdam, The Netherlands

Transplantation 106(12):p 2360-2369, December 2022.

ABSTRACT

Extracellular vesicles (EVs) are tissue-specific particles released by cells containing valuable diagnostic information in the form of various biomolecules. The characterization of EVs released by kidney grafts during Normothermic Machine Perfusion (NMP) may present a promising avenue to assess graft status prior to transplantation.

Here, we phenotyped and determined the concentrations of EVs in the perfusate of 8 discarded expanded-criteria donor (ECD) human kidneys during 6 hours of NMP. Perfusate samples were taken at 0/60/180/360 minutes and examined with Nanoparticle Tracking Analysis (NTA) and Imaging Flow Cytometry (IFCM). Using IFCM, EVs were identified by their expression of common EV markers CD9, CD63 and CD81 (tetraspanins) in combination with either platelet endothelial cell adhesion molecule (CD31), pan-leukocyte protein (CD45) or CFSE fluorescence.

NTA measurements revealed the release of nanoparticles <400 nm into the perfusate during NMP. With IFCM, tetraspanin protein signatures of the released nanoparticles were characterized, and the majority (~75%) of CFSE+ EV were found to be CD81+ while ~16% were CD9+ and ~8% CD63+. Correlation analysis of concentrations of identified EV subset with crude donor characteristics and NMP viability characteristics revealed significant correlations with cold ischemia time, donor age, and renal flow.

Our findings demonstrate that discarded ECD kidney grafts release distinct subsets of EV during NMP. As these subsets correlate with well-established indicators of transplant outcome, EV might represent new potential candidates for assessment of kidney graft quality.

INTRODUCTION

The shortage of available grafts, the increasing number of patients on the waiting list and the general aging of the population has led to an increased use of expanded-criteria donor (ECD) grafts as well as grafts procured from donation after circulatory death (DCD) [1]. Both ECD and DCD grafts are associated with poorer transplant outcomes when compared to organs from standard criteria donors [2, 3]. This is in part because older grafts are more susceptible to ischemia reperfusion injury (IRI) as well as the inability to fully recover after transplantation as a consequence of natural loss of nephron mass [4]. Moreover, an essential problem with the usage of these kidneys is the lack of quality measures needed to guide the clinician in deciding whether to accept or decline the organ. Combined, this has forced the transplant community to 1) investigate new methods of organ preservation aimed at reducing IRI and 2) to develop tools to evaluate transplant kidney quality.

The most recent development in organ preservation is normothermic machine perfusion (NMP). In contrast to hypothermic machine perfusion (HMP), NMP aims to restore cellular metabolism and function to the organ, which is achieved through circulation of a warm, oxygenated red blood cell based solution through the organ prior to transplantation [5, 6]. Because metabolism is activated, NMP offers the possibility to assess graft status prior to transplantation through monitoring of the perfusion dynamics and analysis of biomarkers in the perfusion fluids [2, 5, 7, 8].

Potential candidates for the assessment of graft status are Extracellular vesicles (EVs). EVs are lipid bilayer membrane structures (30-8000 nm in diameter [9]) involved in cellular communication [10]. They express surface markers and carry a 'cargo' (e.g. DNA / RNA / Lipids / proteins [11]), both of which are thought to be indicative for the status of its cell of origin. EVs are excreted by virtually all cell types and are considered an excellent, stable biomarker platform as their cargo is protected from fragmentation and degradation by the lipid bilayer [12]. In transplantation, levels of (human) donor-specific EVs in animal models have been shown to be associated with acute rejection of the allograft [13, 14]. Additionally, miRNA, RNA and proteomic profiling of EVs obtained from kidney preservation fluids [15] or the urine of kidney recipients [16, 17] suggest that EV analysis might enable kidney health assessment and prognostication in kidney transplantation.

Despite the interest in EVs as biomarker, the analysis of EVs is hampered by their physical characteristics such as their small size, low epitope copy number [18], the

variety of protein markers depending on the cell source and the confinement of some markers on the luminal side of the vesicles [19, 20]. In the absence of a specific marker, EVs are identified by their expression of common markers such as CD9, CD63 and CD81. These proteins have a broad tissue distribution, belong to the tetraspanin superfamily, and are enriched on EVs [21].

Previously, our group was able to quantify the release of nanoparticles (such as protein aggregates and EVs) by ECD kidneys during NMP [22]. Here we apply our recently developed Imaging Flow Cytometry (IFCM)-based methodology [23] to identify, phenotype and determine the concentration EVs ≤ 400 nm in diameter released by discarded human kidney grafts during NMP. We show the identification of distinct EV subsets based on their tetraspanin profile in combination with the detection of esterase activity, platelet endothelial cell adhesion molecule (CD31) or the pan-leukocyte protein (CD45). Additionally, in the absence of post-transplantation kidney function, we perform correlation analysis of the identified EV subsets with crude donor and NMP viability characteristics to explore the potential clinical implications of the identified EVs.

RESULTS

Kidneys release nanoparticles during NMP

To study whether discarded kidneys release nanoparticles during NMP, perfusate samples drawn at 0 / 60 / 180 / 360 minutes were measured with NTA to determine the particle concentration and size distribution (Figure 1). We observed a baseline concentration of $2.05E^{9}$ ± $2.13E^{8}$ particles/mL (mean ± standard deviation, area under the curve) within the perfusate prior to contact with the kidney (T0, baseline perfusate). Total particle concentrations were observed to increase over time during NMP: $1.96E^{10}$ ± $7.21E^{8}$ / $2.54E^{10}$ ± $7.85E^{8}$ / $3.06E^{10}$ ± $6.27E^{8}$ objects/mL at 60, 180 and 360 minutes respectively. Average particle size was established to be < 400 nm irrespective of the time of sampling.

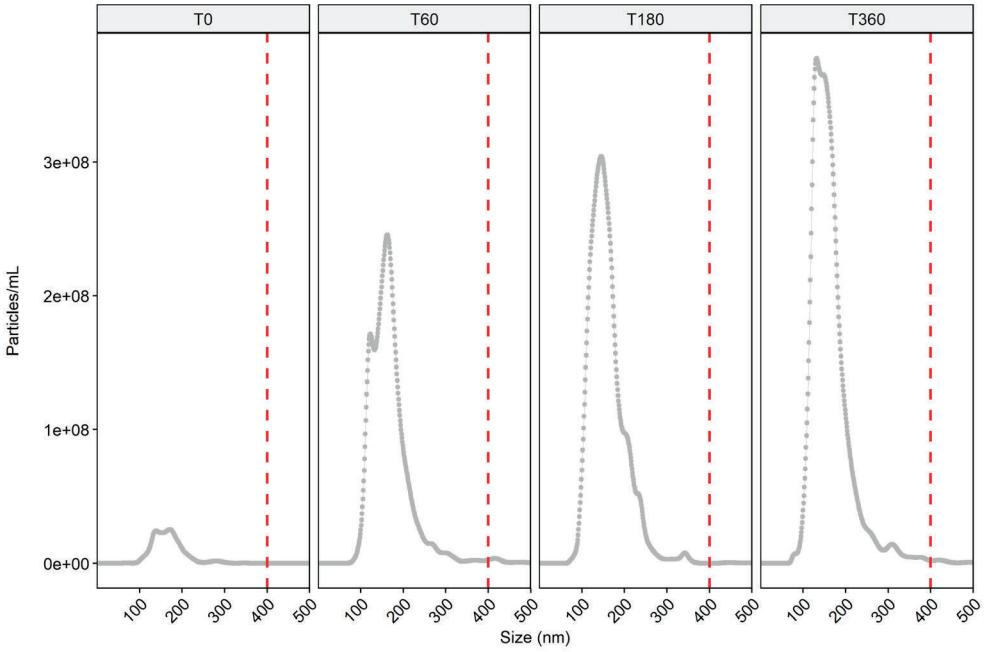

Figure 1 – Concentration and size distribution of particles released by a discarded kidney during (60, 180, 360 minutes - T60 / T180 / T360, respectively) Normothermic Machine Perfusion (NMP), as measured with Nanoparticle Tracking Analysis (NTA). T0 represents particle concentration and size distribution in baseline perfusate. A clear increase in particle concentration was observed during NMP and the majority of released particles were observed to be < 400 nm (red striped lines).

Detergent treatment confirms the analysis of EVs

Next, we stained the perfusate samples of 8 NMP kidneys with CFDA-SE and an anti-tetraspanin antibody mixture (anti-CD9/anti-CD63/anti-CD81) labeled with APC, and measured the samples with Imaging Flow Cytometry (IFCM). CFDA-SE is converted to CFSE (carboxyfluorescein succiminidyl ester) by intravesicular esterases and was used to discriminate EVs from contaminating agents such as lipoproteins. Identification and validation of single EV measurement by IFCM is presented in Supplemental Figure 1.

For the stained samples, we observed CFSE and tetraspanin single positive – but very few double-positive (< 70 events) - fluorescent background events in perfusate samples drawn before exposure to the kidney (T0). Samples collected after 60 / 180 / 360 minutes of NMP showed increases in fluorescent events across all three populations (CFSE single-positive, Tetraspanin single-positive and CFSE and

Tetraspanin double-positive). Detergent treatment was applied on each sample after initial acquisition to discriminate between vesicular and non-vesicular events (Figure 2A).

First, concentrations of fluorescent objects before and after detergent treatment were compared for each time point. For CFSE single-positive objects we observed a ~69% / 72% / 76% reduction in concentration after detergent treatment at T60 / T180/ T360, respectively (Figure 2B). This implies that a large fraction (~31% / 28% / 24%) of these objects represent non-vesicular (background) objects as they had not been dissolved by the detergent treatment. Consequently, the CFSE single-positive population was excluded from further analysis. Detergent treatment reduced Tetraspanin single-positives (Figure 2C) and CFSE and Tetraspanin double-positives (Figure 2D) with 97.7% ± 0.004% and 99.8% ± 0.0002% respectively (normalized mean ± standard deviation, average reduction over all time points). Background levels (concentrations obtained after detergent treatment) of the Tetraspanin single-positive population resided around ~E^6 objects/mL whereas the level of CFSE and Tetraspanin double-positives were observed to be <E^5 objects/mL. These background levels were comparable to the baseline perfusate (T0) samples before detergent treatment.

Second, for Tetraspanin single-positive and CFSE and Tetraspanin double-positive populations we observed ~43 / 56 / 57 and ~507 / 572 / 471 – fold increases after 60 / 180 / 360 minutes of NMP compared to T0, respectively (comparison of means). Comparing the mean concentration of Tetraspanin single-positive events to the mean concentration of Tetraspanin and CFSE double-positive events revealed ~4 / 5 / 6 – fold differences at 60 / 180 / 360 minutes of NMP respectively – indicating that less CFSE-positive EVs were detected as NMP progressed.

Taken together, these findings indicate that 1) kidneys release EVs during NMP and 2) different subpopulations (based on tetraspanin expression in combination with the absence/presence of CFSE) can be identified using IFCM.

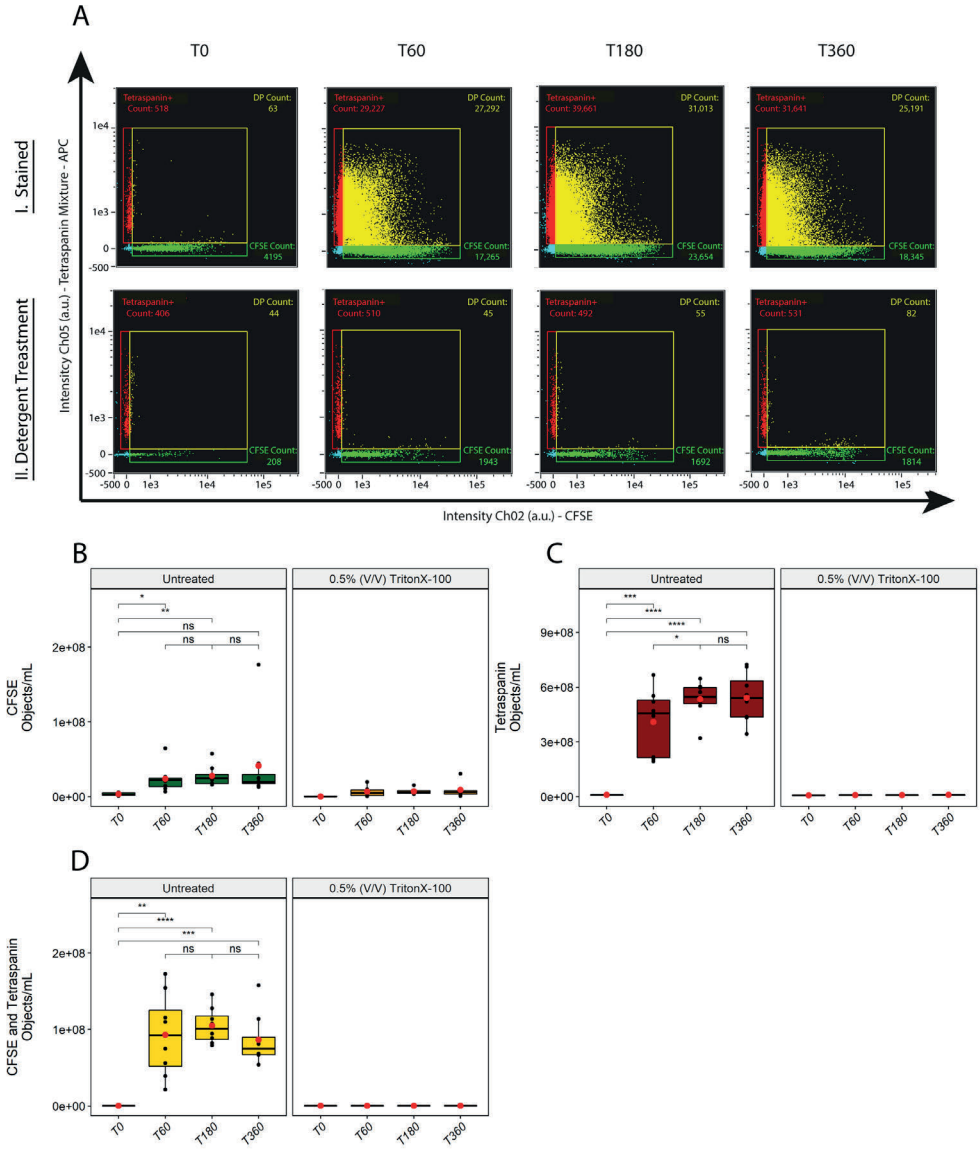

Figure 2 – EV release by discarded kidneys during NMP. **A**) Representative scatter plots of a stained sample (top row) and the corresponding sample after detergent treatment (bottom row) for each time point measured (T0 / T60 / T180 / T360, minutes). **B-D**) Concentrations of single-positive CFSE, single-positive Tetraspanin and double-positive CFSE and Tetraspanin fluorescent objects/mL respectively, before and after detergent treatment per time point measured. Red dots/black lines representing the means/median values of each time point, respectively. Statistical analysis (unpaired t-test, two sided, (*$p < 0.05$, **$p < 0.01$, ***$p < 0.001$, ****$p < 0.0001$)) showed significant release of EV for all time points with respect to pre-NMP samples (**C** and **D**); Only the Tetraspanin single positive population (**C**) showed a significant increase from 60 to 180 minutes. No significant differences in release were observed between the other time points/populations.

EVs released during NMP express predominantly CD81

Following the identification of EVs on the basis of tetraspanin expression, we examined the tetraspanin distribution on the released EVs by staining the NMP samples with CFDA-SE and one of the individual components of the anti-tetraspanin antibody mixture at a concentration equal to that used within the mixture. We observed that CD81+ EVs represented ~ 86% and ~74% of single and double-positive fluorescent events, respectively, across the time points analyzed (normalized average of time points 60, 180 and 360 minutes, Figure 3A-B). CD9+ and CD63+ EV were found to represent ~5% and ~9% of the detected single positive, and 16% and 9% of the double-positive fluorescent events, respectively.

These findings show that tetraspanin CD81 is predominantly expressed on EVs released during NMP. Additionally, CFSE fluorescence was detected in conjunction with all tetraspanins studied, indicating that esterase activity is not exclusively linked to any of these tetraspanins.

Leukocyte and Endothelial-derived EVs are released during NMP

Surface proteins on EVs reflect the biological origin of their parental cells and next we determined the expression of either CD45 (as pan-leukocyte marker) or CD31 (as prominent endothelial marker) on the CD81+ EVs. We performed double staining of the perfusates with anti-CD45 or anti-CD31 in combination with anti-CD81, and analyzed each fluorescent population. For the CD45 single-positive events, ~52% of the events were still present after detergent treatment (data not shown) and no significant increases were observed during NMP when compared to baseline perfusates (T0 – $2.7E^{7}$ ± $5.4E^{6}$ objects/mL) despite high specificity of the mAbs as indicated by isotype controls (dashed lines - $1.7E^{5}$ ± $9.8E^{4}$ objects/mL, Figure 3C). Thus, CD45 single-positive EVs could not be discriminated from baseline perfusate signals. Analysis of CD81 and CD45 double-positive events yielded ~97.5% reduction after detergent treatment, a significant 18 / 19 / 23 – fold difference in objects/mL at 60 / 180 / 360 minutes of NMP compared to T0 ($2.6E^{6}$ ± $1.4E^{5}$ objects/mL), and high specificity as indicated by isotype controls ($4.3E^{4}$ ± $4.1E^{4}$ objects/mL, Figure 3C).

Analysis of CD31 single-positive events showed ~91% reduction after detergent treatment, 11 / 14 / 13 – fold difference in objects/mL at each time point of sample drawing compared to T0 ($2.6E^{5}$ ± $1.8E^{4}$ objects/mL), and an isotype background of

$6.39E^5 \pm 4.67E^5$ objects/mL. For CD81 and CD31 double-positive events, we observed >99% reduction of fluorescent events after detergent treatment, ~950 / 1130 / 1100 – fold difference in objects/mL at each time point of sample drawing compared to T0 ($2.2E^4 \pm 1.9E^4$ objects/mL), and an isotype background of $3.28E^4 \pm 1.53E^4$ objects/mL (Figure 3D).

We then analyzed the relative abundance of both double-positive EV populations with respect to the total CD81+ EVs detected. We observed that 6.8% of CD81+ EVs expressed the endothelial cell marker CD31, and only 1.7% of CD81+ EVs was found to express the common leukocyte antigen CD45 (Figure 3E). The far majority of CD81+ EVs detected (91.5%) were found to not express either of the measured markers.

In summary, these data show that leukocyte and endothelial-derived EVs are released during NMP. Surprisingly, the majority of CD81+ EVs did not bear either of the studied markers.

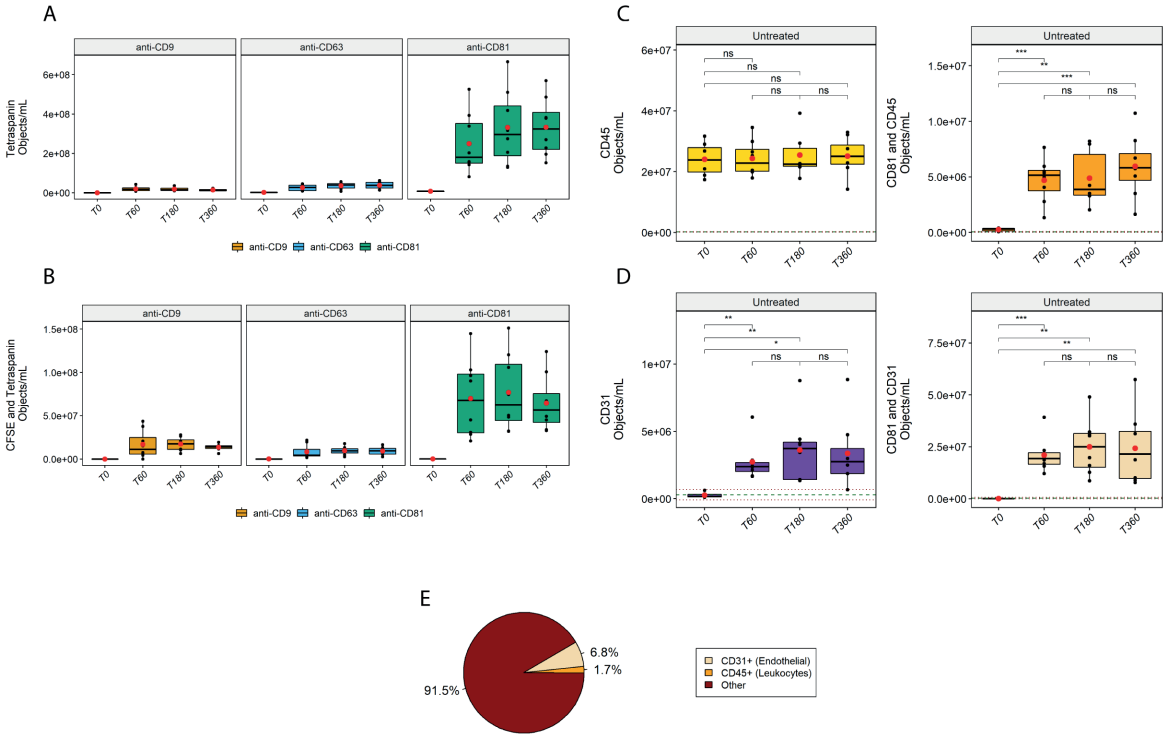

Figure 3 – Phenotyping and determination of the concentration of EVs released during NMP. NMP samples were stained with CFDA-SE in combination with anti-CD9, anti-CD63 or anti-CD81, acquired using IFCM and analyzed using the previously described gating strategies. **A**) Tetraspanin profile of tetraspanin single-positive objects. **B**) Tetraspanin profile of double-positive objects. Additionally, perfusates were stained with anti-CD81 (predominantly expressed on EVs released during NMP) in combination with **C**) anti-CD45 (as pan-leukocyte marker), or **D**) CD31 (as prominent endothelial marker). Significantly increased levels of EVs were detected compared to T0 for all identified subpopulations (*$p < 0.05$, **$p < 0.01$, ***$p < 0.001$, ****$p < 0.0001$), with the exception of CD45 single-positive EVs. Red dots/black lines representing the means/median values of each time point, respectively. Dashed lines: mean (green) ± standard deviation (darkred) of respective isotype controls (shown for **C** and **D**).
E) Assessment of cellular origin of detected CD81+ EVs. For all time points and samples, the fraction of double-positive events compared to total detected CD81+ events (both single-positive and double-positive events) was calculated and averaged to determine the relative abundance of double-positive EVs for either population, thus allowing deduction of cellular origin.

Concentrations of released EV subsets are correlated with donor demographics and NMP viability characteristics.

To determine whether the identified EV subsets can be used as indicators of kidney quality prior to transplantation, we performed correlation analysis between the concentrations of EVs released by each individual kidney, and – in the absence of post-transplantation kidney function - donor kidney characteristics (specified in Table 1) and NMP viability characteristics (as a surrogate for kidney quality - specified in Table 2).

Analysis of anti-CD9 single-positive EVs and CIT revealed a significant correlation after 360 minutes of NMP (R^2 = 0.64, p = 0.017, Figure 4A), whilst no significant correlations with CIT were obtained for any of the other single-positive EV subsets. For CFSE and anti-CD9 double-positive EVs, significant correlations were observed for all time points analyzed ($p < 0.05$, Figure 4B). Additionally, CFSE and anti-CD63 double-positive EV were found to be significantly correlated after 60 minutes (R^2 = 0.79, p = 0.003) – but not after 180 and 360 minutes – of NMP (Figure 4C). Analysis of CD81 and CD45 double-positive EVs revealed a positive correlation with donor age after the first 60 minutes of NMP only (R^2 = 0.81 and p = 0.0023, Figure 4D). Anti-CD31 single-positive EVs were found to be the only EV subset that showed significant correlations with an NMP viability characteristic. For all time points analyzed, a positive correlation between concentrations of CD31+ EVs and renal blood flow was observed (Figure 4E), whilst negative correlations were found with intrarenal vascular resistance (Figure 4F). Although we did observe trends between some of the other donor kidney characteristics or NMP viability characteristics (e.g., kidney weight or impact of initial cold preservation – SCS vs HMP) and EV subset concentrations, none were found to be statistically significant.

The differences between the individual ECD kidneys in terms of NMP viability characteristics (Table 2) did not correspond to e.g. matched kidney grafts retrieved from the same donor (K1 and K2, K7 and K8) or transplantability assessment post NMP (K3 and K5 were deemed of sufficient quality to be transplantable after 6 hours of NMP) when analyzing each kidney individually (as represented by the different shapes in Figure 5).

Altogether, these findings indicate that the release of the identified EV subsets are differentially correlated to donor kidney characteristics and NMP viability characteristics.

Kidney ID	K1 #	K2 #	K3	K4	K5	K6	K7 ##	K8 ##
Donor age (years)	71	71	65	53	70	63	75	75
Donor gender (F/M)	M	M	M	M	M	M	M	M
Donor type (DBD/DCD)	DCD	DCD	DBD	DCD	DBD	DCD	DCD	DCD
Cause of death	Circ/CA	Circ/CA	CVA	CVA/CI	Trauma: capitis	Circ/CA	CVA/ICB	CVA/ ICB
Warm ischemia time (minutes)	11	11	/	27	/	19	14	14
Cold ischemia time (hours)	2,2	6,4	17,8	14,3	14,3	16,1	11,4	20,2
Initial cold preservation (SCS/HMP)	SCS	SCS	HMP	SCS	SCS	HMP	SCS	SCS
Left/right kidney	Left	Right	Left	Right	Left	Right	Right	Left
Reason for discard	Severe kidney failure	Severe kidney failure	Suspected malignancy	Duodenum perforation	Hepatitis B	Surgical, ureter too short	Medical reasons	Medical reasons
Kidney weight (g)	266	352	377	519	298	308	410	213

Table 1 – Donor and retrieval data. F, female; M, male; DCD, donation after cardiac death; DBD, donation after brain death; Circ/CA, circulational: cardiac arrest; CVA, cerebral vascular bleeding; CI, cerebral ischemia; ICB, intra cerebral bleeding; SCS, static cold storage HMP, hypothermic machine perfusion; # and ## represent paired kidney grafts from same donor.

Kidney ID	K1 #	K2 #	K3	K4	K5	K6	K7 ##	K8 ##
Renal Blood Flow (mL/minute/100gr)								
T60	16,54	84,66	83,02	12,14	30,54	23,38	16,58	25,82
T180	31,20	84,66	93,37	25,63	36,24	35,71	24,39	31,92
T360	45,11	91,48	151,19	30,44	47,99	66,23	58,54	92,96
Intrarenal Vascular Resistance (mmHg/mL/minute)								
T60	1,7	0,25	0,24	1,19	0,82	1,04	1,1	1,36
T180	0,9	0,25	0,21	0,56	0,69	0,68	0,75	1,10
T360	0,63	0,23	0,13	0,47	0,52	0,37	0,31	0,38
Total Urine Production (mL) – Accumulated								
T60	0	71,5	63	0	0	0	0	0
T180	0	100,5	120	0	3	12	0	0
T360	0	116	303	0	3	48	0	0
Transplantability assessment post NMP	No	No	Yes	No	Yes	No	No	No

Table 2 – NMP viability characteristics as measured at 60 / 180 / 360 minutes of NMP. After 6 hours of NMP, each ECD kidney was judged by an independent transplant surgeon and nephorologist whether or not the organ was deemed suitable for transplantation (transplantability assessment). # and ## represent paired kidney grafts from same donor.

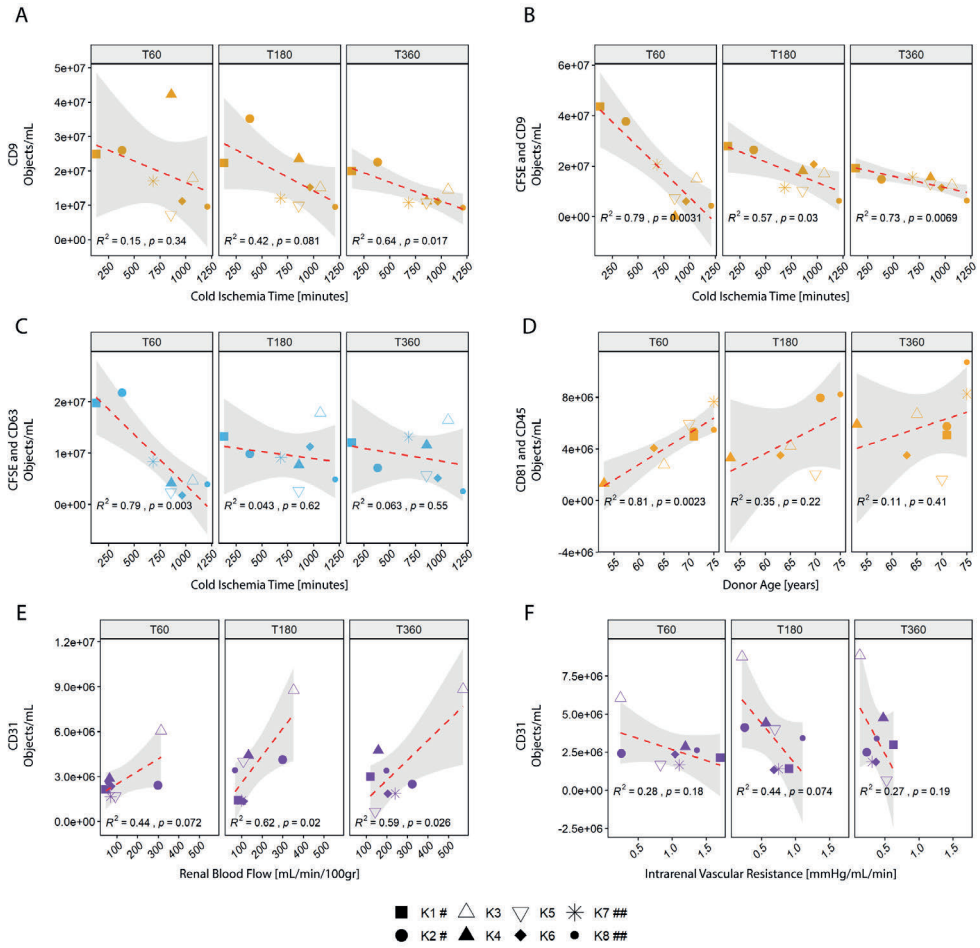

Figure 4 – Correlation analysis of concentrations of released EV subsets with donor kidney and NMP viability characteristics. Overview of the EV subsets for which statistically significant correlations were obtained. Analysis of **A**) correlation between CD9 single-positive, **B**) CFSE and CD9 double-positive, and **C**) CFSE and CD63 double-positive EVs with CIT. **D**) Analysis of correlation between CD81 and CD45 double-positive EVs with donor age. Most notably, correlation analysis of CD31 single-positive EVs with **E**) renal flow and **F**) intrarenal vascular resistance showed inverse correlations. EV concentrations as excreted by each ECD kidney are represented by shape, with open triangles representing K3 and K5 (which were deemed transplantable post NMP – Table 2). # and ## represent paired kidney grafts from same donor.

DISCUSSION

A major benefit of machine perfusion is that it allows for the assessment of kidney quality prior to transplantation through analysis of biomarkers (such as EVs) in the perfusion fluid [2, 5, 7]. Especially during NMP, where cellular metabolism becomes activated, the monitoring of EVs may be a promising tool to infer kidney quality prior to transplantation [26]. Additionally, the characterization of EVs released during NMP may shed light on the origin and composition of EVs released into circulation of transplant recipients and increase our understanding of (distal) immune responses [27-29]. However, although EVs are subject to intensive biomarker studies in various fields [13, 30, 31], little is currently known regarding EV release by kidney grafts during NMP and its association with kidney status.

In this observational study we examined and characterized the release of EVs by discarded human ECD kidneys during NMP. In line with our previous findings [22], we found that the majority of released nanoparticles were <400 nm in size irrespective of the time of sampling and that total particle concentrations increased as NMP progressed. Using IFCM we found that EV concentrations significantly increased during the first 60 minutes of NMP and that concentrations remained relatively stable during the remainder of the NMP procedure (up to 6 hours). We reason that the observed stabilization of EV concentrations are due to the establishment of an equilibrium between EV biogenesis and breakdown during NMP and/or uptake by (endothelial) cells of the kidney. These findings may contribute to the debate regarding optimal NMP perfusion times: since EV release is considered an active process [32], release dynamics during NMP may be dependent on the metabolic status of the kidney graft.

Examination of the tetraspanin profile on the released EVs revealed that the majority of detected EVs expressed tetraspanin CD81. Recently, CD81 has been shown to serve as a regulator of B cell signaling through complex formation with CD19 at the plasma membrane. Upon B cell activation CD19 dissociates from CD81 while in naïve B cells CD81 (epitope 5A6) is complexed by CD19 [33]. Given that the majority of detected EVs released during 6 hours of NMP expressed the CD81 epitope 5A6, the fusion of these CD81+ EVs with recipient B cells may have a dampening effect on B cell signaling as the addition of extra CD81 onto the B cell membrane may affect CD81-CD19 dissociation kinetics. Additionally, it has been shown that allograft-derived EVs bearing intact donor MHC molecules (CD63+ and CD9+CD81+

EV subsets) are able to cross-decorate and activate alloreactive recipient B cells in a mouse skin-transplant model [29]. In a human setting, this cross-decoration might be facilitated by CD81+ EVs.

When determining the origin of detected CD81+ EVs, we found only marginal co-localization of CD81 with endothelial and hematopoietic markers CD31 and CD45. However, part of the CD81+CD31+ EV may represent CD45+ EVs derived from monocytic origin. Additionally, the low percentages of colocalization may be influenced by the usage of mAbs targeting extravesicular epitopes [20] (thus ignoring the presence of markers on the luminal side of EV). Moreover, the released particles were determined to be <400 nm (as shown by NTA, and selected in the IFCM analysis), and therefore were assumed to consist largely of exosomes. Exosomes form through inward budding of the membrane of early endosomes (forming multivesicular bodies in the process) which eventually fuse with the cell plasma membrane, releasing its content into the extracellular space [34]. Consequentially, it is hypothesized that not all exosomes necessarily bear parental cell surface markers – which may explain why >90% of CD81+ EVs were found to not be colocalized with either anti-CD31 or anti-CD45.

Correlation analysis of CFSE+ EVs and CIT revealed negative correlations for EVs bearing tetraspanins CD9 or CD63 (during the first 60 minutes of NMP) - but not CD81. Since CFDA-SE needs intravesicular esterases to acquire its fluorescent properties (CFSE+), these negative correlations may be explained by 1) the negative impact of CIT on cellular (and thus vesicular) enzyme (esterase) activity or 2) reduced release of EVs containing intravesicular esterases as a consequence of CIT. Diminished correlations of CFSE+ and CD9+/CD63+ double-positive EVs with CIT were found after 180 and 360 minutes of NMP – which might be explained by restoration of cellular metabolism during the course of NMP [5, 26].

As the perfusion pressure during NMP is fixed, the perfused kidneys autoregulate their blood flow according to intrarenal vascular resistance. The inverse correlation between low renal blood flow and high intrarenal vascular resistance during NMP has been described in literature, and has been associated with increased vascular injury or interstitial oedema [35]. We demonstrate that the release of CD31+ single-positive EVs (likely to be of endothelial origin) is positively correlated with renal blood flow, and consequently inversely correlated with intrarenal vascular resistance. As it is well-known that the endothelial cell layer of microvessels is a key modulator

of vasodilation through the synthesis and release of vasoactive substances [36], CD31 single-positive EVs might be indicative for kidney quality prior to transplantation. Recently, to aid clinicians in determining kidney quality during NMP, a scoring system has been developed based on the macroscopic appearance and thresholds of renal blood flow and urine output [35]. The presence of different EV subsets (such as CD31+ EVs) might be added – after extensive validation in transplanted cohorts – to this scoring system. Potential identification of other EV subsets and their correlation with kidney function post KTx may provide insight into 1) kidney quality, and 2) the specific compartment(s) of the kidney which are injured/functioning sub-optimally before transplantation. However, in the current work, correlation analysis of the other identified EV subsets with donor kidney characteristics or NMP viability markers did not result in any statistically significant correlations; either when analyzed as a group or when examining EV release for each kidney individually. Although K3 and K5 were determined to be of sufficient quality to be transplantable after 6 hours of NMP, we did not observe any trends that differentiated these kidneys from the other ECD kidneys during NMP for any of the markers examined in this study.

It must be noted that no direct inferences could be made between kidney quality prior to transplantation (or transplant outcome) and the released EV subsets as none of the kidneys studied were actually transplanted. Additionally, as these kidneys represent ECD kidneys the reported concentrations and observed correlations might be different for non-ECD kidneys. Another limitation of this study is the small sample size: the heterogeneity among the ECD kidneys with respect to e.g., cause of donor death and the type of organ storage might (further) impact the amount and/or subsets of EVs released. However, the observed correlations of different EV subsets with CIT and donor age during the first 60 minutes of NMP do indicate that EV release is related to well-established indicators of kidney quality: both CIT and donor age are known to be detrimental to kidney quality/transplant outcome [4, 37].

In conclusion, our findings demonstrate that discarded human ECD kidney grafts release different EV subsets during NMP, and that their release is correlated with well-established indicators of kidney quality such as CIT, donor kidney age, renal blood flow and intrarenal vascular resistance. The identification, quantification and phenotyping of kidney-derived EVs released during NMP may represent a starting point to study the role of EVs as potential biomarkers for kidney graft quality prior to transplantation. How and if the identified (and other) EVs subsets are correlated with kidney function post transplantation will be the focus of future research.

MATERIALS & METHODS

Ethical approval

Ethical approval (number B19.019) for experiments with discarded donor kidneys was granted by the Medical Ethical Committee of the Leiden University Medical Center (LUMC) and University Medical Center Groningen (UMCG). Research consent was obtained from the relatives of all donors prior to organ retrieval.

Procurement, preparation of the kidney, and sample drawing

The included kidney grafts (N=8) were procured from deceased donors according to Dutch national guidelines and were deemed untransplantable because of procurement-related factors or factors determined prior to retrieval (specified in Table 1). After in situ flushing of the abdominal organs with cold University of Wisconsin (UW) preservation solution, the kidneys were retrieved, preserved by either static cold storage (SCS) or HMP, and transported to the participating centers (LUMC or UMCG) where NMP was initiated and performed up to 6 hours (Figure 5). Upon arrival in the participating centers, kidney grafts were inspected and prepared for connection to the NMP circuit under sterile conditions, while the perfusion machine (Kidney Assist, Organ Assist, Groningen, The Netherlands) was primed. The NMP setup was primed as previously described in the PROPER study [24]. Kidneys were subjected to subsequent NMP when the Cold Ischemia Time (CIT) did not exceed 24 hours at arrival.

Perfusate samples were drawn prior to (0) and after 60 / 180 / 360 minutes of NMP, centrifuged at 3700 rpm at room temperature, and the supernatant was stored at -80 ^{0}C.

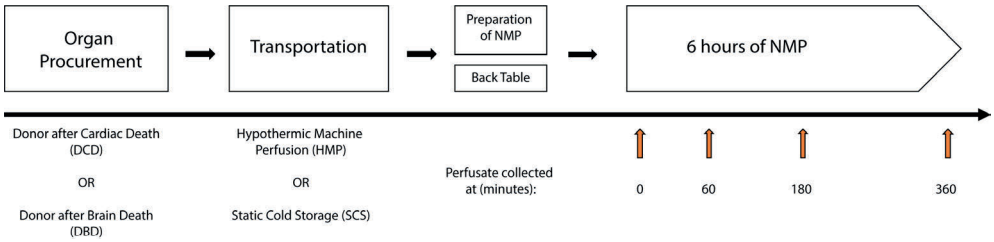

Figure 5 – Schematic overview representing procurement, transportation, preparation of the kidneys, and sample drawing.

Nanoparticle Tracking Analysis

Size distribution and concentration of nanoparticles within the perfusates were measured with the Malvern Panalytical NanoSight NS300 and analyzed with Nanoparticle Tracking Analysis (NTA) software version NTA 3.4 Build 3.4.003. Samples were diluted in 0.2 µm filtered PBS (fPBS) until 20 – 60 particles were in the field of focus during acquisition and 10 videos of 15 seconds were recorded with camera level 11 and analyzed with detection threshold 5.

Sample Labelling and Controls

Perfusates were stained with monoclonal antibodies (mAbs) and Carboxyfluorescein diacetate succinimidyl ester (CFDA-SE) as extensively described in our previous work [23] and detailed in SDC, Materials and Methods; Sample Labelling.

To ascertain EV measurements the following controls were applied, as recommended by the MIFlowCyt-EV framework [25]: buffer only, buffer with reagents, unstained samples, isotype controls, and detergent treatment, which aims to disrupt the membranous structure of EVs thereby allowing discrimination between biological and artificial events. Detergent treatment was performed by adding 20 µL of a 10% (V/V) TritonX-100 detergent to the samples followed by 30 minutes of incubation at room temperature prior to acquisition.

Data acquisition and analysis

All samples were acquired on an ImageStreamX MkII instrument (IS^{x}; Luminex). Settings as extensively described in our previous work [23] and detailed in SDC, Materials and Methods; Acquisition were used.

Data analysis was performed using Amnis IDEAS software (version 6.2). To ensure the analysis of EVs we 1) selected all particles with SSC intensities ≤ 900 a.u., and 2) identified and excluded coincidence detection by counting the number of fluorescent spots within the pixel grid for each event acquired; events showing multiple spots were excluded from analysis [23]. This gating strategy ensures the selection and analysis of single spot fluorescent particles ≤400 nm. Gating areas and cut-offs were established through identification of (fluorescent) populations in unstained and single stained samples, and arbitrary fluorescent intensities were converted into Equivalent Molecules of Fluorescence (ERF) values based on

previously published calibration data [23]. Lower and upper gating area cut-offs were defined as 677 – 112,201 ERF for BV421; 35.40 – 3776 ERF for CFSE; 206 – 14,770 ERF for PE; and 6.40 – 123 ERF for APC.

Statistical Analysis

Statistical analysis was performed using R version 4.0.2 and RStudio (RStudio Team (2016). RStudio: Integrated Development for R. RStudio, Inc., Boston, MA URL http://www.rstudio.com/.) version 1.1.463. Statistical significance between EV concentrations and binary data was determined through two-sided t-tests, 95% CI with unpaired data. Linear correlations with continuous variables were examined using the Pearson correlation method. R^2 values ≥ 0.6 and P values < 0.05 were considered significant.

ACKNOWLEDGMENTS

The authors would like to thank the members of the PROPER Consortium (PROlonged ex-vivo normothermic machine PERfusion for kidney regeneration) for setting up the study, provision of the normothermic machine perfusion samples and input in research design: Prof. Dr. Ian Alwayn, Prof. Dr. Rutger Ploeg, Dr. Dorottya de Vries, Dr. Volkert Huurman, Jason Doppenberg and Asel Arykbaeva from the Leiden University Medical Center, Prof. Dr. Henri Leuvenink, Dr. Robert Pol, Dr. Cyril Moers, Tim Hamelink, Veerle Lantinga and Leonie van Leeuwen from University Medical Center Groningen and Dr. Robert Minnee from the Erasmus Medical Center, Rotterdam, the Netherlands. Additionally, the authors would like to thank Manou van Alphen for her assistance with NMP sample measurements with IFCM.

AUTHOR CONTRIBUTIONS

W.W.W. participated in the research design, performance of the research, data analysis, article drafting and is the corresponding author. A.A. performed the normothermic machine perfusion of kidneys and provided perfusate samples. I.P.J.A. orchestrated the prolonged normothermic machine perfusion study design. C.C.B. participated in the research design. R.C. provided clinical expertise. M.J.H., K.B. participated in the research design and writing of the manuscript. All authors reviewed the manuscript and approved its final version.

CONFLICT OF INTEREST

The authors declare no conflicts of interest.

FINANCIAL DISCLOSURE

The authors declare no funding was received for this study.

REFERENCES

1. Summers DM, Watson CJ, Pettigrew GJ, Johnson RJ, Collett D, Neuberger JM, et al. Kidney donation after circulatory death (DCD): state of the art. Kidney Int. 2015;88(2):241-9.
2. Brat A, Pol RA, Leuvenink HG. Novel preservation methods to increase the quality of older kidneys. Curr Opin Organ Transplant. 2015;20(4):438-43.
3. Callaghan CJ, Harper SJ, Saeb-Parsy K, Hudson A, Gibbs P, Watson CJ, et al. The discard of deceased donor kidneys in the UK. Clin Transplant. 2014;28(3):345-53.
4. Barbari A, Stephan A, Masri MAK, G, Karam, A., Kilani HAD, I. Nephron Mass in Kidney Transplantation. Transplantation Proceedings. 2002;34(6):2401-2.
5. Hosgood SA, Saeb-Parsy K, Wilson C, Callaghan C, Collett D, Nicholson ML. Protocol of a randomised controlled, open-label trial of ex vivo normothermic perfusion versus static cold storage in donation after circulatory death renal transplantation. BMJ Open. 2017;7(1):e012237.
6. Vallant N, Wolfhagen N, Sandhu B, Hamaoui K, Cook T, Pusey C, et al. A Comparison of Pulsatile Hypothermic and Normothermic Ex Vivo Machine Perfusion in a Porcine Kidney Model. Transplantation. 2021;105(8):1760-70.
7. Moers C, Varnav OC, van Heurn E, Jochmans I, Kirste GR, Rahmel A, et al. The value of machine perfusion perfusate biomarkers for predicting kidney transplant outcome. Transplantation. 2010;90(9):966-73.
8. Xu J, Buchwald JE, Martins PN. Review of Current Machine Perfusion Therapeutics for Organ Preservation. Transplantation. 2020;104(9):1792-803.
9. Arraud N, Linares R, Tan S, Gounou C, Pasquet JM, Mornet S, et al. Extracellular vesicles from blood plasma: determination of their morphology, size, phenotype and concentration. J Thromb Haemost. 2014;12(5):614-27.
10. Pitt JM, Kroemer G, Zitvogel L. Extracellular vesicles: masters of intercellular communication and potential clinical interventions. J Clin Invest. 2016;126(4):1139-43.
11. Zaborowski MP, Balaj L, Breakefield XO, Lai CP. Extracellular Vesicles: Composition, Biological Relevance, and Methods of Study. Bioscience. 2015;65(8):783-97.
12. Minciacchi VR, Zijlstra A, Rubin MA, Di Vizio D. Extracellular vesicles for liquid biopsy in prostate cancer: where are we and where are we headed? Prostate Cancer Prostatic Dis. 2017;20(3):251-8.
13. Vallabhajosyula P, Korutla L, Habertheuer A, Yu M, Rostami S, Yuan CX, et al. Tissue-specific exosome biomarkers for noninvasively monitoring immunologic rejection of transplanted tissue. J Clin Invest. 2017;127(4):1375-91.
14. Habertheuer A, Ram C, Schmierer M, Chatterjee S, Hu R, Freas A, et al. Circulating Donor Lung-Specific Exosome Profiles Enable Noninvasive Monitoring of Acute Rejection in a Rodent Orthotopic Lung Transplantation Model. Transplantation. 2021.
15. Gremmels H, de Jong OG, Toorop RJ, Michielsen L, van Zuilen AD, Vlassov AV, et al. The Small RNA Repertoire of Small Extracellular Vesicles Isolated From Donor Kidney Preservation Fluid Provides a Source for Biomarker Discovery for Organ Quality and Posttransplantation Graft Function. Transplant Direct. 2019;5(9):e484.
16. Turco AE, Lam W, Rule AD, Denic A, Lieske JC, Miller VM, et al. Specific renal parenchymal-derived urinary extracellular vesicles identify age-associated structural changes in living donor kidneys. J Extracell Vesicles. 2016;5:29642.

17. Lozano-Ramos SI, Bancu I, Carreras-Planella L, Monguio-Tortajada M, Canas L, Juega J, et al. Molecular profile of urine extracellular vesicles from normo-functional kidneys reveal minimal differences between living and deceased donors. BMC Nephrol. 2018;19(1):189.
18. Welsh JA, van der Pol E, Bettin BA, Carter DRF, Hendrix A, Lenassi M, et al. Towards defining reference materials for measuring extracellular vesicle refractive index, epitope abundance, size and concentration. J Extracell Vesicles. 2020;9(1):1816641.
19. Simonsen JB. What Are We Looking At? Extracellular Vesicles, Lipoproteins, or Both? Circ Res. 2017;121(8):920-2.
20. Blijdorp CJ, Tutakhel OAZ, Hartjes TA, van den Bosch TPP, van Heugten MH, Rigalli JP, et al. Comparing Approaches to Normalize, Quantify, and Characterize Urinary Extracellular Vesicles. J Am Soc Nephrol. 2021.
21. Andreu Z, Yanez-Mo M. Tetraspanins in extracellular vesicle formation and function. Front Immunol. 2014;5:442.
22. Woud WW, Merino A, Hoogduijn MJ, Boer K, van den Hoogen MWF, Baan CC, et al. Nanoparticle Release by Extended Criteria Donor Kidneys During Normothermic Machine Perfusion. Transplantation. 2019;103(5):e110-e1.
23. Woud WW, Pol E, Mul E, Hoogduijn MJ, Baan CC, Boer K, et al. AN IMAGING FLOW CYTOMETRY-BASED METHODOLOGY FOR THE ANALYSIS OF SINGLE EXTRACELLULAR VESICLES IN UNPROCESSED HUMAN PLASMA. bioRxiv. 2022:2022.02.24.481807.
24. Arykbaeva AS, de Vries DK, Doppenberg JB, Engelse MA, Hankemeier T, Harms AC, et al. Metabolic needs of the kidney graft undergoing normothermic machine perfusion. Kidney Int. 2021.
25. Welsh JA, Van Der Pol E, Arkesteijn GJA, Bremer M, Brisson A, Coumans F, et al. MIFlowCyt-EV: a framework for standardized reporting of extracellular vesicle flow cytometry experiments. J Extracell Vesicles. 2020;9(1):1713526.
26. Elliott TR, Nicholson ML, Hosgood SA. Normothermic kidney perfusion: An overview of protocols and strategies. Am J Transplant. 2021;21(4):1382-90.
27. Quaglia M, Dellepiane S, Guglielmetti G, Merlotti G, Castellano G, Cantaluppi V. Extracellular Vesicles as Mediators of Cellular Crosstalk Between Immune System and Kidney Graft. Front Immunol. 2020;11:74.
28. Rutman AK NS, Saberi N, Tchervenkov J, Paraskevas S. Donor Kidney Perfusion Fluid Extracellular Vesicles as Markers of Graft Function [abstract]. Am J Transplant. 2020;20: https://atcmeetingabstracts.com/abstract/donor-kidney-perfusion-fluid-extracellular-vesicles-as-markers-of-graft-function/.
29. Zeng FC, Z. Chen, R. Shufesky, W.J. Bandyopadhyay, M. Camirand, G. Oberbarnscheidt, M.H. Sullivan, M.L.G. Baty, C.J. Yang, M.Q. Calderon, M. Stolz, D.B. Erdos, G. Pelanda, R. Brennan, T.V. Catz, S.D. Watkins, S.C. Larregina, A.T. Morelli, A.E. Graft-derived extracellular vesicles transported across subcapsular sinus macrophages elicit B cell alloimmunity after transplantation. Sci Transl Med. 2021;13(585).
30. McBride JD, Rodriguez-Menocal L, Badiavas EV. Extracellular Vesicles as Biomarkers and Therapeutics in Dermatology: A Focus on Exosomes. J Invest Dermatol. 2017;137(8):1622-9.
31. Karpman D, Stahl AL, Arvidsson I. Extracellular vesicles in renal disease. Nat Rev Nephrol. 2017;13(9):545-62.
32. Raposo G, Stoorvogel W. Extracellular vesicles: exosomes, microvesicles, and friends. J Cell Biol. 2013;200(4):373-83.

33. Susa KJ, Seegar TC, Blacklow SC, Kruse AC. A dynamic interaction between CD19 and the tetraspanin CD81 controls B cell co-receptor trafficking. Elife. 2020;9.
34. Doyle LM, Wang MZ. Overview of Extracellular Vesicles, Their Origin, Composition, Purpose, and Methods for Exosome Isolation and Analysis. Cells. 2019;8(7).
35. Hosgood SA, Barlow AD, Hunter JP, Nicholson ML. Ex vivo normothermic perfusion for quality assessment of marginal donor kidney transplants. Br J Surg. 2015;102(11):1433-40.
36. Durand MJ, Gutterman DD. Diversity in mechanisms of endothelium-dependent vasodilation in health and disease. Microcirculation. 2013;20(3):239-47.
37. Kayler L, Yu X, Cortes C, Lubetzky M, Friedmann P. Impact of Cold Ischemia Time in Kidney Transplants From Donation After Circulatory Death Donors. Transplant Direct. 2017;3(7):e177.

SUPPLEMENTARY DATA

Materials and Methods; Sample Labelling

EVs released by ECD kidneys during NMP were phenotyped and quantitated with Imaging Flow Cytometry. Samples were labelled with an anti-tetraspanin antibody mixture (consisting of anti-CD9/anti-CD63/anti-CD81), anti-CD31, anti-CD45, or CFDA-SE. All mAbs used - (CD9–APC, clone HI9a (6 µg/mL, Biolegend), CD63–APC, clone H5C6 (200 µg /mL, Biolegend), CD81–APC, clone 5A6 (200 µg /mL, Biolegend), CD31–BV421, clone WM-59 (50 µg/mL, BioLegend), CD45-PE, clone HI30 (12.5 µg/mL, BD Biosciences), IgG1,k-BV421, clone MOPC-21 (100 µg/mL, BioLegend); IgG1,k-APC, clone MOPC-21 (200 µg/mL, BioLegend); and IgG1,k-PE, clone MOPC-21 (12.5 µg/mL, BD Biosciences) - were centrifuged at 16,000 x *g* (to remove potential mAb clumps).Tetraspanin mAbs were diluted 30-fold in fPBS before staining (Final concentrations: CD9: 200 ng/mL, CD63: 6.6 µg/mL, CD81: 6.6 µg/mL); CD31-BV421 was diluted 1000-fold (Final concentration: 50 ng/mL); CD45-PE was used undiluted (Final concentration: 12.5 µg/mL).

A 50 µM Carboxyfluorescein diacetate succinimidyl ester stock solution (Vybrant™ CFDA-SE Cell Tracer Kit, Invitrogen) was prepared according to the manufacturers' instructions and, similar to the mAbs, centrifuged for 10 minutes at 16,000 x *g*.

Staining was performed by adding 30 µL of perfusate followed by addition of the diluted mAbs into a pre-determined volume of fPBS (V_{tot} = fPBS + sample + mAbs = 130 µL) followed by O/N incubation at 4 ^{0}C, with 2.5 ng anti-CD9, 83 ng anti-CD63, 83 ng anti-CD81, 0.25 ng anti-CD31, and 156 ng anti-CD45 per test. Staining with CFDA-SE was performed by adding 100 µL of the stock solution to the samples followed by 30 minutes of incubation at room temperature in the dark. All samples were brought to a total volume of 380 µL using fPBS before IFCM measurements.

Materials and Methods; Acquisition

Perfusate samples were interrogated with IFCM (ImageStreamX MkII, Luminex) to phenotype and quantitate Extracellular Vesicles. Lasers were turned on as applicable per fluorophore and set to their maximum power (488 nm : 200 mW, 642 nm :150 mW) with the exception of the 785 nm SSC laser (1.25 mW). Data was acquired over a time period of 180 seconds – to standardize among samples – using the 60x objective with fluidics set to 'low speed / high sensitivity'. This resulted in a flow speed of 43.59 ± 0.07 mm/sec (mean ± standard deviation). Core size was set at 6 µm, autofocus was activated and the 'Remove Speedbead' was option unchecked.

BV421 fluorescence signals were collected in channel 1 (435–505-nm filter), CFSE signals were collected in channel 2 (505–560 nm filter), PE fluorescence signals were collected in channel 3 (560–595-nm filter), APC signals in channel 5 (642–745 nm filter), and SSC signals in channel 6 (745–785 nm filter). Particle enumeration was achieved through the advanced fluidic control of the IS^{x} coupled with continuously running speed beads, resulting in the "objects/mL" feature within the IS^{x} Data Exploration and Analysis Software (IDEAS®).

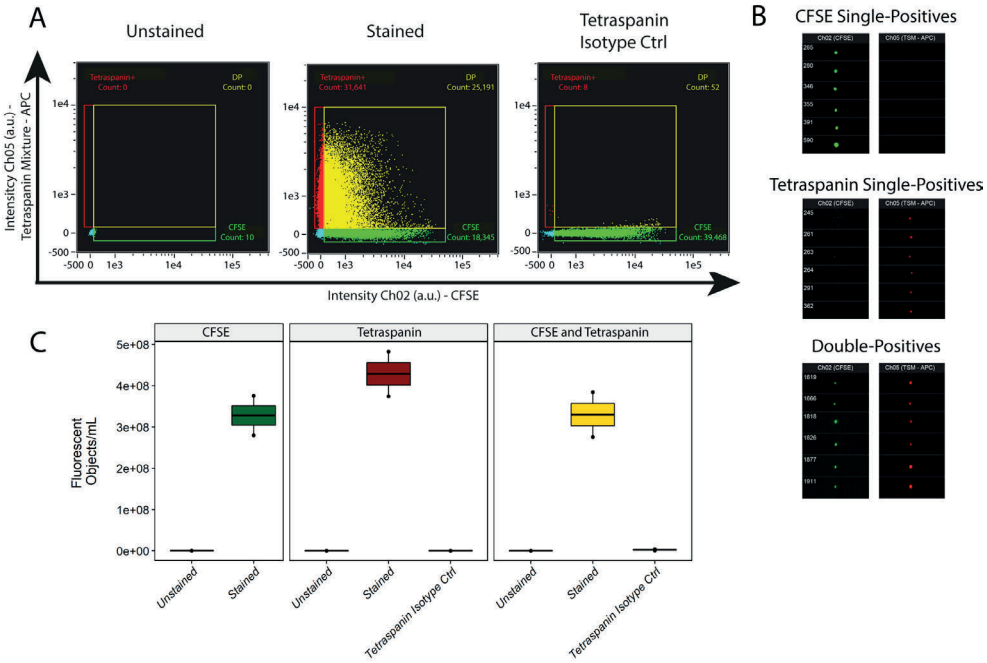

Supplementary Figure 1 – Identification and validation of single EV measurements using Imaging Flow Cytometry (IFCM). **A**) From left to right: fluorescence intensity scatterplots representative for unstained, stained (CFDA-SE & anti-tetraspanin antibody mixture (anti-CD9/anti-CD63/anti-CD81)), and isotype control end-point NMP perfusate samples (T = 360 minutes). Fluorescent populations were established on the basis of unstained and single-stained end-point NMP samples (data not shown). **B**) Visual examination of events representative for each fluorescent population demonstrated the selection and subsequent analysis of particles showing single spot fluorescence (no coincidence events), indicating the selection and analysis of single EVs. **C**) Quantification of fluorescent events in each gate for unstained, stained and isotype control (N=2), showing the specificity of our staining protocol. In unstained samples, no fluorescent events were observed indicating that no auto-fluorescent events were detected. In stained samples, we observed concentrations of fluorescent events (>E^{8} objects/mL) well above unstained and isotype levels (<E^{5} Objects/mL), indicating that the fluorescent events acquired in samples stained with the anti-tetraspanin antibody mixture represent specific fluorescent positive events.

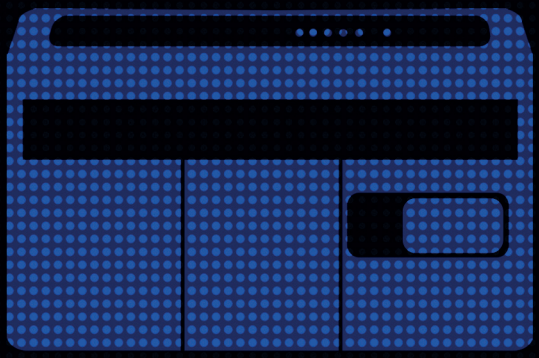

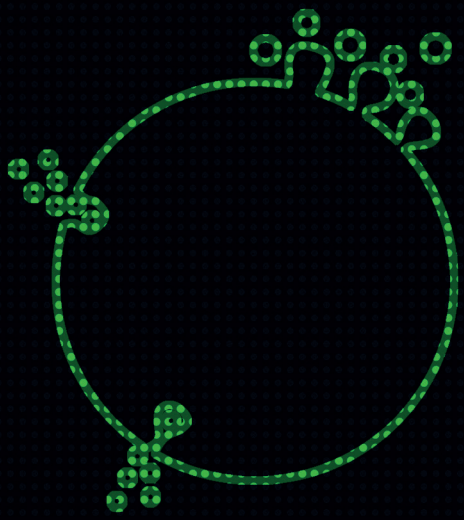

06

DIRECT DETECTION OF CIRCULATING DONOR-DERIVED EXTRACELLULAR VESICLES IN KIDNEY TRANSPLANT RECIPIENTS

Wouter W. Woud[1], Dennis A. Hesselink[1], Martin J. Hoogduijn[1], Carla C. Baan[1], Karin Boer[1]

[1]Erasmus MC Transplant Institute, Department of Internal Medicine, University Medical Center Rotterdam, Rotterdam, The Netherlands

Sci Rep. ***12****, 21973 (2022)*

ABSTRACT

Extracellular vesicles (EVs) are tissue-specific particles containing valuable diagnostic information. However, single EV analysis in blood is challenging due to their physical properties, the molecular complexity of plasma, and a lack of robust data interpretation methods. We assess the applicability of our recently-developed calibrated Imaging Flow Cytometry (IFCM)-based methodology to detect/characterize circulating tissue-specific EV subsets in the clinical setting of kidney transplantation.

Platelet-poor plasma (PPP) was generated from 36 HLA-A3 mismatched donor (HLA-A3+) and kidney transplant recipients (KTRs; HLA-A3-). Samples taken before transplantation, 3 days, 7 days, and 6 months after transplantation as well as before 'for-cause' kidney transplant biopsies were stained with anti-CD9 (plasma EV-marker) and anti-HLA-A3.

Before transplantation, no significant differences in total CD9+ EV concentrations were detected between donor and KTR samples. Tissue-specific EVs were identified as CD9+HLA-A3+. Serial dilution experiments of HLA-A3+ in HLA-A3- PPP showed that single CD9+HLA-A3+ EVs were detectable down to ~1% above the recipient 'self-signal'. After transplantation, CD9+HLA-A3+ EVs were detected above pre-transplantation concentrations in individuals with stable allograft function, but not in individuals with allograft dysfunction.

These results demonstrate the applicability of our calibrated IFCM-based methodology in the direct detection of tissue-specific EV subsets in clinical samples. We believe that this EV methodology is applicable in a variety of clinical contexts.

INTRODUCTION

Extracellular vesicles (EVs) are lipid bilayer-delimited membrane particles (30-8000 nm in diameter[1]) excreted by all cell types, which act as signaling intermediaries during normal homeostasis and during pathologic processes [2-6]. EVs carry proteins on their surface and/or a variety of macromolecules as cargo (e.g. DNA, RNA, lipids and proteins [7]), which are thought to reflect the status of their cell of origin. Indeed, EVs are regarded as "snapshots" of the status of their cell of origin and are examined to assess the presence of various diseases, e.g., cancer or viral infection [8, 9]. As EVs are present in body fluids (e.g. blood[1] / saliva[10] / urine[11, 12]), they are considered to be minimally-invasive biomarkers and so-called "liquid biopsies" [2, 13-16].

The quantification and characterization of EVs is hampered by their physical characteristics such as their small size, low epitope copy number [17], and the variety of protein markers depending on the cell source [18, 19], all of which contribute to the well-documented EV heterogeneity. The identification of EVs in plasma is further hindered by the molecular complexity of the plasma, which contains multiple elements (e.g., lipoproteins, cell debris and soluble proteins), that interfere with EV analysis [18, 20]. Moreover, a lack of robust methods and ambiguities in how data should be interpreted for EV analysis, makes comparison between studies challenging [21, 22].

To overcome the selection biases or introduction of artefacts that are introduced by performing commonly used EV isolation methods [18, 20], our group recently developed a standardized Imaging Flow Cytometry (IFCM)-based methodology for the direct measurement of single EVs ≤400 nm in diameter in diluted plasma samples, *without* prior isolation of EVs [23]. By omitting the need for sample isolation, this method has the potential to directly show the status of an individual by measuring distinct EV subsets, which is greatly beneficial for the monitoring of EVs in health and disease [21, 22].

Expanding upon the previously reported ability of our methodology to directly detect and discriminate human- and mouse-derived EVs in mixed human/mouse plasma samples [23], we here aimed to assess the ability of our protocol to identify, discriminate and analyze EV subsets within human patient plasma samples. To this end, the setting of clinical organ transplantation offers a unique scenario in which tissue-specific EVs originating from the allograft are released into circulation after transplantation [14, 24, 25]. We present an application of our methodology that allows for the direct detection of donor-derived EVs (dd-EVs) in plasma samples from kidney

transplant recipients (KTRs) on the basis of donor-recipient Human Leukocyte Antigen (HLA) mismatching by analyzing samples obtained before (control, no donor EVs present) and after (signal validation, detection of dd-EVs originating from the allograft) transplantation. Dd-EVs were measured against a background of recipient EVs in longitudinally collected KTR samples, and the dynamics of dd-EVs was monitored over time, as well as at time of 'for-cause' biopsy samples.

RESULTS

Direct detection of single EVs ≤ 400 nm in donor and KTR plasma samples

Compared to donor samples, the plasma composition of KTRs contains multiple elements (e.g., elevated creatinine and urea, (medicinal) waste products) which may interfere with single EV detection. Therefore, we first tested the ability of our protocol to directly detect single EVs ≤ 400 nm in diameter in plasma samples obtained from KTRs before transplantation. To this end, PPP samples from living donors (used as healthy controls) and KTRs were diluted in fPBS, and stained with either anti-CD9 (as common plasma EV marker) or isotype control (to infer labelling specificity) before analysis with IFCM. After initial acquisition, detergent treatment was applied on each anti-CD9 labeled sample to discriminate between vesicular and non-vesicular events.

Total concentrations of CD9+ objects/mL (Figure 1A) as measured in donor and KTR plasma samples were compared (Figure 1B). In the donor group, we detected $1.26E^{8}$ ± $6E^{7}$ objects/mL before, and $2.74E^{6}$ ± $6.7E^{6}$ objects/mL after detergent treatment. This represented an approximate 98% reduction – which implies that the majority of CD9+ events analyzed represent EVs. In the plasma samples obtained from KTRs, we detected $1.07E^{8}$ ± $5.3E^{7}$ objects/mL before, and $1.6E^{6}$ ± $5.1E^{6}$ objects/mL after detergent treatment (~97% reduction). No significant differences in total CD9+ EV concentrations were observed between both groups. Additionally, isotype staining resulted in $4.16E^{5}$ ± $3.85E^{5}$ objects/mL and $5.27E^{5}$ ± $1.22E^{5}$ objects/mL for donor and KTR samples, respectively, illustrating the high specificity of our labelling strategy (~300-fold difference with mAb labelling). Buffer only controls (measured each day of sample acquisition) showed no detectable events – indicating that no signals derived from antibody aggregates were detected.

These data suggest that our IFCM protocol is able to directly detect single CD9+ EVs in diluted plasma samples obtained from donors and KTRs before transplantation, despite the differences in molecular composition of the plasma between both groups.

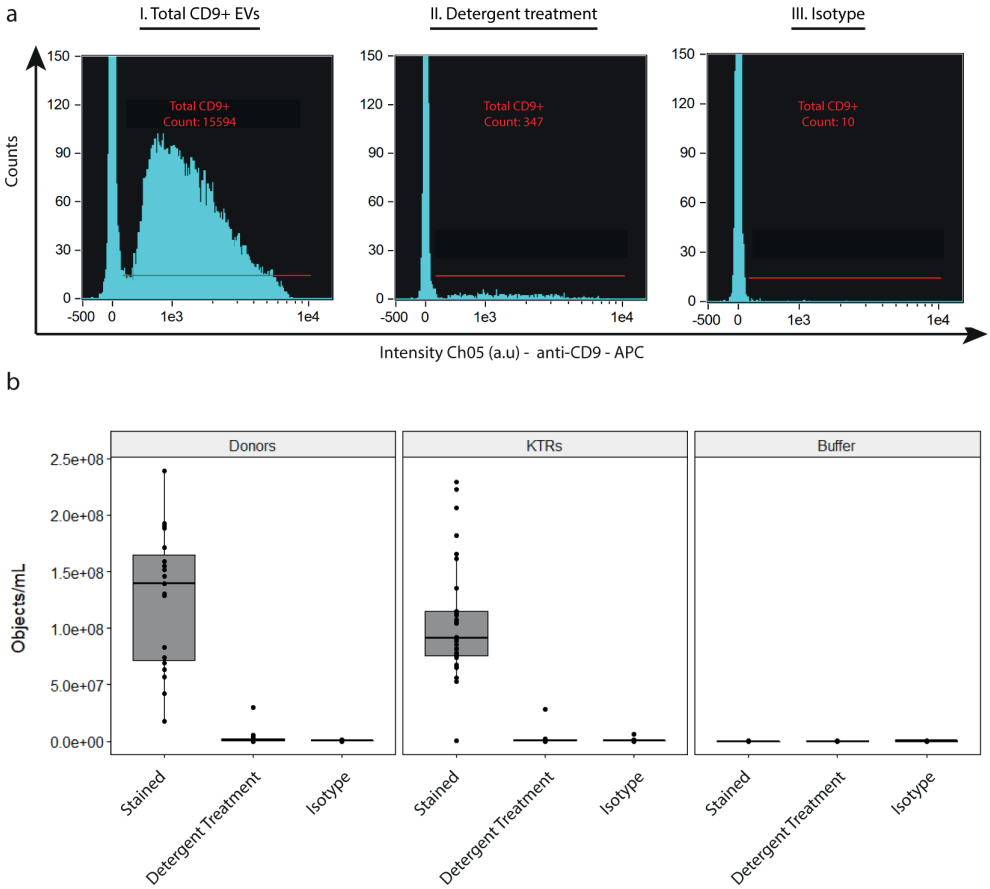

Figure 1 – Detection of CD9+ EVs in both (living) donor and kidney transplant recipient (KTR) samples obtained before transplantation. **A**) left to right: representative histogram plots of a PPP sample stained with anti-CD9, the same sample after detergent treatment (to discriminate between vesicular and non-vesicular events), and isotype staining. **B**) For each of the controls applied: quantification of total CD9+ EV concentrations as detected in PPP samples obtained from (living) donors, KTRs, and buffer only controls.

Identification and discrimination of single dd-EVs based on HLA phenotype

In order to identify dd-EVs in the circulation of KTRs after kidney transplantation, we assessed whether IFCM is capable of discriminating EVs based on HLA phenotype. To this end, we labelled the same PPP samples (donors – HLA-A3+, and recipients (before KTx) – HLA-A3-) with anti-CD9 and anti-HLA-A3, and performed the same control experiments as described above.

Figure 2A shows representative scatter plots for both a donor and recipient PPP sample analyzed with IFCM, before and after detergent treatment. Visual examination of events representative for each fluorescent population (before detergent treatment) demonstrated the selection and analysis of particles showing single spot fluorescence (no coincidence events), indicating the selection and analysis of single EVs [23] (Figure 2B).

For HLA-A3+ single-positive events, we observed only marginal reduction by detergent treatment, showing that these events are not representative of biological particles. Moreover, buffer only controls showed a high degree of fluorescent events, indicating that these signals are most likely representative of antibody aggregates (Figure 2C). Therefore, HLA-A3 single-positive fluorescent events were interpreted to not be representative of EVs, and were excluded from further analysis.

Analysis of CD9+HLA-A3+ double-positive fluorescent event concentrations in the KTR group showed that our assay produced background signals that varied among the different recipients (recipient-specific background) despite recipients all being HLA-A3 negative. Luminex single antigen assay for the anti-HLA-A3 antibody showed no cross reactivity of the antibody with other HLA epitopes (Supplementary Data S1 online), thus validating the specificity of the antibody. Comparison of CD9+HLA-A3+ concentrations between the donor and recipient groups ($1.60E^{7}$ ± $1.03E^{7}$ objects/mL vs $4.29E^{6}$ ± $4.48E^{6}$ objects/mL, respectively) showed that these double-positive fluorescent events can be used to discriminate samples on the basis of HLA phenotype. Concentrations of CD9+HLA-A3+ double-positive events as measured in donor PPP samples showed an approximately 96% reduction after detergent treatment, with concentrations after detergent treatment residing in the range of the isotype and buffer controls (Figure 2D). Consequently, CD9+HLA-A3+ double-positive fluorescent events were identified to represent EVs.

It should be noted that some samples showed low/minimal reduction in concentrations of fluorescent events detected after detergent treatment (as illustrated by 1 recipient sample in Figure 2D). These events were interpreted to not represent membrane-delimited vesicular events, but rather be indicative for protein complexes (which are unaffected by detergent treatment). To identify and exclude such samples from future analysis, we established a threshold of ≥95% reduction (in concentration) after detergent treatment for samples to be included in future analysis. This cut-off value was established to ensure that only samples are included that are representative (≥95%) of membrane-delimited particles (as opposed to protein complexes).

These observations show that our IFCM protocol is able to identify and discriminate single EVs in diluted PPP samples on the basis of their HLA phenotype by analyzing events that are both CD9+ (plasma EV marker) and HLA-A3+ (to discriminate between HLA-A3+ and HLA-A3- individuals).

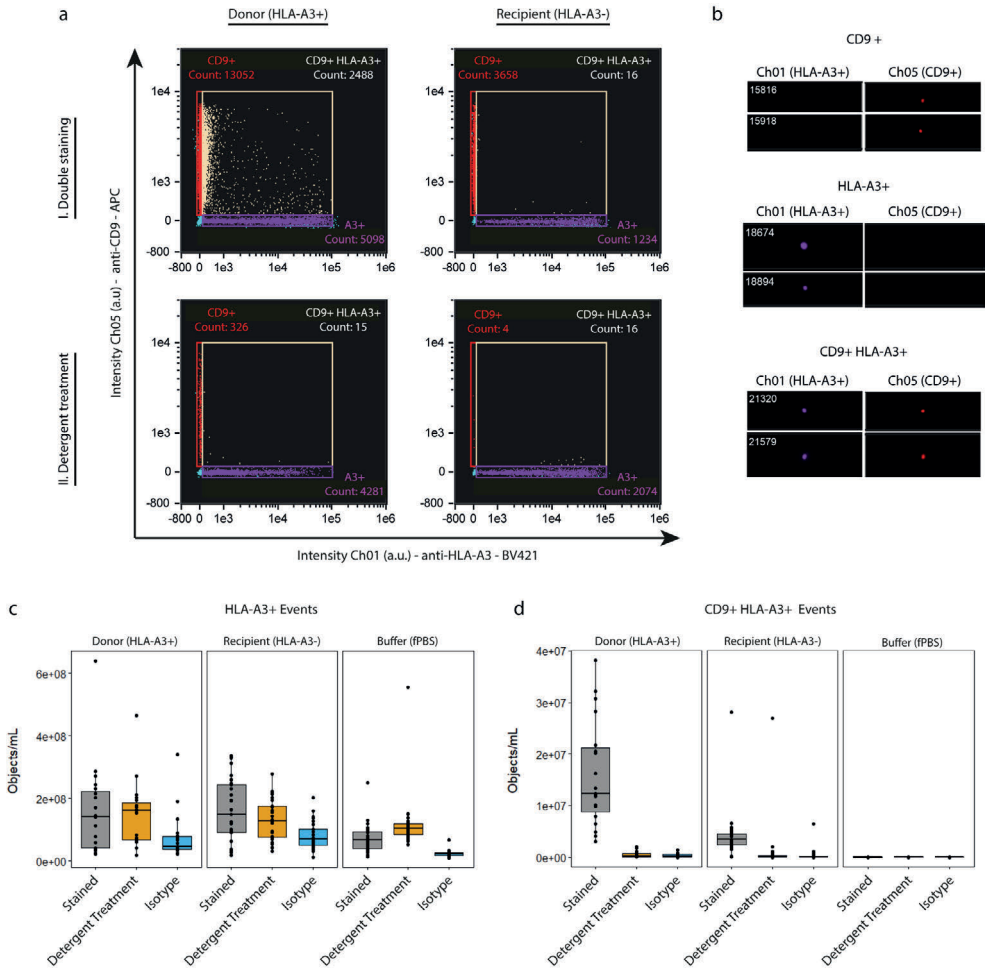

Figure 2 – Discrimination of EVs based on HLA phenotype. **A**) Representative scatter plots of an HLA-A3+ PPP sample (left) and an HLA-A3- PPP sample (right) stained with anti-HLA-A3 (X-axis) and anti-CD9-APC (Y-axis) before and after detergent treatment (top and bottom row, respectively). **B**) Visual examination of events representative for each fluorescent population demonstrated the selection and subsequent analysis of particles showing single spot fluorescence (no coincidence events), indicating the selection and analysis of single EVs. **C-D**) Concentrations of HLA-A3+ and CD9+HLA-A3+ fluorescent events in all pre-transplantation donor, recipient, and buffer only (control) samples before and after detergent treatment, and after isotype staining (grey, orange, and blue boxes, respectively). HLA-A3+ events were found to not be indicative of EV signals and were excluded from analysis. Double-positive events were found to be indicative of EV signals, as well as to be discriminative between HLA-A3+ and HLA-A3- PPP samples.

IFCM discriminates single CD9+HLA-A3+ EVs down to 1% above recipient-specific background

To determine the discriminative power of our IFCM protocol to detect CD9+HLA-A3+ EVs above (recipient-self) background signals in KTR samples, we serially diluted (2-fold dilutions) HLA-A3+ PPP into HLA-A3- PPP (5 matched donor-recipient couples), labelled these samples with anti-CD9 and anti-HLA-A3, and analyzed these with IFCM.

For each of the 5 donor-recipient couples, we quantified the concentrations of CD9+HLA-A3+ EVs as detected for each dilution step (Figure 3A). Similar to the previous observation, we observed that each of the 5 HLA-A3- PPP recipient samples (without any spiked-in HLA-A3+ PPP) yielded varying background concentrations. These were interpreted to represent the recipient-self sample-specific background (indicated with dashed green lines, Figure 3A). We were able to detect CD9+HLA-A3+ EVs above their respective sample-specific background concentrations down to ~100-fold dilution, thus with CD9+HLA-A3+ EVs being detectable ~1% above the recipient 'self' signal.

Next, we examined the accuracy of our IFCM protocol to detect single CD9+HLA-A3+ EVs in mixed plasma samples – as opposed to the coincidence detection of multiple particles recorded as a single event. For each individual (donor-in-recipient) dilution experiment, the concentrations of CD9+HLA-A3+ EVs as detected for each dilution step (range: 100% to 1.56% HLA-A3+ PPP) were analyzed using a linear regression model (Figure 3B). We observed that the concentrations of CD9+HLA-A3+ EVs were linearly proportional to the dilution factor, as indicated by the R^2 values. Additionally, analysis of the (standardized) fluorescent intensities as detected in both detection channels revealed that the fluorescent intensities were unaffected by serial dilution; mean: 1315 (range 1085 – 1604) ERF for BV421 (HLA-A3), and 29.5 (range 25.7 – 35.8) ERF for APC (CD9) (Figure 3C).

Taken together, these data indicate that IFCM is able to detect single dd-EVs directly in recipients' circulation if their fraction exceeds ~1% above their recipient specific background.

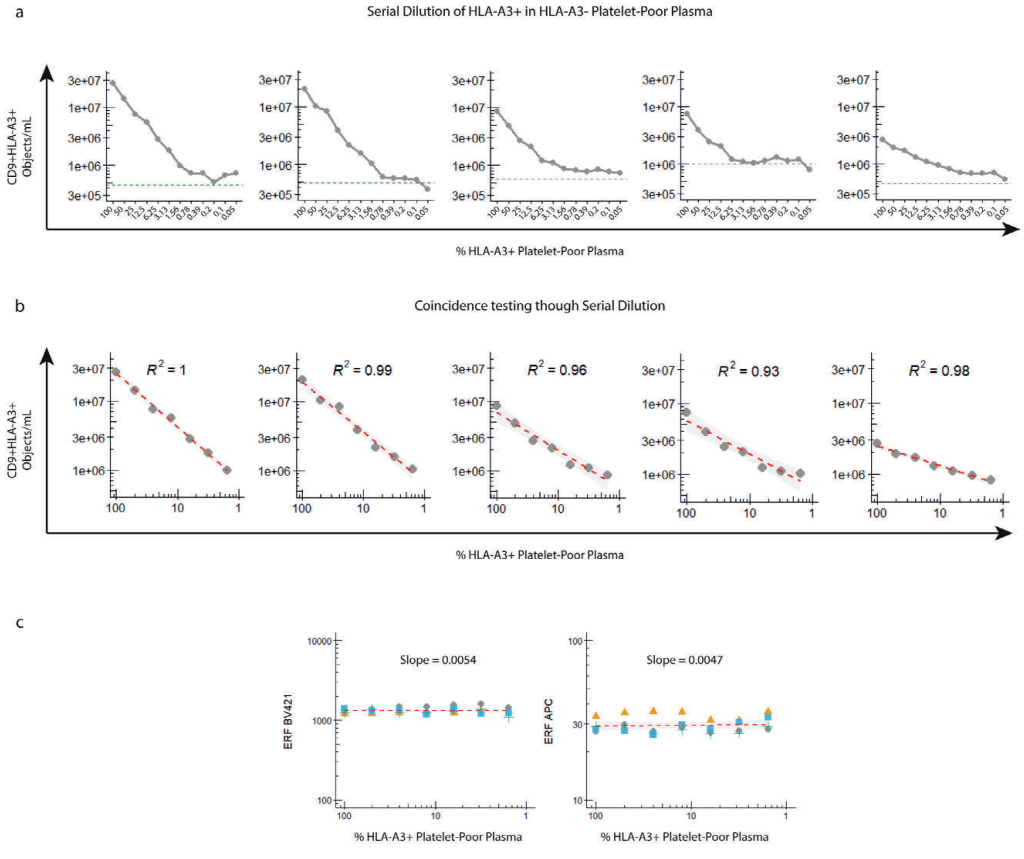

Figure 3 – Quantification of CD9+HLA-A3+ events in mixed PPP samples. **A**) Serial dilutions (2-fold) of 5 double-stained (anti-CD9 and anti-HLA-A3) matched donor-recipient samples shows that our setup is able to discriminate CD9+HLA-A3+ EVs above recipient 'self' background (HLA-A3- recipient signals, indicated by the green dashed lines) down to ~1%. **B**) Coincidence testing through serial dilution. A linear correlation between the concentrations of CD9+HLA-A3+ EVs and dilution factor (range: 100% to 1.56% HLA-A3+ PPP) for each serial dilution experiment confirmed single particle analysis in mixed PPP samples. C) Stable (standardized) fluorescent signals for both detection channels (Ch01 – HLA-A3 / Ch05 – CD9) were observed irrespective of the dilution factor.

dd-EVs are detected in KTRs with stable allograft function

Next, we examined whether dd-EVs could be directly detected in PPP of KTRs after transplantation. As stated previously, samples not passing the threshold of ≥95% reduction after detergent treatment were excluded from analysis; excluded samples were not associated with any specific time-point. Sample exclusion on the basis of detergent treatment resulted in the exclusion of 10 KTR sample series, leaving 26 KTR sample series in the analysis. Table 1 shows the patient characteristics corresponding to the samples included in our analysis, stratified into the four groups as described in the methods section.

First, we compared the total concentrations of double-positive events measured in PPP samples taken before (n = 13) and 2-4 days (n = 17) after transplantation (Figure 4A). We observed a statistically significant difference between these time points which confirms the release of dd-EVs into KTR's circulation.

We then performed a longitudinal analysis of dd-EV concentrations comparing KTRs in the control group with KTRs who underwent a 'for-cause' kidney biopsy ('Biopted' group) (Figure 4B). In the control group, we observed significant increases in dd-EV concentrations at 2-4 days, 6-8 days and 6 months after transplantation compared to the concentrations detected before transplantation. These dd-EV concentrations were observed to be stable throughout follow-up, suggesting that stable allograft function (without a biopsy) leads to a detectable dd-EV signal in KTR plasma. This notion was further strengthened by the observation that dd-EV concentrations did not increase (compared to levels detected before transplantation) in individuals who did experience allograft complications ('Biopted' group); this effect was observed up to at least 6 months after transplantation (Figure 4C).

To examine a potential diagnostic value of dd-EVs, we next compared the concentrations of CD9+HLA-A3+ EVs measured in 'for-cause' biopsy samples taken at 6 days after transplantation (median, range: 2 – 60) with the concentrations as detected in samples taken 6 – 8 days after transplantation from patients in the 'control' group.

The concentration of dd-EVs was higher in time-matched KTR samples without a biopsy compared to concentrations detected at the moment of a for-cause biopsy (irrespective of their pathological classification, $5.36E^6 \pm 2.05E^6$ objects/mL vs $3.24E^6 \pm 8.55E^5$ objects/mL, respectively, $p = 0.05$). However, no statistical differences were

observed when comparing dd-EV concentrations between the control samples and biopsies indicative for ATN (N=2), Presumed Rejection (N=3), or Biopsy Proven Acute Rejection (BPAR – 3x aABMR and 3x aTCMR2a) , demonstrating that dd-EVs were unable to discriminate between the type of complication (Figure 4D).

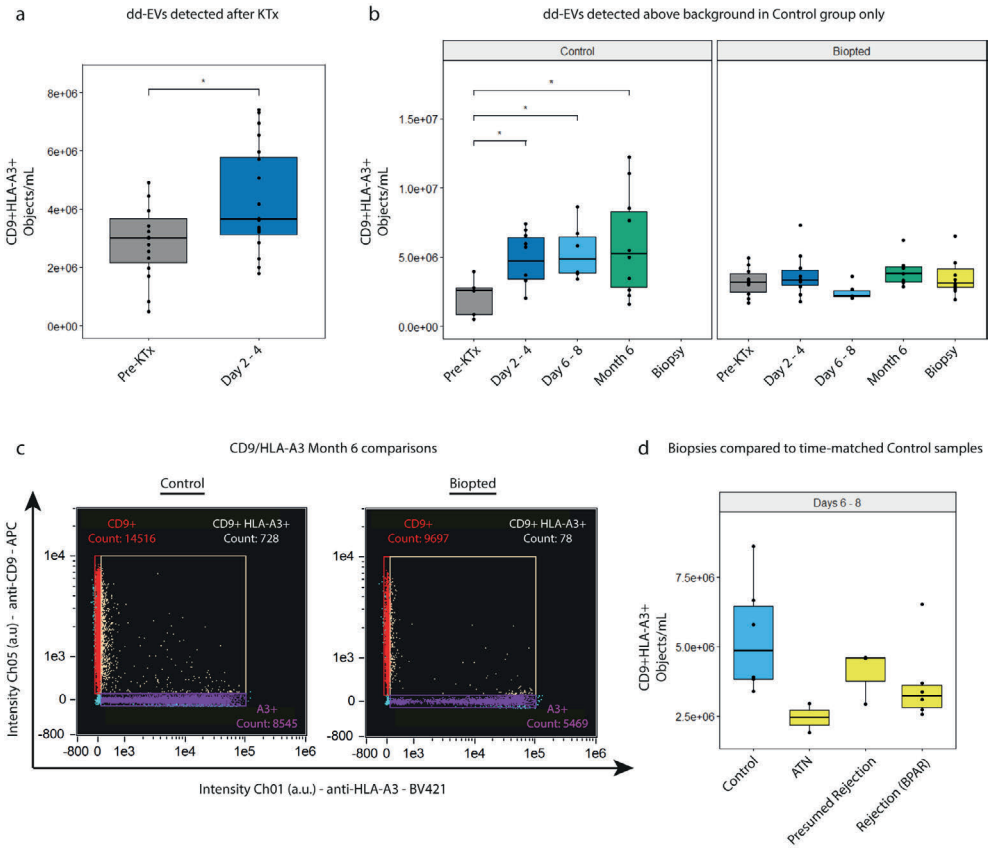

Figure 4 – Detection of dd-EVs after transplantation. **A**) Analysis of the concentrations of CD9+HLA-A3+ events before and 2-4 days after kidney transplantation revealed a significant increase after transplantation. **B**) longitudinal analysis of dd-EV concentrations in KTR blood samples subdivided into either 1) the control group (representing all samples from patients whom did not experience any complications after transplantation) or 2) the biopted group (encompassing all samples from patients whom underwent a biopsy), showing that dd-EVs are detectable above baseline (before transplantation) only in patients whom did not experience complications after transplantation. **C**) Representative CD9 vs HLA-A3 scatter plots of PPP samples taken 6 months after KTx from an individual in the control (left) and biopted (right) group. **D**) dd-EV concentrations as detected in 'for-cause' biopsy samples compared to time-matched control samples.

	Control	Other Diagnosis	Presumed Rejection	Rejection	p-test
n =	11	3	5	7	
Recipient Age (Years)	58.64 (10.06)	62.33 (10.21)	61.20 (14.55)	58.29 (16.43)	0.95
Recipient Gender (Male)	9 (81.8)	3 (100.0)	1 (20.0)	3 (42.9)	0.04
Recipient BMI	27.45 (5.13)	28.03 (11.94)	26.62 (2.27)	27.44 (4.92)	0.99
Donor Type					0.60
DBD	3 (27.3)	1 (33.3)	0 (0.0)	3 (42.9)	
DCD	3 (27.3)	2 (66.7)	1 (20.0)	2 (28.6)	
Living Donor - Related	1 (9.1)	0 (0.0)	1 (20.0)	0 (0.0)	
Living Donor - Unrelated	4 (36.4)	0 (0.0)	3 (60.0)	2 (28.6)	
Donor Age (Years)	54.09 (17.68)	66.00 (2.65)	61.20 (13.55)	64.00 (6.90)	0.38
Donor Gender (Male)	4 (36.4)	1 (33.3)	4 (80.0)	3 (42.9)	0.40
Missmatch HLA-A					0.217
0	0 (0.0)	0 (0.0)	1 (20.0)	0 (0.0)	
1	9 (81.8)	2 (66.7)	1 (20.0)	4 (57.1)	
2	2 (18.2)	1 (33.3)	3 (60.0)	3 (42.9)	
Missmatch HLA-B					0.56
0	2 (18.2)	0 (0.0)	0 (0.0)	0 (0.0)	
1	4 (36.4)	1 (33.3)	1 (20.0)	4 (57.1)	
2	5 (45.5)	2 (66.7)	4 (80.0)	3 (42.9)	
Missmatch HLA-DR					0.02
0	4 (36.4)	0 (0.0)	0 (0.0)	3 (42.9)	
1	5 (45.5)	0 (0.0)	5 (100.0)	2 (28.6)	
2	2 (18.2)	3 (100.0)	0 (0.0)	2 (28.6)	
Induction Therapy					
Basiliximab	11 (100.0)	3 (100.0)	5 (100.0)	5 (71.4)	0.12
Alemtuzumab	0 (0.0)	0 (0.0)	0 (0.0)	2 (28.6)	0.12
Maintenance Immunosuppression					
TAC / MMF / Prednisolone	11 (100.0)	3 (100.0)	5 (100.0)	7 (100.0)	NA

Table 1 – Patient characteristics corresponding to the samples included in our analysis after exclusion of samples not passing the 95% reduction after detergent treatment. For the dd-EV analysis, samples from a total of 26 KTRs were included in the analysis (Figure 4B). Continued variables are described as mean (SD). Categorical variables as number of cases (%). ATG, antithymocyte globulin; BMI, body mass index; DBD, donation after brain death; DCD, donation after circulatory death; MMF, mycophenolate mofetil; MPA, Mycophenolic Acid; TAC, tacrolimus.

DISCUSSION

EVs have great potential value as (minimally invasive) biomarkers [26], but sensitive and reproducible methods for single EV analysis are essential to understand the role of EVs in human health and disease [22]. In the current work, we assessed the applicability of our recently developed IFCM-based methodology [23] to directly measure EV subsets in human patient plasma samples – as exemplified by the detection of single dd-EVs in KTR plasma samples after kidney transplantation.

In addition to their physical properties and current technological challenges, the detection of EV subsets during health and disease may – depending on the disease – be hampered by the presence of 'contaminating' agents in the sample matrix. In the current study, components such as urea and creatinine are elevated as a consequence of kidney failure and may interfere with single EV detection. We show that our IFCM protocol is able to detect single CD9+ EVs in plasma samples obtained from both donors (healthy controls) and KTRs before transplantation, thereby suggesting that single EV detection by our IFCM protocol is uninfluenced by such contaminating components. The concentration of EVs in urine is related to nephron mass, explaining a lower concentration of total CD9+ EVs in KTRs compared to donors [27]. Here, we did not observe a difference in total CD9+ EVs between both groups in blood plasma, which is most likely due to the contribution of multiple organs to the total plasma CD9+ EV pool.

The concept of plasma circulating dd-EV detection and characterization with IFCM has been presented previously [4]. Mastoridis et al. showed that by analyzing CFSE+ events in combination with an exosome-specific marker (CD63) and an origin-specific marker (donor-HLA), circulating dd-EVs could be detected in the circulation of a liver transplantation recipient [4]. However, our protocol provides several improvements over the approach presented in previous work: 1) our IFCM platform is both SSC (size) and fluorescence calibrated – which enhances reproducibility, 2) no EV isolation was performed – thus the 'full spectrum' of detectable EVs was analyzed, and 3) by analyzing CD9+ EVs (shown to be highly prevalent in plasma samples) [4, 23] in combination with donor-HLA, we were able to analyze a broad spectrum of circulating dd-EVs – as opposed to the analysis of donor-derived CFSE+CD63+ exosomes (a donor EV subset). Additionally, we prove the detection of single dd-EVs by our IFCM protocol and determined its sensitivity through serial dilution of HLA-A3+ plasma into HLA-A3- plasma demonstrating a linear correlation with the dilution factor and stable ERF [22].

Currently, it is consensus that CD9+ EVs detected in PPP are most likely platelet-derived. As platelets express HLA Class I antigens on their surface, one might expect a high degree of co-localization of HLA Class I antigens with CD9 on these EVs. However, we found that CD9+HLA-A3+ particles are only a fraction (~16%) of the total CD9+ particles in HLA-A3+ donors. This observation may be explained by 1) different modes of EV biogenesis influencing whether HLA Class I antigens are present on EVs and/or whether their epitope topology is directed to the vesicular surface (and thus detectable with our setup), and 2) CD9 (but not HLA Class I antigens) may also be found on lipoproteins [18].

The identification and quantification of single dd-EVs with IFCM as presented here is also subject to limitations. First, IFCM needs a minimum of 3 pixels before an event is recorded [23]. Consequently, EVs with a low HLA-A3 epitope-density might be missed by our assay. Second, although we calibrated the arbitrary fluorescent SSC intensities of our platform to reflect particle-size, we obtained a goodness-of-fit measure (R^2) of 91%, which implies a 9% error when selecting particles with SSC intensities corresponding to EVs ≤400 nm [23]. For reference, (conventional) clinical-grade Flow Cytometers typically result in R^2 values >0.99 – although lacking the resolution to detect EVs <300 nm [18, 28, 29]. Additionally, we excluded samples not passing the threshold of ≥95% reduction after detergent treatment from analysis, which imposes an analytical bias towards samples containing 'high' concentrations of fluorescent events. However, by applying this selection criteria on our samples we ensured the analysis of fluorescent events of biological origin well above the (fluorescent) background of our assay. An alternative to the detergent treatment threshold could be the selective analysis of samples with a minimum number of events in the gate of interest (exceeding the number of events acquired in negative control samples e.g., buffer + reagents, unstained plasma, plasma + isotype staining) after acquisition.

In transplantation, the potential of EVs as biomarker for the detection of allograft rejection has been reported by a few groups[30-36]. Most notably, animal models of heterotopic heart transplantation (mouse into mouse)[24], islet xenotransplantation (human into mouse)[14], and a lung transplantation model between rats (Wistar into Lewis)[25], have provided evidence that concentrations of allograft-derived EVs diminish during rejection well before alterations in classical biomarkers occur or histologic manifestations of injury were observed. In the current study, we observed a stable release of dd-EVs in KTRs who did not experience allograft dysfunction

after transplantation but were unable to detect dd-EVs above pre-transplantation signals in KTRs who underwent a 'for-cause' biopsy.

Mechanistically, it is currently unknown whether the lower concentrations of dd-EVs during allograft dysfunction is a consequence of decreased production of EVs by the allograft, increased consumption of dd-EVs by recipient immune cells, or a combination of both [24]. Donor exosomes have been shown to be involved in donor antigen presentation to recipient alloreactive T cells in lymphoid organs by the recipient dendritic cells in a phenomenon known as cross-dressing [35, 37-39]. As Habertheuer et al. suggested, this mechanism of T cell activation may suppress production of exosomes by the transplanted tissue even before there is targeted injury to the allograft [24]. At any rate, the detection of dd-EVs can be associated with stable allograft function – which is in contrast to the detection of e.g. donor-derived cell-free DNA, which has been observed to increase in concentration as a consequence of allograft damage [40].

In conclusion, our calibrated IFCM-based methodology to directly detect and characterize plasma-derived EV subsets is applicable in patient human plasma samples. We believe that this methodology – after validation of markers of interest – could boost the EV biomarker research in a variety of clinical contexts, of which monitoring of kidney transplant integrity appears especially promising.

MATERIALS & METHODS

Clinical sample selection

To analyze distinct donor-derived EVs (dd-EVs) in KTR plasma samples, 36 donor-KTR couples were selected on the basis of an HLA-A3 mismatch between donors (HLA-A3+) and KTRs (HLA-A3-). KTRs had not received a previous HLA-A3+ graft. All donor-KTR couples participated in an observational study which aimed to identify minimally invasive biomarkers for the diagnosis of acute kidney transplant rejection, and was approved by the institutional review board of the Erasmus MC (Medical Ethical Review Board number 2018-035); details of this study are described elsewhere [40]. All patients provided written informed consent. Blood samples from living donors were obtained before donation and collected as part of our ongoing Biobank program (Medical Ethical Review Board number 2010-022). These donors served as healthy controls. The study was conducted in accordance with the principles of the Declaration of Helsinki.

Sample collection and processing

From both donors and KTRs, whole blood samples (EDTA) were collected before transplantation, and, for KTRs, 3 days, 7 days, and 6 months after transplantation. Additionally, blood samples were collected on the morning of (or the day preceding) a 'for-cause' kidney transplant biopsy.

Blood was drawn from each individual into two BD Vacutainer K3-EDTA-coated collection tubes (BD Biosciences, San Jose, USA). Whole blood was centrifuged at 1910 x g for 10 minutes at room temperature and the plasma layer was then collected at 16,000 x g for 10 minutes at room temperature in 1 mL aliquots using Safe-Lock Eppendorf tubes (Eppendorf AG, Hamburg, Germany). The resulting platelet-poor plasma (PPP) was first pooled before being divided into 700-µL aliquots in cryovials containing 28 µL of a 25x concentrated protease inhibitor cocktail solution (4% v/v) (cOmplete Protease inhibitor cocktail tablets, Roche, Mannheim, Germany) according to the manufacturers' instructions and stored at -80 °C.

Stratification of KTRs based on biopsy scores

Biopsies were scored by an experienced renal pathologist, and KTRs were divided into 4 groups based on 1) no 'for-cause' biopsy and no anti-rejection therapy ('Control' group), 2) acute tubular necrosis (ATN) as the main finding in the biopsy and no anti-rejection therapy ('ATN' group), 3) no histopathological signs of rejection but treated with anti-rejection therapy on the basis of clinical suspicion of rejection ('Presumed Rejection' group), and 4) biopsy-proven acute rejection (BPAR – aABMR or aTCMR2A) in combination with anti-rejection therapy ('Rejection' group). In case patients underwent multiple biopsies over the course of the study, only the first biopsy was used in the analysis.

Sample labelling

PPP samples were stained with monoclonal antibodies (mAbs) and isotype controls as extensively described in our previous work [23]. In the absence of a specific marker, EVs are identified by their expression of common markers such as CD9, CD63 and CD81 [41]. In this study, we used CD9 (which has been shown to be highly prevalent on plasma-derived EVs) as common EV marker [23]. Additionally, following the characterization of kidney-derived EVs released during normothermic machine perfusion, we determined that CD9 co-localizes to a higher degree with MHC

Class I molecules compared to CD63 (~3-fold difference) (Supplementary Figure S1 online). mAbs used in this study were CD9–APC, clone HI9a (6 µg/mL, Biolegend, San Diego, USA), and HLA-A3-BV421, clone GAP-A3 (200 µg/mL, BD Biosciences, New York, USA). Matched isotype controls were IgG1, k-APC, clone MOPC-21 (200 µg/mL, BioLegend), and IgG2a, k-BV421, clone G155-178 (200 µg/mL, BD Biosciences). Specificity of the anti-HLA-A3 mAbs was confirmed by Luminex single antigen assay (Supplementary Data S1 online). Prior to staining, mAbs and isotypes were centrifuged at 16,000 x g for 10 minutes at room temperature to remove potential mAb clumps (to reduce false-positive signals from analysis), and were diluted in 0.20 µm filtered PBS (fPBS) before staining (final concentrations: 200 ng/mL).

Staining was performed by addition of the diluted mAbs/isotypes to 30 µL of PPP followed by a pre-determined volume of fPBS (V_{tot} = fPBS + sample + mAbs = 130 µL) followed by O/N incubation at 4 ^{0}C. All samples were brought to a total volume of 380 µL using fPBS before IFCM measurements.

Controls

To ascertain EV measurements the following controls were applied, as recommended by the MIFlowCyt-EV framework [22]: buffer only, buffer with reagents, unstained samples, isotype controls, and detergent treatment, which aims to disrupt the membranous structure of EVs thereby allowing discrimination between membrane-enclosed vesicles (which lyse upon detergent treatment) and other protein complexes (which are unaffected by detergent treatment). Detergent treatment was performed by adding 20 µL of 10% (V/V) TritonX-100 to the samples followed by 30 minutes of incubation at room temperature prior to acquisition.

Data acquisition

All samples were acquired on an ImageStreamX MkII instrument (IS^{x}; Luminex). Settings as extensively described elsewhere were used [23]. In brief, lasers were turned on as applicable per fluorophore and set to their maximum power (405 nm : 200 mW, 642 nm :150 mW) with the exception of the 785 nm SSC laser (1.25 mW). High Gain mode – an upgrade of the IFCM that increases the photonic sensitivity and object detection of the system – was activated. Data was acquired over fixed time periods – to standardize among samples – of 180 seconds using the 60x objective with fluidics set to 'low speed / high sensitivity'. This resulted in a flow

speed of 43.59 ± 0.07 mm/sec (mean ± standard deviation). Core size was set at 6 µm, autofocus was activated and the 'Remove Speedbead' option was checked. BV421 fluorescence signals were collected in channel 1 (435–505-nm filter), APC signals in channel 5 (642–745 nm filter), and SSC signals in channel 6 (745–785 nm filter). Particle enumeration was achieved through the advanced fluidic control of the IS^{x} coupled with continuously running speed beads, resulting in the "objects/mL" feature within the IS^{x} Data Exploration and Analysis Software (IDEAS).

Data Analysis

Data analysis was performed using Amnis IDEAS software (version 6.2). Image display mapping was linearly adjusted for all fluorescent events for each channel and then applied to all files of the respective experiment. To ensure the analysis of EVs we 1) selected all particles with SSC intensities ≤ 900 a.u., and 2) identified and excluded coincidence detection by counting the number of fluorescent spots within the pixel grid for each event acquired; events showing multiple spots were excluded from analysis [23]. This gating strategy ensures the selection and analysis of single spot fluorescent particles ≤400 nm. Gating areas and cut-offs were established through identification of (fluorescent) populations in unstained and single stained samples, and arbitrary fluorescent intensities were converted into Equivalent number of Reference Fluorophores (ERF) values based on previously published calibration data [23]. Lower and upper gating area cut-offs were defined as 677 – 112,201 ERF for BV421, and 6.40 – 123 ERF for APC.

Statistical Analysis

Statistical analysis was performed using R version 4.0.2 and RStudio (RStudio Team (2016). RStudio: Integrated Development for R. RStudio, Inc., Boston, MA URL http://www.rstudio.com/.) version 1.1.463. All concentrations reported in this work were corrected for sample dilution (before acquisition – 380 µL total volume per test containing 30 µL sample = ~12.33-fold dilution factor) and are shown as the mean ± standard deviation unless specified otherwise. Statistical significance between EV concentrations and groups was determined through two-sided t-tests, 95% CI with unpaired data.

ACKNOWLEDGMENTS

The authors would like to thank Manou van Alphen and Wenda Verschoor for their assistance in sample measurements with IFCM, Marian C. Clahsen – van Groningen for the pathological scoring of the biopsy samples, and the Immunohaematology and Blood Transfusion lab of the Leiden University Medical Center (LUMC) for performing the Luminex single antigen assay for the HLA-A3 mAb.

AUTHOR CONTRIBUTIONS

W.W.W. participated in the research design, performance of the research, data analysis, article drafting and is the corresponding author. D.A.H., C.C.B., M.J.H., K.B. participated in the research design and writing of the manuscript. All authors reviewed the manuscript and approved its final version.

DATA AVAILABILITY

All source data underlying the figures presented in this work are provided as 'Supplementary Data Figures 1-4'. Any other relevant data are available from the corresponding author upon reasonable request.

CONFLICT OF INTEREST

In the last three years, D.A. Hesselink has received lecture fees and consulting fees from Astellas Pharma, Chiesi Pharma, Medincell, Novartis Pharma, Sangamo Therapeutics and Vifor Pharma. He has received grant support from Astellas Pharma and Chiesi Pharma [paid to his institution]. D.A. Hesselink does not have employment or stock ownership at any of these companies, and neither does he have patents or patent applications.

All other authors declare to not have competing interests.

FINANCIAL DISCLOSURE

The authors declare that the research was conducted in the absence of any commercial or financial relationships that could be construed as a potential conflict of interest.

REFERENCES

1. Arraud N, Linares R, Tan S, Gounou C, Pasquet JM, Mornet S, et al. Extracellular vesicles from blood plasma: determination of their morphology, size, phenotype and concentration. J Thromb Haemost. 2014;12(5):614-27.
2. Karpman D, Stahl AL, Arvidsson I. Extracellular vesicles in renal disease. Nat Rev Nephrol. 2017;13(9):545-62.
3. Marar C, Starich B, Wirtz D. Extracellular vesicles in immunomodulation and tumor progression. Nat Immunol. 2021;22(5):560-70.
4. Mastoridis S, Bertolino GM, Whitehouse G, Dazzi F, Sanchez-Fueyo A, Martinez-Llordella M. Multiparametric Analysis of Circulating Exosomes and Other Small Extracellular Vesicles by Advanced Imaging Flow Cytometry. Front Immunol. 2018;9:1583.
5. Pitt JM, Kroemer G, Zitvogel L. Extracellular vesicles: masters of intercellular communication and potential clinical interventions. J Clin Invest. 2016;126(4):1139-43.
6. Ashcroft J, Leighton P, Elliott TR, Hosgood SA, Nicholson ML, Kosmoliaptsis V. Extracellular vesicles in kidney transplantation: a state-of-the-art review. Kidney Int. 2022;101(3):485-97.
7. Zaborowski MP, Balaj L, Breakefield XO, Lai CP. Extracellular Vesicles: Composition, Biological Relevance, and Methods of Study. Bioscience. 2015;65(8):783-97.
8. Han L, Lam EW, Sun Y. Extracellular vesicles in the tumor microenvironment: old stories, but new tales. Mol Cancer. 2019;18(1):59.
9. Urbanelli L, Buratta S, Tancini B, Sagini K, Delo F, Porcellati S, et al. The Role of Extracellular Vesicles in Viral Infection and Transmission. Vaccines (Basel). 2019;7(3).
10. Han Y, Jia L, Zheng Y, Li W. Salivary Exosomes: Emerging Roles in Systemic Disease. Int J Biol Sci. 2018;14(6):633-43.
11. Salih M, Zietse R, Hoorn EJ. Urinary extracellular vesicles and the kidney: biomarkers and beyond. Am J Physiol Renal Physiol. 2014;306(11):F1251-9.
12. Wang S, Kojima K, Mobley JA, West AB. Proteomic analysis of urinary extracellular vesicles reveal biomarkers for neurologic disease. EBioMedicine. 2019;45:351-61.
13. McBride JD, Rodriguez-Menocal L, Badiavas EV. Extracellular Vesicles as Biomarkers and Therapeutics in Dermatology: A Focus on Exosomes. J Invest Dermatol. 2017;137(8):1622-9.
14. Vallabhajosyula P, Korutla L, Habertheuer A, Yu M, Rostami S, Yuan CX, et al. Tissue-specific exosome biomarkers for noninvasively monitoring immunologic rejection of transplanted tissue. J Clin Invest. 2017;127(4):1375-91.
15. Verhoeven JGHP, Boer K, Van Schaik RHN, Manintveld OC, Huibers MMH, Baan CC, et al. Liquid Biopsies to Monitor Solid Organ Transplant Function: A Review of New Biomarkers. Therapeutic Drug Monitoring. 2018;40(5):515-25.
16. Wu L, Boer K, Woud WW, Udomkarnjananun S, Hesselink DA, Baan CC. Urinary Extracellular Vesicles Are a Novel Tool to Monitor Allograft Function in Kidney Transplantation: A Systematic Review. Int J Mol Sci. 2021;22(19).
17. Welsh JA, van der Pol E, Bettin BA, Carter DRF, Hendrix A, Lenassi M, et al. Towards defining reference materials for measuring extracellular vesicle refractive index, epitope abundance, size and concentration. J Extracell Vesicles. 2020;9(1):1816641.
18. Simonsen JB. What Are We Looking At? Extracellular Vesicles, Lipoproteins, or Both? Circ Res. 2017;121(8):920-2.

19. Blijdorp CJ, Tutakhel OAZ, Hartjes TA, van den Bosch TPP, van Heugten MH, Rigalli JP, et al. Comparing Approaches to Normalize, Quantify, and Characterize Urinary Extracellular Vesicles. J Am Soc Nephrol. 2021.
20. Karimi N, Cvjetkovic A, Jang SC, Crescitelli R, Hosseinpour Feizi MA, Nieuwland R, et al. Detailed analysis of the plasma extracellular vesicle proteome after separation from lipoproteins. Cell Mol Life Sci. 2018;75(15):2873-86.
21. Konoshenko MY, Lekchnov EA, Vlassov AV, Laktionov PP. Isolation of Extracellular Vesicles: General Methodologies and Latest Trends. Biomed Res Int. 2018;2018:8545347.
22. Welsh JA, Van Der Pol E, Arkesteijn GJA, Bremer M, Brisson A, Coumans F, et al. MIFlowCyt-EV: a framework for standardized reporting of extracellular vesicle flow cytometry experiments. J Extracell Vesicles. 2020;9(1):1713526.
23. Woud WW, van der Pol E, Mul E, Hoogduijn MJ, Baan CC, Boer K, et al. An imaging flow cytometry-based methodology for the analysis of single extracellular vesicles in unprocessed human plasma. Commun Biol. 2022;5(1):633.
24. Habertheuer A, Korutla L, Rostami S, Reddy S, Lal P, Naji A, et al. Donor tissue-specific exosome profiling enables noninvasive monitoring of acute rejection in mouse allogeneic heart transplantation. J Thorac Cardiovasc Surg. 2018;155(6):2479-89.
25. Habertheuer A, Ram C, Schmierer M, Chatterjee S, Hu R, Freas A, et al. Circulating Donor Lung-Specific Exosome Profiles Enable Noninvasive Monitoring of Acute Rejection in a Rodent Orthotopic Lung Transplantation Model. Transplantation. 2021.
26. Yanez-Mo M, Siljander PR, Andreu Z, Zavec AB, Borras FE, Buzas EI, et al. Biological properties of extracellular vesicles and their physiological functions. J Extracell Vesicles. 2015;4:27066.
27. Blijdorp CJ, Hartjes TA, Wei KY, van Heugten MH, Bovee DM, Budde RPJ, et al. Nephron mass determines the excretion rate of urinary extracellular vesicles. J Extracell Vesicles. 2022;11(1):e12181.
28. Larson MC, Luthi MR, Hogg N, Hillery CA. Calcium-phosphate microprecipitates mimic microparticles when examined with flow cytometry. Cytometry A. 2013;83(2):242-50.
29. Gyorgy B, Modos K, Pallinger E, Paloczi K, Pasztoi M, Misjak P, et al. Detection and isolation of cell-derived microparticles are compromised by protein complexes resulting from shared biophysical parameters. Blood. 2011;117(4):e39-48.
30. Zhang H, Huang E, Kahwaji J, Nast CC, Li P, Mirocha J, et al. Plasma Exosomes From HLA-Sensitized Kidney Transplant Recipients Contain mRNA Transcripts Which Predict Development of Antibody-Mediated Rejection. Transplantation. 2017;101(10):2419-28.
31. Morelli AE. Exosomes: From Cell Debris to Potential Biomarkers in Transplantation. Transplantation. 2017;101(10):2275-6.
32. Tower CM, Reyes M, Nelson K, Leca N, Kieran N, Muczynski K, et al. Plasma C4d+ Endothelial Microvesicles Increase in Acute Antibody-Mediated Rejection. Transplantation. 2017;101(9):2235-43.
33. Kennel PJ, Saha A, Maldonado DA, Givens R, Brunjes DL, Castillero E, et al. Serum exosomal protein profiling for the non-invasive detection of cardiac allograft rejection. J Heart Lung Transplant. 2018;37(3):409-17.
34. Gunasekaran M, Xu Z, Nayak DK, Sharma M, Hachem R, Walia R, et al. Donor-Derived Exosomes With Lung Self-Antigens in Human Lung Allograft Rejection. Am J Transplant. 2017;17(2):474-84.

35. Campana S, De Pasquale C, Carrega P, Ferlazzo G, Bonaccorsi I. Cross-dressing: an alternative mechanism for antigen presentation. Immunol Lett. 2015;168(2):349-54.
36. Golebiewska JE, Wardowska A, Pietrowska M, Wojakowska A, Debska-Slizien A. Small Extracellular Vesicles in Transplant Rejection. Cells. 2021;10(11).
37. Burlingham WJ. “Cross-Dressing” Becomes Fashionable Among Transplant Recipients. Am J Transplant. 2017;17(1):5-6.
38. Macedo C, Tran LM, Zahorchak AF, Dai H, Gu X, Ravichandran R, et al. Donor-derived regulatory dendritic cell infusion results in host cell cross-dressing and T cell subset changes in prospective living donor liver transplant recipients. Am J Transplant. 2021;21(7):2372-86.
39. Mastoridis S, Londono MC, Kurt A, Kodela E, Crespo E, Mason J, et al. Impact of donor extracellular vesicle release on recipient cell “cross-dressing” following clinical liver and kidney transplantation. Am J Transplant. 2021;21(7):2387-98.
40. Verhoeven J, Boer K, Peeters AMA, Clahsen-van Groningen MC, Roodnat JI, van de Wetering J, et al. A Novel High-Throughput Droplet Digital PCR-Based Indel Quantification Method for the Detection of Circulating Donor-derived Cell-free DNA After Kidney Transplantation. Transplantation. 2022.
41. Andreu Z, Yanez-Mo M. Tetraspanins in extracellular vesicle formation and function. Front Immunol. 2014;5:442.


REJECTED
REJECTED
REJECTED

WHAT HAVE WE LEARNED?

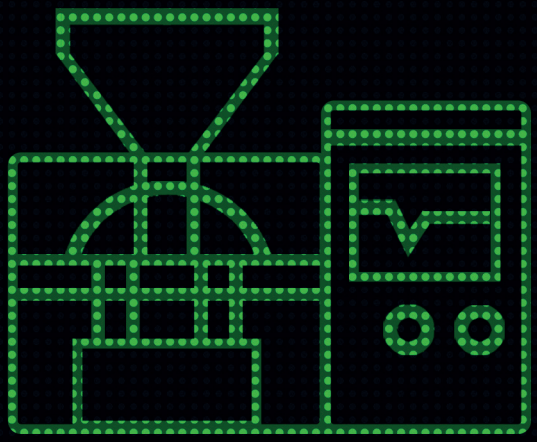

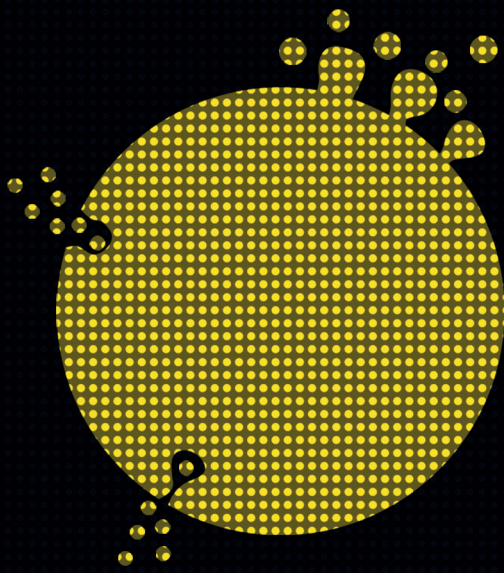

07

SUMMARIES

- ENGLISH SUMMARY
- NEDERLANDSE SAMENVATTING

ENGLISH SUMMARY

Extracellular Vesicles (EVs) are submicron-sized particles released by all cells. EVs carry proteins on their surface and a variety of macromolecules as cargo – which are thought to reflect the status of their cell of origin. As 'snapshots' of the releasing cells, EVs gain more and more interest as potential biomarkers for various diseases. In the context of clinical kidney transplantation, allograft status may be deduced through the analysis of EVs in perfusion fluids, blood plasma, or urine.

The current gold standard for the analysis of EVs in such (complex) biological samples involves the separation of EVs from "contaminating" components. In practice, this is complicated as the nature of these components differ according to the sample of interest, but often overlap with EVs in terms of their biophysical properties (e.g. size, density). In recent years it has become clear that isolation methods such as ultracentrifugation (the most used EV-isolation method to-date) may alter EV properties – thus influencing down-stream analysis and data interpretation. Additionally, as numerous methodologies to isolate and analyze EVs are employed, the EV-field struggles with the reproducibility of EV research – which is a prerequisite for understanding the biological significance of EVs.

Introductory **chapter 1** outlines these challenges, as well as the limitations of current EV detection techniques, and identifies the unmet need for an EV analysis platform which allows accurate, reproducible quantitation and characterization of single EVs in complex biological samples. The chapter then continues to describe a set of criteria for a reproducible EV analysis platform, and postulates Imaging Flow Cytometry (IFCM) as a potential technique for the analysis of single EVs in suspension.

Before exploring IFCM as a potential EV detection platform, in **chapter 2** we first describe the quantitation of nanoparticles released into the perfusion fluids by Expanded-Criteria Donor (ECD) kidneys during Normothermic Machine Perfusion (NMP). The term 'nanoparticles' is used to indicate all uncharacterized sub-micron particles (including, but not limited to EVs) in a given sample.

NMP is an experimental organ-preservation technique in which a 37 °C, oxygenated perfusion fluid is pumped through the donor kidney. Consequently, cellular metabolism is activated, and we demonstrate that ECD kidneys release nanoparticles during NMP. However, the analysis platform used in these experiments (nanoparticle tracking analysis – NTA) has limited phenotyping capabilities, and consequently, is

unsuitable to further characterize the released nanoparticles, and thus unsuitable to confirm that the released nanoparticles represent EVs.

In **chapter 3** we present, following the criteria established in **chapter 1**, an IFCM method for the detection of single EVs in plasma samples which omits the use of EV isolation techniques. Therefore, our method is able to directly show the status of an individual (as reflected by EV concentrations and phenotypes), which is greatly beneficial in the monitoring of EVs in health and disease. As plasma is considered to be the most complex bio fluid for single EV detection (due to the interference of protein aggregates, cell debris and lipoproteins), this methodological development has the potential to push the EV-field further. Additionally, this chapter demonstrates that light scattering signals generated by IFCM can be correlated to particle size through Mie theory. This latter achievement represents a much needed step towards the calibration of IFCM light scattering signals and this standardization improves the reproducibility of EV measurements. Ultimately, the methodology as described in this chapter allows the analysis of single EVs ≤ 400 nm in diameter.

The direct detection of single EVs in urinary samples required an adaptation of the IFCM methodology as developed for the direct detection of single EVs in plasma, as 'Auto-Fluorescent' particles in urine interfere with true EV signals (**chapter 4**). These 'Auto-Fluorescent' particles are not representative of uEVs as they are not lysed by detergent treatment, and consequently should be removed from analysis. We designed a gating strategy which removes such particles from analysis, whilst maintaining events representative for uEVs.

Chapter 5 returns to the clinical setting of organ preservation with NMP (**chapter 2**). In a new ECD kidney cohort, we validate that ECD kidneys release nanoparticles (<400 nm in diameter) into the perfusion fluids. Using our developed IFCM methodology, we 1) are able to show that these nanoparticles are indeed representative of EVs, 2) identify different EV subsets based on the detection of different antigens on the EV surface, and 3) show that some of the identified EV subsets correlate with well-established indicators of transplant outcome. This suggests that EVs might represent new potential candidates for the assessment of kidney graft quality prior to transplantation.

As a first step towards clinical applicability, **chapter 6** sets out to determine whether the developed IFCM methodology is able to detect and follow-up single,

donor tissue-derived EVs in plasma samples of kidney transplant recipients. In this 'needle-in-a-haystack' scenario, we demonstrate that our IFCM methodology is able to 1) differentiate between donor- and recipient-derived EVs on the basis of HLA phenotype differences, 2) detect donor-derived EVs down to ~1% above pre-transplantation background levels, and 3) detect donor-derived EVs above pre-transplantation background levels in individuals with stable allograft function, but not in individuals with allograft dysfunction. In conclusion, this chapter demonstrates the applicability of our calibrated IFCM-based methodology in the direct detection of tissue-specific EV subsets in clinical samples.

In **chapter 8**, the findings and implications of the research described in chapters 2-6 are discussed, conclusions are drawn, and recommendations for future research are made.

NEDERLANDSE SAMENVATTING

Extracellulaire vesikels (EVs) zijn miniscule (sub-micron) blaasjes die door alle cellen worden uitgescheiden en opgenomen. EVs hebben verschillende eiwitten op hun oppervlak (de buitenzijde) en ook een verscheidenheid aan macromoleculen als lading (aan de binnenzijde). Aangenomen wordt dat de combinatie van deze eiwitten en macromoleculen de status van de ouderlijke cel weerspiegelen. Als 'momentopnames' van cellen staan EVs steeds meer in de belangstelling als potentiële biomarkers voor verschillende ziekten. In de context van klinische niertransplantatie zou de status van de getransplanteerde nier wellicht kunnen worden afgeleid door EVs aanwezig in perfusievloeistoffen, bloedplasma of urine te analyseren.

De huidige gouden standaard voor de analyse van EVs in dergelijke (complexe) biologische monsters houdt in dat de EVs worden gescheiden van 'niet-EVs'. In de praktijk is dit lastig omdat deze 'niet-EVs' verschillend zijn afhankelijk van het monster van interesse, terwijl de biofysische eigenschappen (bijv. grootte, dichtheid) van de 'niet-EVs' vaak overlappen met die van EVs. In de afgelopen jaren is het duidelijk geworden dat isolatiemethoden zoals ultracentrifugatie (de meest gebruikte EV-isolatiemethode tot nu toe) de eigenschappen van EVs kunnen veranderen, waardoor de analyse en gegevensinterpretatie worden beïnvloedt. Naast ultracentrifugatie wordt er een verscheidenheid aan verschillende methoden gebruikt om EVs te isoleren en te analyseren, waardoor het EV-veld worstelt met de reproduceerbaarheid van EV-onderzoek. Dit laatste is een belangrijke vereiste voor het interpreteren van de biologische waarde van EVs.

Hoofdstuk 1 beschrijft deze uitdagingen, de beperkingen van de huidige EV-detectietechnieken, en identificeert de onvervulde behoefte aan een optimaal EV-analyseplatform. Dit analyseplatform moet nauwkeurig en reproduceerbaar individuele EVs kunnen kwantificeren en karakteriseren in complexe biologische monsters. Het hoofdstuk beschrijft vervolgens een aantal criteria waaraan dit EV-analyseplatform zou moeten voldoen, en presenteert Imaging Flow Cytometry (IFCM) als een potentiële techniek voor de analyse van individuele EVs in klinisch relevante biologische monsters.

Voordat IFCM als potentieel EV-detectieplatform onderzocht wordt, beschrijft **hoofdstuk 2** de kwantificering van nanodeeltjes in de perfusievloeistoffen van marginale (sub-optimale) donornieren tijdens normotherme machine perfusie

(NMP). De term ‘nanodeeltjes’ wordt hier gebruikt om alle niet-gekarakteriseerde sub-micron deeltjes (inclusief, maar niet beperkt tot EVs) in een bepaald monster aan te duiden.

NMP is een experimentele orgaanconserveringstechniek waarbij een zuurstofrijke perfusievloeistof van 37 °C door de donornier wordt gepompt, met als doel het activeren van cellulair metabolisme. Duidelijk wordt dat marginale donornieren nanodeeltjes uitscheiden tijdens NMP. Het analyseplatform dat in deze experimenten wordt gebruikt (nanoparticle tracking analysis - NTA) heeft echter beperkte mogelijkheden om de vrijgekomen nanodeeltjes te karakteriseren, en is dus ongeschikt om te bevestigen dat deze nanodeeltjes werkelijk EVs zijn.

Hoofdstuk 3 presenteert, in overeenstemming met de in **hoofdstuk 1** opgestelde criteria, een IFCM-methode voor de detectie van individuele EVs in plasmamonsters zonder dat isolatie van EVs nodig is (‘directe-detectie’). Hierdoor is deze methode in staat om direct de status van een individu weer te geven, zoals weerspiegeld in EV-aantallen en aanwezigheid van specifieke eiwitten/moleculen aan de buitenzijde van de EVs. Dit biedt een voordeel bij het analyseren van EVs ten tijden van gezondheid en ziekte aangezien er geen EV modulatie plaats vindt d.m.v. EV isolatie. Omdat plasma wordt beschouwd als het meest complexe biologische monster met betrekking tot de detectie van individuele EVs, heeft deze methodologische ontwikkeling het potentieel om het EV-veld verder te brengen. Daarnaast laat dit hoofdstuk zien dat lichtverstrooiingssignalen gegenereerd door IFCM gecorreleerd kunnen worden aan deeltjesgrootte met behulp van Mie-theorie. Deze laatste ontwikkeling vertegenwoordigt een essentiële stap in de richting van de kalibratie van IFCM-lichtverstrooiingssignalen, waardoor de reproduceerbaarheid van EV-metingen wordt verbeterd. Al met al maakt de methode zoals beschreven in dit hoofdstuk de analyse van individuele EVs met een diameter ≤ 400 nm mogelijk in plasma monsters.

De directe-detectie van individuele EVs in urinemonsters vereist een aanpassing van de IFCM-methodologie aangezien ‘auto-fluorescente’ deeltjes in urine interfereren met EV-signalen (**hoofdstuk 4**). Aangetoond werd dat deze deeltjes niet uit lipiden zijn opgebouwd aangezien de ‘auto-fluorescente’ signalen niet veranderden na behandeling met een detergens (gericht op het verbreken van lipide structuren). Om deze ‘auto-fluorescente’ deeltjes te verwijderen uit de analyse werd een strategie ontwikkeld waarbij signalen die representatief zijn voor urine EVs behouden blijven.

Hoofdstuk 5 keert terug naar de klinische setting van orgaanpreservatie met NMP (**hoofdstuk 2**). In een nieuw cohort van marginale donornieren vonden we opnieuw nanodeeltjes (<400 nm in diameter) in de perfusievloeistoffen. Met behulp van de ontwikkelde IFCM-methodologie (**hoofdstuk 3**) wordt duidelijk dat 1) deze nanodeeltjes inderdaad representatief zijn voor EVs, 2) verschillende EV-subsets, te herkennen aan verschillende eiwitten op hun oppervlak, aanwezig zijn, en 3) dat specifieke EV-subsets correleren met welbekende parameters van transplantatie uitkomst. Samengenomen suggereren deze bevindingen dat EVs nieuwe, potentiële biomarkers kunnen zijn om de kwaliteit van donornieren te beoordelen vóór de transplantatie.

Als eerste stap op weg naar klinische toepasbaarheid wordt in **hoofdstuk 6** onderzocht of de ontwikkelde IFCM-methode in staat is om individuele, van donorweefsel afkomstige EVs te detecteren in plasmamonsters afgenomen van patienten vóór en na niertransplantatie. In dit 'naald-in-een-hooiberg'-scenario wordt duidelijk dat de IFCM-methode in staat is om 1) onderscheid te maken tussen EVs afkomstig van donoren en ontvangers door gebruik te maken van verschillen in HLA-moleculen, 2) donor-EVs te detecteren zijn tot ~1% boven de patiënt-specifieke achtergrondniveaus vóór transplantatie, en 3) donor-EVs te detecteren zijn (na transplantatie) boven deze achtergrondniveaus bij patienten met een stabiele transplantaatfunctie. Deze verhoging van donor-EVs werd niet waargenomen bij patiënten die in verband met een achteruitgang in nierfunctie een nierbiopt kregen. Dit hoofdstuk demonstreert de toepasbaarheid van de ontwikkelde, gekalibreerde IFCM-methode ten behoeve van de directe-detectie van weefselspecifieke EV-subsets in klinisch relevante plasmamonsters.

In **hoofdstuk 8** worden de bevindingen en implicaties van het onderzoek beschreven in de hoofdstukken 2-6 besproken, worden conclusies getrokken en worden aanbevelingen gedaan voor toekomstig onderzoek.

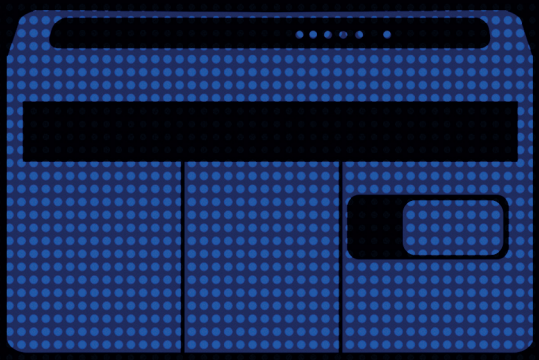

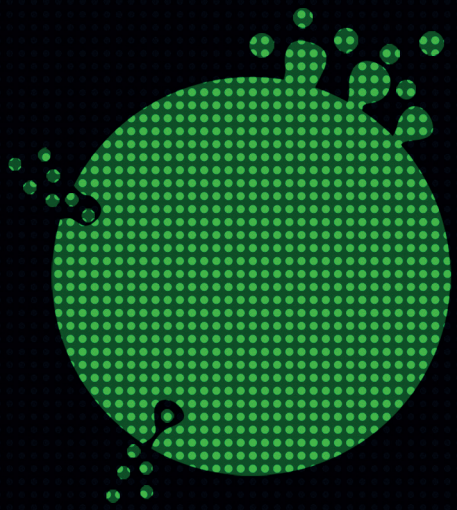

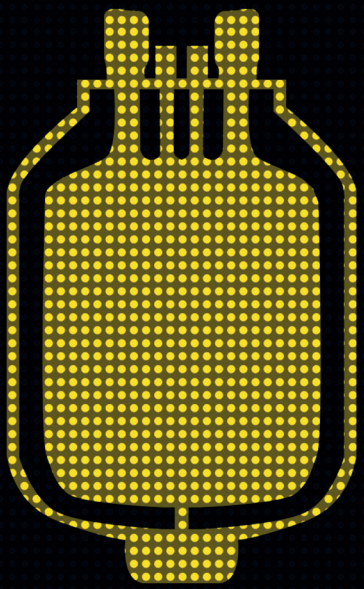

08

GENERAL DISCUSSION AND FUTURE PERSPECTIVES

How did we get here?

The ideas that EVs could have physiological roles, could be used as biomarkers, and could have therapeutic applications, led to an explosion of interest in EVs in the early 21st century [1, 2]. This resulted in the tremendous growth of EV-related research, and, consequently, in the development of a plethora of techniques for the isolation and characterization of EVs – often designed for specific downstream purposes. However, many of these techniques are poorly standardized, and as such reproducibility between studies - which is a prerequisite for understanding the biological significance of EVs - is hindered [3]. To address this issue, the research in this thesis describes the development and validation of a standardized methodology which allows the direct-detection and analysis of single EVs in suspension.

PART 1 – SINGLE EV-DETECTION: DEVELOPMENT

Pre-analytical variables – minus one

The current gold standard approach for EV analysis is based on the isolation or concentration of EVs (**chapter 1**) despite yielding low-purity EV samples due to the co-isolation of non-desired molecules [4, 5]. However, emerging evidence suggest that some widely used EV isolation methods may alter EV properties and thus modulate EV function [6,7]. Therefore, while researchers are encouraged to follow the guidelines established in the 'Minimal Information for Studies on Extracellular Vesicles' (MISEV) [8] – downstream observations with respect to EV-isolates may not necessarily be representative of either the natural biological state of EVs, or EVs at all.

If EVs are to be translated into clinical practice (as a diagnostic tool), it is imperative to reduce, or, better yet, avoid any form of EV modulation. The benefits of eliminating EV-isolation methods are two-fold. First, given the plethora of EV-isolation techniques available to EV researchers, omitting the need for sample isolation prior to EV analysis will lead to improved reproducibility. Secondly, the status of an individual (as reflected in EV concentration, size, protein makeup and content) can be directly monitored and related to well-established indicators of disease, which is greatly beneficial in the monitoring of EVs in health and disease. Thus, while the guidelines postulated by MISEV regarding the reporting of pre-analytical variables (e.g., EV source, sample collection, storage conditions, isolation methods performed) are a good step towards increasing standardization and reproducibility, this thesis argues that the full removal of EV isolation will also increase reproducibility between studies.

Controls are key

Omitting EV isolation requires an analysis platform that is able to 1) detect and discriminate EVs from contaminating components in molecularly complex samples, and 2) report the results in a standardized manner (e.g. according to the international system of units). In this thesis, we identified Imaging Flow Cytometry (IFCM) as a suitable technique that can detect EVs, discriminate distinct EV subpopulations, and distinguish EVs from non-EV particles in complex biofluids without prior EV isolation (**chapters 3 and 4**). The protocols as developed and described in this thesis are compliant with MIFlowCyt-EV [9] - a reporting framework for single EV flow cytometry designed by members of MISEV.

To ensure the identification and analysis of single EVs, we performed a strict set of assay controls designed to prove the detection of single EVs, and discriminate them from interfering components such as e.g. lipoproteins or protein aggregates (highly abundant in platelet-poor plasma [4]). These controls included buffer only, buffer with reagents, unstained controls, isotype controls, single-stained controls, and procedural controls. Additionally, serial dilution and detergent-treated EV samples are used throughout this thesis.

Serial sample dilution assists in evaluating whether EVs are detected as single particles, or to identify potential coincidence detection - also known as “swarm detection” [10]. Obtaining a linear particle count consistent with the dilution factor, and maintaining a stable fluorescence and/or light scatter signal are indicative of single particle analysis [9-11]. Using the imaging capabilities of IFCM, we designed a gating strategy which allows the simultaneous (selective) analysis of both single and multiple fluorescent events, thereby providing insight into the degree of coincidence detection for any given sample. This is (currently) a unique feature for IFCM which may prove to be beneficial in identifying highly concentrated samples – which consequently need to be further diluted to reduce/eliminate coincidence detection.

Detergent controls aid in determining whether detected events represent membrane-enclosed particles. Following incubation with a detergent, the membranous structures of EVs are lysed – reducing their numbers and signals – whilst protein complexes or other particles will persist [9, 12, 13]. In this thesis, in all biofluids assessed, we identified double-positive fluorescent events to be largely comprised of EVs as a ≥ 94% reduction in concentration was observed following

detergent treatment. However, it should be noted that detergent treatment is non-discriminatory between EVs or other lipid-composed particles (such as lipoproteins) – which stipulates the importance of the assay controls described above.

Standardized reporting

Like conventional flow cytometry (FCM), the signals generated by IFCM are expressed in arbitrary units, which hinders data interpretation and comparison of measurement results between instruments and laboratories. As multicenter studies are needed to validate the clinical relevance of EVs during health and disease, e.g. with different instruments measuring the same concentration of cell-type specific EVs in a given sample [14], it is imperative that EV detection assays produce results in a standardized manner. One way to achieve standardization is through calibration, which is a conversion of arbitrary units into standard units [15]. While the calibration of fluorescence signals can be readily achieved by measuring beads with known fluorescent intensities (e.g., expressed Equivalent number of Reference Fluorophores (ERF – **chapter 3**) or in units of Molecules of Equivalent Soluble Fluorochrome (MESF – **chapter 4**) [16], the calibration of light scattering signals into particle size presents an ongoing challenge for IFCM.

In this thesis, we demonstrated – for the first time – the calibration of light scatter signals into particle size for IFCM using Mie theory. The high degree of correlation between predicted and measured side scatter (SSC) intensities for polystyrene beads beads (R^2 = 0.91) underlines the utility of the SSC channel to relate scatter signals to standard units. This development enhances reproducibility between different IFCMs, and even across FC platforms with different optical configurations and settings. However, it should be noted that heterogeneity of the membrane and cargo composition of EVs affects their refractive index (and thus their level of scattering) and may potentially introduce errors in the estimated EV sizes.

In summary, following the application of strict assay controls, and calibration of both fluorescence and SSC signals for IFCM, we developed a standardized methodology which allows analysis of single EVs in complex biofluids such as platelet-poor plasma, urine, and perfusion fluids. Our methodology does not require prior isolation of EVs (thus limiting EV modulation), is able to simultaneously analyze EV concentration, phenotype, and size, and reports these parameters in standardized units.

Single-EV FC Strategies

The ideal platform for single EV analysis would 1) be widely available in clinical laboratories, 2) be technically validated, 3) have a high throughput, 4) have high reproducibility, and 5) be able to reveal EV subpopulations via phenotyping [17]. Consequently, bulk EV analysis methods – which report only average properties of an EV preparation – such as Western Blot, ELISA/TR-FIA, or mass-spec proteomics are limited in their usefulness [13] when aiming to examine the diagnostic potential of EVs.

Flow Cytometry (FC) as an analysis platform fits all the above criteria, but – as described in **chapter 1** - most FCs are designed for cell measurements and are not readily adapted to measure EVs [4,18,19]. To address this issue, several different strategies have been introduced to the field. For example, using an optimized configuration of the commercially available BD Influx FC, Vlist et al have demonstrated the detection of isolated cell supernatant-derived EVs ~100 nm in diameter [20]. However, applying these configurations to the FC requires an experienced operator with technical-expertise. Additionally, such modifications will turn the FC into a dedicated EV detection platform, thus 'losing' the ability to be used for cell analysis.

Another published FC-based method, performed on a commercially available Beckman Coulter CytoFlex, describes a strategy to directly measure EVs in plasma by labelling the EVs with a fluorescent lipid probe (vFRed) in combination with CFDA-SE or an anti-tetraspanin mixture [21]. In this study, rather than relating SSC signals into particle size through Mie calculations, EV size (surface area) is determined by calibration of EV membrane fluorescence by using a synthetic vesicle size standard, as provided in the vFC EV Analysis kit from Cellarcus Biosciences. Staining with the lipid membrane dye should be consistent for applicability, meaning that either the amount of dye needs to be approximately matched to the number of EVs (which is unknown before analysis), or an excess of dye should be used so that the membrane becomes saturated with dye [22]. An excess of dye will, however, lead to increased background signals, which, in turn, will hinder discrimination of EVs above background.

These two examples highlight the current status of the EV FC field, where either dedicated EV-detection platforms are being developed, or existing platforms are tested for their sensitivity to detect sub-micron particles. The development of the IFCM-methodology as described in the first part of this thesis falls into the second

category. At the moment of writing, IFCM as a platform has been commercially available for over a decade, yet its ability to detect EVs has only relatively recently been discovered [23-26]. Key features or advantages that contribute to IFCM being a more powerful platform for EV analysis compared to conventional FC include the slower flow rate, CCD-camera based detection (enabling higher quantum efficiency compared to conventional photon multiplier tubes), and integration of detected signals over time using Time Delayed Integration [27]. Additionally, IFCM does not require an experienced operator with technical-expertise, allows standardized reporting following calibration (this thesis), and can be used for the analysis of both cells and/or EVs (even simultaneously) [27].

As promising as this platform seems, there are some inherent limitations. First, due to the recording of images associated with detected events, the size of individual data files are large compared to conventional FC data files. As clinical trials often involve the measurement of large sample cohorts, the accumulation of many large data files will lead to an increased need for computational storage space, as well as analysis power. Second, the low flow rate (approximately 0.3 µL/minute as used in our setup) hinders the rate of sample throughput. This becomes especially apparent when increasing sample acquisition times to identify rare EV subpopulations. However, this can be resolved by automating the process of sample acquisition with a 96-well plate reader and performing overnight measurements.

PART 2 – SINGLE EV-DETECTION: VALIDATION

The Promise of Perfusion

At the moment of writing, the field of organ transplantation is suffering from a shortage of donor organs. To increase the donor-pool, increasing numbers of expanded-criteria donor (ECD) kidneys as well as kidneys procured from donation after circulatory death (DCD) [28] are used in kidney transplantation (**chapter 1**). ECD kidneys are, however, associated with poorer transplant outcomes when compared to kidneys from standard criteria donors [29, 30], and as such the field is exploring options to infer kidney quality prior to transplantation. Normothermic machine perfusion (NMP) is extensively being researched as a platform which may allow assessment, preservation, and even treatment of marginal quality donor kidneys [29, 31, 32]. Because metabolism is activated at 37 °C, NMP offers the possibility to assess kidney status prior to transplantation through monitoring of

the perfusion dynamics and analysis of biomarkers (e.g., neutrophil gelatinase-associated lipocalin, kidney injury molecule-1, and endothelin-1 [33]) in the perfusion fluids [29, 31, 34, 35].

Probing Perfusion Fluids

In the first-ever kidney NMP pilot trial in the Netherlands, we examined the release of nanoparticles by ECD kidneys during NMP with Nanoparticle Tracking Analysis (NTA) (**chapter 2**). Whilst 11 ECD kidney were included in this trial [36], we were able to demonstrate significant nanoparticle release (compared to baseline perfusion fluids) in 3 out of 11 kidneys. In the other 8 kidneys, we observed high concentrations of nanoparticles already present in the perfusion fluids before the perfusion procedure, which was attributed to the addition of Olimel (a mixture of glucose, amino acids, and lipids) as an energy source for cellular metabolism. Given that NTA is a technique which detects light scattering of individual particles in suspension, the addition of lipids to the perfusion fluids interfered with nanoparticle detection.

In a second NMP study, Olimel was replaced with a non-lipid containing solution, and nanoparticle release during NMP was confirmed with NTA in 8 ECD kidneys (**chapter 5**). Characterization of these nanoparticles (using our single-EV IFCM protocol as developed in part I of this thesis) confirmed that these nanoparticles are representative of EVs, and showed that the detected EVs are representative of several subtypes based on their phenotypes. For example, after labelling the perfusion samples with a mixture of three common EV-markers (CD9, CD63, and CD81 – all belonging to the tetraspanin protein family), we found that the majority of detected EVs expressed CD81. This was a surprising find given that platelet-poor plasma or urine samples predominantly yielded CD9+ (**chapter 3**) or CD63+ (**chapter 4**) EVs, respectively. These findings suggest that the phenotypes and subsets of EVs differ dependent on the type of bio-fluid, representing a starting point for future researchers when examining EVs in different complex bio-fluids.

To determine the cellular origin of the CD81+ EVs released during NMP, we labelled the perfusion fluids with anti-CD81 and anti-CD31 (endothelial marker). However, we found only marginal co-localization of these markers, suggesting that the majority of CD81+ EVs are either not of endothelial origin, or do not express CD31 on the vesicular surface.

A last observation was the correlation of the identified EV-subsets with crude donor kidney and NMP viability characteristics cold ischemia times (CIT) and renal blood flow. Both CIT and renal blood flow are parameters in a recently developed scoring system to aid clinicians in determining kidney quality during NMP [37]. We therefore postulate that EV release during NMP is not random, but rather indicative of the biological status of the (ECD) kidneys.

The needle in the haystack

Compared to perfusion fluids (which contain multiple components released by a single organ), the biological complexity of platelet-poor plasma (containing multiple components from multiple organs) makes single-EV detection much more challenging. To examine the applicability of the protocol (as developed in part I of this thesis) in the detection of low abundant EVs, we utilized the unique setting of clinical organ transplantation.

In **chapter 6** we aimed to directly analyze donor tissue-derived EVs (dd-EVs) in plasma samples of kidney transplant recipients (KTRs). To detect dd-EVs, we took advantage of two concepts: 1) plasma EVs express surface MHC antigens, and 2) donor-recipient MHC mismatch enables identification of transplant organ-derived EVs from recipient bodyfluids [38, 39]. These concepts enabled the detection of a relatively low abundant population of dd-EVs with the recipient serving as its own control (pre-transplantation) to rule out non-specific antibody targeting, and confirm the detection of dd-EVs post transplantation (signal validation).

Although the detection of human dd-EVs through IFCM has been demonstrated by other research groups [25, 40], our protocol provides several improvements over the approach presented in previous work. First, the full calibration (both size and fluorescence) of our IFCM platform enhances the reproducibility of our findings. Second, as no EV isolation (and thus modulation) was performed, our protocol allows the analysis of the 'full spectrum' of detectable EVs representative of their natural biological state. Third, we omitted the use of CFDA-SE as 'pan-EV' marker as to date no marker capabale of identifying all EV has been reported. Fourth, we demonstrated the analysis of single dd-EVs by our IFCM protocol and determined its sensitivity through serial dilution of donor plasma into KTR plasma.

What have we learned?

This thesis started by presenting an analogy between the studying (quantification) of bees and EVs to infer environmental or cellular status. In both cases, specific tools are needed to fulfil this purpose. For example, bee-keepers may count the number of inter-frames covered with adult bees from above the hive body to estimate the adult worker population size of a given colony [41]. In this thesis we developed and validated a standardized assay for the direct detection of single EVs in complex biofluids using IFCM. Although many techniques for EV characterization and quantification have been (and continue to be) developed, the method as presented in this thesis represents an important step towards the standardized reporting of analytical parameters such as size and fluorescence for single EVs. The ability of our protocol to detect even low abundant subpopulations of EVs without performing EV isolation demonstrates its potential to become a key tool in the EV-field, and we expect that EV IFCM may one day be used in the diagnosis, prognosis and monitoring of health and disease.

FUTURE DIRECTIONS

Is the technology ready for the clinic?

Single EV FC is considered the holy grail in EV characterization as it has the potential to detect, size, and phenotype thousands to millions of single EVs per minute [14]. The work described in this thesis has identified IFCM as a suitable platform for single EV detection. We believe that IFCM could serve as a diagnostic tool in the clinic, especially given its ability to detect low abundant EV subpopulations as demonstrated in this thesis. However, there are some areas in which the technique can be further improved.

In this thesis, we calibrated the light scattering intensities as detected by our IFCM to reflect particle sizes (through Mie theory). However, the obtained degree of correlation between predicted and measured scatter intensities for polystyrene (PS) beads (R^2 = 0.91) was not on the level of conventional, state-of-the art FCMs ($R^2 \geq 0.99$). This implies an approximate 8% error when estimating the size of EVs, which, in turn, impairs reproducibility. Thus, the calibration of light scattering signals into particle size should be further optimized for IFCM. Ongoing efforts are currently examining whether light scattering signals generated by a 405-nm laser may lead to improved scatter-to-size resolutions, using PS beads to calibrate light scatter signals and hollow organosilica beads (HOBs - with refractive resembling that of EVs [42]) to validate these calibrations [14].

The development of reference materials such as HOBs reflects the ongoing efforts of the EV-field in cross-platform standardization. The benefit of using HOBs, rather than PS beads, is that HOBs with a given size will allow the gating of EVs of the same size without the need of Mie theory to correct light scattering signals into particle size [42]. Therefore, HOBs are ideal reference beads with which to standardize optical measurements of EV concentrations within a predefined size range. Future improvements to HOBs could be fluorescent labelling (similar to PS beads with attributed MESF or ERF values), with the aim of creating a single reference reagent which allows simultaneous calibration of both light scattering and fluorescent signals.

On a less technical note, the low flow rates and consequential long acquisition times, as well as the sizes of data files generated by IFCM may impair its clinical implication. Newer platforms, such as the recently developed CellStream, may solve these problems as this platform has an approximate 10-fold higher flow rate, and does not record images for each detected event – thus leading to smaller data files and shorter acquisition times. However, the downside of not having images associated with recorded events is that it would be impossible to 1) perform spot counts on individual events to determine potential coincidence detection ('swarm' effect) in individual samples, and 2) visually assess outlying events to determine whether these represent contaminating components such as cellular debris (which show brightfield images).

Is the clinic ready for the technology?

It is apparent that EV FC is state-of-the-art nanoparticle characterization and thereby more demanding that conventional (cellular) FC. At the moment of writing, this is largely due to the current technical limitations and rapid technological developments, which demand a high level of expertise – both on the level of sample acquisition as well as data analysis. Although the field is regularly updating its consensus on standardization efforts (through MISEV position papers), and more easy-to-use reference materials are being introduced, we have only just began to fully appreciate and recognize the biological significance of EVs in health and disease.

The observation that ECD kidneys release EVs during NMP, and that subsets of EVs are correlated with well-established indicators of transplant outcome provides a stepping stone for future research into the potential of EVs as indicators of kidney quality prior to transplantation. For example, EV parameters such as concentration, size, and phenotype may be analyzed in perfusion fluids of both ECD and non-ECD

kidneys to examine potential differences. Alternatively, perfusion fluids obtained after hypothermic (4 degrees Celsius) machine perfusion of kidneys may be analyzed and compared with perfusion fluids obtained after NMP to determine if cellular activation has an influence on EV release. Ideally, future research should aim to correlate EV parameters to post-transplantation graft status such as delayed graft function and creatinine levels.

The clinical kidney transplantation samples demonstrated that circulating donor-derived EVs are present at higher concentrations in recipients with stable allograft function than in recipients with allograft dysfunction. These findings are in line with animal models [38, 39, 43], which demonstrated reduced concentrations of dd-EVs before histological proof of allograft rejection. Mechanistically, it is currently unknown whether the lower concentrations of dd-EVs during allograft dysfunction is a consequence of decreased production of EVs by the allograft, increased consumption of dd-EVs by recipient immune cells, or a combination of both [43]. These intriguing questions may be answered by future researchers ideally using a secondary patient cohort using both the same donor-recipient HLA mismatch (HLA-A3) to validate our findings (serving as a technical replicate), as well as using a different donor-recipient HLA mismatch (to validate the biological significance).

In summary, although EV FC requires a higher level of expertise compared to conventional FC, its potential as a tool for single EV characterization in both health and disease is promising. It must be noted that EV analysis with IFCM has been performed in fields other than transplantation e.g., oncology (to characterize glioblastoma-derived EVs [26, 44] or leukemia-derived EVs [45]), diabetes (to examine the protective effects of EVs released by adipose-derived stem cells on obesity [46]), or immunology (to study the interface between pathogen-derived EVs and host recipient cells [47]). However only a few studies have performed calibration of their fluorescent signals, and none - other than those presented in this thesis - have performed calibration of light scattering intensities when using IFCM. As multicenter studies are needed to validate the clinical relevance of EVs during health and disease, e.g. with different instruments measuring the same concentration of cell-type specific EVs in a given sample [14], it is imperative that EV detection assays produce results in a standardized manner. The calibration of arbitrary signals generated by IFCM into standard units as presented in this thesis represents an important step towards increasing the reliability of EV measurements between instruments and laboratories, which are pre-requisites for understanding the biological and diagnostic significance of EVs.

REFERENCES

1. Couch Y, Buzas EI, Di Vizio D, Gho YS, Harrison P, Hill AF, et al. A brief history of nearly EV-erything - The rise and rise of extracellular vesicles. J Extracell Vesicles. 2021;10(14):e12144.
2. Roy S, Hochberg FH, Jones PS. Extracellular vesicles: the growth as diagnostics and therapeutics; a survey. J Extracell Vesicles. 2018;7(1):1438720.
3. Gardiner C, Vizio DD, Sahoo S, Théry C, Witwer KW, Wauben M, et al. Techniques used for the isolation and characterization of extracellular vesicles: results of a worldwide survey. Journal of Extracellular Vesicles. 2016;5:10.3402/jev.v5.32945.
4. Simonsen JB. What Are We Looking At? Extracellular Vesicles, Lipoproteins, or Both? Circ Res. 2017;121(8):920-2.
5. Karimi N, Cvjetkovic A, Jang SC, Crescitelli R, Hosseinpour Feizi MA, Nieuwland R, et al. Detailed analysis of the plasma extracellular vesicle proteome after separation from lipoproteins. Cell Mol Life Sci. 2018;75(15):2873-86.
6. Jang SC, Kim OY, Yoon CM, Choi DS, Roh TY, Park J, et al. Bioinspired exosome-mimetic nanovesicles for targeted delivery of chemotherapeutics to malignant tumors. ACS Nano. 2013;7(9):7698-710.
7. Linares R, Tan S, Gounou C, Arraud N, Brisson AR. High-speed centrifugation induces aggregation of extracellular vesicles. J Extracell Vesicles. 2015;4:29509.
8. Thery C, Witwer KW, Aikawa E, Alcaraz MJ, Anderson JD, Andriantsitohaina R, et al. Minimal information for studies of extracellular vesicles 2018 (MISEV2018): a position statement of the International Society for Extracellular Vesicles and update of the MISEV2014 guidelines. J Extracell Vesicles. 2018;7(1):1535750.
9. Welsh JA, Van Der Pol E, Arkesteijn GJA, Bremer M, Brisson A, Coumans F, et al. MIFlowCyt-EV: a framework for standardized reporting of extracellular vesicle flow cytometry experiments. J Extracell Vesicles. 2020;9(1):1713526.
10. van der Pol E, van Gemert MJ, Sturk A, Nieuwland R, van Leeuwen TG. Single vs. swarm detection of microparticles and exosomes by flow cytometry. J Thromb Haemost. 2012;10(5):919-30.
11. Morales-Kastresana A, Musich TA, Welsh JA, Telford W, Demberg T, Wood JCS, et al. High-fidelity detection and sorting of nanoscale vesicles in viral disease and cancer. J Extracell Vesicles. 2019;8(1):1597603.
12. Tertel T, Gorgens A, Giebel B. Analysis of individual extracellular vesicles by imaging flow cytometry. Methods Enzymol. 2020;645:55-78.
13. Nolan JP, Duggan E. Analysis of Individual Extracellular Vesicles by Flow Cytometry. Methods Mol Biol. 2018;1678:79-92.
14. Kuiper M, van de Nes A, Nieuwland R, Varga Z, van der Pol E. Reliable measurements of extracellular vesicles by clinical flow cytometry. Am J Reprod Immunol. 2021;85(2):e13350.
15. Welsh JA, van der Pol E, Bettin BA, Carter DRF, Hendrix A, Lenassi M, et al. Towards defining reference materials for measuring extracellular vesicle refractive index, epitope abundance, size and concentration. J Extracell Vesicles. 2020;9(1):1816641.
16. Lannigan J, Erdbruegger U. Imaging flow cytometry for the characterization of extracellular vesicles. Methods. 2017;112:55-67.
17. Ayers L, Pink R, Carter DRF, Nieuwland R. Clinical requirements for extracellular vesicle assays. J Extracell Vesicles. 2019;8(1):1593755.

18. Larson MC, Luthi MR, Hogg N, Hillery CA. Calcium-phosphate microprecipitates mimic microparticles when examined with flow cytometry. Cytometry A. 2013;83(2):242-50.
19. Gyorgy B, Modos K, Pallinger E, Paloczi K, Pasztoi M, Misjak P, et al. Detection and isolation of cell-derived microparticles are compromised by protein complexes resulting from shared biophysical parameters. Blood. 2011;117(4):e39-48.
20. van der Vlist EJ, Nolte-'t Hoen EN, Stoorvogel W, Arkesteijn GJ, Wauben MH. Fluorescent labeling of nano-sized vesicles released by cells and subsequent quantitative and qualitative analysis by high-resolution flow cytometry. Nat Protoc. 2012;7(7):1311-26.
21. Sandau US, Duggan E, Shi X, Smith SJ, Huckans M, Schutzer WE, et al. Methamphetamine use alters human plasma extracellular vesicles and their microRNA cargo: An exploratory study. J Extracell Vesicles. 2020;10(1):e12028.
22. de Rond L, Coumans FAW, Nieuwland R, van Leeuwen TG, van der Pol E. Deriving Extracellular Vesicle Size From Scatter Intensities Measured by Flow Cytometry. Curr Protoc Cytom. 2018;86(1):e43.
23. Erdbrugger U, Rudy CK, Etter ME, Dryden KA, Yeager M, Klibanov AL, et al. Imaging flow cytometry elucidates limitations of microparticle analysis by conventional flow cytometry. Cytometry A. 2014;85(9):756-70.
24. Headland SE, Jones HR, D'Sa AS, Perretti M, Norling LV. Cutting-edge analysis of extracellular microparticles using ImageStream(X) imaging flow cytometry. Sci Rep. 2014;4:5237.
25. Mastoridis S, Bertolino GM, Whitehouse G, Dazzi F, Sanchez-Fueyo A, Martinez-Llordella M. Multiparametric Analysis of Circulating Exosomes and Other Small Extracellular Vesicles by Advanced Imaging Flow Cytometry. Front Immunol. 2018;9:1583.
26. Ricklefs FL, Maire CL, Reimer R, Duhrsen L, Kolbe K, Holz M, et al. Imaging flow cytometry facilitates multiparametric characterization of extracellular vesicles in malignant brain tumours. J Extracell Vesicles. 2019;8(1):1588555.
27. Gorgens A, Bremer M, Ferrer-Tur R, Murke F, Tertel T, Horn PA, et al. Optimisation of imaging flow cytometry for the analysis of single extracellular vesicles by using fluorescence-tagged vesicles as biological reference material. J Extracell Vesicles. 2019;8(1):1587567.
28. Summers DM, Watson CJ, Pettigrew GJ, Johnson RJ, Collett D, Neuberger JM, et al. Kidney donation after circulatory death (DCD): state of the art. Kidney Int. 2015;88(2):241-9.
29. Brat A, Pol RA, Leuvenink HG. Novel preservation methods to increase the quality of older kidneys. Curr Opin Organ Transplant. 2015;20(4):438-43.
30. Callaghan CJ, Harper SJ, Saeb-Parsy K, Hudson A, Gibbs P, Watson CJ, et al. The discard of deceased donor kidneys in the UK. Clin Transplant. 2014;28(3):345-53.
31. Hosgood SA, Saeb-Parsy K, Wilson C, Callaghan C, Collett D, Nicholson ML. Protocol of a randomised controlled, open-label trial of ex vivo normothermic perfusion versus static cold storage in donation after circulatory death renal transplantation. BMJ Open. 2017;7(1):e012237.
32. Noah CV, Tratnig-Frankl P, Raigani S, Cetrulo CL, Uygun K, Yeh H. Moving the Margins: Updates on the Renaissance in Machine Perfusion for Organ Transplantation. Current Transplantation Reports. 2020;7(2):114-23.
33. Hosgood SA, Nicholson ML. An Assessment of Urinary Biomarkers in a Series of Declined Human Kidneys Measured During Ex Vivo Normothermic Kidney Perfusion. Transplantation. 2017;101(9):2120-5.

34. Moers C, Varnav OC, van Heurn E, Jochmans I, Kirste GR, Rahmel A, et al. The value of machine perfusion perfusate biomarkers for predicting kidney transplant outcome. Transplantation. 2010;90(9):966-73.
35. Xu J, Buchwald JE, Martins PN. Review of Current Machine Perfusion Therapeutics for Organ Preservation. Transplantation. 2020;104(9):1792-803.
36. Rijkse E, de Jonge J, Kimenai HJAN, Hoogduijn MJ, de Bruin RWF, van den Hoogen MWF, et al. Safety and feasibility of 2 h of normothermic machine perfusion of donor kidneys in the Eurotransplant Senior Program. BJS Open. 2021;5(1).
37. Hosgood SA, Barlow AD, Hunter JP, Nicholson ML. Ex vivo normothermic perfusion for quality assessment of marginal donor kidney transplants. Br J Surg. 2015;102(11):1433-40.
38. Habertheuer A, Ram C, Schmierer M, Chatterjee S, Hu R, Freas A, et al. Circulating Donor Lung-Specific Exosome Profiles Enable Noninvasive Monitoring of Acute Rejection in a Rodent Orthotopic Lung Transplantation Model. Transplantation. 2021.
39. Vallabhajosyula P, Korutla L, Habertheuer A, Yu M, Rostami S, Yuan CX, et al. Tissue-specific exosome biomarkers for noninvasively monitoring immunologic rejection of transplanted tissue. J Clin Invest. 2017;127(4):1375-91.
40. Mastoridis S, Londono MC, Kurt A, Kodela E, Crespo E, Mason J, et al. Impact of donor extracellular vesicle release on recipient cell “cross-dressing” following clinical liver and kidney transplantation. Am J Transplant. 2021;21(7):2387-98.
41. Chabert SR, F. Chadoeuf, J. Guilbaud, L. Morison, N. Vaissière, B. Rapid measurement of the adult worker population size in honey bees. Ecological Indicators. 2021;122(107313).
42. Varga Z, van der Pol E, Palmai M, Garcia-Diez R, Gollwitzer C, Krumrey M, et al. Hollow organosilica beads as reference particles for optical detection of extracellular vesicles. J Thromb Haemost. 2018.
43. Habertheuer A, Korutla L, Rostami S, Reddy S, Lal P, Naji A, et al. Donor tissue-specific exosome profiling enables noninvasive monitoring of acute rejection in mouse allogeneic heart transplantation. J Thorac Cardiovasc Surg. 2018;155(6):2479-89.
44. Maire CL, Fuh MM, Kaulich K, Fita KD, Stevic I, Heiland DH, et al. Genome-wide methylation profiling of glioblastoma cell-derived extracellular vesicle DNA allows tumor classification. Neuro Oncol. 2021;23(7):1087-99.
45. Wierz M, Pierson S, Gargiulo E, Guerin C, Moussay E, Paggetti J. Purification of Leukemia-Derived Exosomes to Study Microenvironment Modulation. Methods Mol Biol. 2019;1884:231-45.
46. Zhao H, Shang Q, Pan Z, Bai Y, Li Z, Zhang H, et al. Exosomes From Adipose-Derived Stem Cells Attenuate Adipose Inflammation and Obesity Through Polarizing M2 Macrophages and Beiging in White Adipose Tissue. Diabetes. 2018;67(2):235-47.
47. Ofir-Birin Y, Abou Karam P, Rudik A, Giladi T, Porat Z, Regev-Rudzki N. Monitoring Extracellular Vesicle Cargo Active Uptake by Imaging Flow Cytometry. Front Immunol. 2018;9:1011.

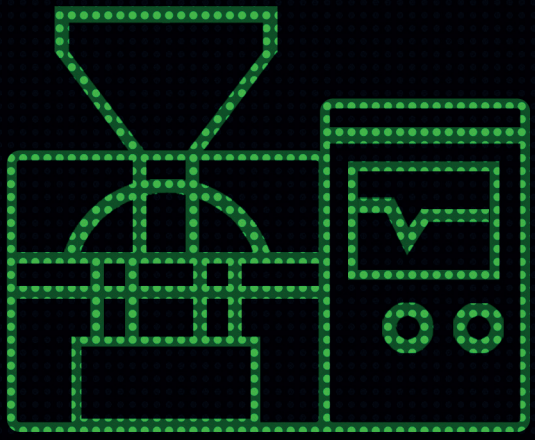

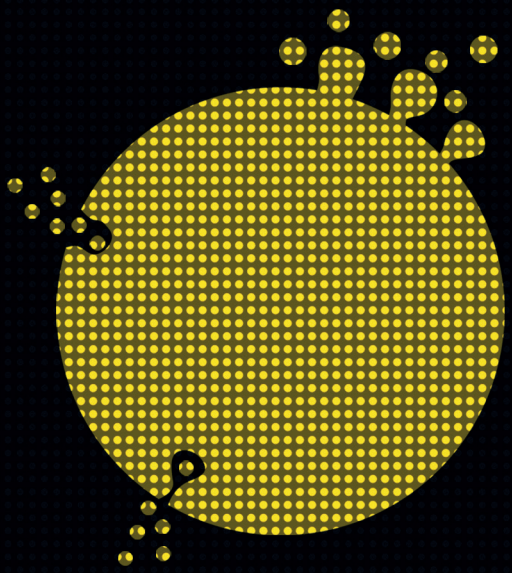

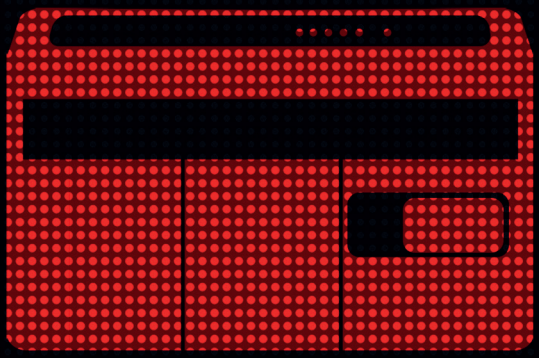

09

ABOUT THE AUTHOR

- CURRICULUM VITAE
- LIST OP PUBLICATIONS
- PHD PORTFOLIO
- ACKNOWLEDGEMENTS

CURRICULUM VITAE

Photo taken by Daan Nieuwland

Wouter Willem Woud was born on the 21st of July 1990 in Zaandam, The Netherlands. He attended the VWO from 2002 to 2008 at the Sint Michael College, Zaandam, with a focus on nature and health. After finishing his BSc Bio-Exact at the University of Amsterdam in 2012 he completed an MSc Life Sciences at the Free University. During his MSc, he specialized in Systems Biology with an emphasis on - and affinity for 'wet lab'-techniques.

After graduating in 2015, he decided to travel through New Zealand, where he later picked up a position as research technician at Innate Immunotherapeutics Limited - a small start-up pharmaceutical company in Auckland. Happily extending his visit into a 15-month experience (acquiring a 'kiwi' accent in the process), he returned to The Netherlands in 2017.

In January 2018, he started his PhD project at the Rotterdam Transplant Institute within the department of Internal Medicine, section Nephrology and Transplantation at the Erasmus MC, under the supervision of prof. Carla C. Baan, dr. Martin J. Hoogduijn, and dr. ir. Karin Boer. In this project, he developed and validated an Imaging Flow Cytometry-based assay for the direct detection of single Extracellular Vesicles in complex, clinically relevant biofluids. This thesis is the culmination of this research.

Wouter now works as a post-doctoral reseacher at ExoVectory, continuing to study the therapeutic applications of Extracellular Vesicles.

LIST OF PUBLICATIONS

Woud WW, Merino A, Hoogduijn MJ, Boer K, van den Hoogen MWF, Baan CC, Minnee RC.
Nanoparticle Release by Extended Criteria Donor Kidneys During Normothermic Machine Perfusion. *Transplantation. 2019;103(5):e110-e1.*

Woud WW, van der Pol E, Mul E, Hoogduijn MJ, Baan CC, Boer K, Merino A.
An imaging flow cytometry-based methodology for the analysis of single extracellular vesicles in unprocessed human plasma. *Commun Biol. 2022;5(1):633.*

Wu L *, **Woud WW ***, Baan CC, Hesselink DA, van der Pol E, Jenster G, Boer K.
Isolation-free measurement of single urinary extracellular vesicles by imaging flow cytometry. *Nanomedicine. 2022;48:102638.*

Woud WW, Arykbaeva AS, Alwayn IPJ, Baan CC, Minnee RC, Hoogduijn MJ, Boer K.
Extracellular Vesicles Released During Normothermic Machine Perfusion are Associated with Human Donor Kidney Characteristics. *Transplantation. 2022.*

Vos J, Tejeda-Mora H, Merino A, Wu L, **Woud WW**, Demmers JAA, van IJcken WFJ, Reinders MEJ, Hoogduijn MJ.
Bio-distribution and longevity of mesenchymal stromal cell derived membrane particles. *J Control Release. 2022;350:642-51.*

Woud WW, Hesselink DA, Hoogduijn MJ, Baan CC, Boer K.
Direct detection of circulating donor-derived extracellular vesicles in kidney transplant recipients. *Sci Rep. 2022;12(1):21973.*

Woud WW, Pugsley HR, Bettin B, Varga Z, van der Pol E.
Size and Fluorescence Calibrated Imaging Flow Cytometry: from Arbitrary to Standard Units. *In Preparation.*

* Equal Contributions

PHD PORTFOLIO

Name	Wouter W. Woud
Erasmus MC Department	Internal Medicine, Erasmus MC Transplant Institute
Research School	Postgraduate School of Molecular Medicine (MolMed)
PhD period	January 2018 – June 2023
Promotor	Prof. dr. C.C. Baan
Co-promotors	Dr. ir. K. Boer Dr. M.J. Hoogduijn

General courses	**Year**	**ECTS**	
Basic Course on R	2018	1.8	
Workshop on Photoshop and Illustrator CS6 for PhD-students and other researchers	2018	0.3	
Advanced Immunology Course	2019	4.5	
Erasmus MC - Scientific Integrity	2022	0.3	
National and international conferences	**Year**	**ECTS**	
Joint NTV-BTS Transplantation Conference, *Rotterdam, The Netherlands*	2018	1	
Young Professionals Networkday, *Utrecht, The Netherlands*	2018	1	
Exosomes & Liquid Biopsies Europe, *Rotterdam, The Netherlands*	2018	1	
HLA Educationday, *Leiden, The Netherlands*	2018	1	
Clinical Review Symposium, *Utrecht, The Netherlands*	2018	1	
Science Days Internal Medicine, *Sint-Michielsgestel, The Netherlands*	2019	1	
ESOT2019 *, *Copenhagen, Denmark*	2019	1.2	
NLSEV2019 *, *Utrecht, The Netherlands*	2019	1	
Science Days Internal Medicine *, *Sint-Michielsgestel, The Netherlands*	2020	1	Best Poster Prize
Boot Conference *, *Roermond, The Netherlands*	2020	1	
Virtual Conference TTS, *Online*	2020	1.2	
Virtual Conference NLSEV **, *Online*	2020	2	
Virtual Mini Symposium PROPER **, *Online*	2020	2	
Boot Conference, *Online*	2021	1	
Virtual Conference ISEV *, *Online*	2021	2	

General courses	Year	ECTS	
American Transplant Conference, *Online*	2021	1	
ESOT ** (2x), *Milano, Italy*	2021	3	
NLSEV * / **, *Amsterdam. The Netherlands*	2021	2	Best Poster Prize
ITS * / **, *Berlin, Germany*	2022	3	3rd Poster Prize
ISEV ** (2x), *Lyon, France*	2022	3	
Bootcongres * / **, *Leiden, The Netherlands*	2022	1.6	
TTS ** (2x), *Buenos Aires, Agentina*	2022	1	
CYTO **, *Philadelphia, USA*	2022	1	
Science days Internal Medicine **, *Sint-Michielsgestel, The Netherlands*	2022		
NLSEV *, *Maastricht, The Netherlands*	2022	1.6	
METVES II Workshop, *Delft, The Netherlands*	2022	0.3	
6e Regionale nascholing - Nefrologische Zorg op Maat, *Rotterdam, The Netherlands*	2022	1	
Additional activities	**Year**	**ECTS**	
Supervision 4th year VMBO student	2019	0.3	
Training ImageStreamX	2020	0.6	
Certified Peer Reviewer Course	2021	0.3	
Supervising HLO Internship student	2021	25	
Erasmus MC EV Meetings	2018 - 22	1.5	
Transplantation Journal Club	2018 - 22	1.5	
Total		**73**	

* Poster Presentation, ** Oral Presentation

ACKNOWLEDGEMENTS

"Laboring five years to write a book that most readers will pick up to flip straight to the acknowledgements, is an excellent exercise in modesty"
- Josje Kok, 2021

I have been told that this section is often the most-read part of any thesis. So if this is the first time you read the words 'Extracellular Vesicle' and 'Imaging Flow Cytometry': please go back to the beginning and actually read this thesis. Chances are you will like it, and – who knows – you might learn a thing or two.

With that out of the way, I would like to dedicate this section to the many people who have in some form contributed to my PhD-trajectory. As every sentence written during these last five years has been scrutinized, structured, debated, changed, and re-written - I here refuse to do any of that. I have, however, roughly organized this section into three parts. Although many of you cannot (and should not ever) be placed into a single category, my (scientific) inclination for order and cataloguing is near compulsive – leaving me no other options ☺.

"I don't know half of you half as well as I should like, and I like less than half of you half as well as you deserve" – John. R. R. Tolkien, 1954

Dear **Prof. dr. Carla C. Baan**, thank you for giving me the opportunity to perform my PhD studies at the Rotterdam Transplantation Lab, for seeing the potential in the (early) ImageStream experiments conducted at Sanquin (Amsterdam), for acquiring our own IFCM at the Transplantation Laboratory, and for your critical approach and comments to all the experiments and writing performed. You allowed me the freedom to 'play' at the lab (although, as scientists we prefer to say 'test'), made sure I did not lose oversight of the bigger picture (the completion of this thesis), and taught me to take my time during presentations (I have the tendency to speed-up in my enthusiasm).

Dear **Dr. ir. Karin Boer**, thank you for being there all along the way, for all the chats (both work and non-work related), for nourishing my enthusiasm when an experiments' outcome was in line with expectations (and for motivating me when it wasn't), and for helping me organize my thoughts on paper. Although I 'derailed' my own project – away from a biomarkers' perspective, and into a more technical approach – you managed to keep up and be as excited as I was when we found/saw something new. Keep speaking your mind and be direct, it is your greatest gift ☺.

Dear **Dr. Martin J. Hoogduijn**, although your expertise lies in the field of mesenchymal stromal cells you managed to stay on top of my project. Thank you for showing me to the world of normothermic machine perfusion (NMP), for introducing me to the Greek gods POSEIDON and APOLLO, and for connecting me to the PROPER-consortium. I found these studies fascinating, and I hope that the research into EVs and NMP will be continued. Also, a big thank you for your endless patience, your constructive feedback, and your good sense of humor – together with Karin you were the best daily supervisor I could have wished for.

Dear **Dr. Ana M. Merino**, you taught me everything I needed to know about EVs, about flow cytometry, and the notorious difficulties of combining the two. I am so grateful that I got to pick your brain during the first two years of my PhD; your no-nonsense attitude was enlightening. It was a loss for the Transplantation Laboratory when you left us for Thermo Fisher, but I am sure we will run into each other again. Until then!

Dear **Dr. Edwin van der Pol**, although you were not my supervisor in any form, I still would like to thank you for all I have learned from you, and all you have done. We met at the NLSEV conference in Amsterdam in 2021 where you offered to help me calibrate the side scatter signals of our IFCM – which turned out to be the missing piece in our assay. You introduced me to Mie theory for spherical sub-micron particles, and awakened in me a curiosity for the technicalities of flow cytometry. I hope we will continue our calibration work, and I am excited for what the future may hold.

Dear **Dr. Haley R. Pugsley**, you were my go-to person for anything related to the analysis of IFCM data. Your knowledge of IFCM design, masking, features, and displaying options in the IDEAS software have helped me understand and make sense of the data I acquired. I hope we stay in contact, I am sure I will have more questions in the future ☺.

To **Manou van Alphen**: thank you for being the best internship student I could have wished for! Your time with us at the lab has been one of the best periods in my PhD trajectory; I thoroughly enjoyed your humor, can-do attitude, analytical insights, eye for detail, patience (a golden-quality in research), your willingness to learn (either lab skills or coding skills), and your *"zachte ch"* (some things are what they are).

To all my fellow **PhD candidate colleagues** – both current and those who have moved on – Jeroen, Aleixandra, Amy, Hector, Steven, Amanda, Suwasin, Liang, Daphne, Hui, Shengbing, Yvette, Reshwan, and Quincy. Thank you so much for making this trajectory memorable: for celebrating the wins (publications), for drinking away the losses (rejections), for cheering each other on during presentations, and for exploring foreign cities during conferences. You are a great group of people – amazing entertainers and sharp scientists – and I wish you all the best in your current and future careers!

To all the **technicians** at the Transplantation Lab: Wenda (*Wennie*), Rens (*Reka*), Mariska (*Misa*), Ronella (*Ronnie*), Sander (*Såndør*), Marjolein (*Marjo*), Annemiek (*Miek*), Frederique (*Frey*), and Derek (*Pretletter*). I gave each of you a nickname from the moment I arrived at the lab, and have since refused to use your given names outside formal meetings. Collectively, you taught me all the 'wet lab' skills I needed, showed me what it entails to run a biomarker study (the sheer amount of samples coming in daily was overwhelming at times), provided expert hands-on advice, and overall helped me perform my experiments. A special shout-out to *Wennie* (for joining the WWW-WV-EV-Team), *Reka* (for all flow cytometry discussions), and *Pretletter* (for making each interaction a delight).

"Good friends don't let their friends do stupid stuff alone" – Anonymous

To Daan, Joey, Stefan, Jasper, Mark, Jesse and Frank (Jetse), you guys are more than just friends – I consider you all family. I tried to explain my work once by using M&Ms to illustrate the identification of different cellular particles, which – to this day – is all you guys have remembered (Daan: "Wel heel be-'hap'-baar uitgelegd hoor"). Despite this lack of understanding, you guys have helped me through these last five years by smothering me with board games, D&D sessions, music (through listening, making, recording, and performing), whiskey evenings, and good long talks. You were, and continue to be, a welcome diversion to the mental exercise I have put myself through. Now that this is over, I am ready to have a life again ☺.

"Dad, you are like a father to me" – Big Lebowski, 1998

A big thanks to my **family** and all those attached! Thank you all for the great family gatherings (always asking 'when are you finished?'), and for providing reality checks whenever I would go on a rant about my exciting findings.

To Mama and Cees, Maus and Harmen, and Storm: thank you for being there for me all along this road, for taking care of me whenever I visited you 'up North', for laughing at me when I accidently speak 'Rotterdams' (wet 't's are a thing now), and for binge watching anime-series with me (looking at you Stormeru). I know you are just as proud as I am on this book, even if you judge it by its cover.

"There is no parking space for my flying carpet!" – The Otter princess

A special thanks goes to **Dara**, *mijn maatje*, travel buddy, dog-admirer, partner in crime, and avocado-addict. We had been living together for 2 months when the pandemic struck (forcing us in a lockdown), and I'd say we passed that new relationship-test ("*bivakkeren op een postzegel"*) with honors. Your laugh is what makes me wake up in the morning (in combination with a fresh cup of coffee), and your drive to build a better future is contagious. I am curious to see where life will take us, but for now we will start by creating our own place – with enough space for that flying carpet of yours. Дара, обичам те!


REJECTED
REJECTED
REJECTED